

SYNTHESIS, CHARACTERIZATION AND DFT STUDIES OF SOME AZOMETHINE AND β -AMINO DERIVATIVES

*Thesis submitted to the
BHARATHIDASAN UNIVERSITY, Tiruchirappalli-620 024
In partial fulfillment of the requirements for the award of the
degree of*

Doctor of Philosophy in Chemistry

By

K.K. MOHAMMED AMEEN
(Ref. No.: 42969/Ph.D.K2/Chemistry/PT/2012)

Under the Guidance of

Dr. M. SYED ALI PADUSHA



**Post Graduate and Research Department of Chemistry
JAMAL MOHAMED COLLEGE (Autonomous)
College with Potential for Excellence
Accredited (3rd Cycle) with 'A' Grade by NAAC
DBT Star Scheme & DST-FIST Funded
(Affiliated to Bharathidasan University)
Tiruchirappalli – 620 020
Tamil Nadu, India**

MARCH 2022

Dr. M. SYED ALI PADUSHA
Associate Professor
Research Advisor and Convener
PG & Research Dept. of Chemistry
Jamal Mohamed College
Tiruchirappalli- 620020
Email: padusha_chem@yahoo.co.in



Res. Address:
64-Mohamed Nagar
J. K. Nagar
Khajamalai Post
Tiruchirappalli- 23
Mobile: 9865447289

CERTIFICATE

This is to certify that the thesis entitled **“SYNTHESIS, CHARACTERIZATION AND DFT STUDIES OF SOME AZOMETHINE AND β -AMINO DERIVATIVES”** submitted by **Mr. K.K. MOHAMMED AMEEN** is a bonafide record of research work done by him under my guidance in the PG and Research Department of Chemistry, Jamal Mohamed College (Autonomous), Tiruchirappalli 620 020 and that the thesis has not previously formed the basis for the award to the candidate, of any Degree/Diploma, Associateship, Fellowship or other similar titles. The thesis as a whole is an independent work of the candidate.

Place: Tiruchirappalli-20.
Date:

Dr. M. SYED ALI PADUSHA
(Research Supervisor)

K.K. MOHAMMED AMEEN

Research Scholar

PG and Research Department of Chemistry

Jamal Mohamed College (Autonomous)

Tiruchirappalli-620 020

DECLARATION

I hereby declare that the thesis entitled **“SYNTHESIS, CHARACTERIZATION AND DFT STUDIES OF SOME AZOMETHINE AND β -AMINO DERIVATIVES”** which I submit for the award of the degree of Doctor of Philosophy to the Bharathidasan University is the original work carried out by me under the guidance and supervision of **Dr. M. SYED ALI PADUSHA**, Associate Professor, PG and Research Department of Chemistry, Jamal Mohamed College (Autonomous), Tiruchirappalli - 620 020.

I further declare that this work has not been submitted earlier in full or in parts to any other university for the award of any other degree or diploma.

Place: Tiruchirappalli-20.













Date:

(K.K. MOHAMMED AMEEN)

Document Information

Analyzed document	K.K. MOHAMMED AMEEN - Chemistry - Ref. No. 42969.pdf (D131393247)
Submitted	2022-03-24T13:03:00.0000000
Submitted by	Dr.S.Vanitha
Submitter email	vanitha@bdu.ac.in
Similarity	5%
Analysis address	navitha.bdu@analysis.orkund.com

Sources included in the report

SA	Janani Manuscript.docx Document Janani Manuscript.docx (D67849637)	 2
SA	Thesis-Sundramoorthy S.pdf Document Thesis-Sundramoorthy S.pdf (D40374307)	 1
SA	1517030018-S.pdf Document 1517030018-S.pdf (D50997848)	 5
SA	Bharathidasan University, Tiruchirappally / (S.Sangeetha Margreat) Thesis.pdf Document (S.Sangeetha Margreat) Thesis.pdf (D110838983) Submitted by: bdulib@gmail.com Receiver: bdulib.bdu@analysis.orkund.com	 2
SA	chapter 5.pdf Document chapter 5.pdf (D35631008)	 3
SA	1216060011-SSS.doc Document 1216060011-SSS.doc (D21279067)	 4
SA	1216060003-S.docx Document 1216060003-S.docx (D17682077)	 7
SA	Tintu K Kuruvilla.pdf Document Tintu K Kuruvilla.pdf (D43303222)	 3
SA	A17MPPH02.docx Document A17MPPH02.docx (D41026489)	 1
SA	09-12-16sathesh Thesis aligned.docx Document 09-12-16sathesh Thesis aligned.docx (D24163307)	 1
SA	1615799112-thesis-14112019.pdf Document 1615799112-thesis-14112019.pdf (D58843842)	 1
SA	Abstract and Chapters (1).docx Document Abstract and Chapters (1).docx (D128637526)	 1

ACKNOWLEDGEMENT

All Praise to the **Almighty**, the most beneficent and merciful who blessed me with enough strength and mercy to complete this research work successfully.

I express my hearty gratitude to **Dr. M. Syed Ali Padusha**, a dynamic academician and vibrant research advisor, Associate Professor of Chemistry, Jamal Mohamed College (Autonomous), Tiruchirappalli, for his copious guidance throughout my research work. May the almighty bless him and his family with utmost grace.

I express my sincere gratitude to **Dr. A. K. Khaja Nazeemudeen Sahib**, Secretary and Correspondent, **Hajee. M. J. Jamal Mohamed Sahib**, Treasurer, **Dr. K. Abdus Samad**, Assistant Secretary and Directors of Management committee of Jamal Mohamed College (Autonomous), for provided me an opportunity to pursue the research work in this esteemed institution.

I convey my deep sense of gratitude to **Dr. S. Ismail Mohideen**, Principal, Jamal Mohamed College (Autonomous), for his enthusiastic support and motivation.

I whole heartedly thank **Dr. M. Mohamed Sihabudeen**, Additional Vice-Principal, Associate Professor and Head, PG and Research Department of Chemistry, Jamal Mohamed College (Autonomous), for his motivation and encouragement throughout the research work.

I express my sincere thanks to the Doctoral committee members **Dr. J. Princy Merlin**, Associate Professor and Head, PG and Research Department of Chemistry, Bishop Heber College (Autonomous), Tiruchirappalli and **Dr. J. Sirajudeen**, Assistant Professor of Chemistry, Jamal Mohamed College (Autonomous) for their valuable suggestions and support throughout the period of research.

It is my pleasure to express my gratitude to my teachers **Dr. M. Seeni Mubarak**, **Dr. A. Jafar Ahamed**, Associate Professors, PG and Research Department of Chemistry, Jamal Mohamed College (Autonomous) and (Late) **Dr. A. Burkanudeen** for their encouragement and motivation during my research work.

I also thank **Dr. R. Khader Mohideen** , **Dr. A.M. Mohamed Sindhasha** and **Dr. S. Mohamed Salique** Former Principals, Jamal Mohamed College, Tiruchirappalli and **Dr. A. Abdul Jameel** and **Dr. M.I. Fazal Mohamed** Former Heads, PG and Research Department of Chemistry, Jamal Mohamed College (Autonomous) for their continuous support during the course of study.

I extend my immense thanks to **Dr. F. M. Mashood Ahamed**, Assistant Professor, PG and Research Department of Chemistry, Jamal Mohamed College (Autonomous), for his helping hands during this research.

It is a great joy to express my thanks to **Dr. N. Mujafarkani**, Assistant Professor, PG and Research Department of Chemistry, Jamal Mohamed College (Autonomous) and the fellow research scholars, **Dr. T. Chandrasekaran**, **Dr. M. Suresh**, **Mr. D. Parthasarathi** and **Mr. R. Manoj Kumar** for their support during this tenure.

I am grateful to **Mr. Senthil Kumar**, EUMIC Laboratory, Tiruchirappalli, **SAIF IIT** Chennai, **VIT University**, Vellore for the technical support provided.

I wish to record my thanks to all the **Teaching** and **Non-Teaching Staff Members** of the Department for their timely help during my research.

It is my great honor to thank my parents **Mr. Aboobacker K.K** and **Mrs. Rukiyya MT**, Uncle **Mr. Hamza VK**, Aunt **Mrs. Jameela VK**, my beloved wife **Mrs. Saniya VK**, Daughters **Nihla**, **Minha** and **Tamanna**, Sister, **Haseena KK** and Cousin **Abul Falal A** for their support and encouragement during this research work.

I take this opportunity to thank Manager, **Janab PP. Unneen Kutty Moulavi**, Correspondent **Raheem** and my colleagues of Puliyparamb Higher Secondary School, Kodunthirapully, Palakkad, Kerala for their help rendered during my research work.

(K.K. MOHAMMED AMEEN)

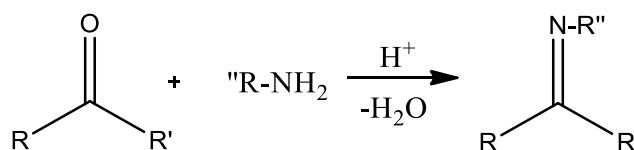
Content

	Page. No
Chapter-I Introduction	1
Chapter-II Synthesis of azomethine compounds via Schiff reaction (MA1-MA5)	42
Chapter-III Synthesis of azomethine compounds via Schiff reaction (MA6-MA10)	68
Chapter-IV Synthesis of β -amino carbonyl compounds	92
Chapter-V Synthesis, characterization and DFT studies of MA14 & MA15	106
Summary and Conclusion	149
References	152

Introduction

1.1. Schiff Condensation

Imines are the compounds derived from the reaction of an aldehyde or ketone with primary amine in the presence of an acid as catalyst and were first reported by Hugo Schiff. The common structural feature of these compounds is the azomethine group with a general formula $\text{RHC}=\text{N-R}'$, where R and R' are alkyl, aryl, cyclo alkyl or heterocyclic groups which may be variously substituted. These compounds are also known as anils, imines or azomethines.



Schiff bases are the intermediates in organic reactions and are further explored for their utility. Azomethine group of these compounds has a great attention as precursor in huge organic synthesis due to their biological applications such as antitubercular, anticancer, CNS depressant, antibacterial antimicrobial activity, anti-inflammatory, anticonvulsant, antitumor, antihypertensive activity, anti HIV activity, plant growth inhibitors, and insecticidal properties. The Schiff bases are an intermediate in the biologically important transamination, racemization reactions and amino protective groups in organic synthesis.

They were used as protective agent in natural rubber. An example of a biologically important aldehyde is *pyridoxalphosphate*, which is the active form of the vitamin B6. Vitamin B6 serves as a coenzyme by forming an imine with an amino acid grouping an enzyme. The coenzyme, bound to the enzyme, is involved in transamination reaction, the transfer of the amino group from one amino acid to another, which is important in the metabolism and the biosynthesis of amino acids. In the last step, enzyme-catalyzed hydrolysis cleaves the imine to pyridoxal and the modified amino acid. An imine linkage between the aldehyde derived from vitamin A and the protein opsin in the retina of the eye plays an important role in the chemistry of vision. Vitamins are also called coenzymes, meaning that they are important to the functioning of many enzymes, which are large proteins that catalyze chemical changes in cell.

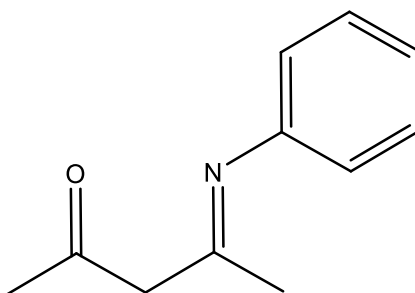
Moreover the reactions of azomethine involving in ring closure reaction to generate a wide range of five, six and seven members rings of heterocyclic molecules by reacting with 2-aminopyridine, 4-isopropyl benzaldehyde, 3,4,5-trimethoxy benzaldehyde, 3-aminobenzo trifluoride derivatives are playing vital role as active substances in biological systems and liquid-crystalline compounds. Therefore the synthesis of such compounds has gained greater importance. A large number of different Schiff base ligands have been used as cation carriers in potentiometric sensors as they have shown excellent selectivity, sensitivity and stability for specific metal ions. Schiff bases have been

studied for their important properties in catalysis. They show catalytic activity in hydrogenation of olefins. They find applications in biomimetic catalytic reactions.

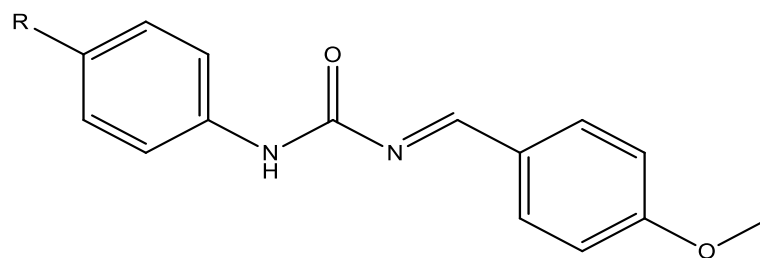
An interesting application of Schiff bases is their use as an effective corrosion inhibitor, which is based on their ability to form a monolayer spontaneously on the surface to be protected. Many commercial inhibitors include aldehydes or amines, but presumably due to the C=N bond the Schiff bases function more efficiently in many cases. The principal interaction between the inhibitor and the metal surface is chemisorption. The inhibitor molecule should have centers capable of forming bonds with the metal surface by electron transfer. In such cases the metal acts as an electrophile and the inhibitor acts as a Lewis base. Nucleophilic centers, such as oxygen and nitrogen atoms, of the protective compound have free electron pairs which are readily available for sharing. Together with the atoms of the benzene rings they create multiple absorption sites for the inhibitor thus enabling stable monolayer formation. Synthesis, characterization and structure activity relationship (SAR) of Schiff bases have been studied worldwide. Several studies showed that the presence of a lone pair of electrons in sp^2 hybridized orbital of nitrogen atom of the azomethine group is of considerable chemical and biological importance. They involved in normal cell processes by the formation of a hydrogen bond between the

active centers of cell constituents and sp^2 hybridized nitrogen atom of the azomethine group.

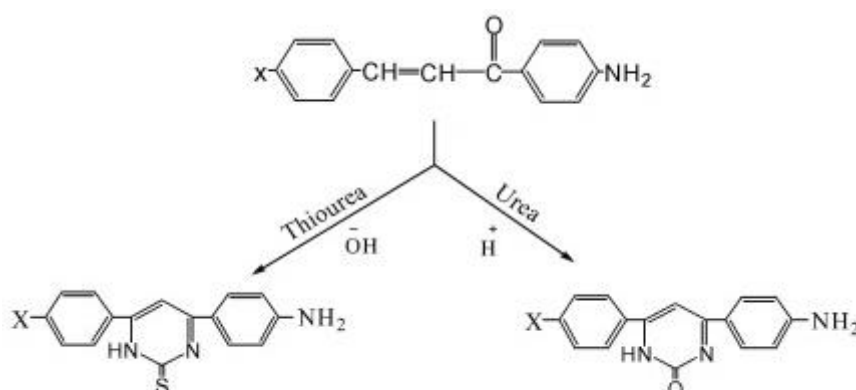
J.Popelis et.al., have reported the synthesis of imines by reacting furylacroleins and amino pyridines. They have employed zeolite molecular sieves as adsorbent. An interesting result revealed from their study was that the zeolites served as good dehydrating agents and catalyst for the synthesis [1]. Adnan dib has reported the synthesis of imines derived from acetyl acetone. The author also carried out computational study to explain the geometry, heat of formation and binding energy [2].



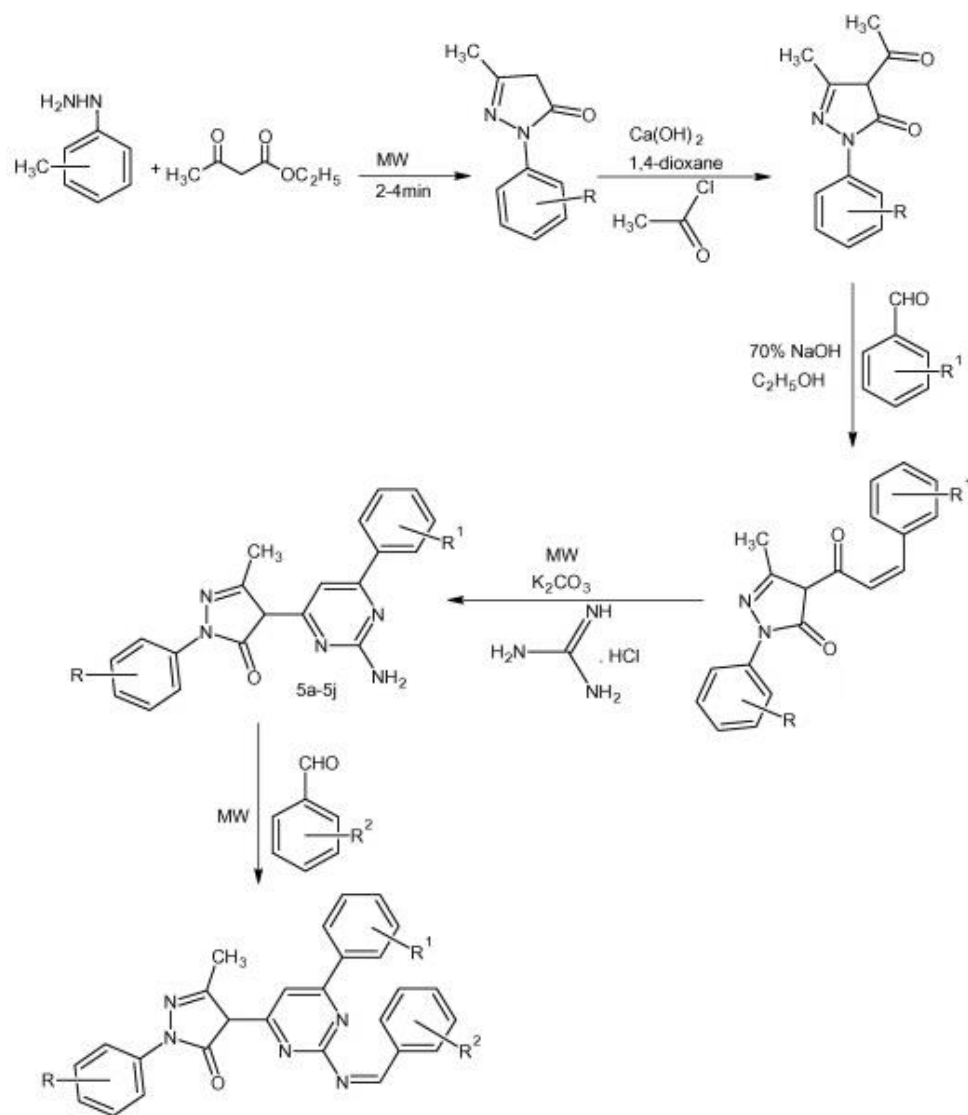
Synthesis of 1-(4-methoxyphenyl)-3-[(1E)-2-(pyrimidin-5-yl)ethylidene]urea and its analogues using phenyl urea derivatives and aldehyde were reported by V.R.Nagavolu et.al. The team also reported the in-vitro anti-oxidant activities of the compounds employing hydrogen peroxide free radical inhibition method [3].



Sunita Bhagat et.al, have reported aqueous mediated synthesis of imines by reacting salicylaldehyde and aromatic amines employing microwave irradiations and established that the yield obtained by this method is higher than the conventional method [4]. Jumbad.H. Tomma et.al, have reported the Schiff bases containing pyrimidine units obtained by reacting chalcones with urea/ thio urea [5].



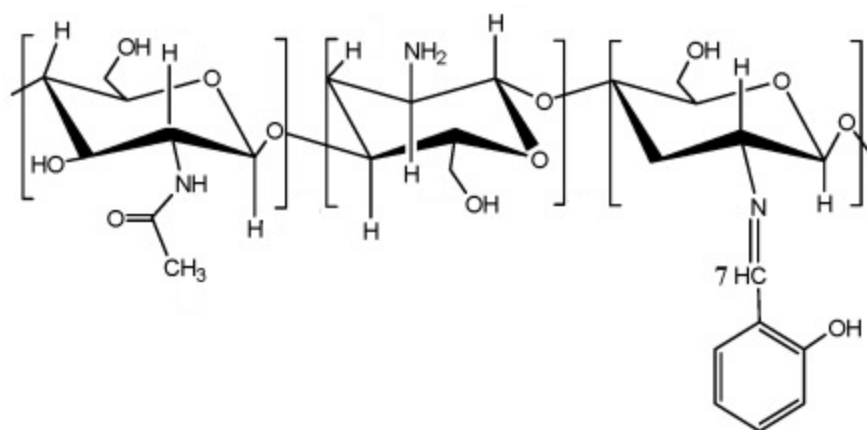
2N-salicylidene-5-(*p*-nitro phenyl)-1,3,4-thiadiazole was prepared by reacting 4-nitrobenzoic acid and thiosemicarbazide in the presence of phosphorous oxy chloride and its antibacterial activity was reported by Emad yousif et.al, The results showed that the compound was active against *S.aureus*, *S.typhi* and *E.Coli* [6]. Rishikesh.V.Antre et.al. have reported the microwave irradiated synthesis of imines derived from pyridines attached with pyrazolone moiety [7].



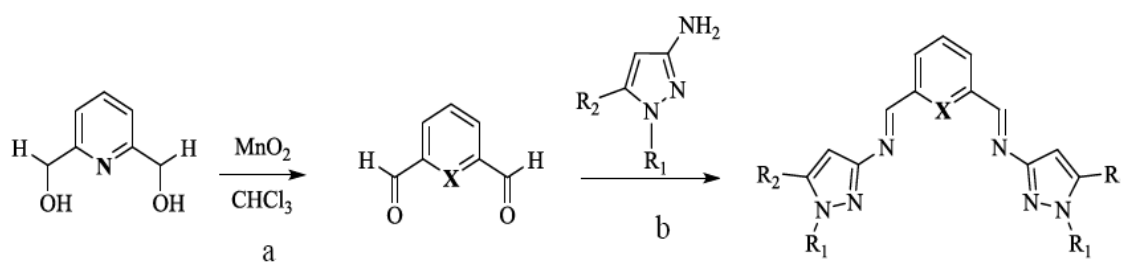
Hina zafar et. al, have reported the synthesis of macrocyclic Schiff base by reacting 1,2-diphenylethane-1,2-dione dihydrazone and dimethyl/diethyloxalate. They also investigated the antimicrobial and anticancer activities of the compounds. The results revealed that the synthesized compounds were possessed good activity against HeLa, MCF7 and Hep3B human cancer cell lines [8]. Wound healing bio materials was synthesized by Y. Dong and W. Wang. The authors have

prepared the Schiff bases as bio active hydrogels and employed it for healing the wounds and in the delivery of stem cells [9].

Hellen et.al, have synthesized the biopolymeric scaffolds using Chitosan and salicylaldehyde derivatives and investigated their antimicrobial and anti cancer activities. The results showed that the synthesized compounds were potent against MCF-7 human breast cancer cell line [10].

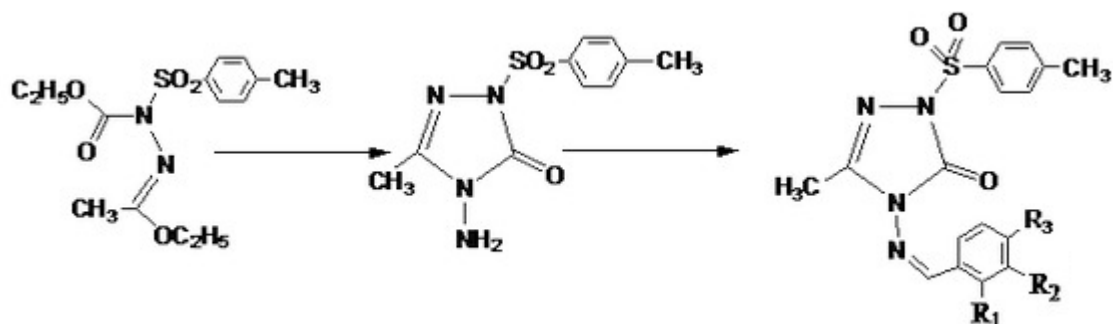


DNA interaction, molecular docking and antitumor activities of the compounds derived from o-vanillin have been reported. The results revealed that the compounds have effective binding via hydrogen bonding with active receptor protein DNA topoisomerase [11]. Anti cancer activity of the compounds derived from 3-aminopyrazole and dialdehydes were reported. The investigation showed that the synthesized compound possessed higher cytotoxicity and suggested that the heterocyclic moiety have effective bio activity [12].

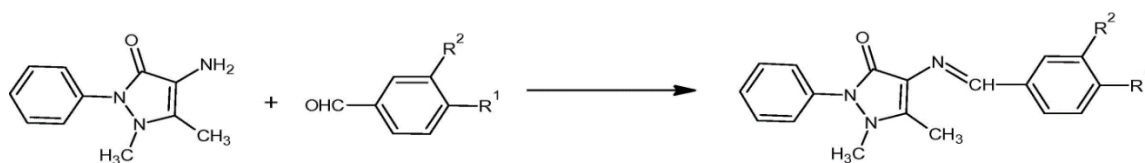


The compounds derived by reacting ethyl amino benzo nitro furan and salicylaldehyde derivatives were reported. The study reveals that the derived compounds are effective scaffolds on combating microbial infections [13].

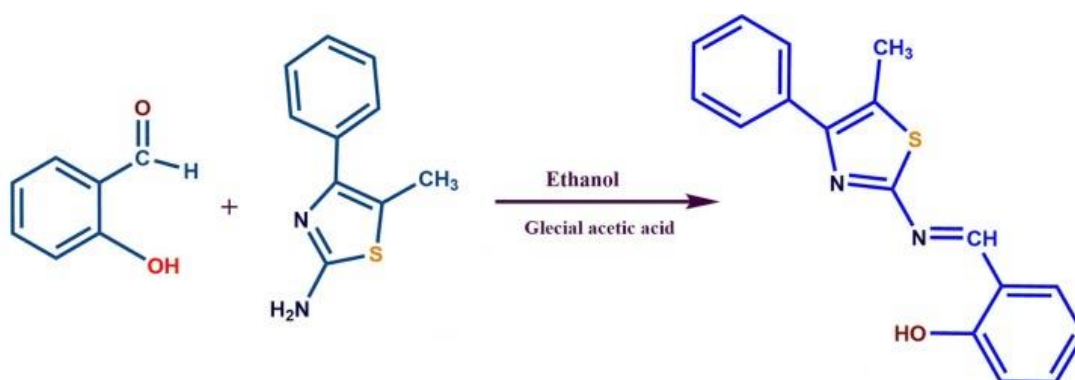
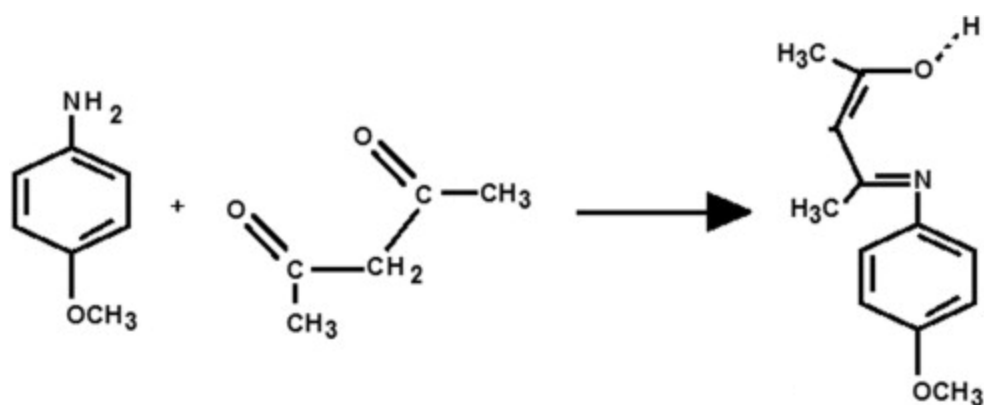
Antioxidant activity, antihypertensive activity and angiotensin-I converting enzyme inhibition activities of the compounds synthesized by reacting amino triazole and aromatic aldehydes were reported [14].



Aminophenazone and benzaldehyde derived compounds were reported and their analgesic and anti-inflammatory activities in mice and antipyretic activity in rabbits were investigated. The results showed that the compounds are effective in reducing fever in rabbits after 3-4 hours [15].

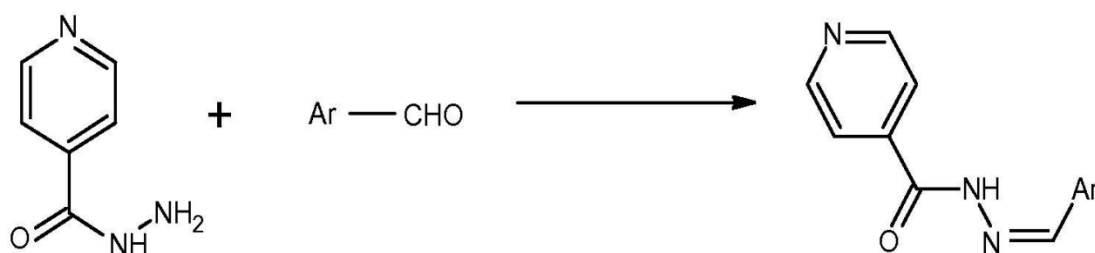


Condensation product of salicylaldehyde and amino phenylmethyl thiazole and its anticancer activity against breast cancer MCF-7, liver cancer HepG2, lung carcinoma A549 and colorectal cancer HCT116 cell lines were evaluated. The results showed that the compound exhibits activity against the cell line in the order HepG2>MCF-7>A549>HCT116 [16]. The compound derived from anisaldehyde and their adsorption properties were reported [17].



The synthesis and pharmacological activity of *N*-[(1*Z*)-(substituted aromatic) methyldene] pyridine-4-carbohydrazides and *N*-[3-chloro-2-

(substituted aromatic)-4-oxoazetidin-1-yl]pyridine-4-carboxamides were reported. The compounds were investigated for their antidepressant activity and in the elevated plus maze test and passive avoidance test in mice for the evaluation of nootropic activity. The compounds exhibited higher antidepressant activity and the compounds with para nitro substitution on the aryl ring showed the highest nootropic activity. The results further confirm the fact that the 2-azetidinone skeleton has potential as a CNS active agent and can be explored for the development of more potent and safe CNS active agents for therapeutic use [18].



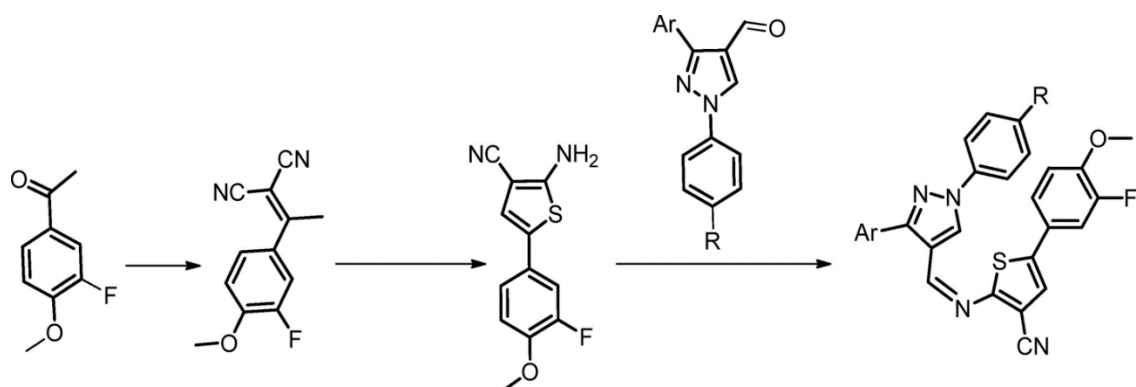
The synthetic protocol of 2-Amino-benzimidazole condensation with acetyl acetone, ethyl cyanoacetate and 3, 4-dimethoxy benzaldehyde established to develop Schiff bases was reported. Further the antimicrobial activity of the ligands against bacterial strains and fungal strains were investigated [19]. The Schiff bases derived from the condensation between mono and diacetyl ferrocene and 2-aminobenzenthion in different molar ratio, lead to series of mono and binuclear complexes was reported. Synthesized Schiff bases were tested for the growth inhibitory activity against phytopathogenic bacteria and

fungi, including some antibiotic resistant, make it interesting for a practical use as antimicrobial agent. It is obvious that the activity become more pronounced when two ferrocene rings are coupled and more toxic against bacteria and fungi [20].

The synthesis and structural characterization of mixed ligand complexes derived from 2,6-pyridinedicarboxaldehyde bis(*o*-hydroxyphenylimine), 2,6-pyridine dicarboxaldehyde bis(*p*-hydroxyphenylimine) and 2-aminopyridine are reported. The compounds have been screened for their antimicrobial activities and their findings have been reported by comparing with some known antibiotics [21]. Schiff base derived from 2-thiophene carboxaldehyde and 2-aminobenzoic acid are reported. The synthesized compounds were screened for their antibacterial activity against bacterial species, *Escherichia coli*, *Pseudomonas aeruginosa*, *Staphylococcus pyogenes* and Fungi (*Candida*). The activity data show that the compounds exhibit potent antimicrobial activity [22].

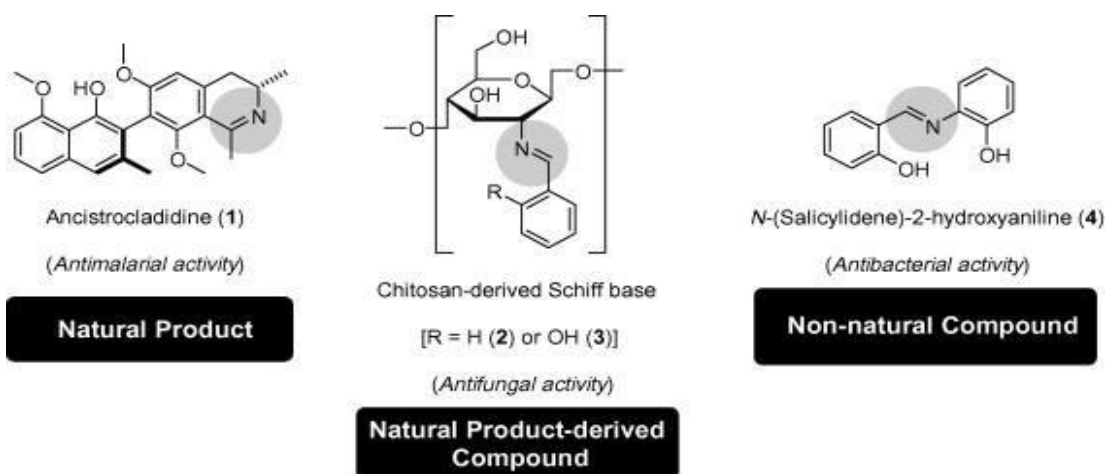
2-Amino-5-(3-fluoro-4-methoxyphenyl)thiophene-3-carbonitrile was synthesized from 1-(3-fluoro-4-methoxyphenyl)ethanone, malononitrile, a mild base and sulfur powder using Gewald synthesis technique and the intermediate was treated with 1,3-disubstituted pyrazole-4-carboxaldehyde to obtain the Schiff bases. 1,3-disubstituted pyrazole-4-carboxaldehyde derivatives have been synthesized by Vilsmeier-Haack reaction in the course of a multi-step reaction. The

compounds have been screened for their *in vitro* antimicrobial activity and the results showed that the compounds have excellent activity [23].

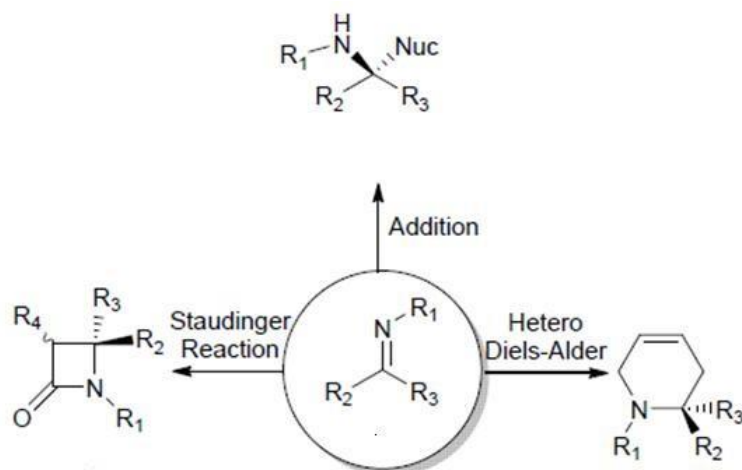


5-methyl thiophene-2-carboxaldehyde-carbohydrazone was synthesized and evaluated for antioxidant activity employing hydroxyl radical scavenging, DPPH, NO, reducing power methods *in vitro*. The obtained IC₅₀ value of the DPPH activity for the compound was found to be high. Microbial assay values of the above compound against *Staphylococcus aureus*, *Escherichia coli*, *Rhizocotonia bataticola* and *Alternaria alternata* were found to be higher [24].

Przybylski P et. al., investigated the wide application of Schiff bases like pigments and dyes, catalysts, intermediates in organic synthesis as polymer stabilisers. Further, biological activities such as antifungal, antibacterial, antimalarial, antiproliferative, anti-inflammatory, antiviral, and antipyretic properties have also been studied [25]. Guo Z et. al., reported that Imine or azomethine groups are present in various natural, natural-derived, and non-natural compounds which are responsible for their biological activity [26].

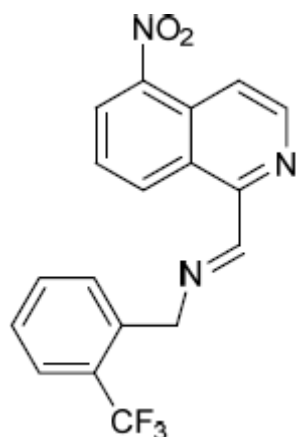


Kobayashi et.al, studied the addition of organometallic reagents or hydride which undergo reduction in the C=N group to form asymmetric carbon-carbon bond [27]. Ueno et.al, concludes that imines are useful in the formation of six member nitrogen containing heterocyclic compounds employing hetero Diel's- Alder reaction [28]. Allen and Tidwell proposed Staudinger reaction with ketene to furnish biologically important β -lactam ring [29].

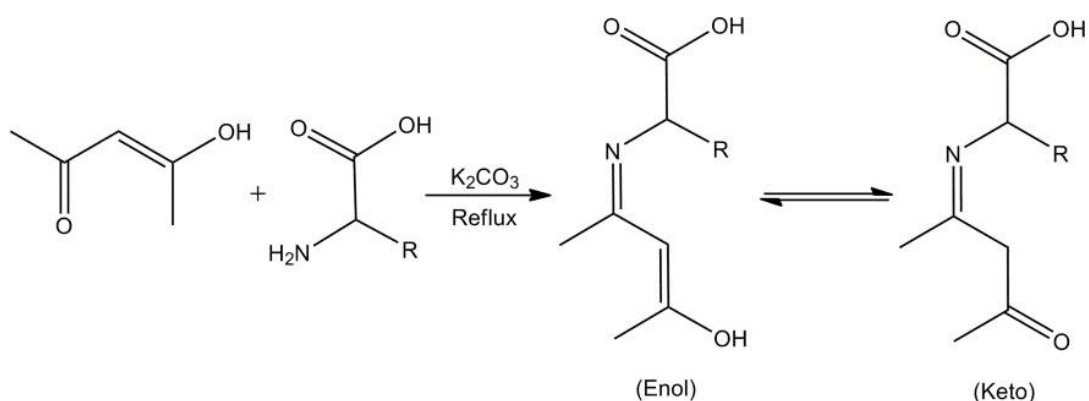


Malaria is a severe morbidity of humans and other animals. The imino group of Schiff bases has been found to be valuable

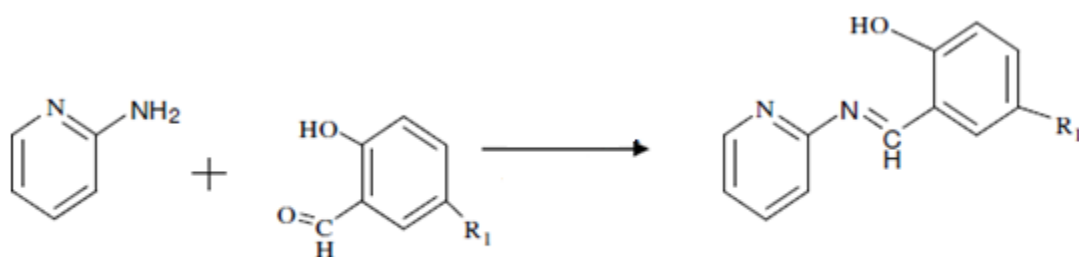
function to confer antimalarial activity. Secondary metabolite produced by plants belonging to the families *Ancistrocladaceae* and *Dioncophyllaceae* features an imine group in its structure. The compound has shown potent activity against *P. falciparum*. Some novel aldimine and hydrazone isoquinoline derivatives prepared by reacting 1-formyl-5-nitroisoquinoline with amines showed activity against a chloroquine-resistant *Plasmodium falciparum* strain (ACC Niger). In particular the compound *N*-[(1*E*)-(5-nitro-1-naphthyl)methylene]-1-[2-(trifluoromethyl)phenyl]methanamine showed an IC₅₀ of 0.7 µg/mL against *P. falciparum* was reported by Rathelot et.al [30].



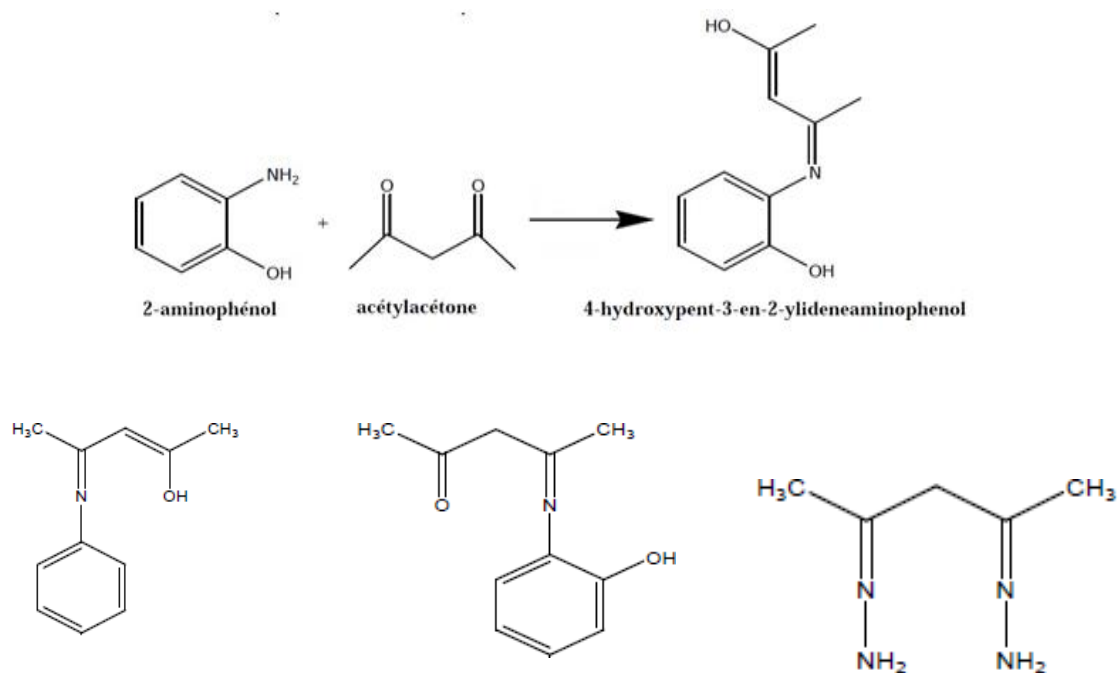
Misbah ur Rehman et.al., reported the *In-vitro* antimicrobial studies of acetyl acetone derived compounds against *B.subtilis*, *S. aureus*, *E.coli*, *P. aeruginosa*, *C. albicans*, and *A. niger*. All the compounds were reported to exhibit moderate to good antimicrobial activity [31].



Dueke-Eze et.al., reported that 2-amino pyridine derivatives inhibit metabolic growth of *S. aureus* and *E. coli*. The antibacterial activity of the compounds depends on the nature of substituent present on the aldehyde [32].



Francis K. Ngounoue et.al, worked on acetyl acetone derivatives and their antimicrobial activity against *E. coli*, *P. aeruginosa*, *S. typhi*, *S. aureus* and antifungal activities against *C.albicans* [33]. Prasad A et al., investigated the compounds derived from acetyl acetone with amines such as aniline, 2-amino phenol, para-anisidine and hydrazine hydrate. The compounds exhibit high activity against the Bacterial strains [34].

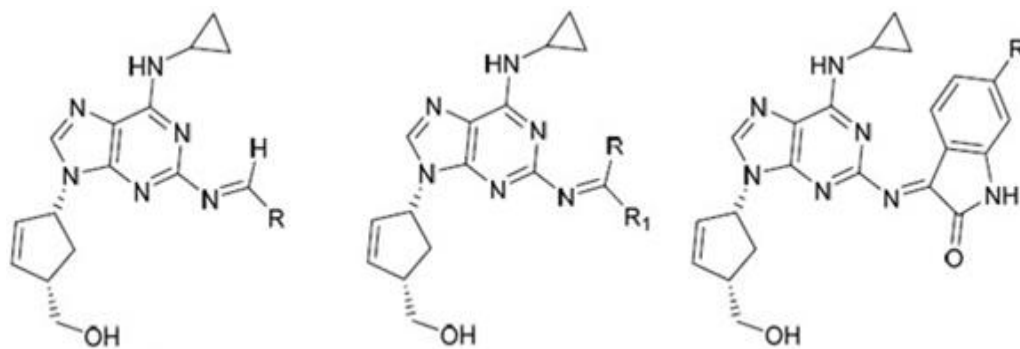


A series of novel 3-(4-(benzylideneamino) phenylimino) 4-fluoroindolin-2-one derivatives were synthesized and evaluated for analgesic, anti-inflammatory, and ulcerogenic index activities. Results displayed that compounds exhibited significant analgesic activity and anti-inflammatory activity comparable to reference standard diclofenac sodium. Interestingly, the test compounds showed only mild ulcerogenic side effect when compared to aspirin [35]. Schiff base derived from 4-aminoantipyrine (4-amino-1,5-dimethyl-2-phenylpyrazole-3-one) and benzaldehyde derivative was tested for its anti-inflammatory activity. The results showed promising anti-inflammatory activity which could be use in the treatment of inflammatory diseases. The results of this study may lead to the development of a new therapeutic agent useful in fighting diseases caused by oxidative stress and inflammation [36].

A series of Schiff base derivatives of 4-aminophenazone (4APZ-1,5-dimethyl-2-phenyl-1,2-dihydro-3*H*-pyrazol-3-one) with different aldehydes were synthesized. The synthetic compounds were screened for their anti-inflammatory, analgesic and antipyretic activities. Carrageen, an-induced paw oedema (CIPO) and histamine induced paw oedema (HIPO) methods were used to determine the anti-inflammatory activity of commercial sample of 4APZ and its synthesized Schiff bases in mice. The anti-inflammatory activity was in the order of 4APZAB > 4APZBB > 4APZCB > 4APZVn and all the test compounds exhibited considerable dose dependent inhibition of the paw oedema. The effect of the compounds on membrane stabilization was also determined which showed that compounds 4APZ (120 and 240 mg/kg doses), 4APZAB (160 mg/kg) and 4APZVn (600 mg/kg) produced highly significant inhibition ($P < 0.001$) of hypotonicity-induced haemolysis. Further, it was also observed that 4APZ (120 and 240 mg/kg doses), 4APZBB (500 mg/kg) and APZCB (150, 300 and 600 mg/kg dose) produced highly significant inhibition ($P < 0.001$) of albumin denaturation; a consistent dose dependent anti-inflammatory effect of test compounds was compared to the standard drug. Analgesic activity of the compounds was investigated by formalin-induced paw licking (FIPL) and acetic acid-induced writhing (AIW) methods in mice. It was observed that 4APZ (240 mg/kg), 4APZAB (160 mg/kg), 4APZBB (500 mg/kg), 4APZCB (600 mg/kg) and 4APZVn (600 mg/kg) showed analgesic effect with highly significant ($P < 0.001$) reduction of paw licking and writhing activity in the treated mice. The order of analgesic effect of the

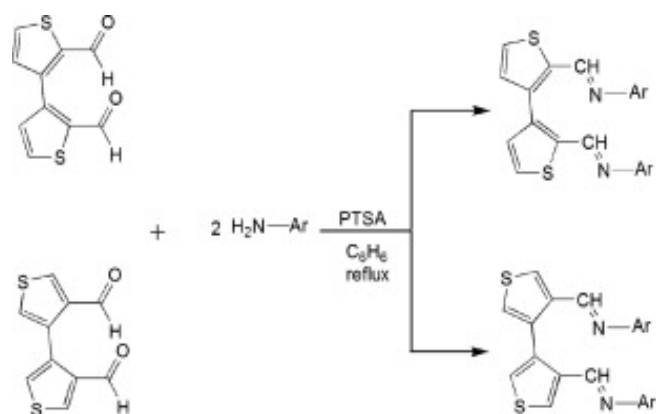
compounds was 4APZAB > 4APZBB > 4APZVn > 4APZCB. Moreover, phenobarbitone-induced sleeping time (PIST) in mice was also studied but only 600 mg/kg of 4APZVn significantly increased the duration of induced sleep which also suggested its sedative property. Brewer's yeast was used to induce fever in rabbits and analyzed the compounds for their antipyretic activity. Different doses of 4APZ for different time durations (240 mg/kg-after 1 h, 120 and 240 mg/kg doses-after 2 h) produced highly significant ($P < 0.001$) inhibition of hyperpyrexia. Other compounds showed good antipyretic activity after 2, 3 and 4 h [37].

Although there are many therapeutic options for viral infections, currently available antiviral agents are not yet fully effective, probably due to the high rate of virus mutation. They may also cause any of a number of side effects. Salicylaldehyde Schiff bases of 1-amino-3-hydroxy-guanidine tosylate are a good platform for the design of new antiviral agents. In fact, from a set of different 1-amino-3-hydroxyguanidine tosylate-derived Schiff bases, 2-(3-allyl-2-hydroxybenzylidene)-N-hydroxyhydrazine carboxi-midamide derivative was shown to be very effective against mouse hepatitis virus(MHV), inhibiting its growth by 50% when employed at concentrations as low as 3.2 μ M [38].

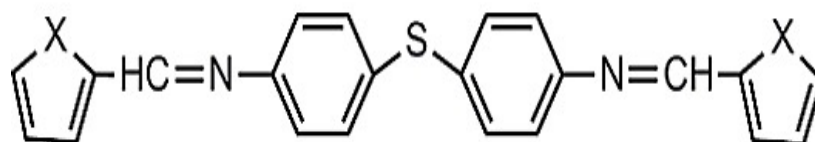


A new series of 3-(benzylideneamino)-2-phenylquinazoline-4(3H)-ones were prepared through Schiff base formation of 3-amino-2-phenylquinazoline-4H-one with various substituted carbonyl compounds and their cytotoxicity and antiviral activity were evaluated against herpes simplex virus-1(KOS), herpes simplex virus-2 (G), vaccinia virus, vesicular stomatitis virus, herpes simplex virus-1 TK-KOS ACVr, para influenza-3 virus, reovirus-1, Sindbis virus, Coxsackie virus B4, Punta Toro virus, felinecorona virus (FIPV), feline herpes virus, respiratory syncytial virus, influenza A H1N1 subtype, influenza A H3N2 subtype and influenza B virus. Compounds showed better antiviral activity against the entire tested virus [39].

Reactions of aromatic amines with 3,3'-bithiophene-2,2'-dicarbaldehyde and 3,3'-bithiophene-4,4'-dicarbaldehyde gave the 2,2'-(*N*-(aryl)diimino)-3,3'-bithiophene and 4,4'-(*N*-(aryl)diimino)-3,3'-bithiophene in good yields. Orthophenylenediamine reacted with dicarbaldehyde to give dithieno[3,4-*c*;4',3'-*e*]azepino[1,2-*a*]benzimidazole and dithieno[2,3-*c*;3',2'-*e*]azepino[1,2-*a*]benzimidazole and their characterization were reported [40].



Three new Schiff-base compounds were synthesized by treating 4,4'-diaminodiphenyl sulfide and pyrrole/thiophene/furan-2-carboxaldehyde in ethanol. The *in vitro* antibacterial and antifungal activities of the synthesized compounds were investigated using disc diffusion method. Schiff bases synthesized individually exhibited varying degrees of inhibitory effects on the growth of the tested microbial species [41].



Some new Schiff bases have been synthesized by the condensation of 2-aminophenol, 2-amino-4-nitrophenol/2-amino-4-methylphenol/2-amino benzimidazole with thiophene-2-carboxaldehyde/pyrrole-2-carboxaldehyde. The *in-vitro* antibacterial activity of the synthesized compounds has been tested against *Salmonella typhi*, *Bacillus coagulans*, *Bacillus pumills*, *Escherichia coli*, *Bacillus circulans*,

Pseudomonas, *Clostridium* and *Klebsilla pneumonia* by disc diffusion method. The quantitative antimicrobial activity of the test compounds was evaluated using resazurin based microtiter dilution assay. *Ampicillin* was used as standard antibiotics. Schiff bases individually exhibited varying degrees of inhibitory effects on the growth of the tested bacterial species. The antioxidant activity of the synthesized compounds was determined by the 1,1-diphenyl-2-picrylhydrazyl(DPPH) method. IC₅₀ value of synthesized Schiff bases were calculated and compared with standard BHA [42]. An inexpensive and efficient catalyst, P₂O₅/SiO₂ was employed to synthesize Schiff bases in higher yield was reported. The reaction was carried out at solvent-free condition and with simple synthetic procedure [43]. A new Schiff base, 3,5-dihydroxy-N'-(2,4,5-trimethoxybenzylidene)benzohydrazide hydrate (DTBH) was synthesized and characterized by elemental analysis and X-ray single crystal diffraction. The compound crystallized in a monoclinic system. The antibacterial activities, cytotoxicities and effects of the compound on the contractility of isolated jejunal smooth muscle (IJSM) of rats were evaluated. The compound showed no antibacterial activity. No cytotoxic effects were found on Caco-2 cell line within 360 μM. However, it indicated significant inhibitory effect on the contractility of isolated jejunal smooth muscle in a dose dependent manner. The inhibitory effects are related to the activation of α and β-adrenoceptors [44].

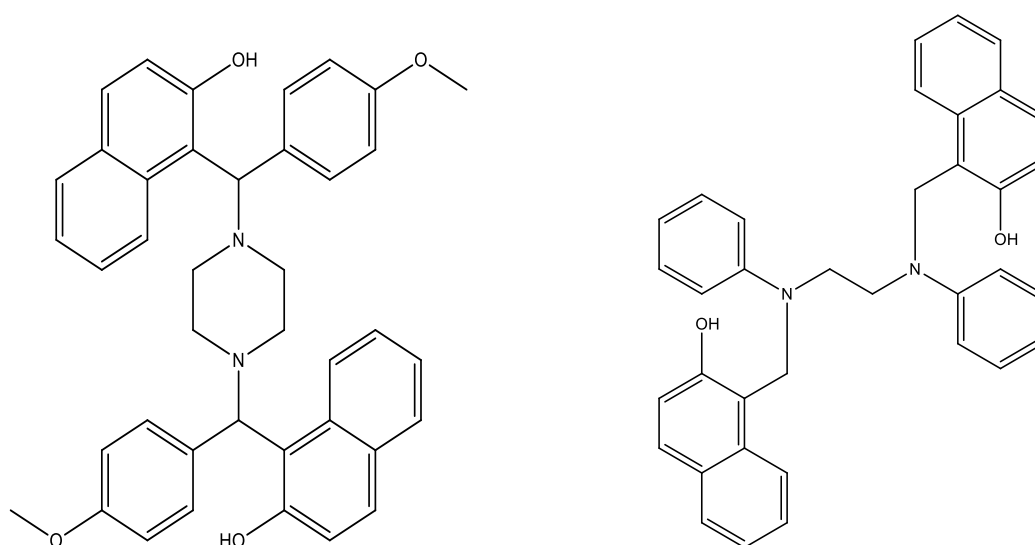
1.2. Mannich Reaction

Mannich Reaction is a multi component reaction (**MCR**) reported by Carl Mannich in 1912 which involves the reaction of non-enolizable aldehydes, amines, and enolizable ketones produced β -amino carbonyls also known as Mannich base. They have gained importance due to their applications in pharmaceutical industry and other applications including as agro chemicals and plant growth regulators. The chemistry of the amino alkylation of aromatic substrates by the Mannich reaction is of great interest for the synthesis and modification of biologically active compound having physical and chemical importance as well as physiological properties because the amino group can be easily converted into a variety of other functionalities. Mannich reaction offers a judicious method for introduction of basic amino alkyl chain in various drugs/compounds. Owing to its special features, a serious attention has been focused by several researchers on the synthesis and development of new Mannich bases.

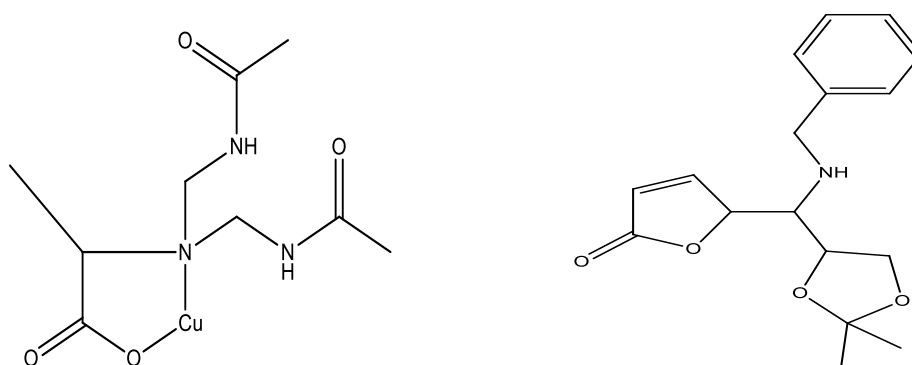
One-pot Mannich reaction of vanillin, aniline and cyclohexanone catalyzed by ionic liquid triethanol ammonium chloroacetate was reported. Mechanism of the reaction was investigated using the density functional theory. The reaction started with a nucleophilic attack of aniline nitrogen at the carbonyl group of vanillin. The intermediate α -amino alcohol formed in this way was further subjected to protonation by the triethanol ammonium ion yielding the iminium ion. Theoretically, the obtained iminium ion and the enol form of cyclohexanone can build the protonated Mannich base via the *anti* and *syn* pathways. The

chloroacetic anion spontaneously abstracts the proton yielding the final product of the reaction *anti* 2-[1-(*N*-phenylamino)-1-(4-hydroxy-3-methoxyphenyl)]methyl cyclohexanone. The *syn* pathway requires lower activation energy but the *anti* pathway yields a thermodynamically more stable product, which implies that the examined Mannich reaction is thermodynamically controlled [45].

Subrahmanian Supriya et al. have reported Mannich amino methylation reactions of a series of bis(α -aminoacidato)metal(II) complexes and their Single crystal XRD studies. One of the amino methylated product has been employed as a catalyst in the colour removal of the pyrocatechol violet dye [46]. Two series of *N,N'*-bis[aryl-(2-hydroxynaphthalen-1-yl)-methyl]-piperazines and *N,N'*-bis(arylmethyl)-*N,N'*-bis(2-hydroxynaphthalen-1-yl)-methyl)-ethylenediamines were synthesized under solvent free conditions using micro wave irradiation and their X-ray diffraction studies have also been reported by Po-Jung J. Huang et al. [47].

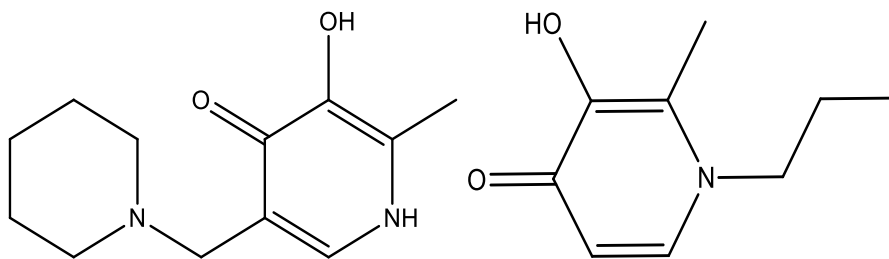


Chew Hee Ng et al. have reported the effect of different α -substituents in the reaction of copper (II) chelated amino acids with formaldehyde and acetamide [48]. Scott K. Bur and Stephen F. Martin have investigated the stereoselectivity and synthetic utility of some vinylogous derivatives synthesized by the addition of a dienol into an iminium ion [49].

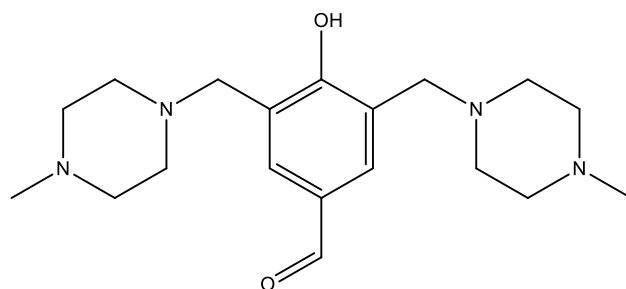


Three-component Mannich reaction of ketones, aromatic aldehydes and aromatic amines catalyzed by four Bronsted acidic ionic liquids comprising of iodide and borate was reported. Ionic liquids have been used as catalyst and solvent to produce some Mannich bases in high yield (75%) and shorter reaction time (20 minutes). Work up has been facilitated by simple extraction with water to recover ionic liquid for recycling up to four times without any significant loss in activity [50].

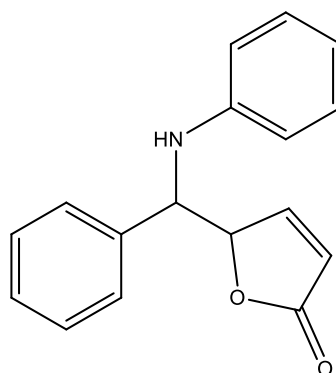
3-hydroxy-2-methyl-5-(piperidin-1-ylmethyl)pyridin-4(1H)-one, 3-hydroxy-2-methyl-1-propylpyridin-4(1H)-one and their analogues have been reported by Ahshin Fassihi et al. Further it is revealed from the antimicrobial evaluation, multiple linear regression analysis and QSAR studies of the synthesized compounds that are active against *C. albicans* and *S. aureus* [51].



A new end-off type acyclic ligand possessing highly reactive aldehyde group and two N-methyl piperazine arms, 2,6-bis[[4-methyl piperazin-1-yl]-4-formyl phenol which may lead to the extension of its structure in to a supramolecular moiety have been reported by K. Shanmuga Bharathi et al. [52].

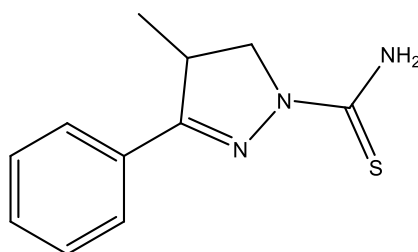


Zhi-Liang Yuan et al. have reported a series of trimethyl siloxyfuran derivatives via asymmetric vinylogous Mannich reaction involving aldimines and trimethylsiloxyfuran using silver acetate as catalyst [53].

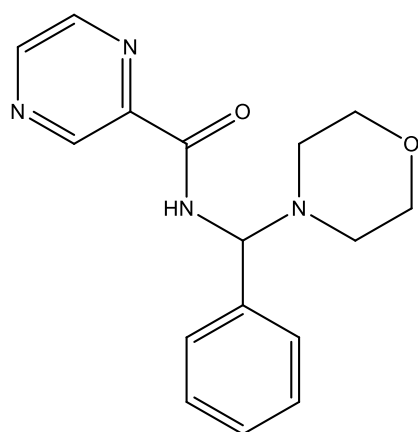


Regioselective synthesis of 2-[(4-methylpiperzine-1-yl)methyl]-2H-1,2,4-triazole-3(4H)-thiones and their pharmacological properties have been reported by Arun M. Isloor et al. Further they have studied that the compounds possessing p-chloro, p-methoxy and p-methyl substituents in phenyl ring exhibits potent antimicrobial activity [54].

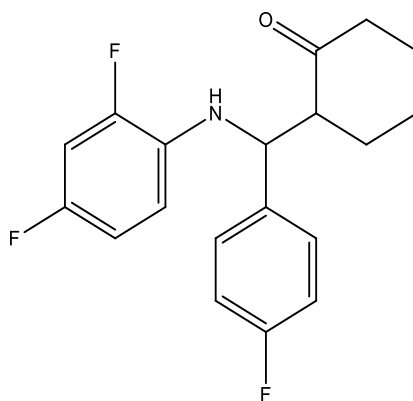
Cyclization of N-substituted thiosemicabazides resulted in pyrazoline derivatives with two chelating arms possessing in-vitro antiamoebic activities have been reported by Kakul Husain et al. [55].



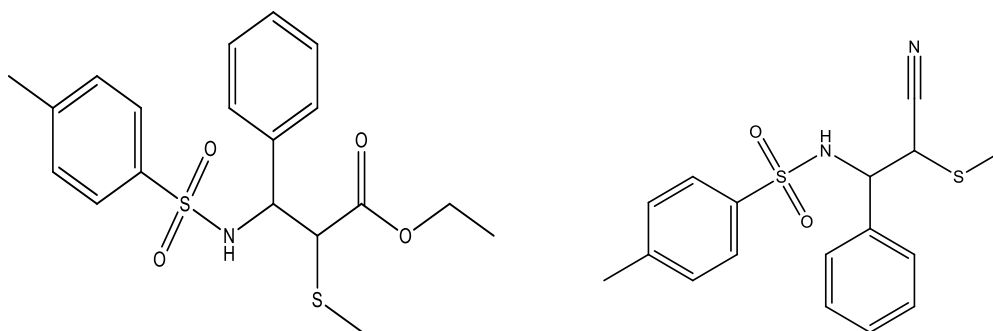
A series of pyrazinamide derivatives were synthesized by Chaluvvaraju K C and Ishwar Bhat K and their antimicrobial screenings were evaluated against *E. coli*, *B. substilis*, *S. aures*, *A. Niger* and *C. albicans* using amoxicillin, ciprofloxacin and ketoconazole as standard drugs [56].



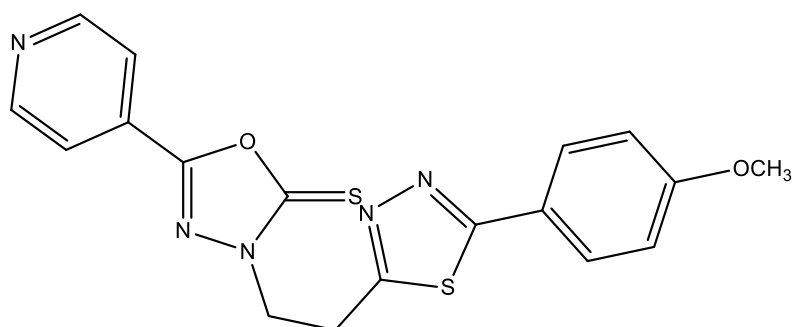
Cerium Chloride catalysed reaction and solvent free microwave irradiation methods were employed to synthesize 2-((2,4-difluorophenylamino)(4-fluorophenyl)methyl)cyclohexanone and its analogous and their X-ray diffraction studies have been reported by U. Sankappa Rai et al. Further the antimicrobial evaluation of the synthesized compounds show that the compounds bearing halogen substitution, pyridine and indole substitution and methoxy substitution possess enhanced activity [57].



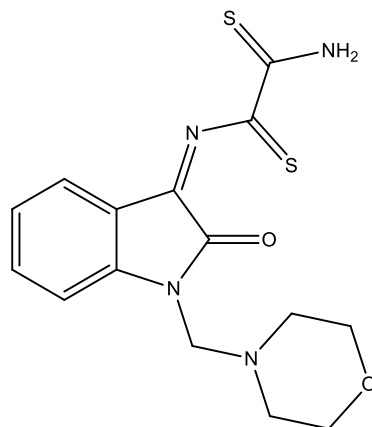
M. Lakshmi Kantam et al. have reported the nano crystalline magnesium oxide catalyzed synthesis of Ethyl-3-[[4-methylphenyl)sulfonyl]amino}-2-(methyl-sulfanyl)-3-phenylpropanoate, N-[2-Cyano-2-(methylsulfanyl)-1-phenylethyl]-4-methyl-1-benzenesulfonamide and their analogues by reacting N-sulfonyl aldimines with sulfonium salts. Further was reported that the synthesized compounds bearing sulphur atom possess diverse biological activities [58].



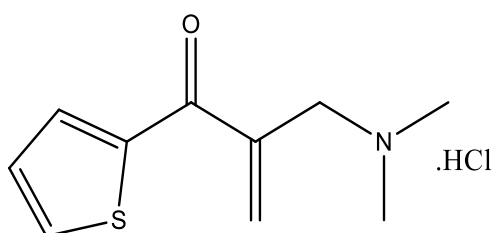
Trupti S. Chitre et al. have reported the synthesis, molecular docking studies and antimycobacterial evaluation of 1,3,4-(thiadiazol-2-ylamino)methyl-5-(pyridin-4-yl)-1,3,4-oxadiazol-2-thiones. It is revealed from the study that the compound having methoxy group exhibit significant antimycobacterial activity [59].



Ahlam J. Abdul ghani and Nada M. Abbas have reported the synthesis of (Z)-N1-(1-(morpholinomethyl)-2-oxoindolin-3-ylidene)ethane bis(thioamide), (Z)-N1-(1-((diphenylamino)methyl)-2-oxoindolin-3-ylidene)ethane bis(thioamide) and their antimicrobial and cytotoxicity studies against human epidermoid larynx carcinoma (Hep-2) cell line. [60]

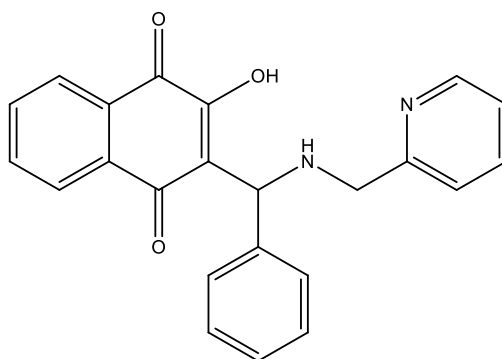


Synthesis of acetophenone and 2-acetyl thiophene derivatives via conventional heating method and microwave irradiation method was reported by Ebru Mete et al. From the study it has been found that the compounds bearing unsaturated ketones show potent biological activity [61].

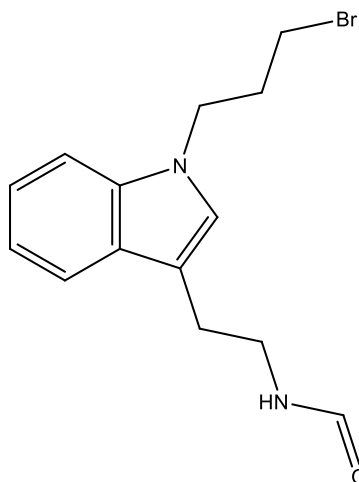


QSAR studies of quinoline derivatives have been reported by Arthur Y. Shaw et al. They have examined the variation in the anticancer activity by replacing some substituents. It is revealed that the replacement of sulfonyl group with methylene group or the replacement of piperazine ring with ethylenediamine group increase the potency. On the other hand, as 8-hydroxyquinoline was replaced with phenol, 3-hydroxypyridine and 1-naphthol, a dramatic decrease in activity was observed. These results indicating that 8-hydroxyquinoline is a crucial scaffold for activity [62].

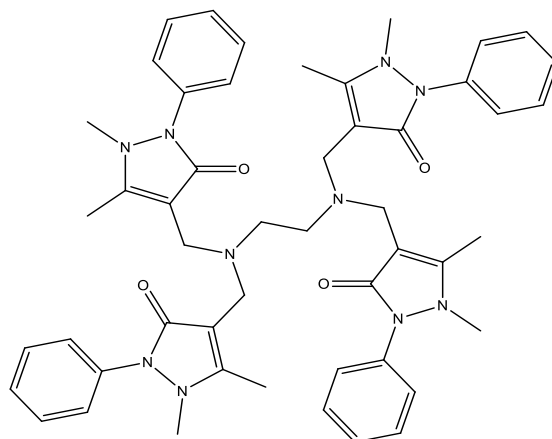
2-hydroxy-3-(phenyl((pyridin-2-ylmethyl)amino)methyl) naphthalene-1,4-dione¹⁵ and its derivatives exhibiting various biological and pharmacologic properties were reported by Amanda P. Neves et al [63].



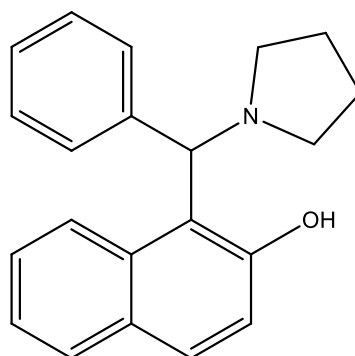
Elizabeth Malamidou-Xenikaki et al. have reported the synthesis of 9-(ω -nitroalkyl)-4,9-dihydro-3H β -carbolines using 2-[1-(ω -Nitroalkyl)-1H-indol-3-yl]ethylformamides through a diastereoselective intramolecular N-acyliminium cyclization reactions. Further they have investigated the improvement of the diastereoselectivity of the reactions using chiral tryptamine substrates and chiral acylating agents [64].



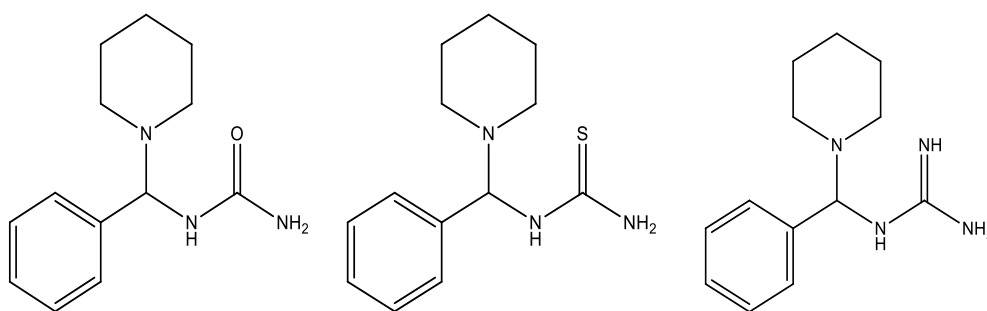
Elena Maria Mosoarca et al. have reported the synthesis of N,N-tetra-(4-antipyrilmethyl)-1,2-diaminoethane their cytotoxic evaluation against human tumor cell lines, glioblastoma multiforme, breast cancer, hepatoma and lung carcinoma and nontumor cell lines MDBK and BALB/c 3T3 clone 31 [65].



Nanocrystalline MgO catalysed synthesis of Betti bases (1-(α -aminoalkyl)-2-naphthols) via Mannich pathway involving the condensation of naphthol, aldehyde and alkylamine was reported by Bikash Karmakar and Julie Banerji. The report reveals that the metal oxide catalyst employed in the synthesis find excellent applications such as active adsorbent for gases and for destruction of hazardous chemicals [66].

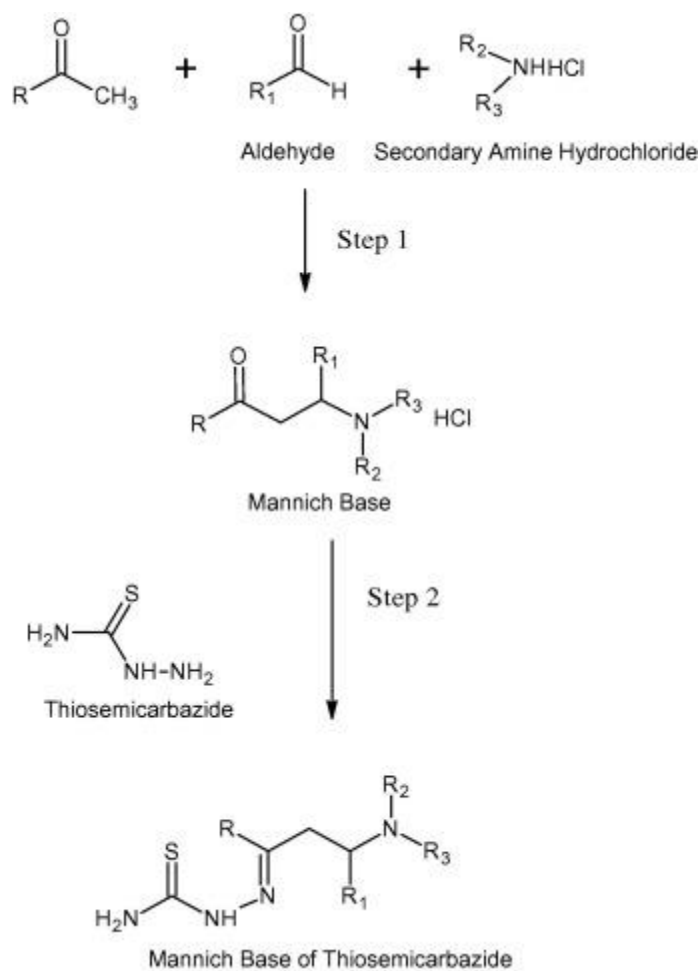


Resacetophenone derivatives synthesized using three variable electronegative atoms of urea, thiourea and guanidine and their antioxidant activities by DPPH have been reported by Arpit D. Shah et al. Further they have reported that the synthesized compounds bearing oxygen and sulphur possess increased activity [67].

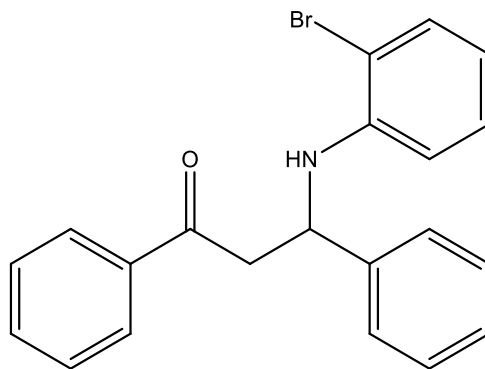


Synthesis of Mannich bases of thiosemicarbazide as mutual prodrugs was reported. The compounds were screened for antifungal activity using BHI (brain heart infusion) broth dilution method against *Candida albicans* and *Aspergillus niger*. Docking of synthesized compounds was done on CYP51A1, P45014DM (Lanosterol 14 α -demethylase enzyme) using Vlife MDS 3.5 to confirm the mechanism of antifungal activity. Docking study showed a strong hydrophobic interaction between amino acid residues Arginine (ARG141), Glutamine (GLU146), Leucine (LEU54), Lysine (LYC227), and Threonine (THR147) with the carbon of ketone, nitrogen of amine and sulfur of thiosemicarbazide. Strong Vander wall's interactions are also observed with the carbon of ketone, nitrogen of amine and sulfur of thiosemicarbazide. Analogs with aromatic and substituted aromatic aldehydes showed least activity, while analogs with aliphatic aldehyde,

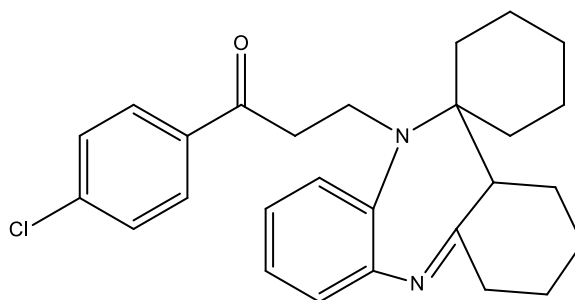
ketones and amines showed greater activity in *C. albicans* compared to *A. niger*. Analogs having morpholine as amine showed almost similar activity in both [68].



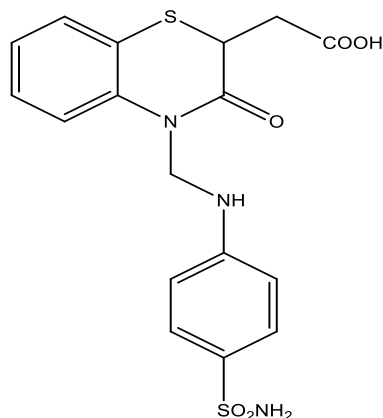
Recyclable bismuth nitrate catalyzed, environmental pollution free, one pot synthesis was reported by sheik Mansoor et al. by reacting benzaldehyde, acetophenone and substituted aromatic amines employing simple procedure and mild condition [69].



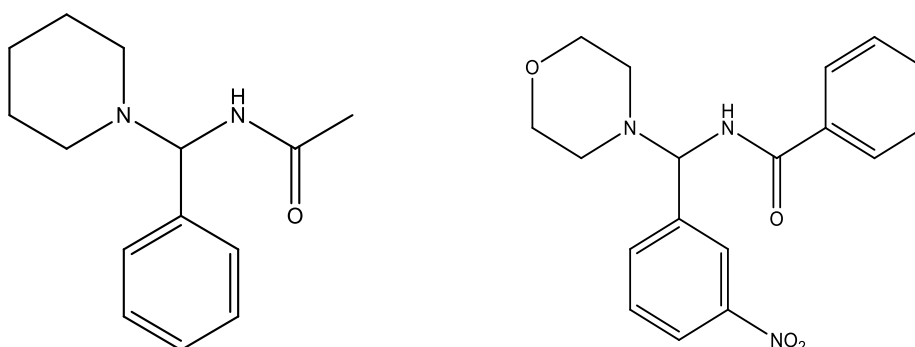
Pandeya S N and Neha Rajput have reported sulphated zirconia catalyzed synthesis of benzodiazepine derivatives which are having chloro group found to possess anticonvulsant activity and good central and peripheral analgesic activity [70, 71].



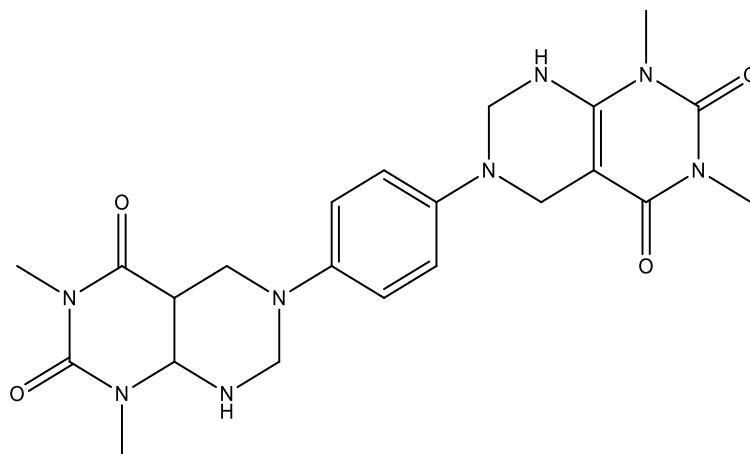
Sindhu T. J et al. have reported the synthesis, comparative molecular docking studies and antibacterial activities of 1, 4-Oxazine and 1, 4- Thiazine derivatives [72]. 1-((2E)-1-[(2-methylphenyl) amino]-3-phenylprop-2-en-1-yl) thiourea and 1-((2E)-1-[(2-methylphenyl) amino]-3-phenylprop-2-en-1-yl)urea exhibit antibacterial activity against *Staphylococcus aureus*, *Klebsiella Pneumonia*, *Salmonella typhi*, *Escherichia coli* and *Pseudomonas aeruginosa* and anti oxidant activity have been reported by G.Vishnuvardhanaraj et al. [73].



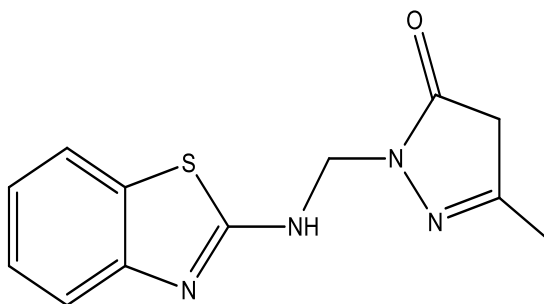
N-[1-piperidinobenzyl] acetamide, N-[1-morpholino(-4-nitrobenzyl)] benzamide³⁶ and their analogues and their antibacterial activity against *Agrobacterium sp* have been reported by Rimpyp Gupta et al. [74].



Wafaa S. Hamama et al. have investigated the behavior of Mannich reaction towards 6-amino-1,3-dimethylpyrimidine-2,4(1H,3H)-dione. Further they have reported a series of cyclized derivatives viz, 6-(4-(6,8-Dimethyl-5,7-dioxooctahydropyrimido[4,5-d]pyrimidin-3(4H)-yl)phenyl)-1,3-dimethyl-5,6,7,8-tetrahydropyrimido[4,5-d]pyrimidine-2,4(1H,3H)-dione employing different pathways with varying yield [75].



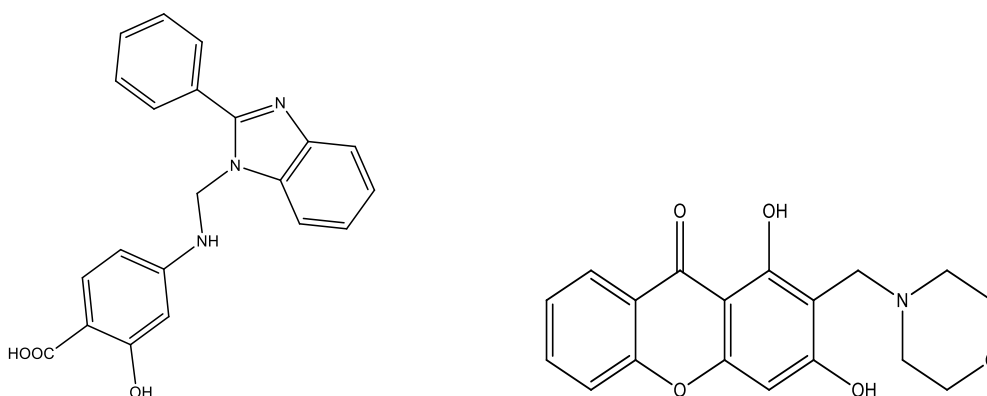
Rathi Paresh P et al. have reported the synthesis of 2-[(1, 3-benzothiazol-2-ylamino) methyl]-5-methyl-2, 4-dihydro-3h-pyrazol-3-one and its in-vitro anti-inflammatory activity by bovine serum albumin denaturation inhibition method [76].



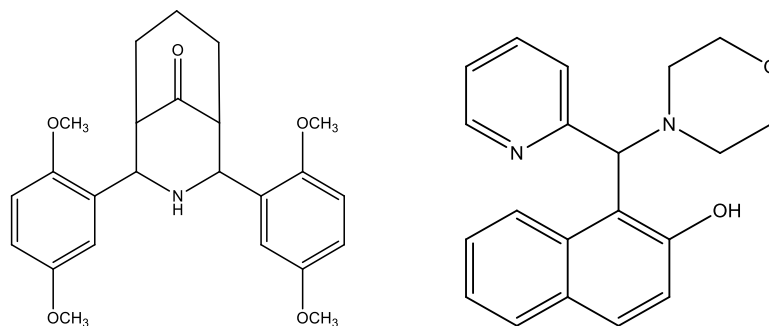
A series of N-Mannich bases of benzimidazolyl substituted derivatives were reported. The synthesized compounds were evaluated for their antimicrobial, anthelmintic and insecticidal activities using standard drugs, streptomycin, Nystatin, piperazine hydrochloride and cypermethrin respectively. The result showed that all the compounds possess promising activity against the selected microbes [77].

Baldwin Mathew V et al. have reported the synthesis, antitubercular activities and molecular docking studies of some pyrazine

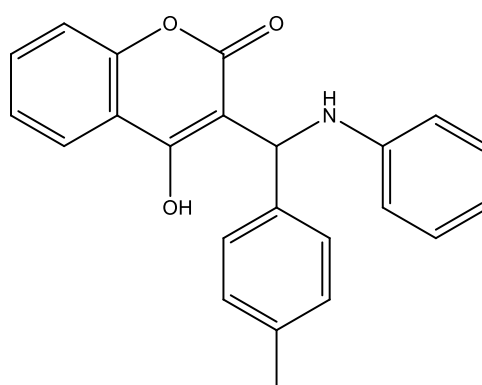
derivatives. The synthesized compounds were subjected to docking studies against viral protein CFP 10-ESAT6 complex (3FAV) from *Mycobacterium tuberculosis* using Argus lab software. The result indicates that the compounds having sulfadimidine shows best ligand pose energy and potent antitubercular activity [78]. Synthesis of 3-dihydroxanthone derivatives and their molecular docking studies and kinetic studies show their potency as anticholinesterase agents were reported by Jiangke Qin et al. [79].



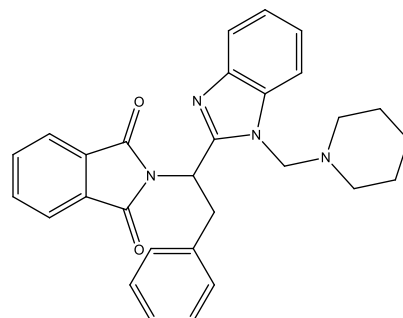
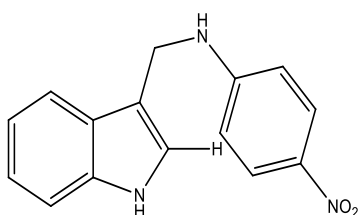
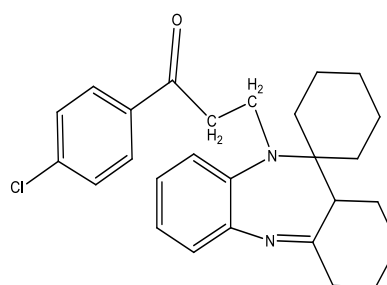
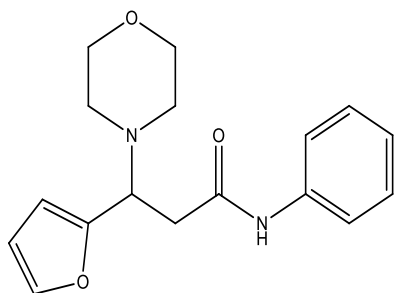
Dong Ho Park et al. have reported a series of 2,4-diaryl-3-azabicyco[3.3.1]nonan-9-ones and their antioxidant properties [80]. Iodine catalyzed flavanone and tetrahydropyrimidine derivatives were reported by Veerababurao Kavala et al. [80]. Someshwar D. Dindulkar et al. have reported the synthesis of 2-naphthol derivatives employing copper triflates as an efficient catalyst under solvent free conditions [81].



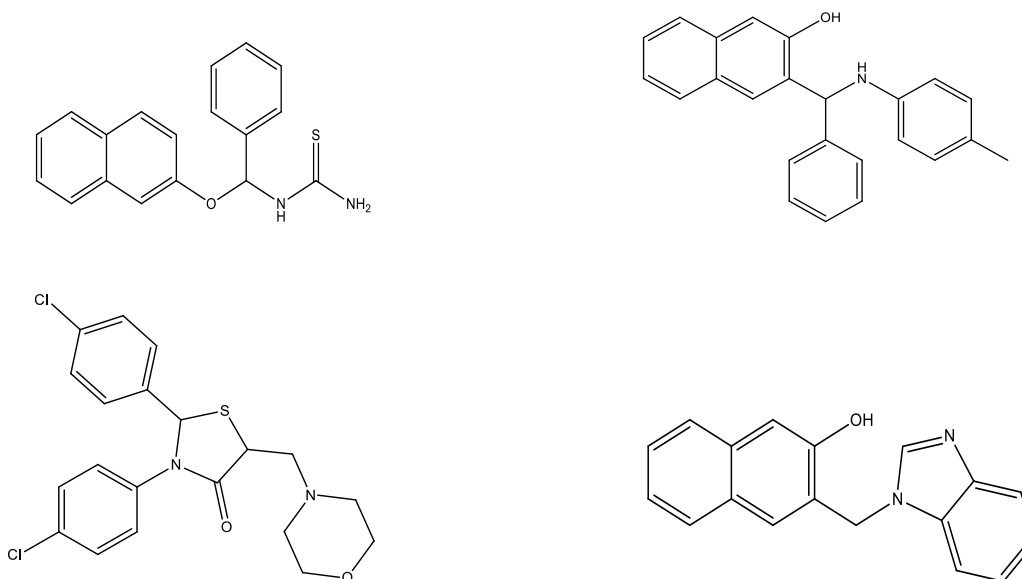
Onkara. P et al. have reported the ionic liquid phase and microwave assisted synthesis of 3-substituted aminophenyl-4-hydroxycoumarins. Further docking studies of the synthesized compounds were carried out using VLife MDS 3.5 software incorporating GA docking method to study their antimicrobial activity. [82].



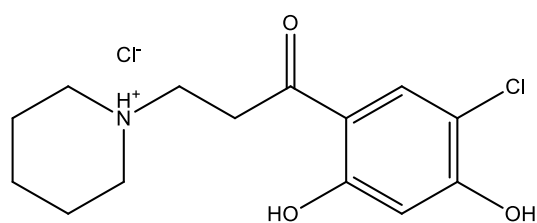
Suman bala et al. have reported the synthesis of β -amino carbonyl derivatives possessing heterocyclic ring with two/three hetero atoms and their diverse biological and pharmacological activities viz., antimicrobial, anticonvulsant, anti-inflammatory, anthelmintic, anticancer, antioxidant and analgesic activities [83].



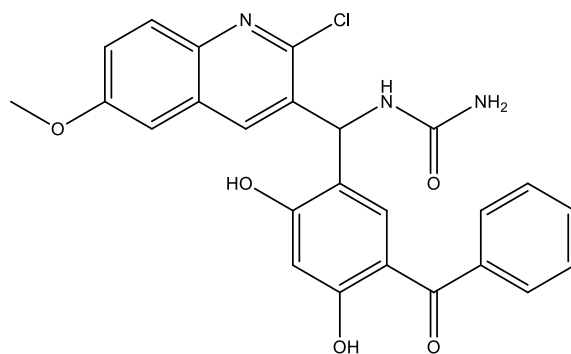
M. Sivakami et al. have reported the synthesis, antioxidant and cytotoxic activities of 1-(naphthalen-2-yl)oxy(phenyl)(methyl) thiourea using HeLa cell line . Further the report shows that the synthesized compound contains thio urea has enhanced antimicrobial and cytotoxic activities [84]. K. Chakkaravarthi et al. have reported the synthesis of 3-(phenyl(*p*-tolylamino)methyl) naphthalene-2-ol and 3-((1H-benzo[d]imidazole-1-yl)methyl)naphthalene -2-ol. Further the study reveals that the compound possessing benzimidazole and naphthol moiety have excellent antioxidant property [85]. Beena Thomas et al. have reported 2, 3-bis(4-chlorophenyl)-5-(morpholin-4-ylmethyl)-1,3-thiazolidin-4-one and its analogues and their antitubercular activities [86].



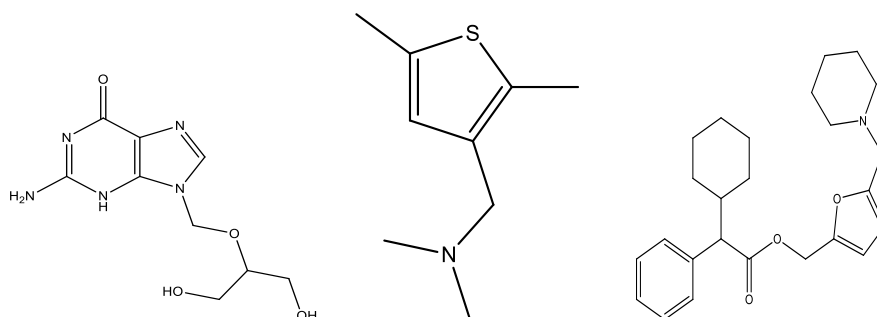
Synthesis of 1-(3-(5-Chloro-2,4-dihydroxyphenyl)-3-oxopropyl)piperidin-1-ium chloride and their analogues. These compounds are subjected to evaluation of Hsp90 ATPase inhibition activity by the colorimetric Malachite green assay and antiproliferative effect against PC3 pancreatic carcinoma cells have been reported by Sayan Dutta Gupta et al. The activity profiles of the synthesized compounds were correlated well with their docking results [87].



Ionic liquid phase synthesis and antitubercular activities of 1-((5-benzoyl-2,4-dihydroxyphenyl)(2-chloro-6-methoxyquinolin-3-yl)methyl)piperidin-1-ium chloride and its analogues were reported by Hitendra M. Patel et al. [88].



Sheela Joshi et al. have reported the synthesis and LD₅₀ test of derivatives of 2-amino-9-[(1,3 di hydroxy propane-2yl) oxy] methyl] 6-9 dihydro-3H-purine-6-one (Ganciclovir derivatives). This study reveals that the compounds are potential source with less side effect [89]. Gheorghe Roman have investigated the chemistry of electron-rich, monocyclic five-membered heterocycles with one heteroatom, thiophene and furan derivatives and their reactivity and applications [90].



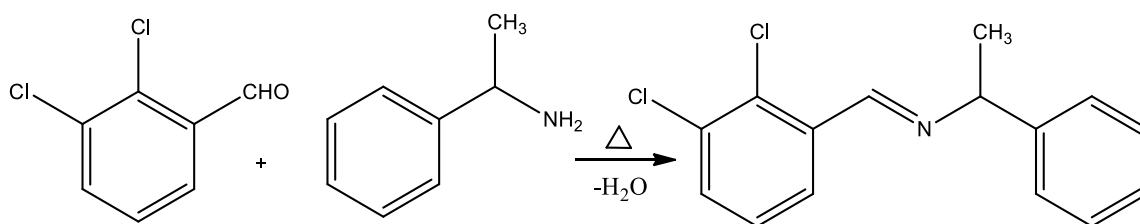
Synthesis of azomethine compounds via Schiff reaction (MA1-MA5)

Materials and Methods

Melting points were measured in an open capillary on Mel-Temp apparatus and are uncorrected. IR spectra were recorded on Perkin Elmer spectrometer using KBr pellets. ^1H and ^{13}C NMR spectra were recorded on a Bruker AM-400 spectrometer for solution in DMSO- d_6 with tetramethyl silane (TMS) as an internal standard. All the chemical shifts values were recorded as δ ppm. Mass spectra were recorded by EI method and HRMS was measured on a JEOL GC mate II mass spectrometer. Commercially obtained reagents were used without further purification. All reactions were monitored by TLC with silica gel-G coated plates.

2.1. Synthesis of (2, 3-Dichloro-benzylidene)-(1-phenyl-ethyl)-amine (MA1)

To the ethanolic solution of 1-phenylethanamine (12.8 mL, 0.1 M), 2, 3-dichlorobenzaldehyde (17.5 g, 0.1 M) was added and refluxed for 6 h. The mixture was poured into a beaker contain crushed ice. The solid separated out was washed, filtered and dried over vacuum and recrystallized using ethanol. (Colour: Deep Brown solid; M.P: 171 $^{\circ}\text{C}$)



Scheme: 2.1- Synthesis of (2, 3-Dichloro-benzylidene)-(1-phenyl-ethyl)-amine (MA1)

2.1.1. FTIR spectrum of (2, 3-Dichloro-benzylidene)-(1-phenyl-ethyl)-amine (MA1)

The FT-IR spectrum of MA1 is presented in the Fig. 2.1. Aromatic C-H stretching in phenyl ring exhibits a band at 3068 cm⁻¹. A strong absorption band appeared at 2964 cm⁻¹ is due to C-H stretching. An absorption band at 1562 cm⁻¹ indicates C=N stretching. A band appeared at 719 is due to C-Cl stretching.

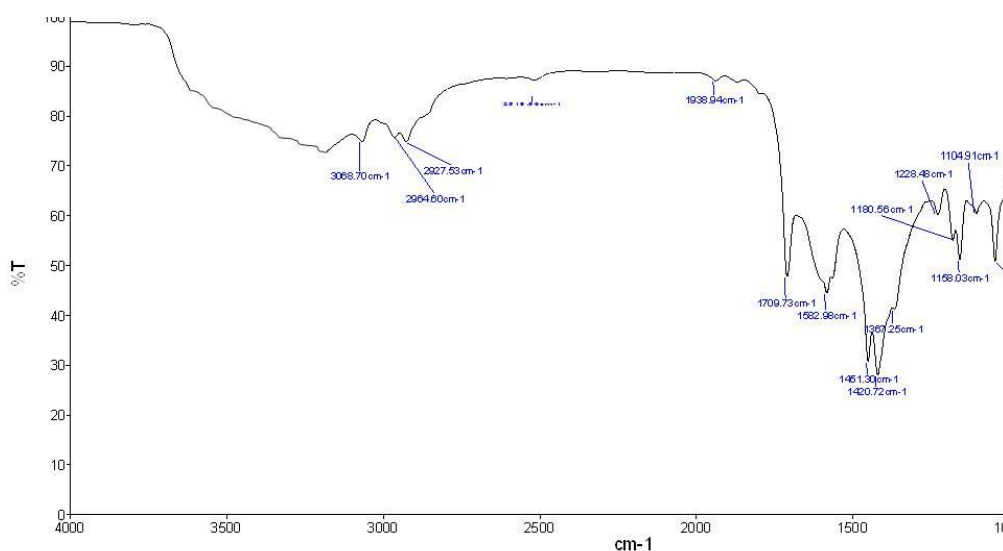


Fig. 2.1. FTIR spectrum of (2, 3-Dichloro-benzylidene)-(1-phenyl-ethyl)-amine (MA1)

2.1.2. ^1H -NMR spectrum of (2, 3-Dichloro-benzylidene)-(1-phenyl-ethyl)-amine (MA1)

^1H - NMR spectrum of MA1 in the Fig 2.2 has peaks ranges from 7.2-7.5 are due to aromatic protons. Presence of azomethine and methine protons revealed from the peaks exhibited at 6.9 ppm and 5.9 ppm respectively. Methyl protons exhibited peak at 1.5 ppm.

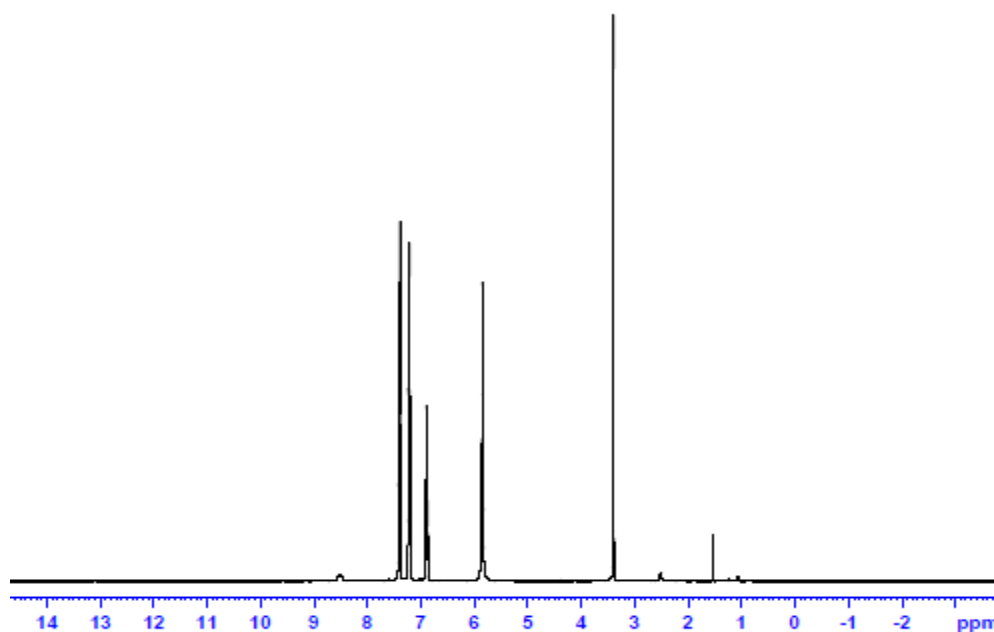


Fig.2.2. ^1H -NMR spectrum of (2, 3-Dichloro-benzylidene)-(1-phenyl-ethyl)-amine (MA1)

2.1.3. ^{13}C -NMR spectrum of (2, 3-Dichloro-benzylidene)-(1-phenyl-ethyl)-amine (MA1)

Fig. 2.3 represents the ^{13}C -NMR spectrum of MA1. Azomethine carbon exhibits a peak at 162 ppm. Aromatic carbons show signals from 120 to 128 ppm. A peak appeared at 72 ppm shows the presence of methine carbon. A peak obtained at 22 ppm is due to methyl carbon.

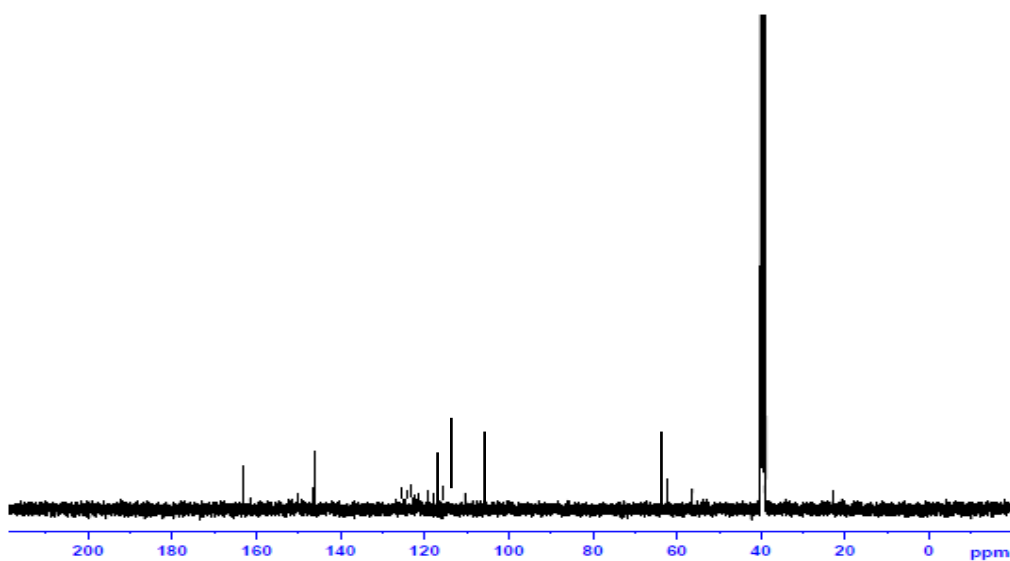


Fig.2.3. ^{13}C -NMR spectrum of (2, 3-Dichloro-benzylidene)-(1-phenyl-ethyl)-amine (MA1)

2.1.4. Mass spectrum of (2, 3-Dichloro-benzylidene)-(1-phenyl-ethyl)-amine (MA1)

The Mass spectrum of MR4 is shown in the Fig 2.4. Exact mass of MA1 has been confirmed by its m/z appeared at 277.04.

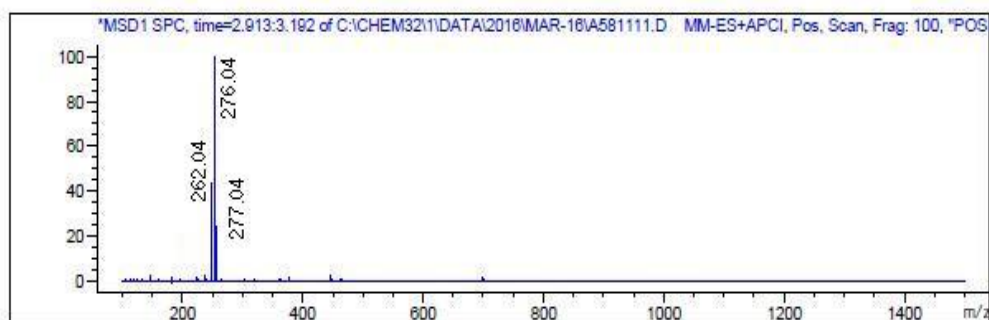


Fig.2.4. Mass spectrum of (2, 3-Dichloro-benzylidene)-(1-phenyl-ethyl)-amine (MA1)

2.1.5. Antimicrobial Screening

Materials and Methods

Bacterial cultures were obtained from Eumic analytical Lab and Research Institute, Tiruchirappalli. Bacterial strains were maintained on Nutrient agar slants (Hi media) at 4°C. Ofloxacin and Amphotericin B are positive standards for bacteria and fungi strains respectively.

Inoculum Preparation

Bacterial cultures were sub cultured in liquid medium (Nutrient broth) at 37°C for 8 h and further used for the test (10^5 - 10^6 CFU/mL). These suspensions were prepared immediately before the test was carried out.

Preparation of Culture Media

Muller Hinton Agar (MHA) medium

Muller Hinton agar medium is exclusively used for diffusion oriented Bacteriological experiments.

Ingredients	Grams / Liter
Beef infusion	300 g
Casein acid hydrolysate	17.50 g
Starch	1.50 g
Agar-agar	20 g

The ingredients were added into the distilled water and boiled until the medium dissolve completely and the same was sterilized by autoclaving at 15 lb psi pressure (121⁰ C) for about 15 minutes. The nutrient broth was prepared by the same composition without agar.

Antimicrobial evaluation of MA1

S. No	Pathogen	Zone of inhibition (mm/mL)				
		25 μ L	50 μ L	75 μ L	100 μ L	Control
1.	<i>S. aureus</i>	12	15	17	20	20
2.	<i>E. coli</i>	12	14	16	18	28
3.	<i>A. niger</i>	17	20	22	25	30

Table 2.1. Zone of inhibition of MA1

Zone of inhibition of the compound MA1 given in the Table 2.1 and Fig 2.5.1-2.5.4 reveals that the compound exhibits very less activity against *E.coli*. It shows moderate activity against *A. niger*. Potency of the compound is found to be high against *S. aureus*. The compound is found to be potent against gram positive bacteria and less active against gram negative bacteria and moderate against fungi strain when compared to the standard drug employed.

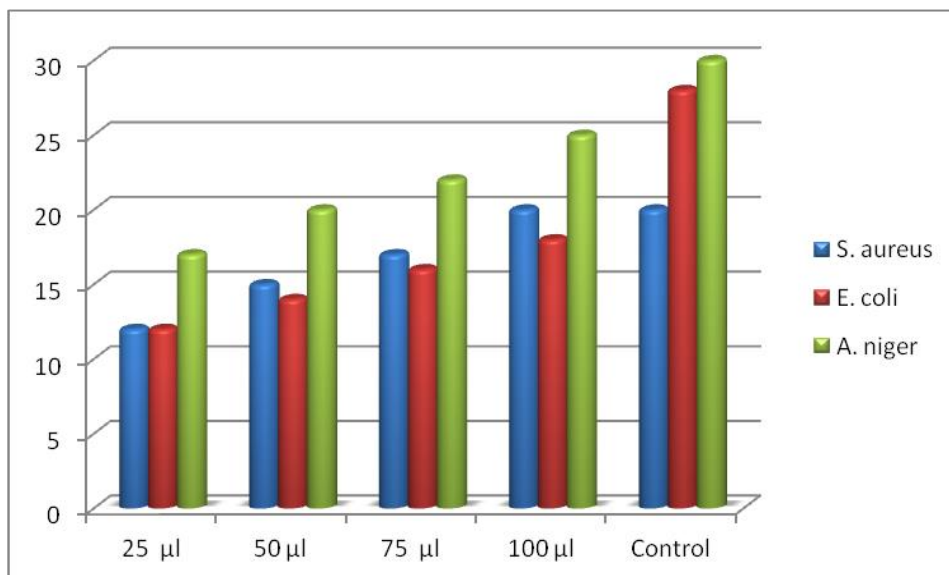


Fig.2.5.1.

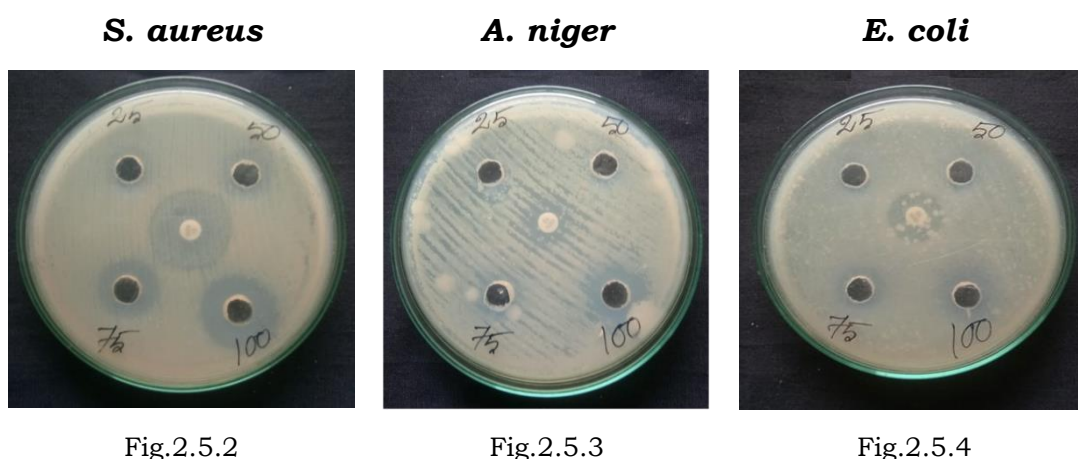


Fig.2.5.2

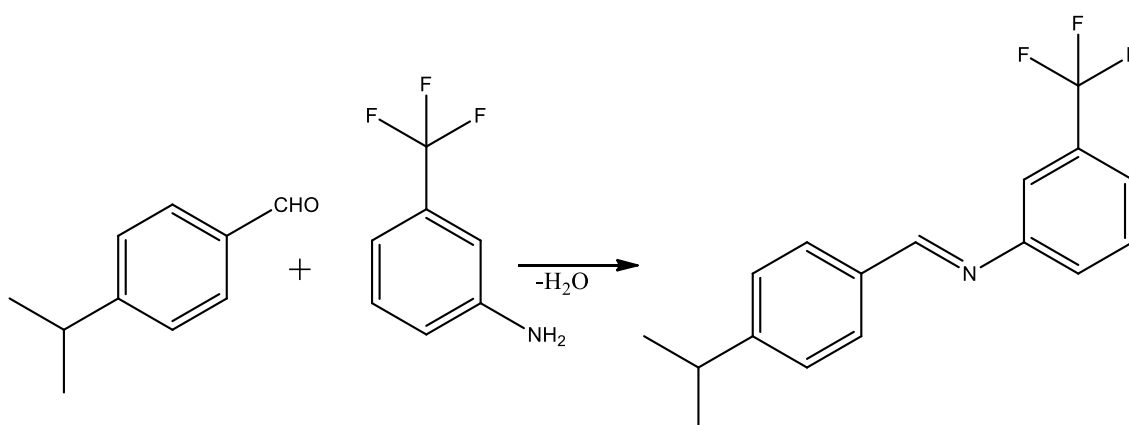
Fig.2.5.3

Fig.2.5.4

Fig.2.5.1-2.5.4.Zone of inhibition of MA1.

2.2. Synthesis of (4-Isopropyl-benzylidene)-(3-trifluoromethyl phenyl)-amine (MA2)

To the ethanolic solution of 4-isopropyl benzaldehyde (14.8 mL, 0.1 M), 3-amino benzotrifluoride (16.0 mL, 0.1 M) was added. The reaction mixture was taken in a RB flask and kept over a magnetic stirrer and stirred for 6 h. The solid separated out was washed, filtered, and dried over vacuum and recrystallized using absolute ethanol. (Colourless solid; M.P: 180 °C)



Scheme: 2.2- Synthesis of (4-Isopropyl-benzylidene)-(3-trifluoromethyl phenyl)-amine (MA2)

2.2.1. IR Spectrum of (4-Isopropyl-benzylidene)-(3-trifluoromethyl phenyl)-amine (MA2)

The FT-IR spectrum of MA2 is presented in the Fig. 2.6. Aromatic C-H stretching in phenyl ring exhibits a band at 2965 cm^{-1} . A strong absorption band appeared at 2876 cm^{-1} is due to C-H stretching. An absorption band at 1631 cm^{-1} indicates C=N stretching. A band appeared at 1018 cm^{-1} is due to C-F stretching.

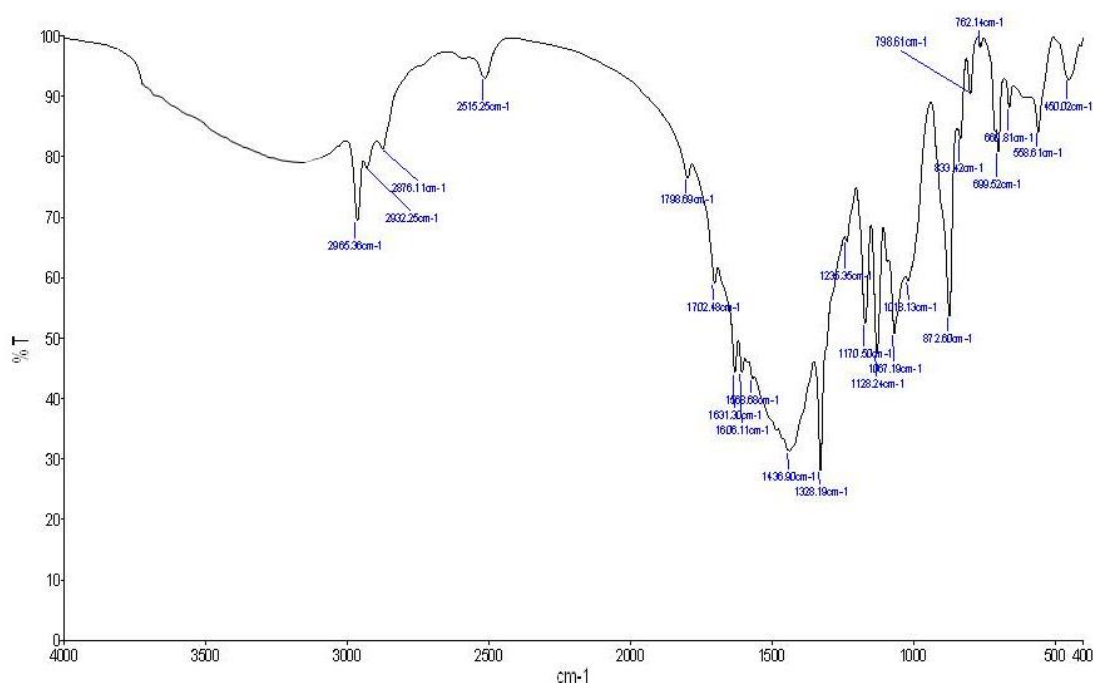


Fig. 2.6. IR Spectrum of (4-Isopropyl-benzylidene)-(3-trifluoromethyl phenyl)-amine (MA2)

2.2.2. $^1\text{H-NMR}$ Spectrum of (4-Isopropyl-benzylidene)-(3-trifluoromethylphenyl)amine (MA2)

$^1\text{H-NMR}$ spectrum of MA2 has been given in the Fig 2.7. A peak at 8.5 ppm indicates the azomethine proton. The signals ranges from 6.9 to 7.5 ppm are assigned to aromatic protons. A peak observed at 2.5 ppm

indicates methine protons. Methyl protons are assigned by the signal obtained at 1.1 ppm.

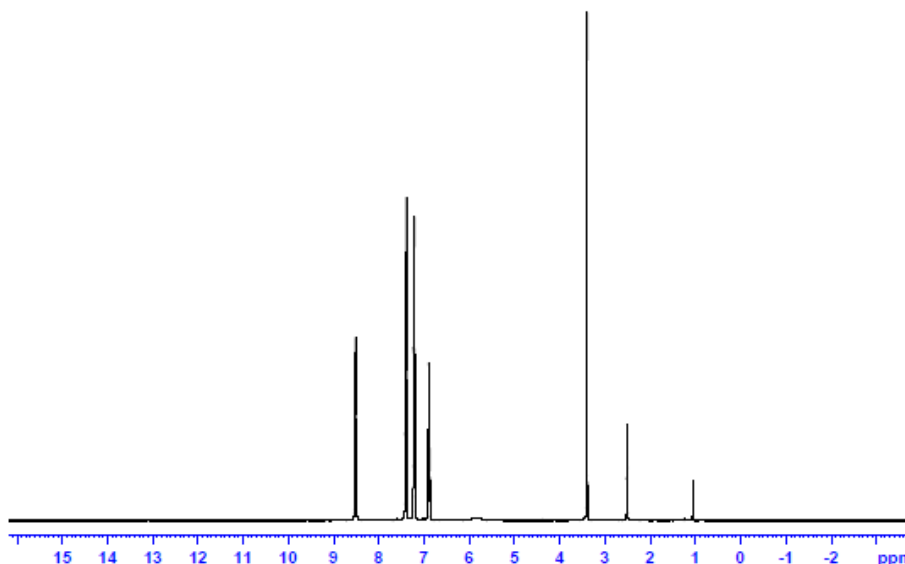


Fig. 2.7. ¹H-NMR Spectrum of (4-Isopropyl-benzylidene)-(3-trifluoromethylphenyl)amine (MA2)

2.2.3. ¹³C-NMR Spectrum of (4-Isopropyl-benzylidene)-(3-trifluoromethyl phenyl)-amine. (MA2)

¹³C-NMR of the compound MA2 has been presented in the Fig 2.8. Azomethine carbon shows a peak at 161 ppm. The peaks ranging from 124-138 indicate the aromatic carbons. CF₃ carbon is indicated by a peak at 122 ppm.

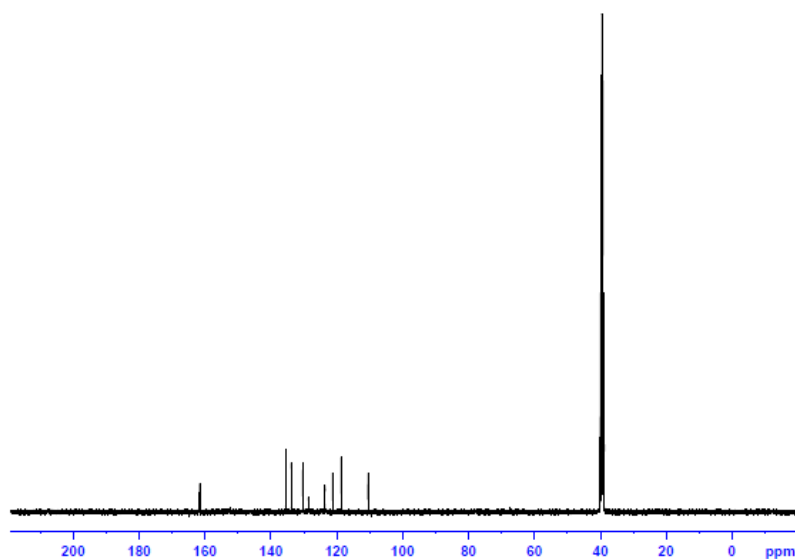


Fig.2.8. ¹³C-NMR Spectrum of (4-Isopropyl-benzylidene)-(3-trifluoromethyl phenyl)-amine. (MA2)

2.2.4. Mass Spectrum of (4-Isopropyl-benzylidene)-(3-trifluoromethyl phenyl)-amine. (MA2)

Fig. 2.9 represents the mass spectrum of the compound MA2. The peak appearing at m/z 291.12 confirms the calculated molecular mass of the compound. The intense peak at m/z 248.12 is the base peak.

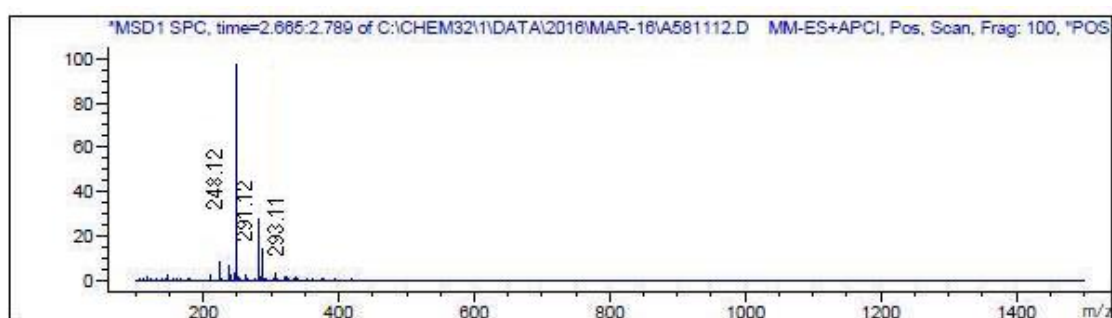


Fig.2.9. Mass Spectrum of (4-Isopropyl-benzylidene)-(3-trifluoromethyl phenyl)-amine. (MA2)

2.2.5. Antimicrobial evaluation of MA2

S. No	Pathogen	Zone of inhibition (mm/mL)				
		25 μ L	50 μ L	75 μ L	100 μ L	Control
1.	<i>S. aureus</i>	10	12	15	19	20
2.	<i>E. coli</i>	11	12	14	16	30
3.	<i>A. niger</i>	10	14	16	18	30

Table 2.2. Zone of inhibition of MA2

The compound MA2 possesses very high activity against *S. aureus*, less activity against *E.coli* and considerable activity against the fungi strain, *A. niger* when compared to the positive standard. In general the compound exhibit moderate activity against fungi pathogen and potent against gram positive bacteria. The results are shown in the Table 2.2 and in the Fig. 2.10.1-2.10.4

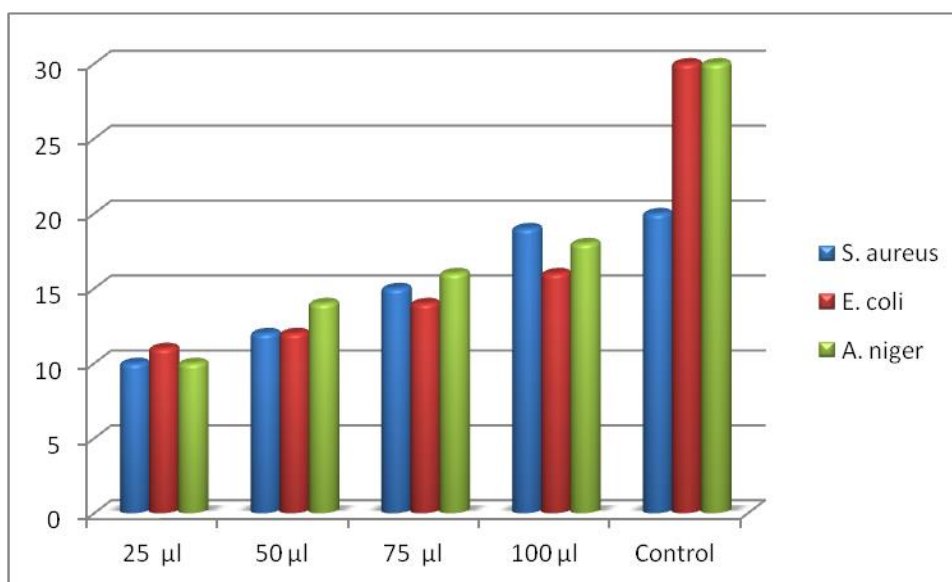


Fig.2.10.1

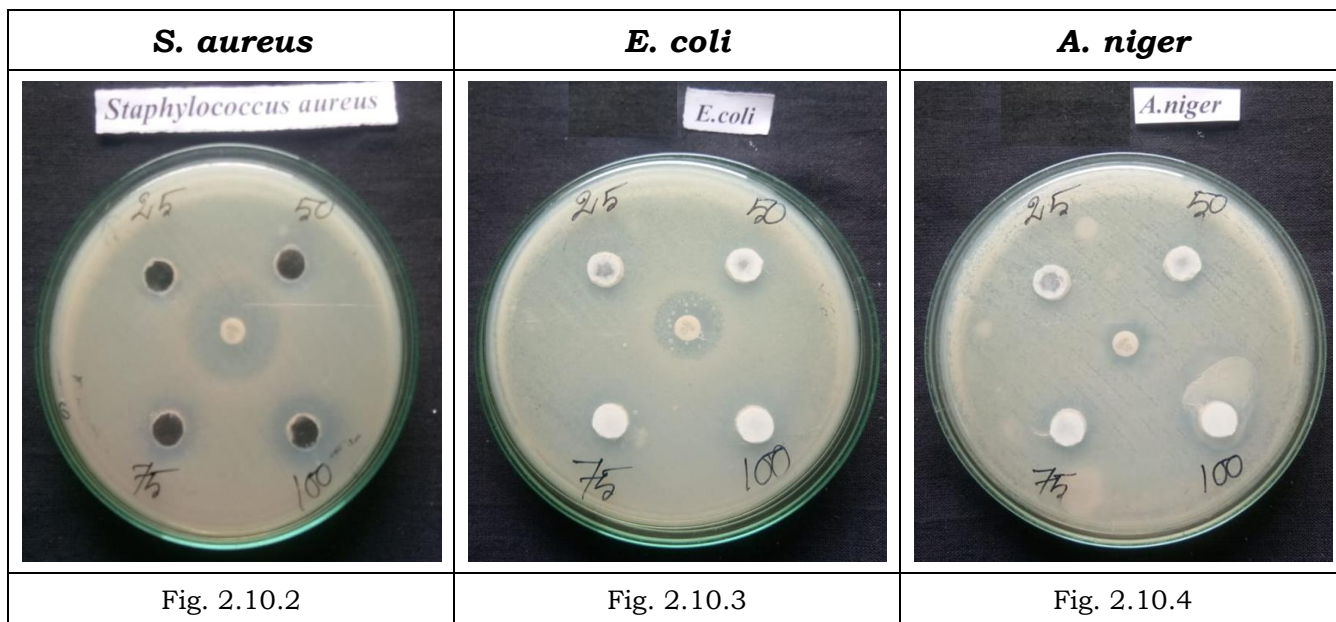
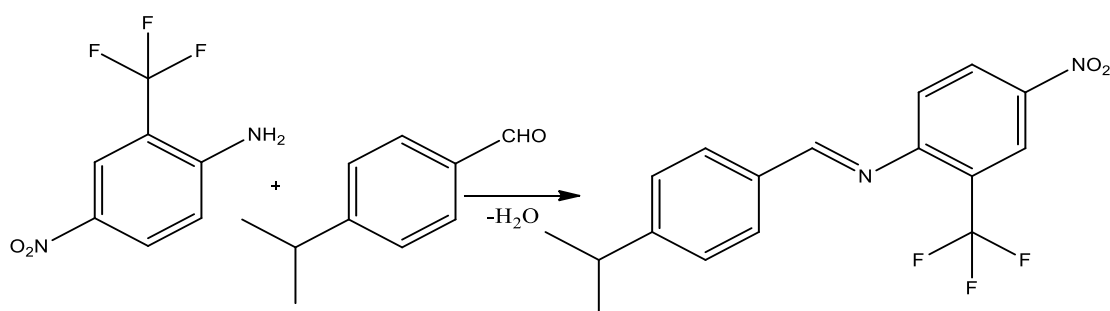


Fig.2.10.1-2.10.4. Zone of inhibition of MA2

2.3. Synthesis of N-(4-isopropylbenzylidene)-4-nitro-2-(trifluoromethyl)aniline (MA3)

To the ethanolic solution of 2-amino-5-nitrobenzenetrifluoride (20.4 g, 0.1 M), 4-isopropylbenzaldehyde (15.0 mL, 0.1M) was added. The reaction mixture was taken in a RB flask and kept over a magnetic stirrer and stirred for 6 h. The solid separated out was washed, filtered, and dried over vacuum and recrystallized using absolute ethanol. (Colour: Brown solid; M.P: 106 °C)



Scheme: 2.3- Synthesis of N-(4-isopropylbenzylidene)-4-nitro-2-(trifluoromethyl)aniline (MA3)

2.3.1. IR spectrum of N-(4-isopropylbenzylidene)-4-nitro-2-(trifluoromethyl)aniline (MA3)

FT-IR spectrum of MA3 is shown in the Fig 2.11. Aromatic C-H stretching frequencies are indicated by the band at 3024 cm^{-1} . C=N stretching frequency is noticed by a band at 1632 cm^{-1} . A band at 1584 cm^{-1} shows the NO_2 stretching. C-F absorption exhibited a band at 1055 cm^{-1} .

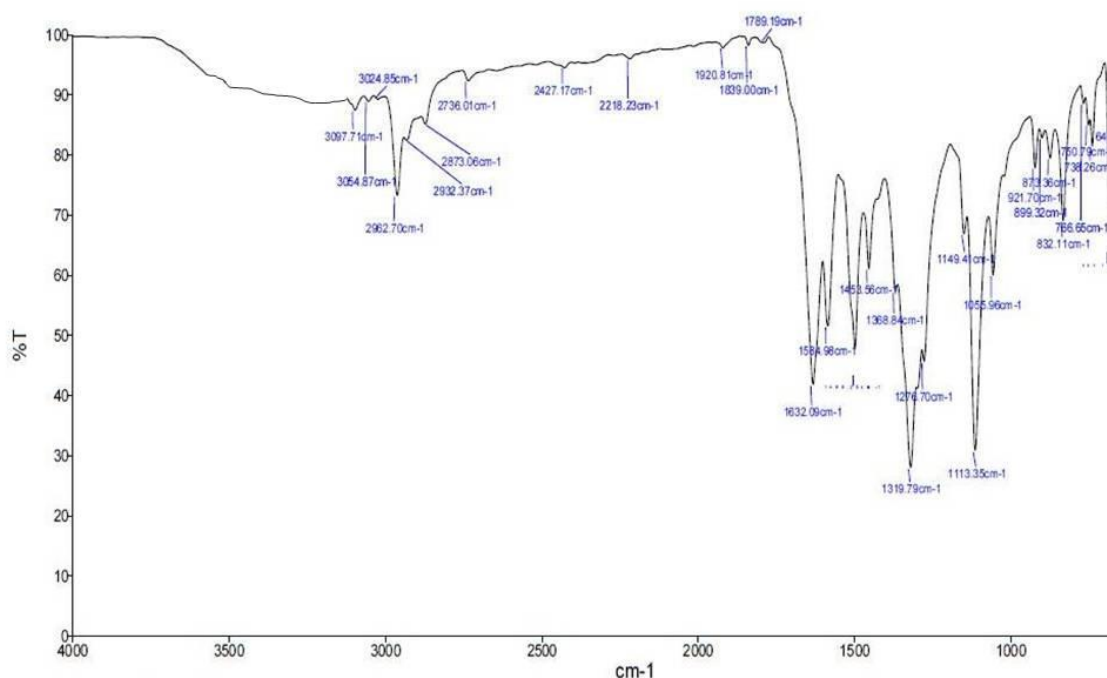


Fig.2.11. IR spectrum of N-(4-isopropylbenzylidene)-4-nitro-2-(trifluoromethyl)aniline (MA3)

2.3.2. $^1\text{H-NMR}$ spectrum of N-(4-isopropylbenzylidene)-4-nitro-2-(trifluoromethyl)aniline (MA3)

$^1\text{H-NMR}$ spectrum of MA3 is given in the Fig 2.12. A peak at 8.5 ppm indicates the azomethine proton. The signals ranges from 6.9 to 7.5 ppm are assigned to aromatic protons. A peak observed at 2.5 ppm

indicates methine protons. Methyl protons are assigned by the signal obtained at 1.2 ppm.

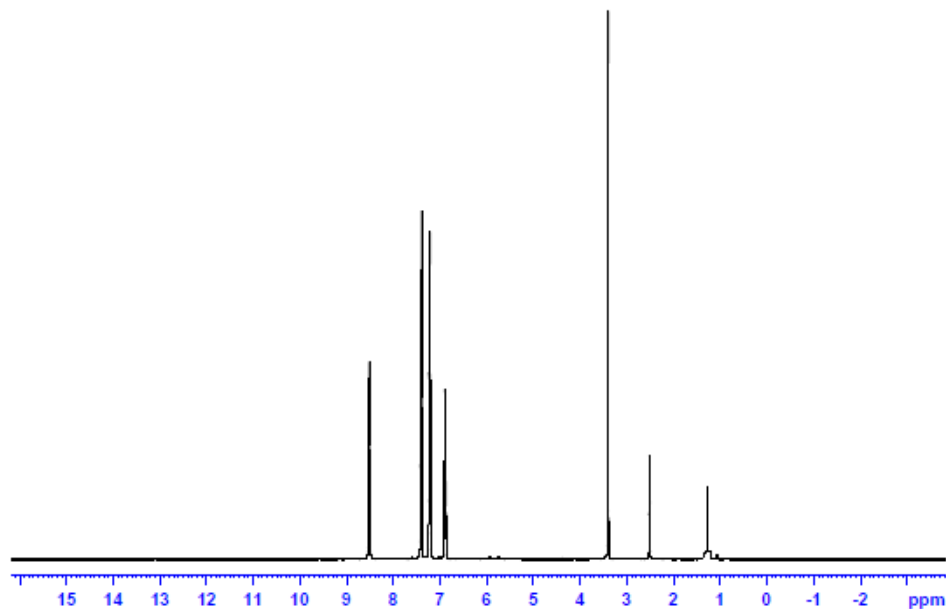


Fig.2.12. ^1H -NMR spectrum of N-(4-isopropylbenzylidene)-4-nitro-2-(trifluoromethyl)aniline (MA3)

2.3.3. ^{13}C -spectrum of N-(4-isopropylbenzylidene)-4-nitro-2-(trifluoromethyl)aniline (MA3)

^{13}C -NMR of the compound MA3 is presented in the Fig 2.13. Azomethine carbon shows a peak at 162 ppm. The signal appeared at 146 ppm is due to nitro group carbon bonded in aromatic ring. The peaks ranging from 122-135 indicate the aromatic carbons. CF_3 carbon is indicated by a peak at 121 ppm.

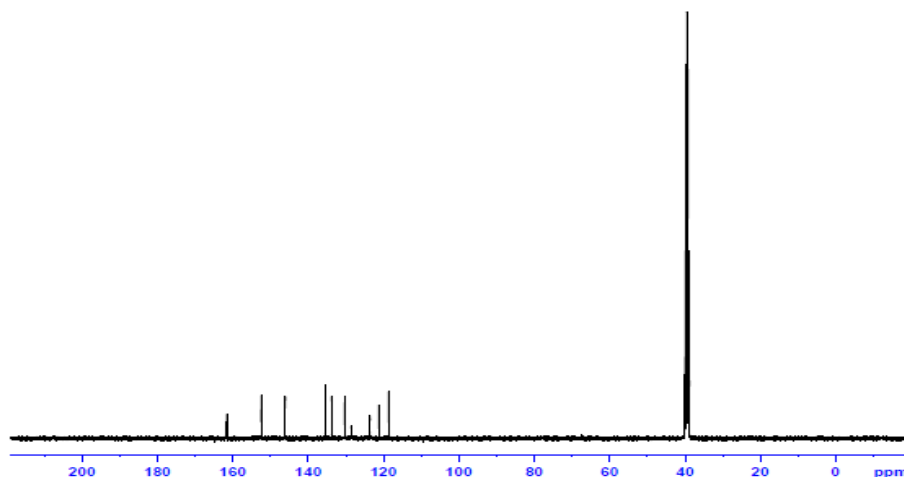


Fig. 2.13. ^{13}C -spectrum of N-(4-isopropylbenzylidene)-4-nitro-2-(trifluoromethyl)aniline (MA3)

2.3.4. Mass spectrum of N-(4-isopropylbenzylidene)-4-nitro-2-(trifluoromethyl)aniline (MA3)

Fig. 2.14 represents the mass spectrum of the compound MA3. The molecular ion peak appearing at m/z 336.31 confirms the calculated molecular mass of the compound. The peak appearing with high intensity at m/z 293.11 is the base peak.

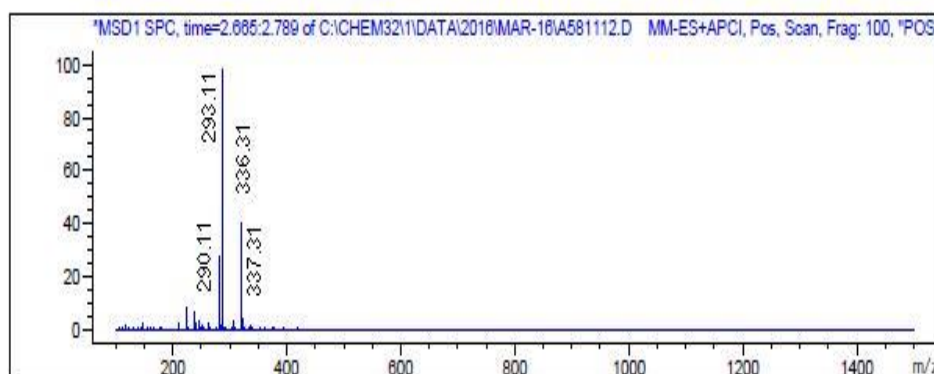
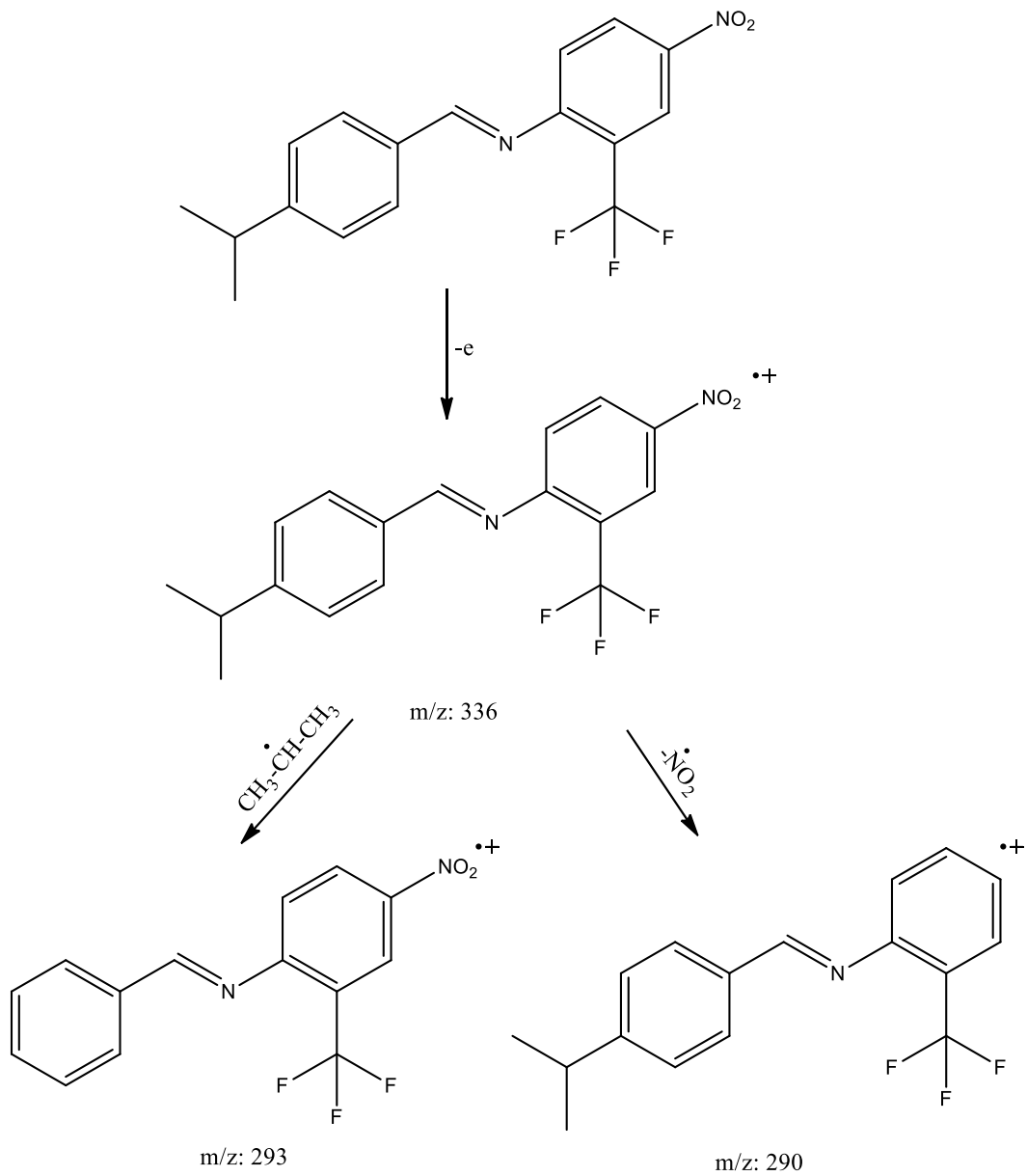


Fig.2.14. Mass spectrum of N-(4-isopropylbenzylidene)-4-nitro-2-(trifluoromethyl)aniline (MA3)

Mass Fragmentation



2.3.5. Antimicrobial evaluation of MA3

S. No	Pathogen	Zone of inhibition (mm/mL)				
		25 μL	50 μL	75 μL	100 μL	Control
1.	<i>S. aureus</i>	17	20	25	30	20
2.	<i>E. coli</i>	18	22	26	30	32
3.	<i>A. niger</i>	13	16	18	20	30

Table 2.3. Zone of inhibition of MA3

Table 2.3 and the Fig 2.15.1-2.15.4 represent the results of the antimicrobial evaluation of the compound MA3. It shows that the compound is found to possess greater activity against *S. aureus* and *E. coli* and moderate activity against *A. niger*. The compound is more active against bacterial stain than the fungi when compared to the positive standard.

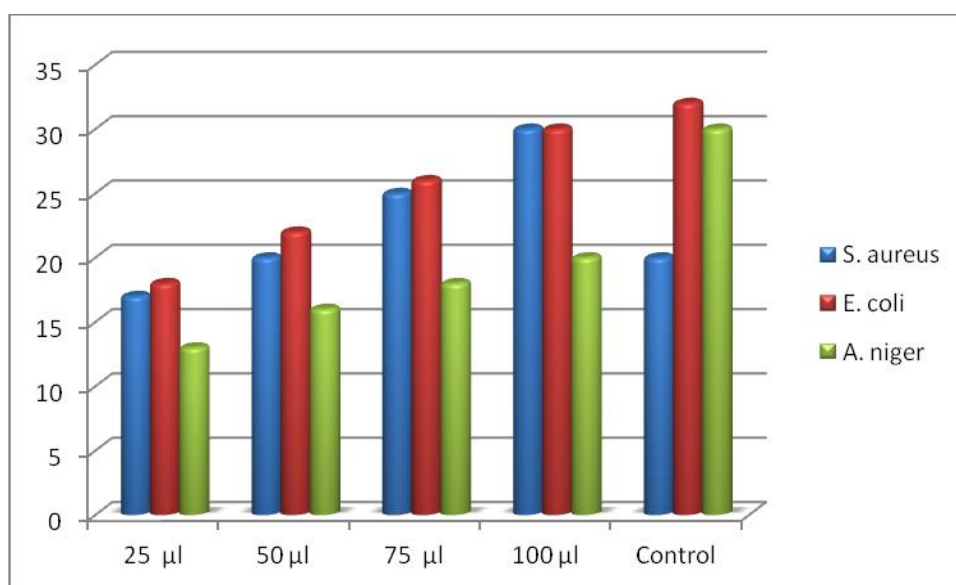


Fig.2.15.1

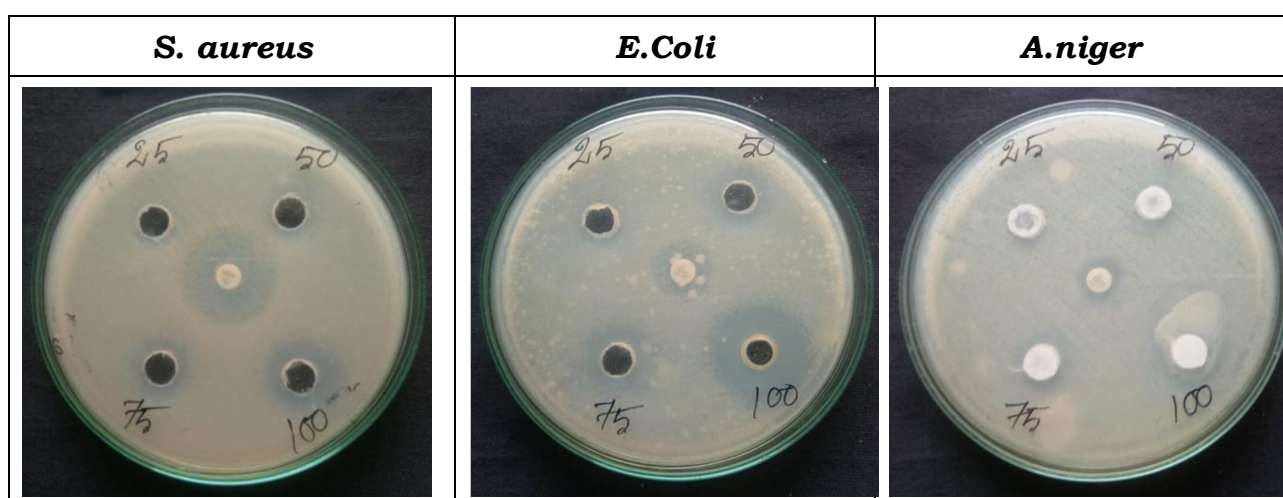
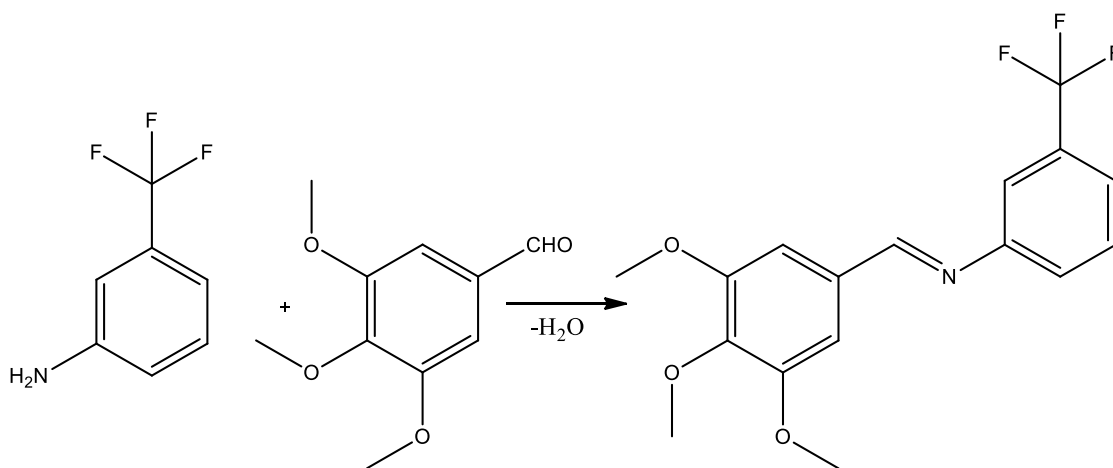


Fig.2.15.2-2.15.4. Zone of inhibition of MA3

2.4. Synthesis of 3-(trifluoromethyl)-N-(3,4,5-trimethoxybenzylidene)aniline (MA4)

To the ethanolic solution of 3, 4, 5-trimethoxy benzaldehyde (19.0 mL, 0.1 M), 3-aminobenzotrifluoride of (16.0 g , 0.1M) was added. The reaction mixture was taken in a RB flask and kept over a magnetic stirrer and stirred for 6 h. The solid separated out was washed, filtered and dried over vacuum and recrystallized using absolute ethanol. (Colour: Brown solid; M.P: 184 °C).



Scheme: 2.4- Synthesis of 3-(trifluoromethyl)-N-(3,4,5-trimethoxybenzylidene)aniline (MA4)

2.4.1. IR spectrum of 3-(trifluoromethyl)-N-(3,4,5-trimethoxybenzylidene)aniline (MA4)

The FT-IR spectrum of MA4 is provided in the Fig. 2.16. Aromatic C-H stretching in phenyl ring exhibits a band at 2939 cm^{-1} . A strong absorption band appeared at 2836 cm^{-1} is due to C-H stretching. An absorption band at 1586 cm^{-1} indicates C=N stretching. A sharp band noticed at 1122 cm^{-1} is attributed to C-O-C Stretching. A band appeared at 1001 cm^{-1} is due to C-F stretching.

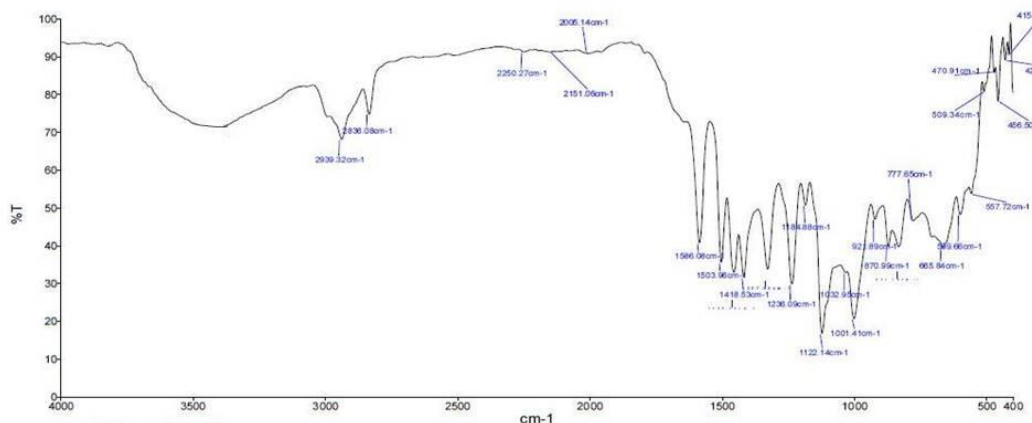


Fig. 2.16. IR spectrum of 3-(trifluoromethyl)-N-(3,4,5-trimethoxybenzylidene)aniline (MA4)

2.4.2. ¹H-NMR spectrum of 3-(trifluoromethyl)-N-(3,4,5-trimethoxybenzylidene)aniline (MA4)

¹H-NMR spectrum of MA4 is shown in the Fig 2.17. A peak at 8.9 ppm indicates the azomethine proton. The signals ranges from 6.9 to 7.5 ppm are assigned to aromatic protons. Methyl protons are assigned by the signal obtained at 3.9 ppm.

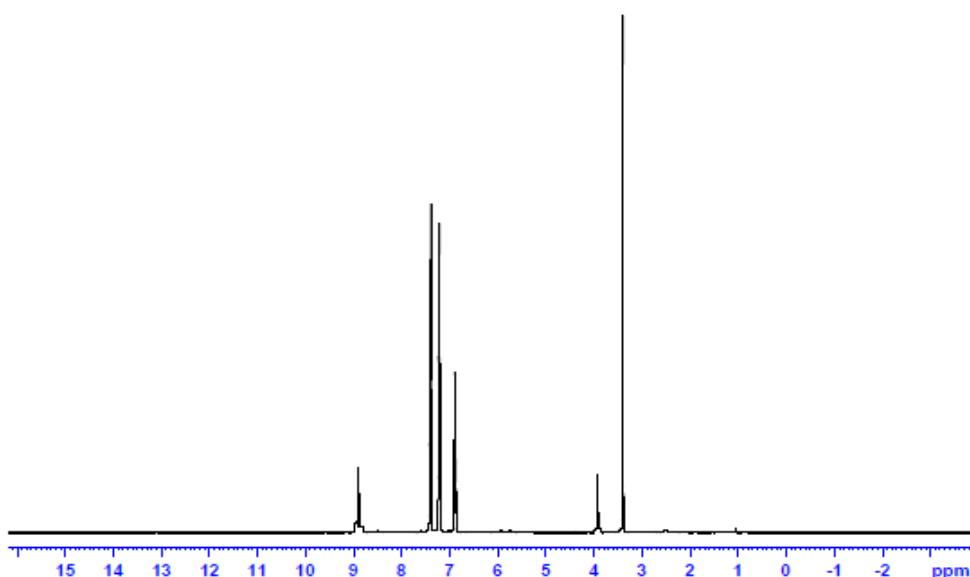


Fig. 2.17. ¹H-NMR spectrum of 3-(trifluoromethyl)-N-(3,4,5-trimethoxybenzylidene)aniline (MA4)

2.4.3. ^{13}C -NMR spectrum of 3-(trifluoromethyl)-N-(3,4,5-trimethoxybenzylidene)aniline (MA4)

^{13}C -NMR spectrum of the compound MA4 has been presented in the Fig 2.18. Azomethine carbon shows a peak at 162 ppm. The signal appeared at 155 ppm is due to methoxy group attached in aromatic ring. The peaks ranging from 125-137 indicate the aromatic carbons. CF_3 carbon is indicated by a peak at 123 ppm. Carbon of methoxy group exhibited a peak 58 ppm.

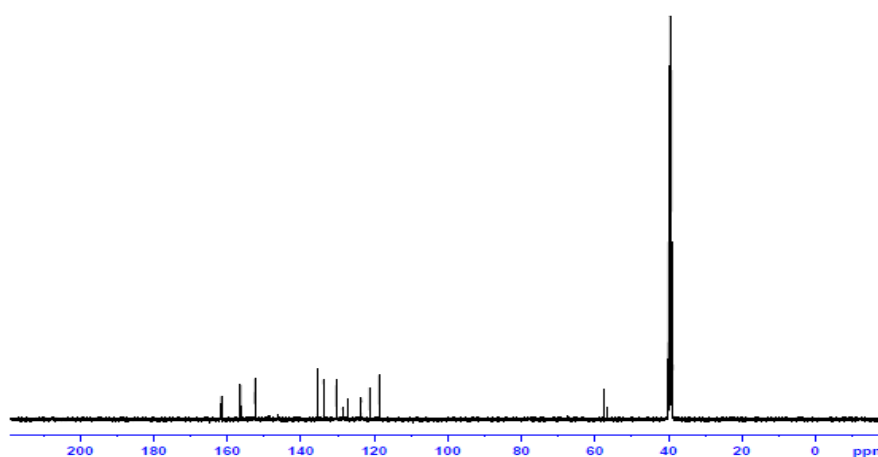


Fig. 2.18. ^{13}C -NMR spectrum of 3-(trifluoromethyl)-N-(3,4,5-trimethoxybenzylidene)aniline (MA4)

2.4.4. Mass spectrum of 3-(trifluoromethyl)-N-(3,4,5-trimethoxybenzylidene)aniline (MA4)

Fig. 2.19 represents the mass spectrum of the compound MA4. The peak appearing at m/z 339.11 confirms the calculated molecular mass of the compound. The intense peak at m/z 255.09 is the base peak.

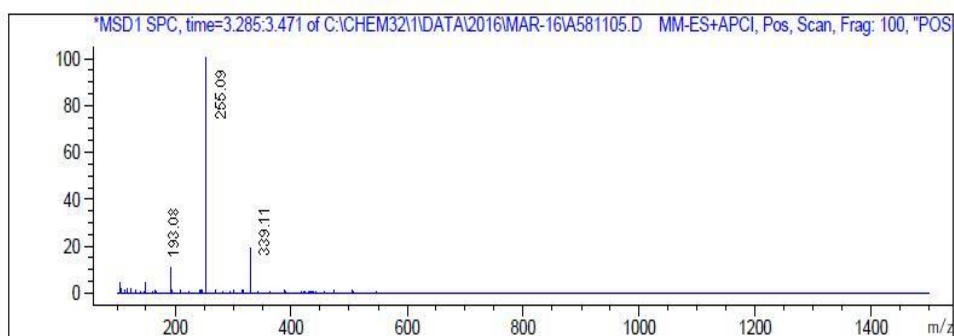


Fig.2.19. Mass spectrum of 3-(trifluoromethyl)-N-(3,4,5-trimethoxybenzylidene)aniline (MA4)

2.4.5. Antimicrobial evaluation of MA4

S. No	Pathogen	Zone of inhibition (mm/mL)				
		25 μ L	50 μ L	75 μ L	100 μ L	Control
1.	<i>S. aureus</i>	11	14	16	18	20
2.	<i>E. coli</i>	14	18	21	25	28
3.	<i>A. niger</i>	10	12	15	16	30

Table 2.4. Zone of inhibition of MA4

Zone of inhibition of the compound MA4 is represented in the Table 2.4 and Fig 2.20. From the table and Fig., it has been understood that the compound is active against gram positive and negative bacteria. Further the compound is found to be less active against fungi.

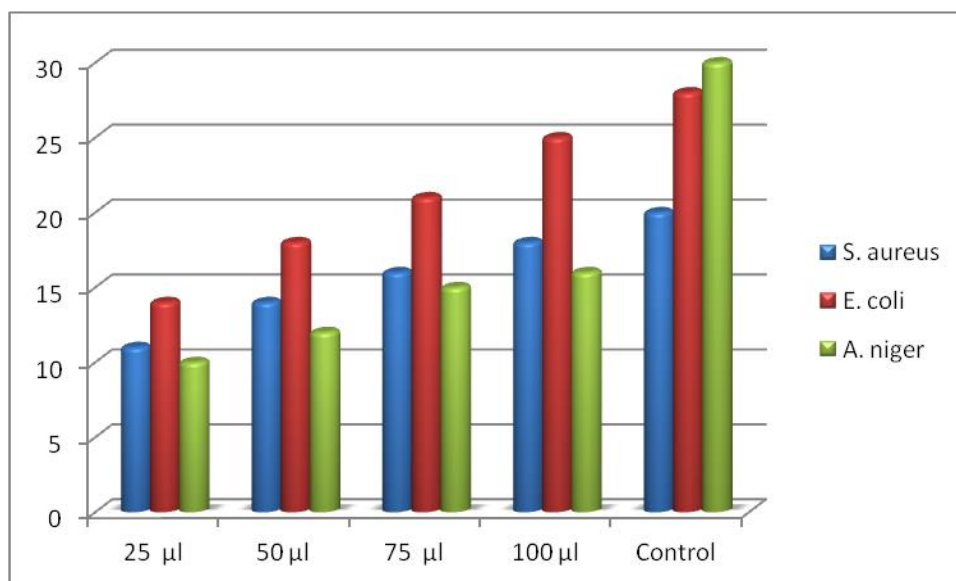


Fig.2.20.1

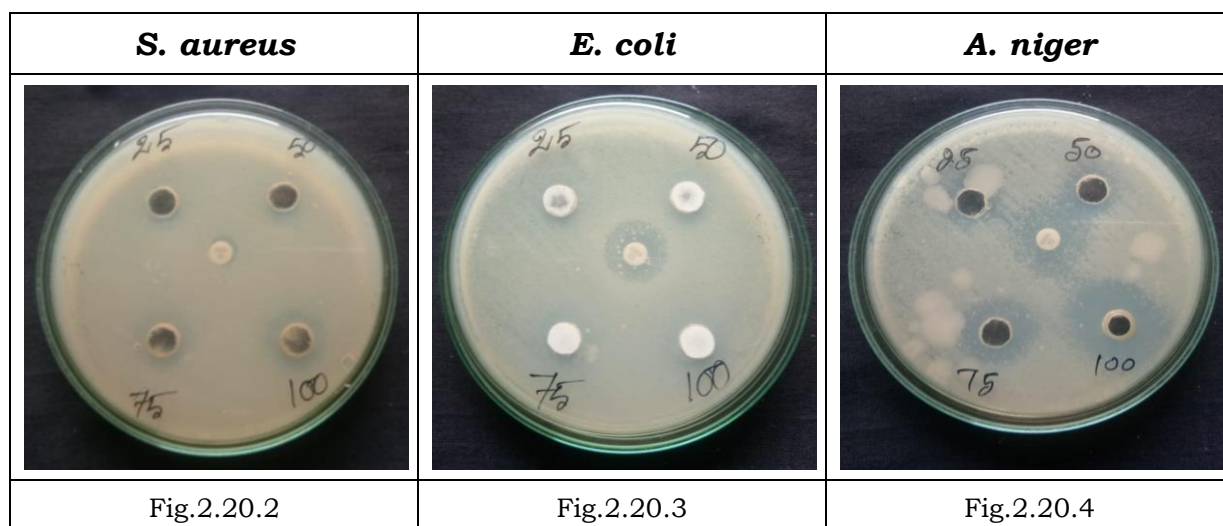
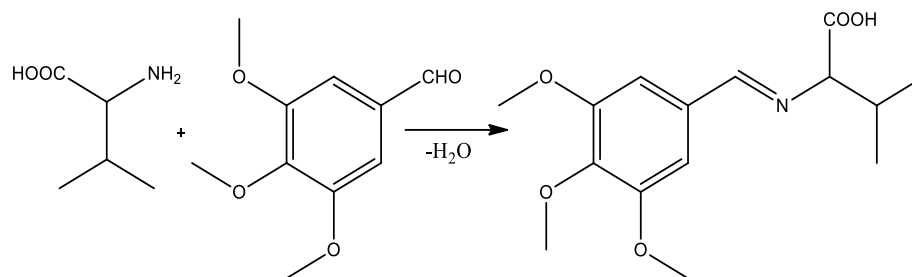


Fig.2.20.1-2.20.4 Zone of inhibition of MA4

2.5. Synthesis of 3-methyl-2-((3,4,5-trimethoxybenzylidene)amino)butanoic acid (MA5)

To the ethanolic solution of 3, 4, 5-trimethoxybenzaldehyde (19.0 mL, 0.1 M), L-Valine (16.0 g, 0.1M) was added. The reaction mixture was taken in a RB flask and kept over a magnetic stirrer and stirred for 6 h.

The solid separated out was washed, filtered and dried over vacuum and recrystallized using absolute ethanol. (Colour: Yellow solid; M.P: 132 °C)



Scheme: 2.5- Synthesis of 3-methyl-2-((3,4,5-trimethoxybenzylidene)amino)butanoic acid (MA5)

2.5.1. FT-IR spectrum of 3-methyl-2-((3,4,5-trimethoxybenzylidene)amino)butanoic acid (MA5)

FT-IR spectrum of MA5 is shown in the Fig 2.21 exhibits a band at 3418 cm⁻¹ indicates OH stretching. A band appeared at 2938 cm⁻¹ is attributed to aromatic C-H stretching. A band at 2836 cm⁻¹ is due to aliphatic C-H stretching. C=N stretching vibration is noticed at 1585 cm⁻¹. An absorption band at 1646 cm⁻¹ indicates the carbonyl stretching of carboxylic acid.

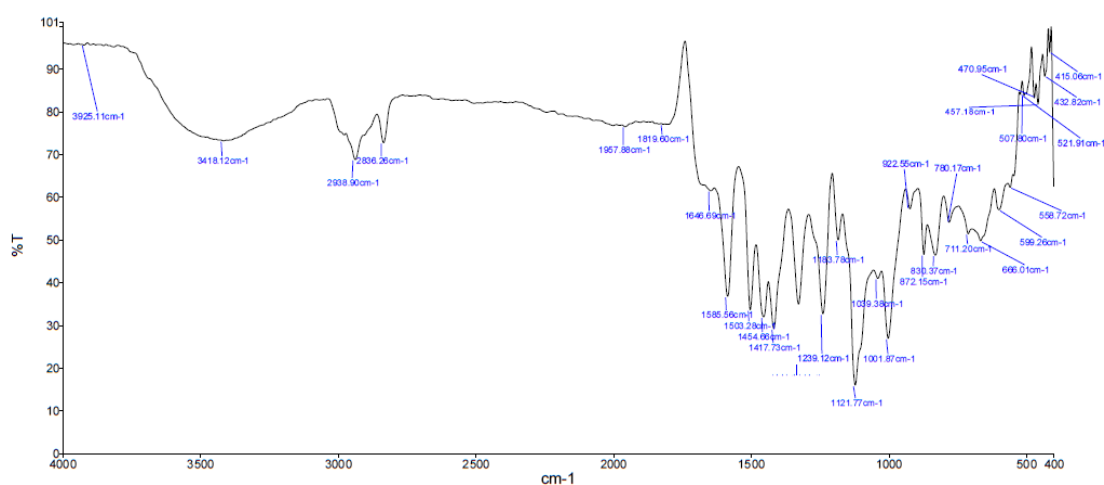


Fig.2.21. FT-IR spectrum of 3-methyl-2-((3,4,5-trimethoxybenzylidene)amino)butanoic acid (MA5)

2.5.2. ¹H-NMR spectrum of 3-methyl-2-((3,4,5-trimethoxybenzylidene)amino)butanoic acid (MA5)

¹H-NMR spectrum of MA5 has been shown in the Fig 2.22. A sharp peak appeared at 9.9 ppm indicates the presence of OH proton. Aromatic protons are indicated by the signals range from 6.9-7.4 ppm. Methine protons in which carboxylic group and methyl groups attached show peaks at 3.9 and 2.5 respectively. Signal of methoxy group proton is appeared at 1.2 ppm.

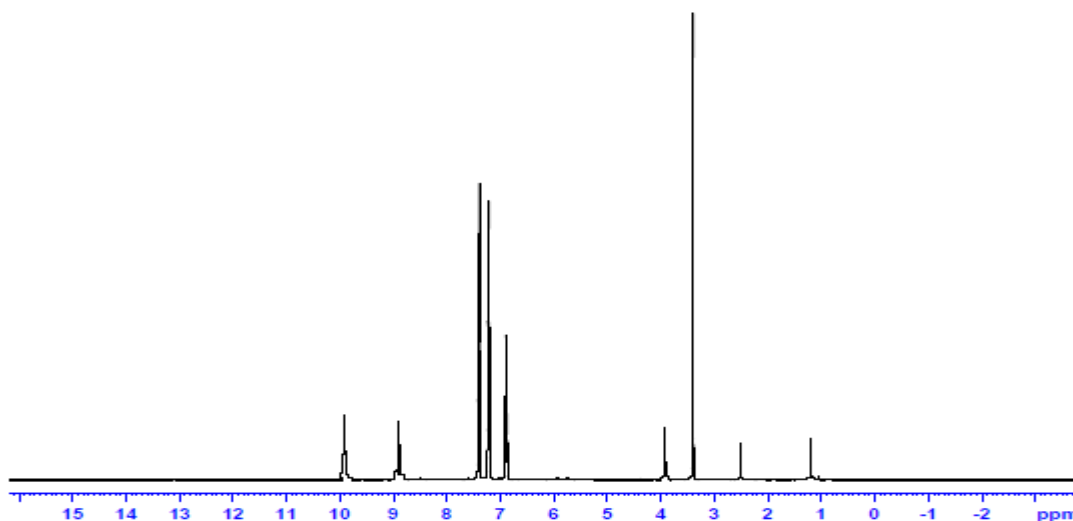


Fig. 2.22. ¹H-NMR spectrum of 3-methyl-2-((3,4,5-trimethoxybenzylidene)amino)butanoic acid (MA5)

2.5.3. ¹³C-NMR spectrum of 3-methyl-2-((3,4,5-trimethoxybenzylidene)amino)butanoic acid (MA5)

¹³C-NMR of the compound MA5 has been presented in the Fig 2.23. Carbonyl carbon of carboxylic acid shows a peak at 178 ppm. Azomethine carbon exhibits a peak at 162 ppm. The peaks ranging from

122-137 indicate the aromatic carbon. CH₃ and CH carbons are indicated by peaks at 62 and 57 ppm respectively.

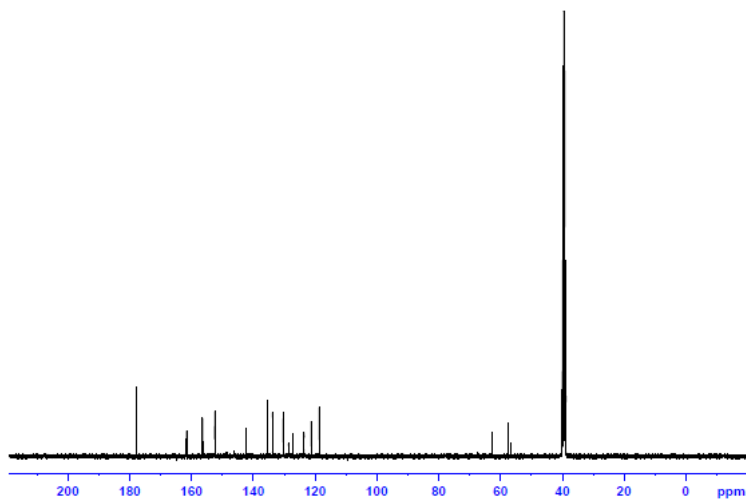


Fig.2.23. ¹³C-NMR spectrum of 3-methyl-2-((3,4,5-trimethoxybenzylidene)amino)butanoic acid (MA5)

2.5.4. Mass spectrum of 3-methyl-2-((3,4,5-trimethoxybenzylidene)amino)butanoic acid (MA5)

Fig. 2.24 represents the mass spectra of the compound MA5. The peak appearing at m/z 295.14 confirms the calculated molecular mass of the compound. The intensity of the molecular ion peak reveals that the peak itself is the base peak.

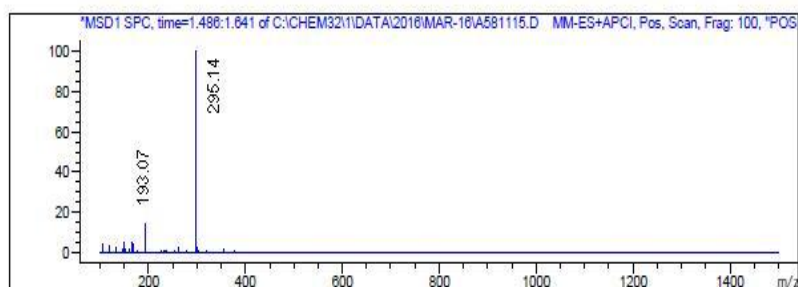


Fig.2. 24. Mass spectrum of 3-methyl-2-((3,4,5-trimethoxybenzylidene)amino)butanoic acid (MA5)

2.5.5. Antimicrobial evaluation of MA5

S.No	Pathogen	Zone of inhibition (mm/mL)				
		25 μ L	50 μ L	75 μ L	100 μ L	Control
1.	<i>S. aureus</i>	10	12	14	16	20
2.	<i>E. coli</i>	11	13	16	18	30
3.	<i>A. niger</i>	12	14	17	18	30

Table 2.5.Zone of inhibition of MA5

Antimicrobial evaluation of the compound MA5 shows that the compound possesses lesser activity against *E.Coli* and *A. niger* and excellent activity against *S.aureus* when compared to the positive standard. The results are given in the Table 2.5 and Fig 2.25.

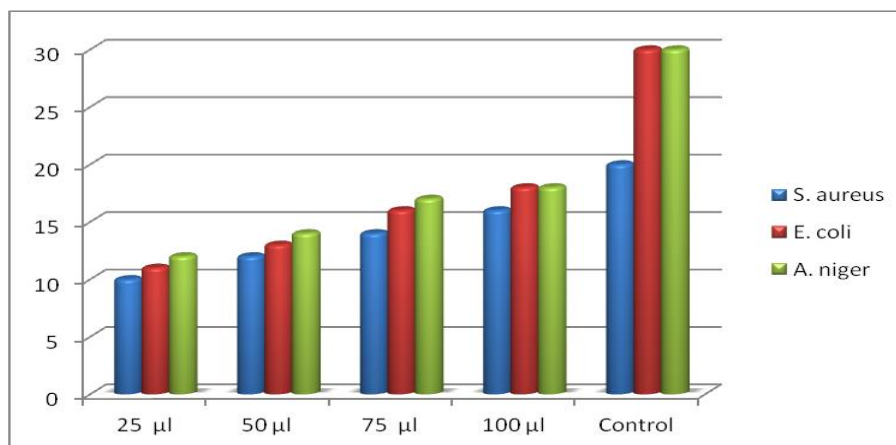


Fig.2.25.1

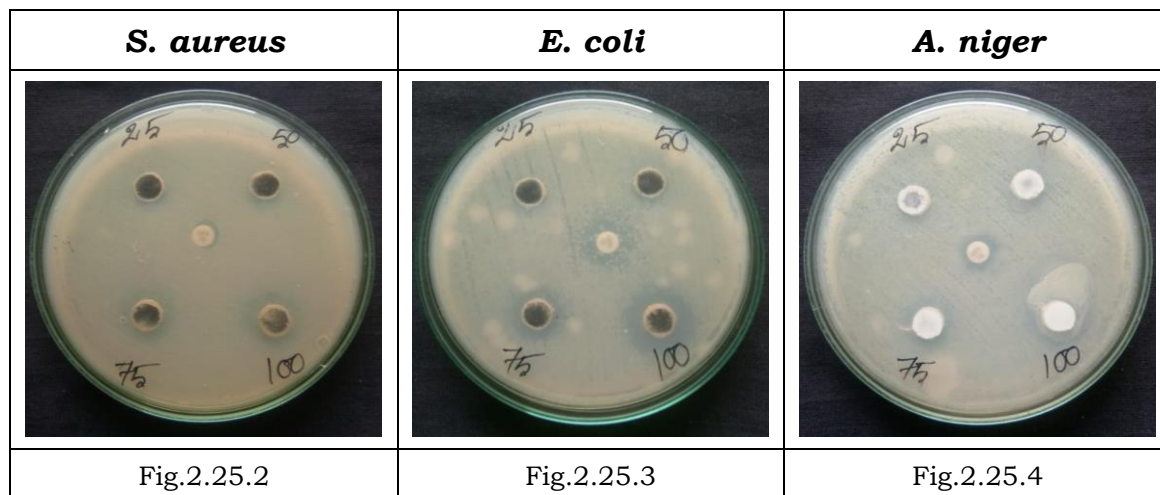
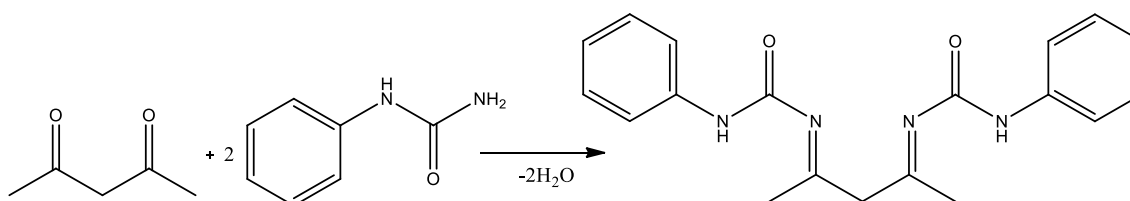


Fig.2.25.1-2.25.4 Zone of inhibition of MA5

Synthesis of azomethine compounds via Schiff reaction (MA6-MA10)

3.1. Synthesis of (E,E)-1,1'-(pentane-2,4-diylidene)bis(3-phenylurea) (MA6)

To the ethanolic solution of acetyl acetone (10.2 mL, 0.1 M), two equivalents of phenyl urea (24.0 g, 0.1 M) was added. The reaction mixture was refluxed for 6 h, cooled and poured into a beaker containing crushed ice. The solid separated out was washed, filtered and dried over vacuum and recrystallized using absolute ethanol. (Pale brown solid, M.P: 132 °C)



Scheme 3.1: Synthesis of (E,E)-1,1'-(pentane-2,4-diylidene)bis(3-phenylurea) (MA6)

3.1.1. IR spectrum of (E,E)-1,1'-(pentane-2,4-diylidene)bis(3-phenylurea) (MA6)

The IR spectrum of MA6 has been presented in the Fig 3.1 NH stretching and bending frequencies exhibited bands at 3428 and 1593 cm⁻¹ respectively. A strong absorption band at 3036 cm⁻¹ is due to aromatic CH stretching. A strong absorption band at 1656 cm⁻¹ is

assigned to C=O stretching. A band appeared at 1613 cm^{-1} is due to C=N stretching.

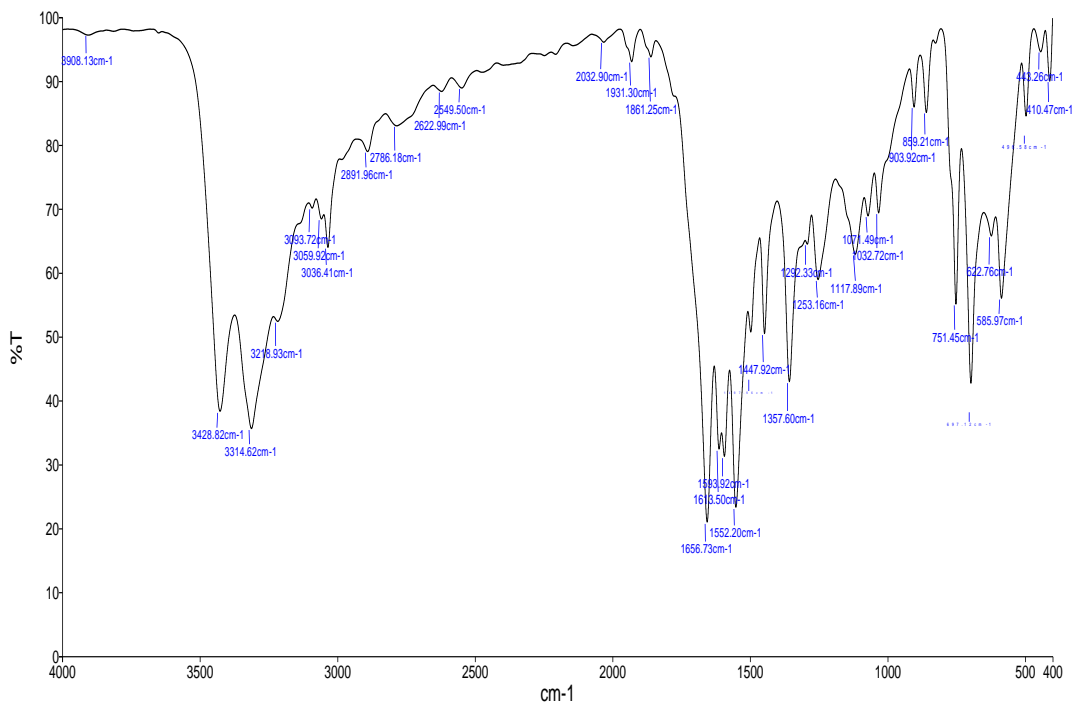


Fig.3.1. IR spectrum of (E,E)-1,1'-(pentane-2,4-diylidene)bis(3-phenylurea) (MA6)

3.1.2. $^1\text{H-NMR}$ spectrum of of (E,E)-1,1'-(pentane-2,4-diylidene)bis(3-phenylurea) (MA6)

$^1\text{H-NMR}$ spectrum of MA6 has been given in the Fig 3.2. A peak observed at 8.5 ppm indicates NH protons. The signals appearing from 6.9 to 7.4 ppm are assigned to aromatic protons. The peaks appeared at 5.9 and 2.5 ppm are due to methylene and methyl protons respectively.

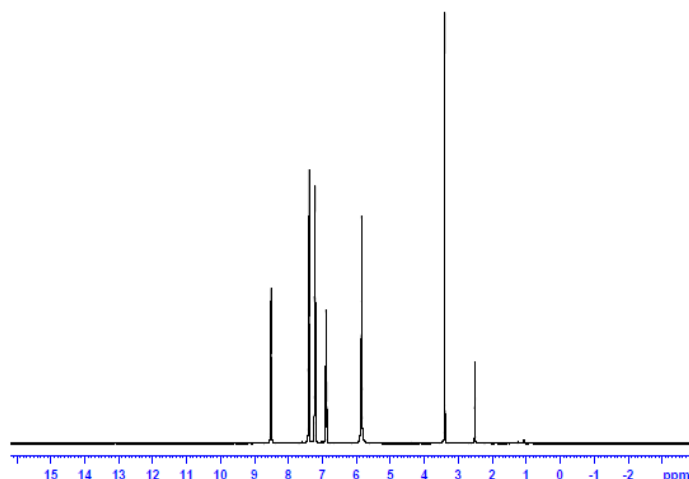


Fig. 3.2. ^1H -NMR spectrum of of (E,E)-1,1'-(pentane-2,4-diylidene)bis(3-phenylurea) (MA6)

3.1.3. ^{13}C -NMR spectrum of of (E,E)-1,1'-(pentane-2,4-diylidene)bis(3-phenylurea) (MA6)

^{13}C -NMR of the compound MA6 has been presented in the Fig 3.3. Azomethine carbon exhibits a peak at 165 ppm. Carbonyl carbon shows a peak at 160 ppm. The peaks ranging from 119-129 indicate the aromatic carbons. CH_2 and CH_3 carbons of ester are indicated by peaks at 35 and 27 ppm respectively. A peak at 42 ppm is due to methine carbon.

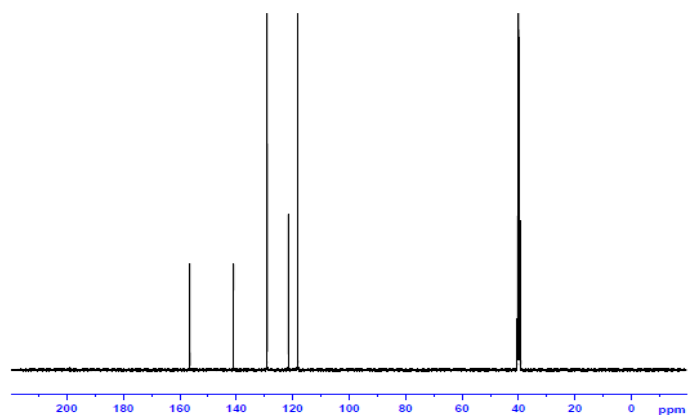


Fig.3.3. ^{13}C -NMR spectrum of of (E,E)-1,1'-(pentane-2,4-diylidene)bis(3-phenylurea) (MA6)

3.1.4. Mass spectrum of (E,E)-1,1'-(pentane-2,4-diylidene)bis(3-phenylurea) (MA6)

Mass spectra of the compound MA6 has been given in the Fig. 3.4. The peak noticed at m/z 336.16 indicates the molecular ion peak. The intense appearing at m/z 216.12 is the base peak.

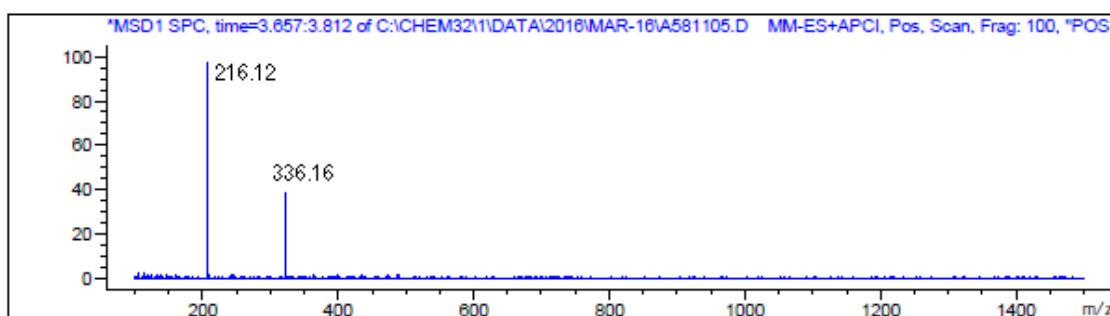


Fig.3.4. Mass spectrum of (E,E)-1,1'-(pentane-2,4-diylidene)bis(3-phenylurea) (MA6)

3.1.5. Antimicrobial evaluation of MA6

The results of antimicrobial evaluation depicted in the Table 3.1 and Fig.3.5.1-3.5.5 shows that the compound MA6 possess moderate activity against *S. aureus*, *C. Albicans* and *A. niger* and higher activity against *E. coli*. Activity of the compound is found to be maximum in the case of gram negative bacteria than the gram positive bacteria and fungi strains when compared to the positive standards. The compound possesses excellent antibacterial activity than the antifungal activity.

S.No	Pathogen	Zone of inhibition (mm/mL)				
		25 μ L	50 μ L	75 μ L	100 μ L	Control
1.	<i>S. aureus</i>	12	14	16	18	21
2.	<i>E.coli</i>	14	16	18	20	18
3.	<i>C. albicans</i>	11	13	15	16	20
4.	<i>A.niger</i>	12	14	16	18	22

Table 3.1: Zone of inhibition MA6

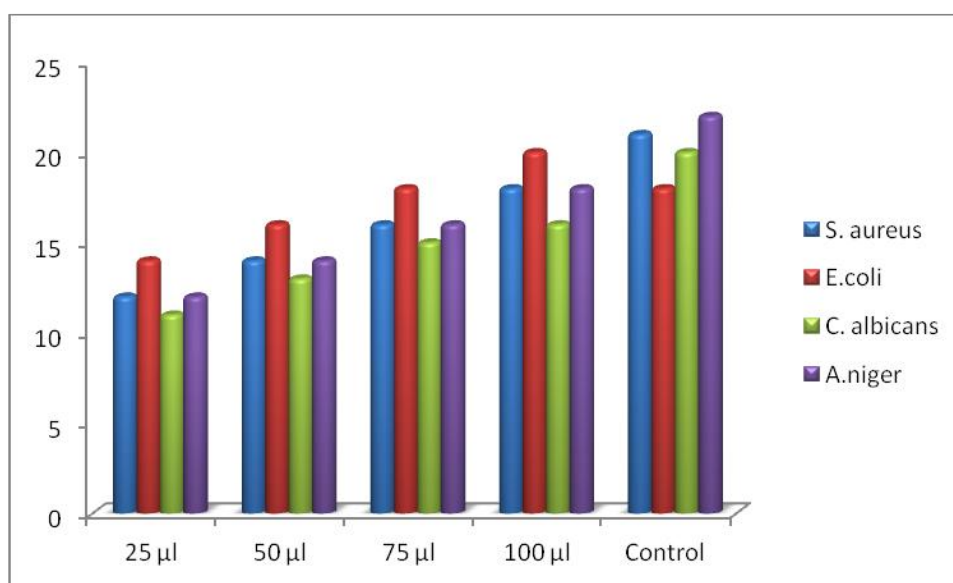


Fig.3.5.1.

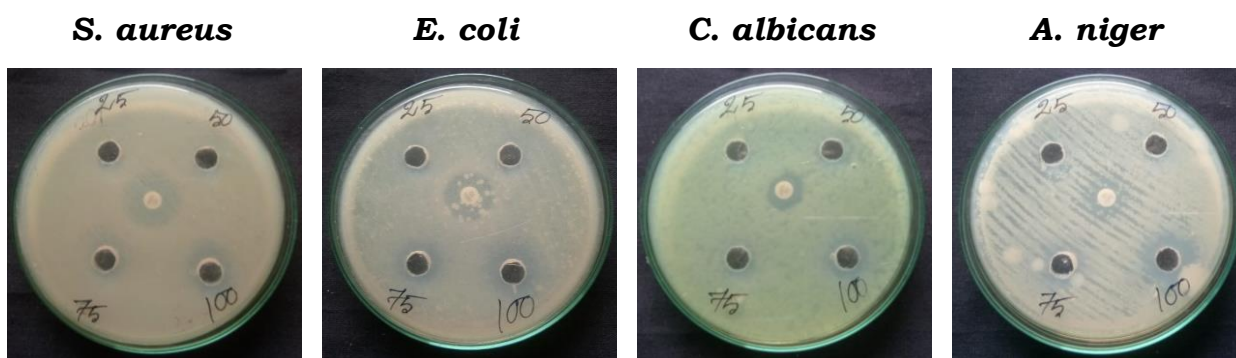


Fig.3.5.2.

Fig.3.5.3.

Fig.3.5.4.

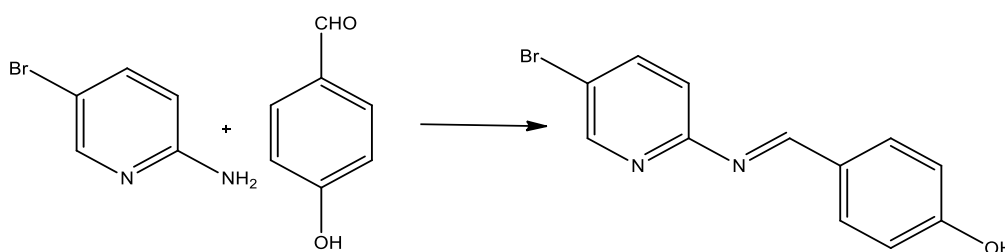
Fig.3.5.5.

Fig.3.5.1-3.5.5.Zone of inhibition MA6

3.2. Synthesis of 4-(((5-bromopyridin-2-yl)imino)methyl)phenol

(MA7)

To the ethanolic solution of 4-hydroxybenzaldehyde (12.2 g, 0.1 M), 2-amino-5-bromopyridine (17.3 g, 0.1 M) was added. The reaction mixture was refluxed for 6 h, cooled and poured into a beaker containing crushed ice. The solid separated out was washed, filtered and dried over vacuum and recrystallized using absolute ethanol. (Yellow solid; M.P: 112 °C)



Scheme 3.2: Synthesis of 4-(((5-bromopyridin-2-yl)imino)methyl)phenol (MA7)

3.2.1. IR spectrum of 4-(((5-bromopyridin-2-yl)imino)methyl)phenol

(MA7)

FT-IR spectrum of the compound MA7 has been given in the Fig. 3.6. A band at 3453 cm^{-1} shows the OH stretching. Aromatic CH stretching frequency is noticed by a band at 3022. C-H and C=N stretching of azomethine are indicated by the band at 2937 and 1628 cm^{-1} respectively. A sharp band appears at 635 cm^{-1} is due to C-Br stretching.

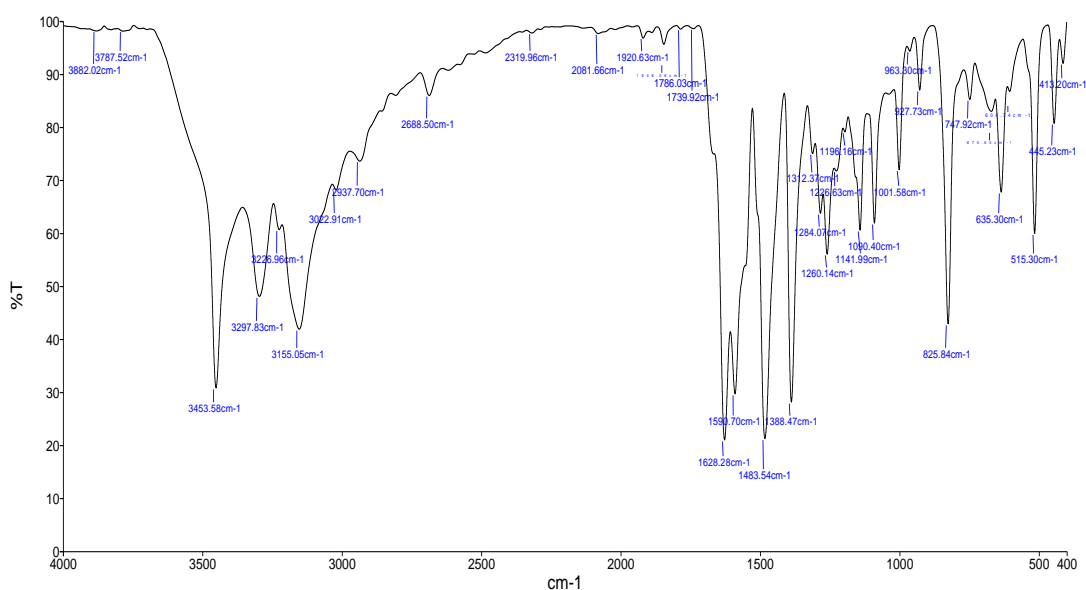


Fig.3.6. IR spectrum of 4-(((5-bromopyridin-2-yl)imino)methyl)phenol (MA7)

3.2.2. ¹H-NMR spectrum of 4-(((5-bromopyridin-2-yl)imino)methyl)phenol (MA7)

¹H-NMR spectrum of the compound MA7 has been represented in the Fig. 3.7. A peak appeared at 8.9 ppm is assigned to OH proton. Aromatic protons are indicated by signals ranging from 7.9 to 6.4 ppm. Methine proton shows a peak at 6.1 ppm.

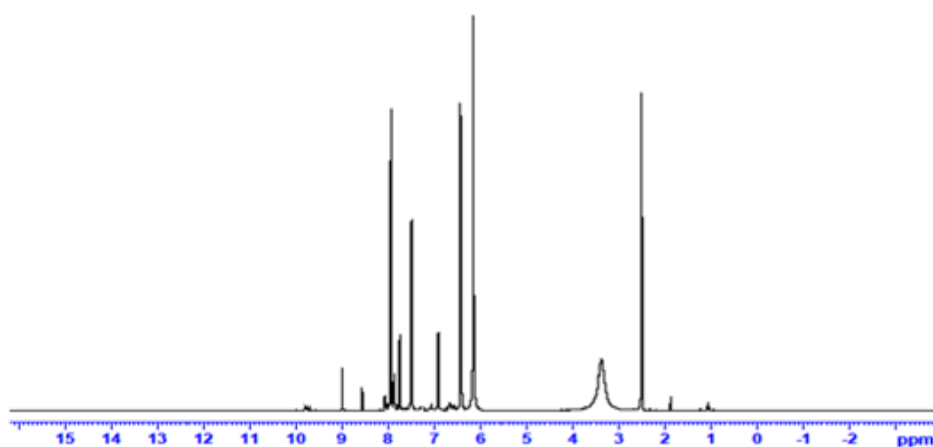


Fig.3.7. ¹H-NMR spectrum of 4-(((5-bromopyridin-2-yl)imino)methyl)phenol (MA7)

3.2.3. ^{13}C -NMR spectrum of 4-(((5-bromopyridin-2-yl)imino)methyl)phenol (MA7)

^{13}C -NMR spectrum of MA7 has been given in the Fig.3.8. A peak appears at 166.2 ppm indicates the carbon in which the OH group is bonded in the phenyl ring. Azomethine carbons exhibit signals at 158 ppm. The signals range from 116-127 ppm is assigned to aromatic carbons. The carbon in which the bromine atom is bonded in the phenyl ring is indicated by the signal at 111.

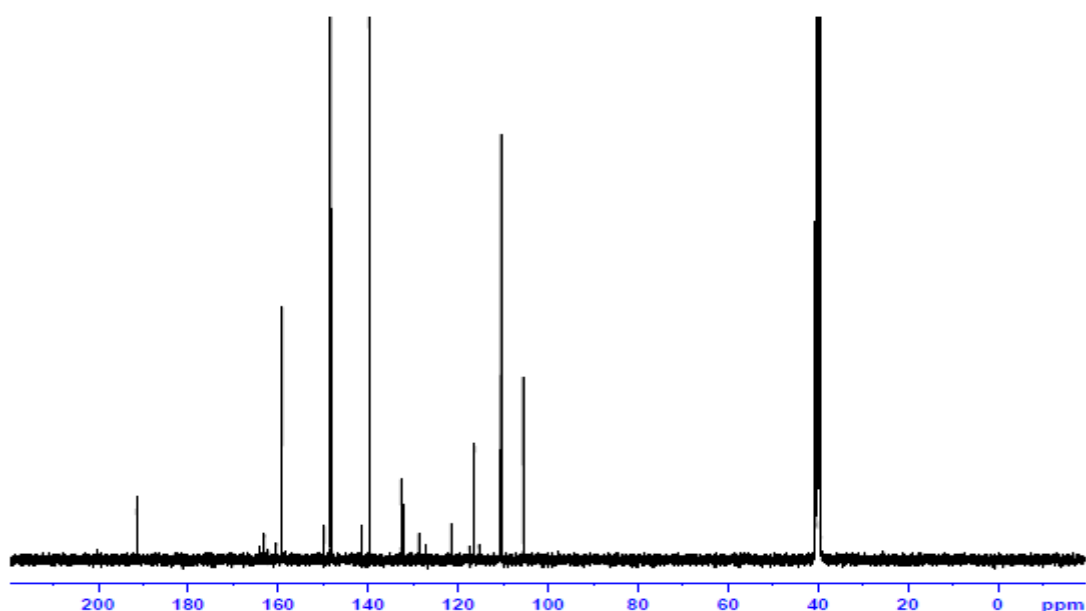


Fig.3.8. ^{13}C -NMR spectrum of 4-(((5-bromopyridin-2-yl)imino)methyl)phenol (MA7)

3.2.4. Mass spectrum of 4-(((5-bromopyridin-2-yl)imino)methyl)phenol (MA7)

Mass spectra of the compound MA7 has been given in the Fig. 3.9. The peak noticed at m/z 276 indicates the molecular ion peak. The intensity of the peak shows that the molecular ion peak itself is the base peak.

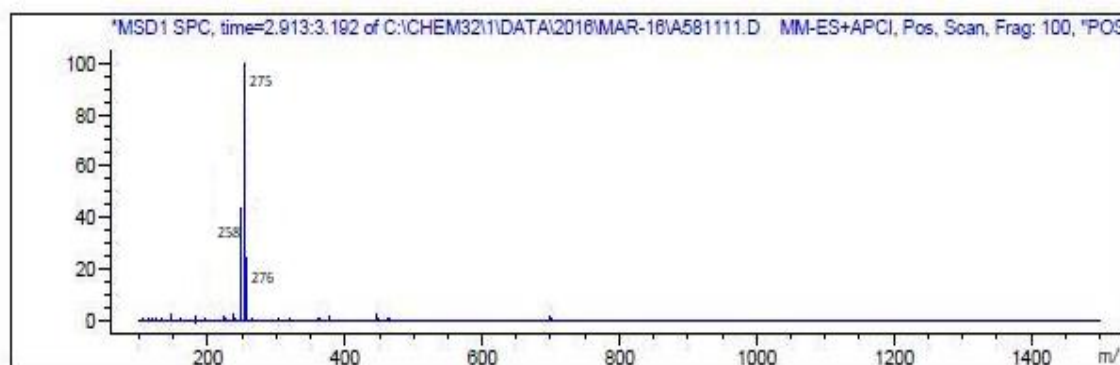


Fig. 3.9. Mass spectrum of 4-(((5-bromopyridin-2-yl)imino)methyl)phenol (MA7)

3.2.5. Antimicrobial evaluation of MA7

The results of antimicrobial evaluation depicted in the Table 3.2 and Fig 3.10 shows that the compound MA7 possess less activity against *S.aureus* and considerable activity against *C.albicans* and *A. niger*. Activity of the compound is found to be maximum in the case of gram positive bacteria than the gram negative bacteria. The compound exhibits greater activity against *E.coli* than the standard drug employed. The compound possesses excellent antibacterial activity than the antifungal activity.

S.No	Pathogen	Zone of inhibition (mm/mL)				
		25 μ L	50 μ L	75 μ L	100 μ L	Control
1.	<i>S. aureus</i>	10	12	14	16	21
2.	<i>E.coli</i>	12	14	16	18	18
3.	<i>C. albicans</i>	12	15	17	19	20
4.	<i>A.niger</i>	12	15	18	20	22

Table 3.2: Zone of inhibition MA7

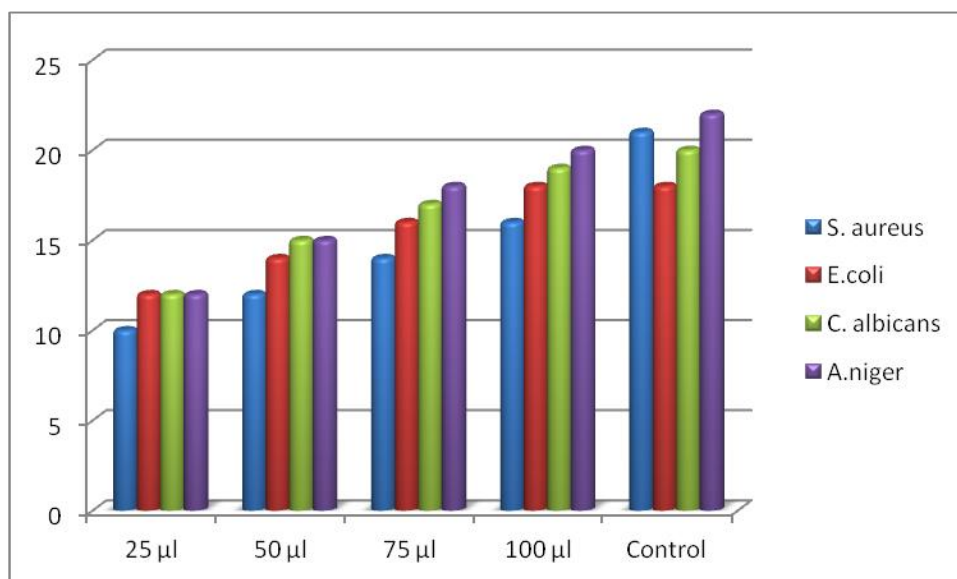


Fig.3.10.1

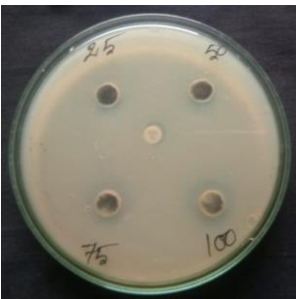
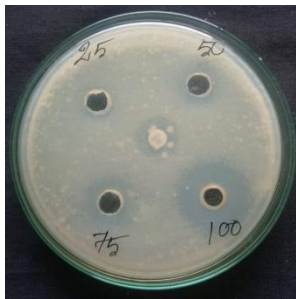
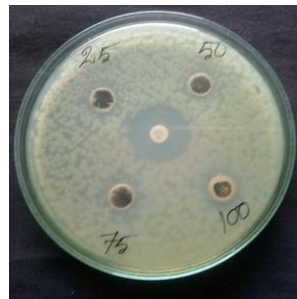

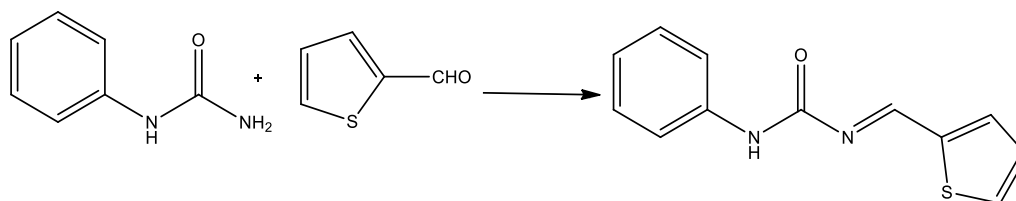
<i>S. aureus</i>	<i>E. coli</i>	<i>C. albicans</i>	<i>A. niger</i>
			
Fig.3.10.2	Fig.3.10.3	Fig.3.10.4	Fig.3.10.5

Fig.3.10.1-3.10.5 Zone of inhibition MA7

3.3. Synthesis of 1-phenyl-3-(thiophen-2-ylmethylene)urea (MA8)

To the ethanolic solution of thiophene-2-carboxaldehyde (9.3 mL, 0.1 M), N-phenyl urea (24.0 g, 0.1 M) was added. The reaction mixture was refluxed for 6 h, cooled and poured into a beaker containing crushed ice. The solid separated out was washed, filtered and dried over vacuum and recrystallized using absolute ethanol. (Silky solid; M.P: 142 °C).



Scheme 3.3: Synthesis of 1-phenyl-3-(thiophen-2-ylmethylene)urea (MA8)

3.3.1. IR spectrum of 1-phenyl-3-(thiophen-2-ylmethylene)urea (MA8)

Fig 3.11 represents the FT-IR spectrum of the compound MA8. It shows a sharp band at 3221 cm^{-1} which indicates the NH stretching. Aromatic CH stretching frequency is exhibited by a band at 3061 . C-H stretching of azomethine is indicated by a band at 1614 . Carbonyl stretching is noticed by a band at 1655 cm^{-1} . Appearance of a band at 773 cm^{-1} indicates the C-S stretching.

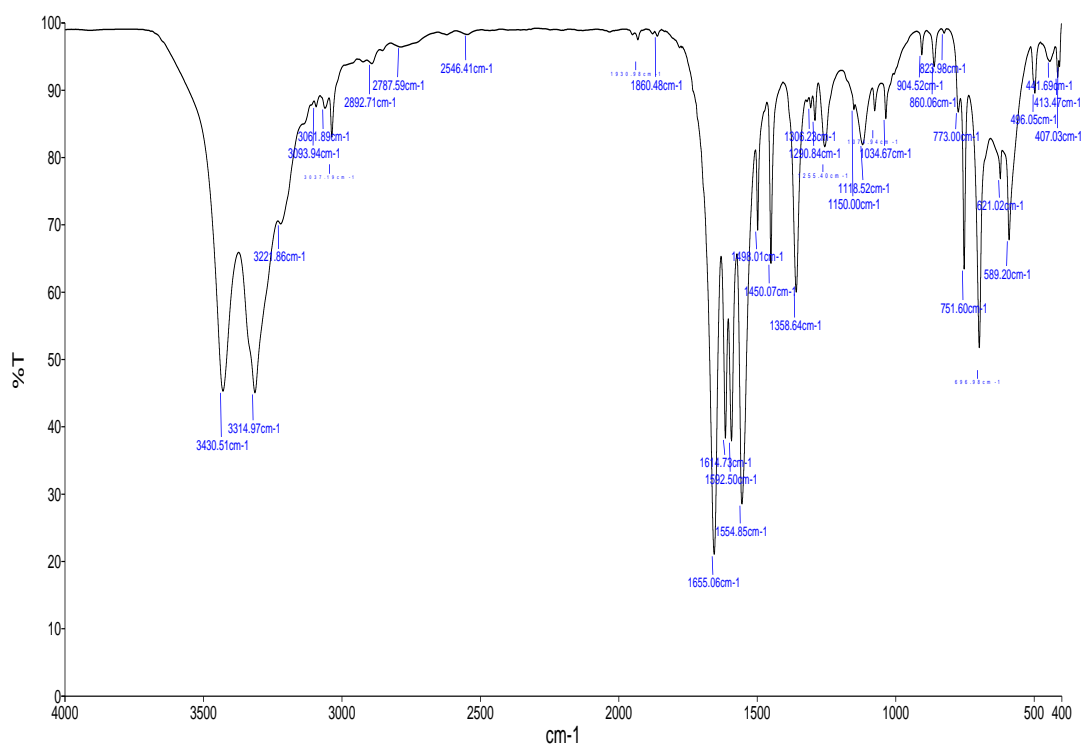


Fig.3.11. IR spectrum of 1-phenyl-3-(thiophen-2-ylmethylene)urea (MA8)

3.3.2. ¹H-NMR spectrum of 1-phenyl-3-(thiophen-2-ylmethylene)urea (MA8)

¹H-NMR spectrum of the compound MA8 is shown in the Fig 3.12. A peak noticed at 9.6 ppm accounts NH proton. Aromatic protons exhibit signals from 6.9 to 7.9 ppm. Presence of a peak at 6.2 ppm reveals azomethine proton.

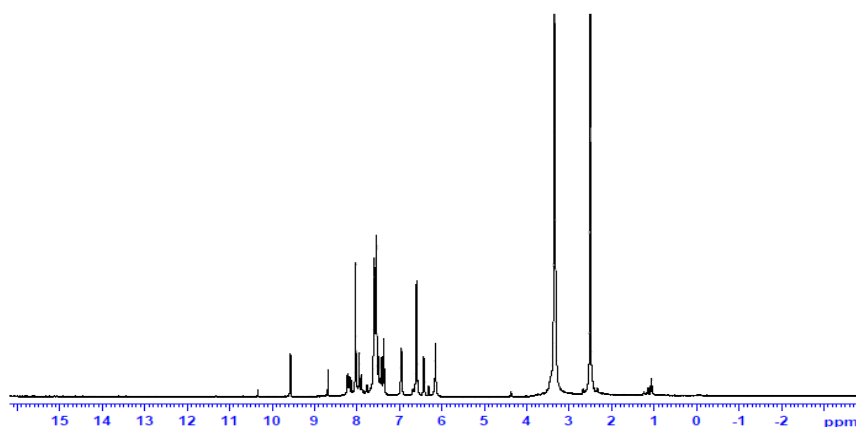


Fig.3.12. ¹H-NMR spectrum of 1-phenyl-3-(thiophen-2-ylmethylene)urea (MA8)

3.3.3. ¹³C-NMR spectrum of 1-phenyl-3-(thiophen-2-ylmethylene)urea (MA8)

¹³C-NMR spectrum of MA8 is shown in the Fig 3.13 has a peak at 162 ppm is due to azomethine carbon. The signal at 159 is attributed to carbonyl carbon. The presence of aromatic carbons is indicated by the peaks ranges from 117-135 ppm.

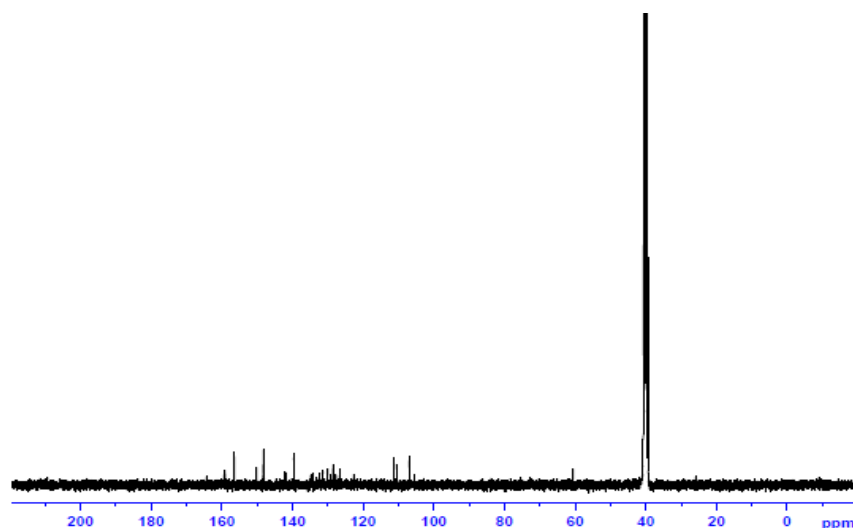


Fig.3.13. ^{13}C -NMR spectrum of 1-phenyl-3-(thiophen-2-ylmethylene)urea (MA8)

3.3.4. Mass spectrum of 1-phenyl-3-(thiophen-2-ylmethylene)urea (MA8)

Mass spectra of the compound MA8 is shown in the Fig.3.14. The peak observed at m/z 230.05 indicates the molecular ion peak. The peak appearing at m/z 153.02 with high intensity is the base peak.

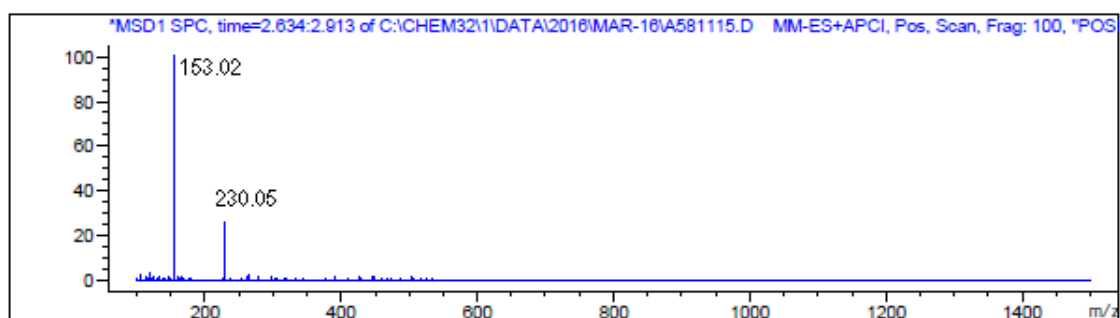
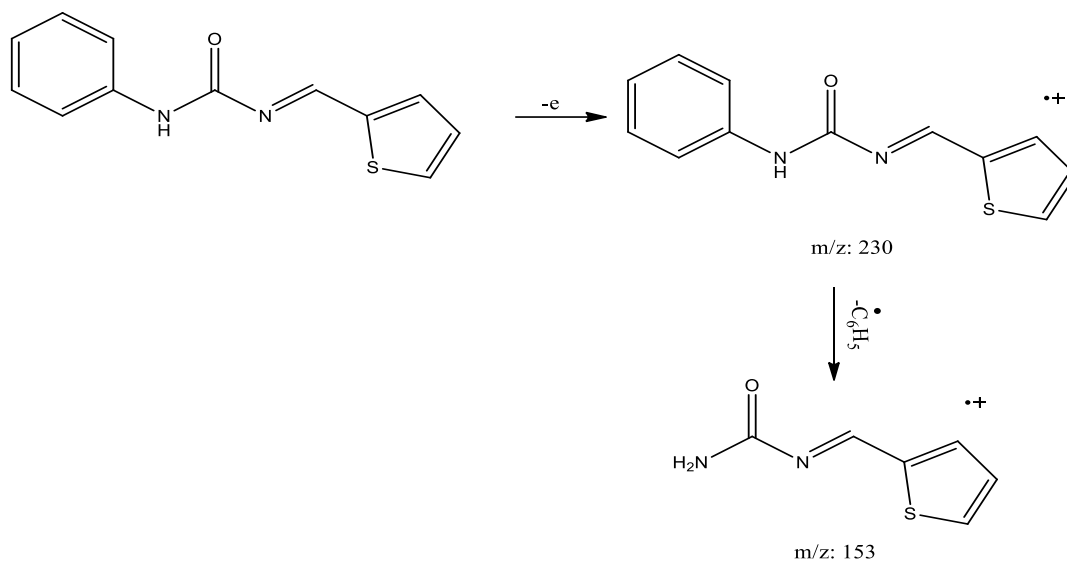


Fig.3.14. Mass spectrum of 1-phenyl-3-(thiophen-2-ylmethylene)urea (MA8)

Mass fragmentation



3.3.5. Antimicrobial evaluation of MA8

Results of antimicrobial screening of the compound MA8 are shown in the Table 3.3 and Fig 3.15.1-3.15.5 reveal that the compound possesses less activity against *C.albicans* and moderate activity against *A.niger* and *E.Coli*. Activity of the compound against *S.aureus* is found to be maximum when comparing to the positive standard. The compound is highly active against gram positive bacteria than the gram negative bacteria and fungi strains. Antibacterial activity of the compound is found to be higher than the antifungal activity.

S.No	Pathogen	Zone of inhibition (mm/mL)				
		25 μ L	50 μ L	75 μ L	100 μ L	Control
1.	<i>S. aureus</i>	13	16	18	20	21
2.	<i>E.coli</i>	10	12	14	16	18
3.	<i>C. albicans</i>	10	11	13	15	20
4.	<i>A.niger</i>	12	14	16	19	22

Table 3.3: Zone of inhibition of MA8

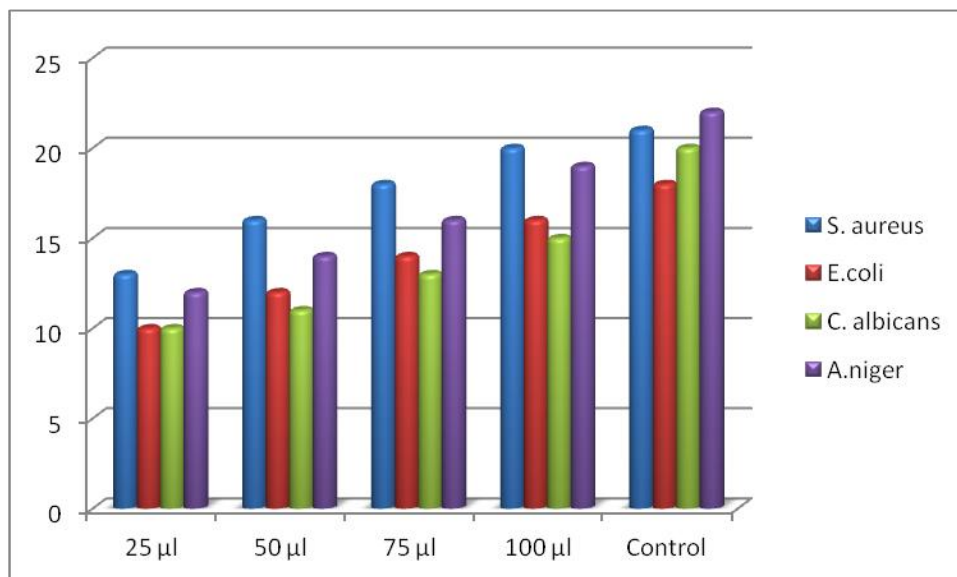


Fig.3.15.1

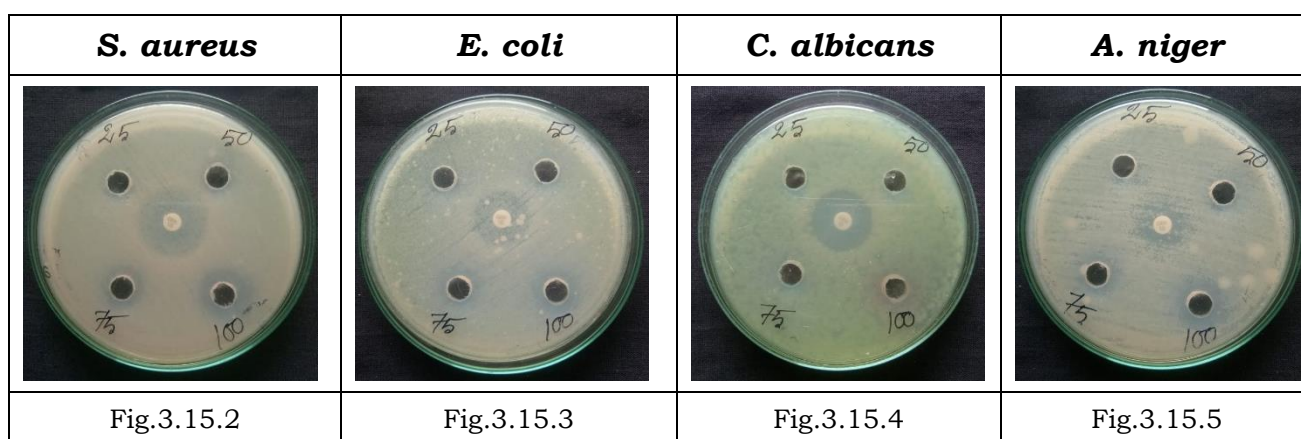
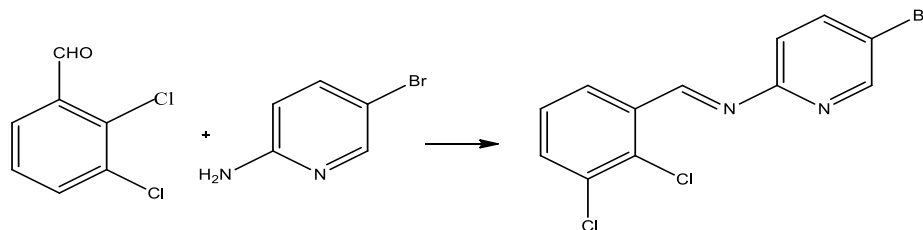


Fig.3.15.1-3.15.5.Zone of inhibition of MA8

3.4. Synthesis of 5-bromo-N-(2,3-dichlorobenzylidene)pyridin-2-amine (MA9)

To the ethanolic solution of 2, 3-dichlorobenzaldehyde (17.5 g, 0.1 M), 2-amino-5-bromopyridine (17.3 g, 0.1 M) was added. The reaction mixture was refluxed for 6 h, cooled and poured into a beaker containing crushed ice. The solid separated out was washed, filtered and dried over vacuum and recrystallized using absolute ethanol. (Ivory solid; M.P: 138 °C)



Scheme 3.4: Synthesis of 5-bromo-N-(2,3-dichlorobenzylidene)pyridin-2-amine (MA9)

3.4.1. IR spectrum of 5-bromo-N-(2,3-dichlorobenzylidene)pyridin-2-amine (MA9)

FT-IR spectrum of MA9 is shown in the Fig 3.16. A band noticed at 3050 cm^{-1} shows aromatic CH stretching. Azomethine C-H and C=N stretching frequency are indicated by the bands at 2961 and 1588 cm^{-1} respectively. The bands appeared at 747 and 712 cm^{-1} are due to C-Br and C-Cl stretching respectively.

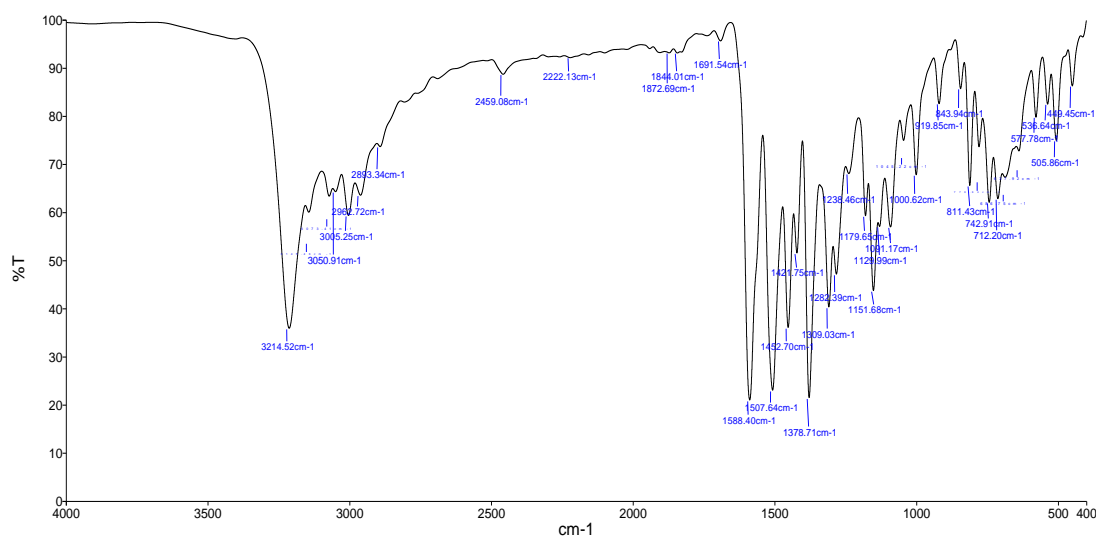


Fig.3.16. IR spectrum of 5-bromo-N-(2,3-dichlorobenzylidene)pyridin-2-amine (MA9)

3.4.2. ¹H-NMR spectrum of 5-bromo-N-(2,3-dichlorobenzylidene)pyridin-2-amine (MA9)

¹H-NMR spectrum of MA9 is shown in the Fig 3.17. The signals at 8.5 is indicating CH proton of azomethine. The signals exhibited from 6.1 to 7.8 ppm indicates the aromatic protons.

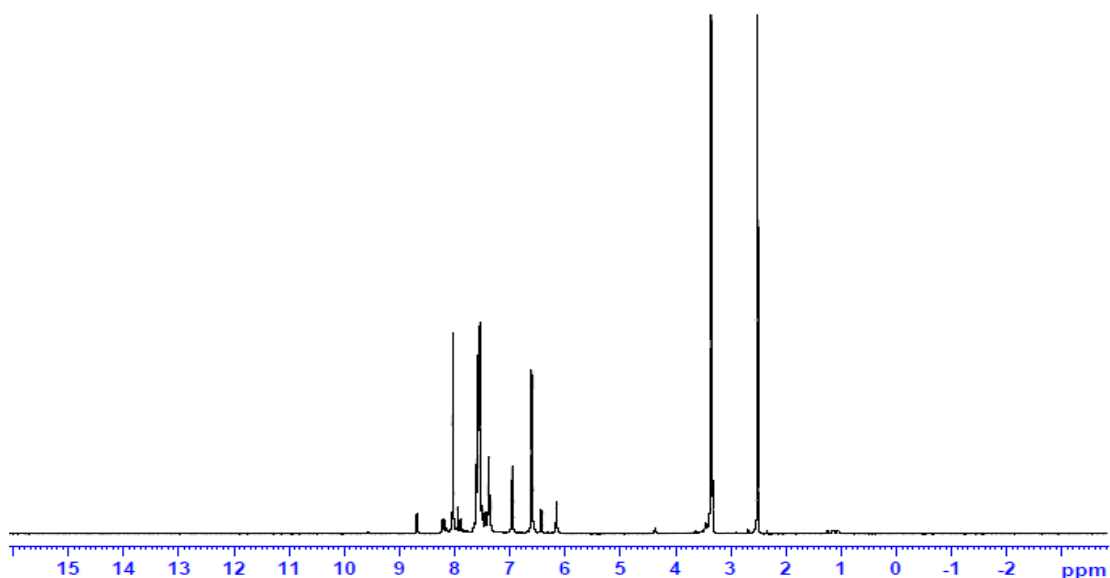


Fig.3.17. ¹H-NMR spectrum of 5-bromo-N-(2,3-dichlorobenzylidene)pyridin-2-amine (MA9)

3.4.3. ¹³C-NMR spectrum of 5-bromo-N-(2,3-dichlorobenzylidene)pyridin-2-amine (MA9)

¹³C-NMR spectrum of MA9 is shown in the Fig 3.18. A peak appears at 160 ppm is due to azomethine carbon. The peaks noticed at 142, 113 ppm are indicating the carbons in which chlorine and bromine atoms attached to the phenyl ring respectively. The signals appeared in the range of 126 to 140 ppm are due to aromatic carbons.

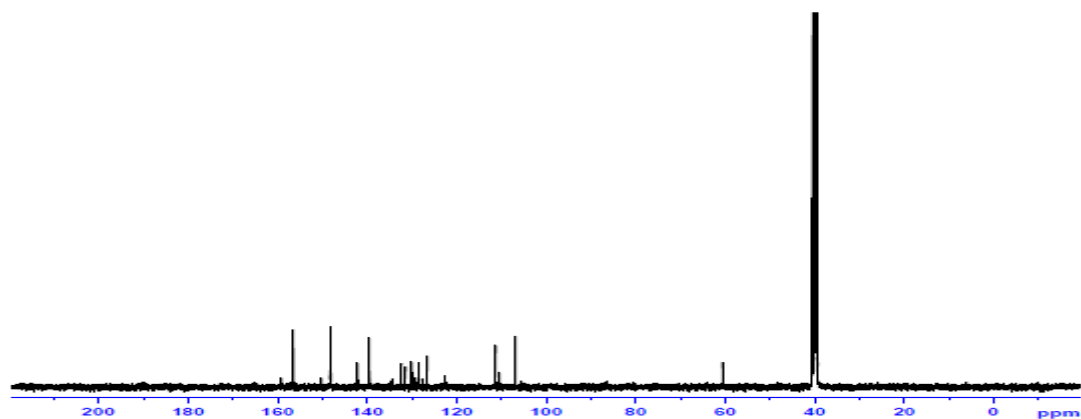


Fig.3.18. ^{13}C -NMR spectrum of 5-bromo-N-(2,3-dichlorobenzylidene)pyridin-2-amine (MA9)

3.4.4. Mass spectrum of 5-bromo-N-(2,3-dichlorobenzylidene)pyridin-2-amine (MA9)

Fig. 3.19 represents the mass spectra of the compound MA9. The molecular ion peak appearing at m/z 327.92 confirms the calculated molecular mass of the compound. The peak appearing with high intensity at m/z 187.0 is the base peak.

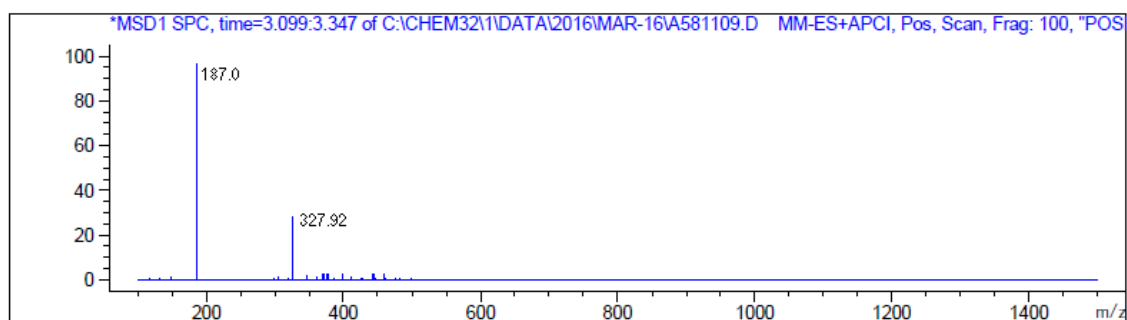


Fig.3.19. Mass spectrum of 5-bromo-N-(2,3-dichlorobenzylidene)pyridin-2-amine (MA9)

3.4.5. Antimicrobial evaluation of MA9

Zone of inhibition of the compound MA9 given in the Table 3.4 and Fig 3.20.1-3.20.5 reveal that the compound exhibits lesser activity against *C. albicans* and moderate against *E. Coli* and *S. aureus*. Potency of the compound is found to be high against *A.niger*. Further it is revealed that the compound is found to be potent against fungi strain than the bacterial strains when compared to the positive standard.

S.No	Pathogen	Zone of inhibition (mm/mL)				
		25 μ L	50 μ L	75 μ L	100 μ L	Control
1.	<i>S. aureus</i>	12	14	16	18	21
2.	<i>E.coli</i>	10	14	14	16	18
3.	<i>C. albicans</i>	10	12	14	16	20
4.	<i>A.niger</i>	12	15	18	20	22

Table 3.4: Zone of inhibition of MA9

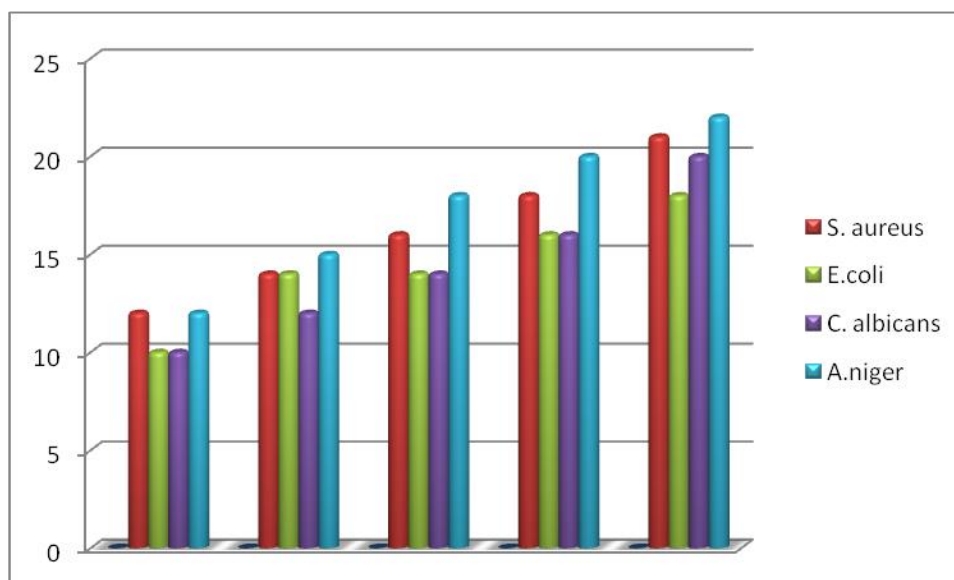


Fig.3.20.1


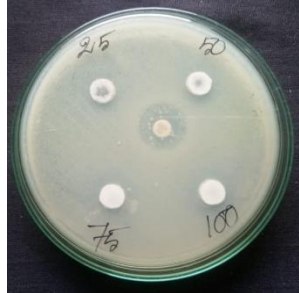
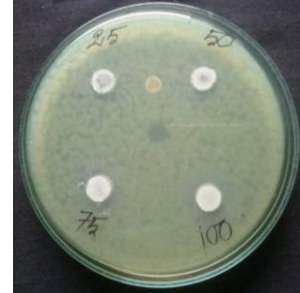

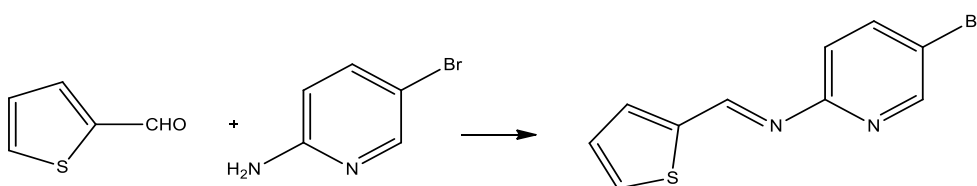
<i>S. aureus</i>	<i>E. coli</i>	<i>C. albicans</i>	<i>A. niger</i>
			
Fig.3.20.2	Fig.3.20.3	Fig.3.20.4	Fig.3.20.5

Fig.3.20.1-3.20.5.Zone of inhibition of MA9

3.5. Synthesis of 5-bromo-N-(thiophen-2-ylmethylene)pyridin-2-amine (MA10)

To the ethanolic solution of thiophene-2-carboxaldehyde (9.30 mL, 0.1 M), 2-amino-5-bromopyridine (17.3 g, 0.1 M) was added. The reaction mixture was refluxed for 6 h, cooled and poured into a beaker containing crushed ice. The solid separated out was washed, filtered and dried over vacuum and recrystallized using absolute ethanol. (Brown solid; M.P: 137 °C)



Scheme 3.5: Synthesis of 5-bromo-N-(thiophen-2-ylmethylene)pyridin-2-amine (MA10)

3.5.1. IR spectrum of 5-bromo-N-(thiophen-2-ylmethylene)pyridin-2-amine (MA10)

FT-IR spectrum of MA10 is shown in the Fig 3.21 exhibits a band at 3023 cm⁻¹ indicates the aromatic CH stretching. The bands at 2943

and 1588 cm^{-1} are due to C-H and C=N stretching vibrations respectively. Bands observed at 824 and 633 cm^{-1} are due to C-Br and C-S stretching respectively.

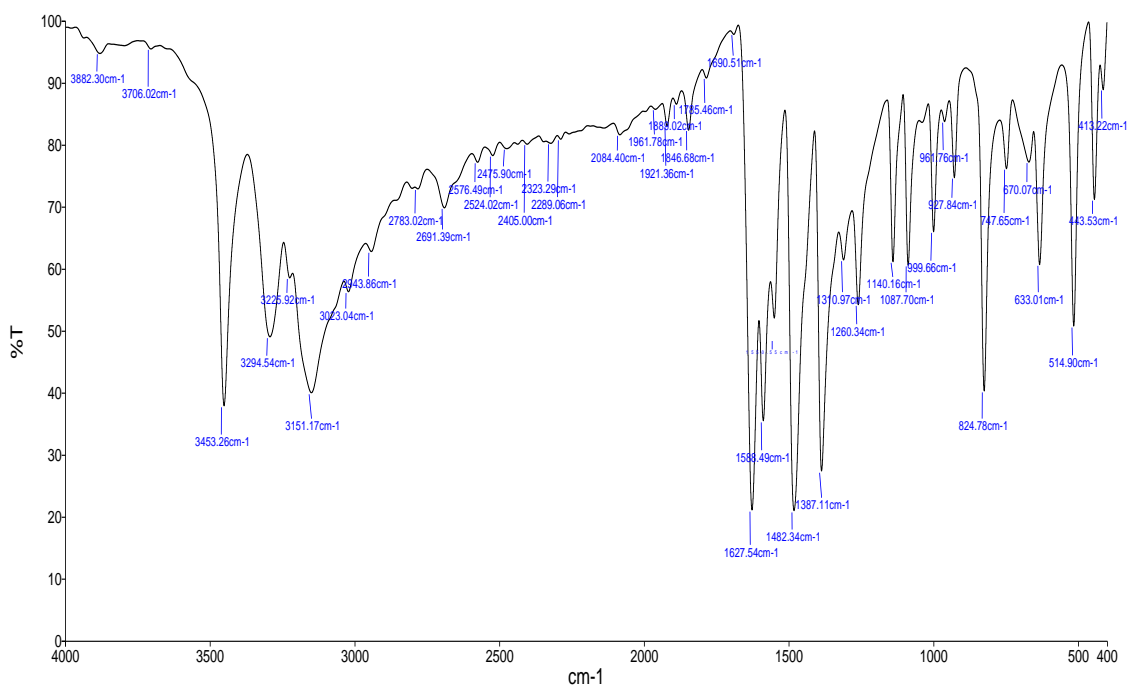


Fig.3.21. IR spectrum of 5-bromo-N-(thiophen-2-ylmethylene)pyridin-2-amine (MA10)

3.5.2.1H-NMR spectrum of 5-bromo-N-(thiophen-2-ylmethylene)pyridin-2-amine (MA10)

$^1\text{H-NMR}$ spectrum of MA10 has been given in the Fig 3.22. Azomethine proton noticed by a peak at 7.9 ppm. The signals ranging from 6.9 to 7.5 ppm are attributable to the aromatic protons.

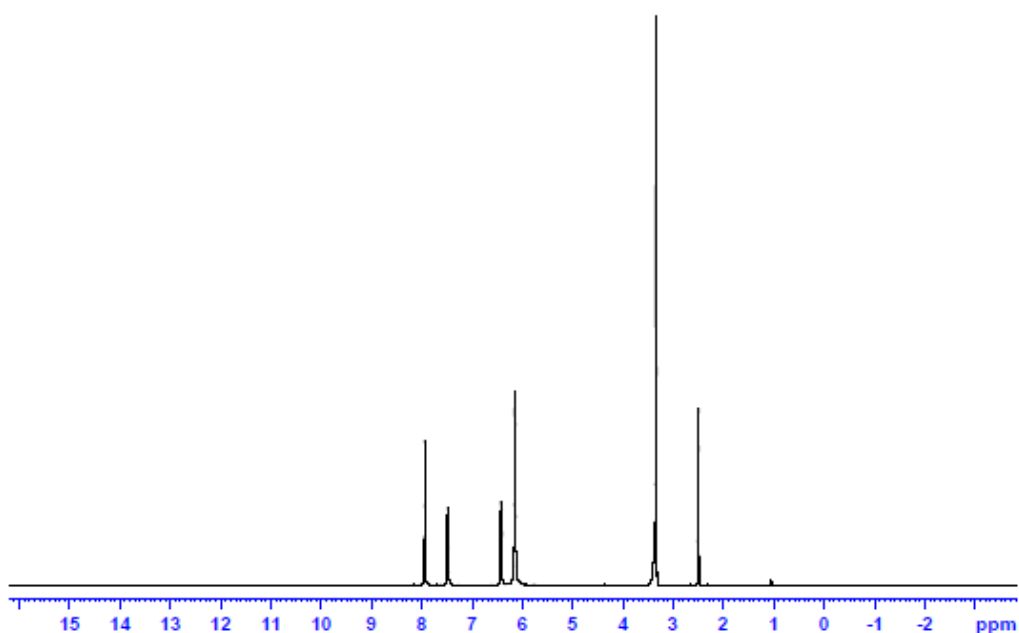


Fig.3.22. ^1H -NMR spectrum of 5-bromo-N-(thiophen-2-ylmethylene)pyridin-2-amine (MA10)

3.5.3. ^{13}C -NMR spectrum of 5-bromo-N-(thiophen-2-ylmethylene)pyridin-2-amine (MA10)

^{13}C -NMR of MA10 has been given in the Fig 3.23. A peak at 159 ppm indicates C=N carbon. The signals at 116, 139 and 147 ppm show the aromatic carbons. A peak at 113 ppm indicates the carbon in which the bromine atom is bonded in the phenyl ring.

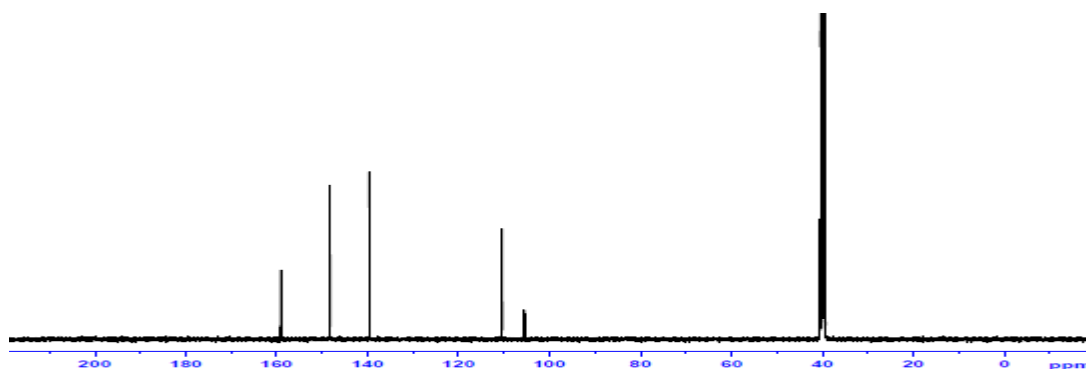


Fig.3.23. ^{13}C -NMR spectrum of 5-bromo-N-(thiophen-2-ylmethylene)pyridin-2-amine (MA10)

3.5.4. Mass spectrum of 5-bromo-N-(thiophen-2-ylmethylene)pyridin-2-amine (MA10)

Mass spectrum of the compound MA10 has been depicted in the Fig. 3.24. The peak appearing at m/z 265.95 is the molecular ion peak. The intense peak noticed at m/z 197.98 is assigned as base peak.

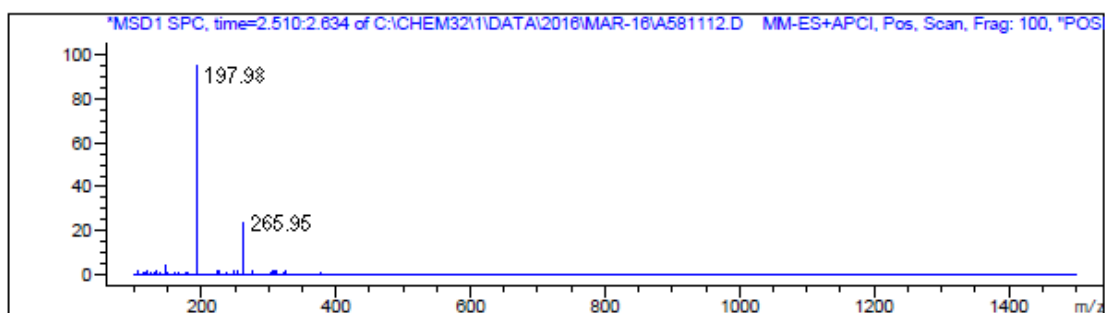


Fig.3.24. Mass spectrum of 5-bromo-N-(thiophen-2-ylmethylene)pyridin-2-amine (MA10)

3.5.4. Antimicrobial evaluation of MA10

The compound MA10 possesses excellent antimicrobial activity against all the tested bacterial and fungi pathogens when compared to the positive standard. Potency of the compound is found to be very high against gram negative bacteria and fungi pathogen. The compound shows equally higher activity on comparing both bacteria and fungi pathogen hence it is observed that the compound may possess broad spectrum antimicrobial activity. The results are shown in the Table 3.5 and in the Fig. 3.25.1-3.25.5

S. No	Pathogen	Zone of inhibition (mm/mL)				
		25 μ L	50 μ L	75 μ L	100 μ L	Control
1.	<i>S. aureus</i>	16	19	21	23	21
2.	<i>E.coli</i>	15	17	20	22	18
3.	<i>C. albicans</i>	14	17	20	22	20
4.	<i>A.niger</i>	16	19	22	25	22

Table 3.5: Zone of inhibition of MA10

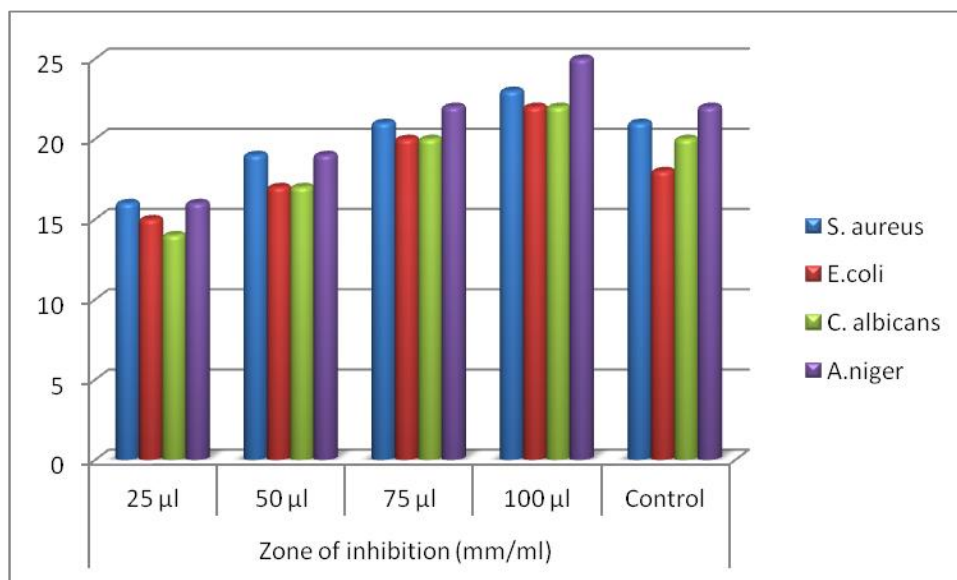


Fig.3.25.1

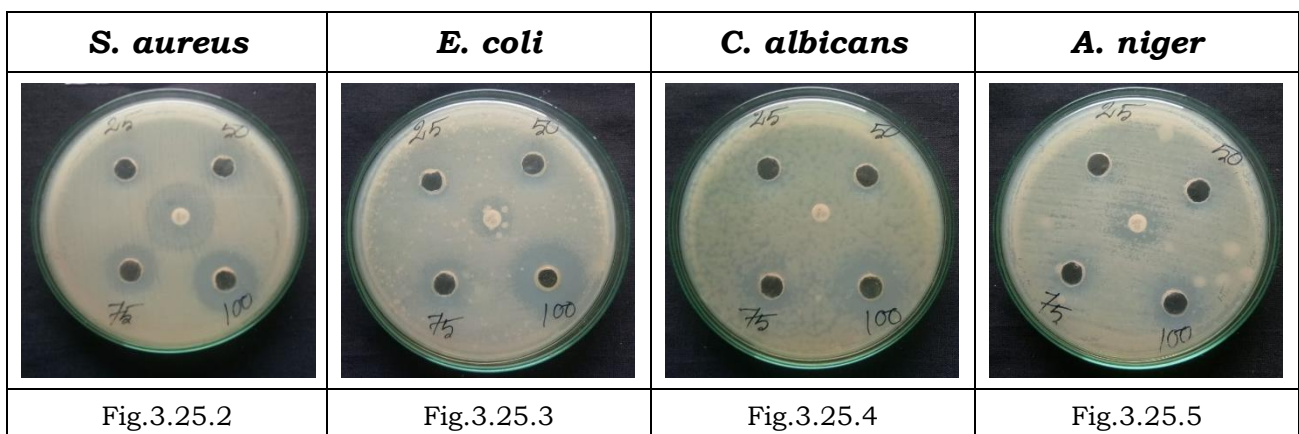
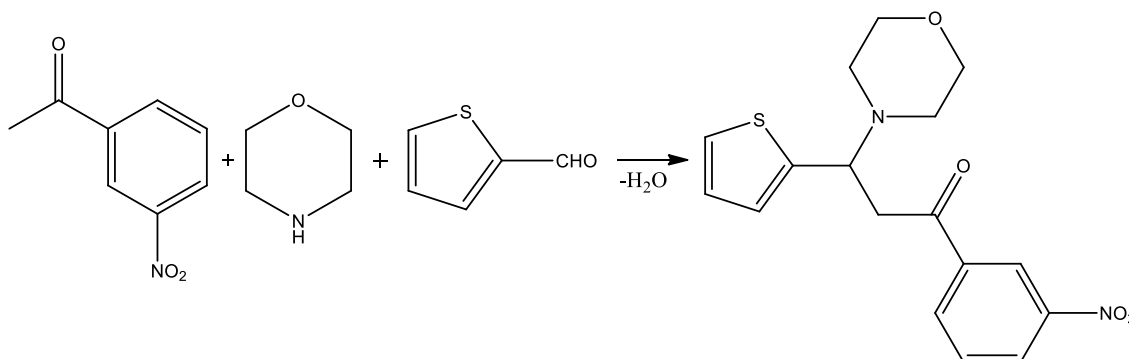


Fig.3.25.1-3.25.5.Zone of inhibition of MA10

Synthesis of β -amino carbonyl compounds using Mannich reaction (MA11-MA13)

4.1. Synthesis of 3-morpholino-1-(3-nitrophenyl)-3-(thiophen-2-yl)propan-1-one (MA11)

To the ethanolic solution of 3-nitro acetophenone, morpholine was added followed by thiophene-2-carboxaldehyde (9.3 mL, 0.1 M). The reaction mixture was kept at ice cold condition over a magnetic stirrer and stirred for about 3 h. The solid separated out was washed filtered and dried over vacuum. (Ivory solid; M.P: 142 °C)



Scheme 4.1: Synthesis of 3-morpholino-1-(3-nitrophenyl)-3-(thiophen-2-yl)propan-1-one (MA11)

4.1.1. IR spectrum of 3-morpholino-1-(3-nitrophenyl)-3-(thiophen-2-yl)propan-1-one (MA11)

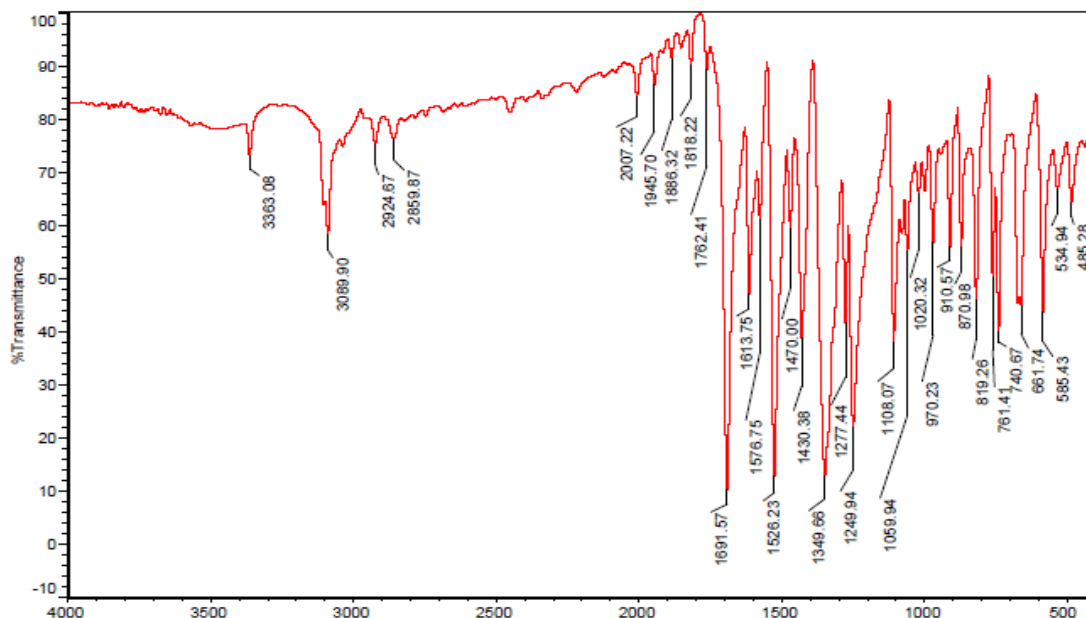


Fig.4.1. IR spectrum of 3-morpholino-1-(3-nitrophenyl)-3-(thiophen-2-yl)propan-1-one

The FT-IR spectrum of MA11 given in the Fig 4.1 shows a band at 3089 cm^{-1} is due to aromatic C-H stretching. C-S stretching of thiophene exhibits a band at 2924 cm^{-1} . C-H stretching of methine group observed at the range of 2859 cm^{-1} . A strong absorption band appeared at 1691 cm^{-1} is attributed to C=O stretching frequency. The band appeared at 1576 cm^{-1} shows the N-O vibrations. The frequency ranges at 1349 and 1059 cm^{-1} are assigned to C-N and C-O-C stretching of morpholine. A band noticed at 661 cm^{-1} is due to C-S stretching.

4.1.2. ¹H-NMR spectrum of 3-morpholino-1-(3-nitrophenyl)-3-(thiophen-2-yl)propan-1-one (MA11)

¹H NMR spectrum of MA11 has been depicted in the Fig 4.2 show peaks ranges from 6.7 to 7.9 ppm indicate the aromatic protons of phenyl and thiophene ring. Methine proton shows a peak at 4.5 ppm. CH₂ protons of morpholine are assigned by the signals at 3.4 and 2.8 ppm.

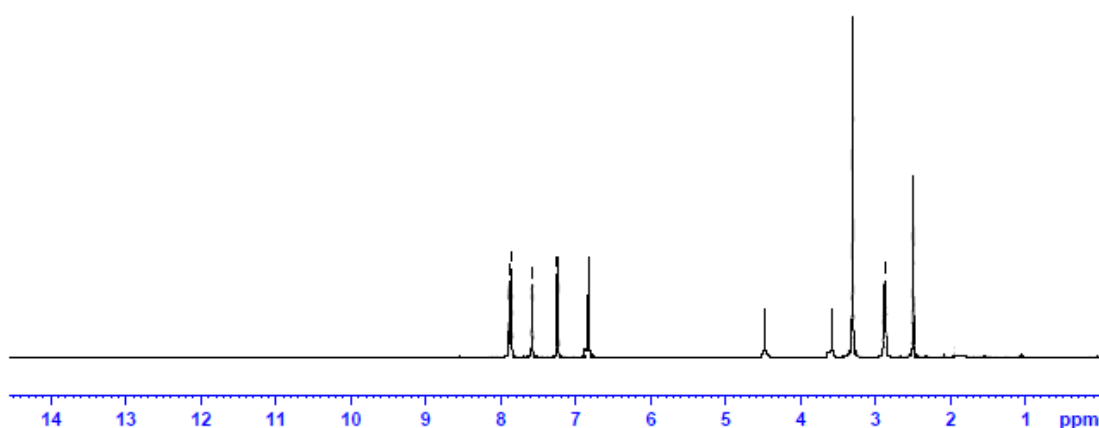


Fig.4.2. ¹H-NMR spectrum of 3-morpholino-1-(3-nitrophenyl)-3-(thiophen-2-yl)propan-1-one (MA11)

4.1.2. ¹³C-NMR spectrum of 3-morpholino-1-(3-nitrophenyl)-3-(thiophen-2-yl)propan-1-one (MA11)

¹³C NMR of MA11 has been given in the Fig 4.3. Carbonyl carbon of the compound is indicated by a signal at 196 ppm. Aromatic carbons of phenyl and thiophene ring shows the signal ranges from 137 to 122 ppm. The peaks obtained at 62 and 52 ppm are due to the carbons of morpholine. A peak appeared at 71 ppm shows the presence of methine carbon.

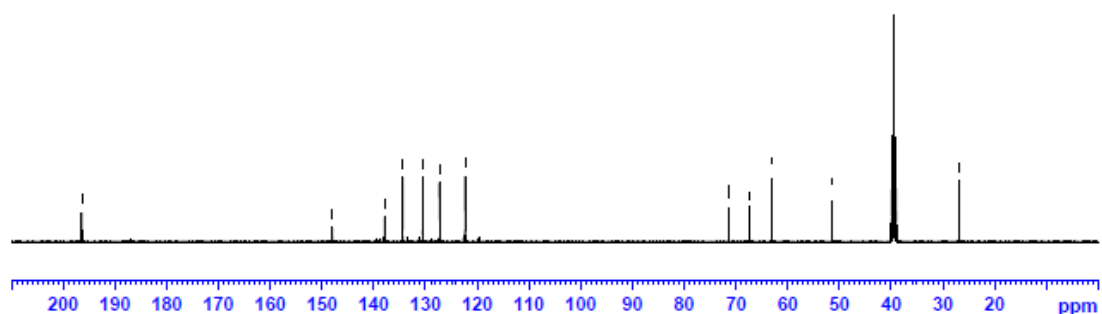


Fig.4.3. ^{13}C -NMR spectrum of 3-morpholino-1-(3-nitrophenyl)-3-(thiophen-2-yl)propan-1-one (MA11)

4.1.4. Mass spectrum of 3-morpholino-1-(3-nitrophenyl)-3-(thiophen-2-yl)propan-1-one (MA11)

The Mass spectrum of MA11 has been represented in the Fig 4.4. The molecular ion peak appeared at m/z 347.8 shows the exact mass of the compound. The highest intensity peak observed at 164 is the base peak.

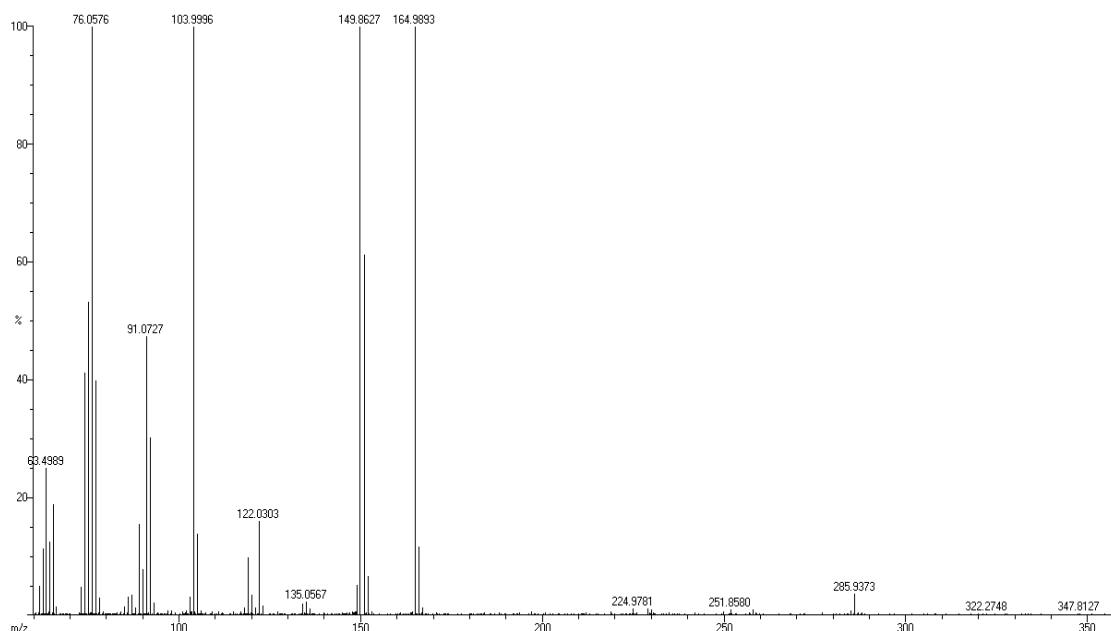


Fig.4.4. Mass spectrum of 3-morpholino-1-(3-nitrophenyl)-3-(thiophen-2-yl)propan-1-one (MA11)

4.1.5. Antimicrobial evaluation of MA11

Results of antimicrobial screening of the compound MA11 are shown in the Table 4.1 and Fig 4.5, reveal that the compound possesses less activity against *A.niger* and *Moraxella*. Activity of the compound against *B. subtilis* and *Trichophyton* is found to be moderate as compared to the positive standards. The compound is highly active against gram positive bacteria than the gram negative bacteria. Antifungal activity of the compound is found to be higher than the antibacterial activity.

S. No.	Pathogens	Zone of inhibition (mm/ μ L)				
		25 μ L	50 μ L	75 μ L	100 μ L	Control
1.	<i>B. subtilis</i>	18	21	23	26	30
2.	<i>Moraxella</i>	13	14	15	16	30
3.	<i>A. niger</i>	9	10	11	12	30
4.	<i>Trichophyton</i>	9	10	12	15	18

Table 4.1: Zone of inhibition of MA11

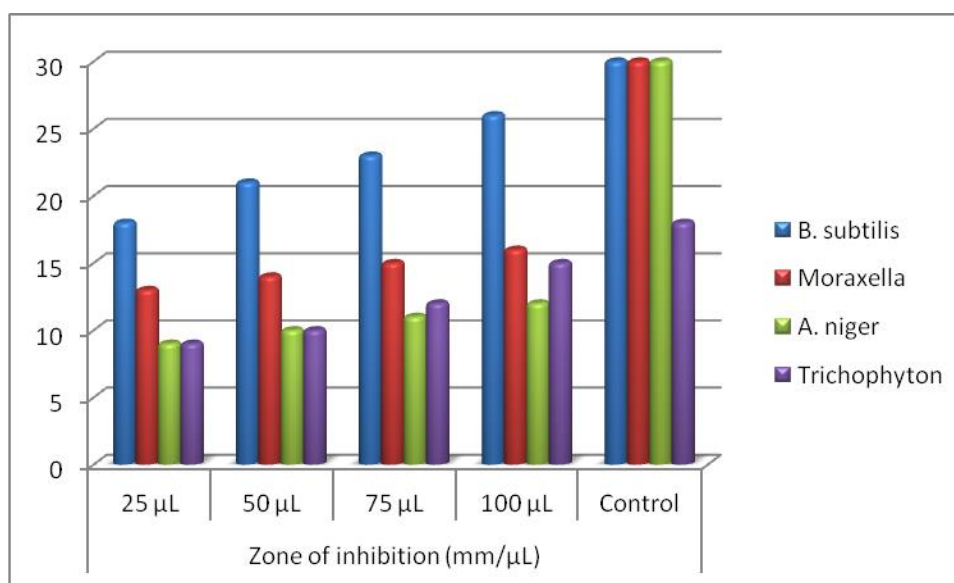
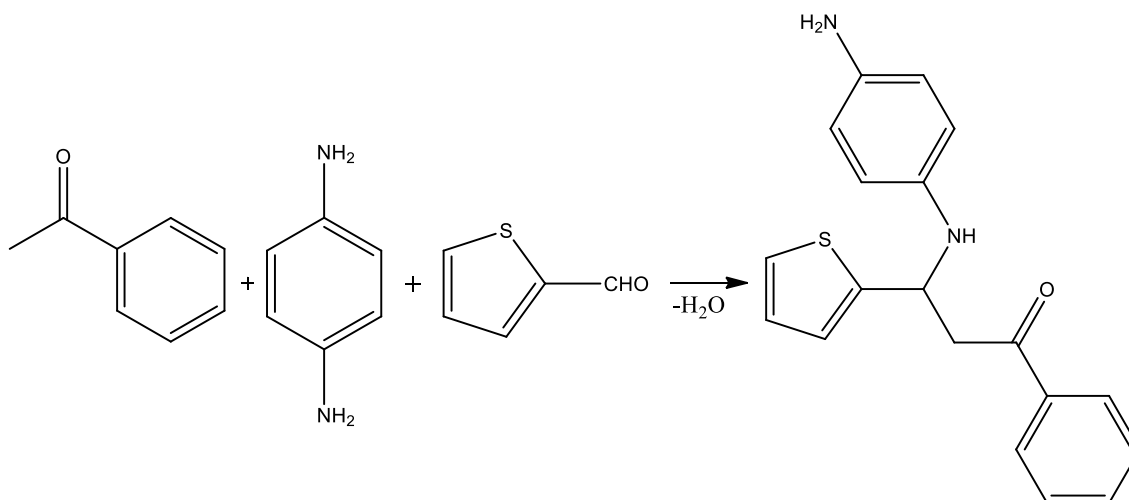


Fig.4.5: Zone of inhibition of MA11

4.2. Synthesis of 3-((4-aminophenyl)amino)-1-phenyl-3-(thiophen-2-yl)propan-1-one (MA12)

To the ethanolic solution of acetophenone, p-Phenylene diammine (10.8 g, 0.1 M) was added followed by thiophene-2-carboxaldehyde (9.3 mL, 0.1 M). The reaction mixture was kept at ice cold condition over a magnetic stirrer and stirred for about 7 h. The solid separated out was washed filtered and dried over vacuum. (Colour: Yellow solid; M.P: 151 °C)



Scheme 4.2: Synthesis of 3-((4-aminophenyl)amino)-1-phenyl-3-(thiophen-2-yl)propan-1-one (MA12)

4.2.1. IR spectrum of 3-((4-aminophenyl)amino)-1-phenyl-3-(thiophen-2-yl)propan-1-one (MA12)

FT-IR spectrum of MA12 is shown in the Fig 4.6. NH stretching is noticed by a band at 3396 cm^{-1} . Aromatic CH and C=C stretching frequencies are exhibited by the bands at 3026 and 1516 cm^{-1} respectively. A sharp absorption band at 1665 cm^{-1} is due to the carbonyl stretching of acetophenone.

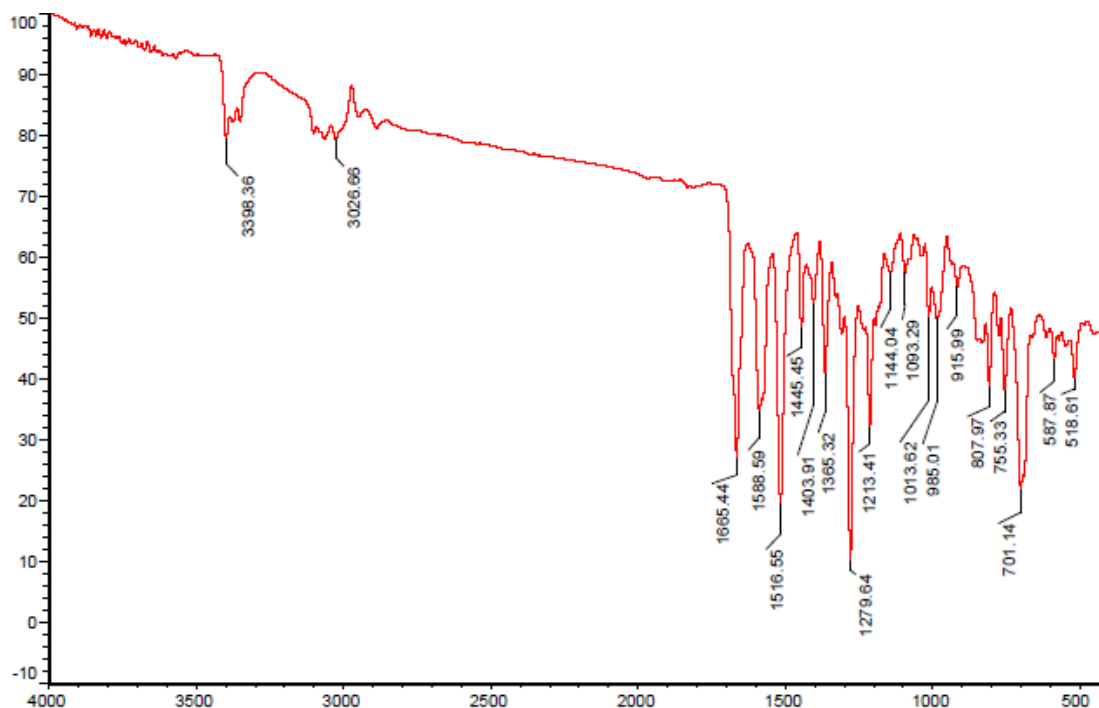


Fig.4.6. IR spectrum of 3-((4-aminophenyl)amino)-1-phenyl-3-(thiophen-2-yl)propan-1-one (MA12)

4.2.2. ¹H-NMR spectrum of 3-((4-aminophenyl)amino)-1-phenyl-3-(thiophen-2-yl)propan-1-one (MA12)

¹H-NMR spectrum of MA12 has been given in the Fig 4.7. The peaks appeared at 9.2 and 7.9 ppm indicates NH₂ and NH protons respectively. The signals range from 7.5 to 6.9 ppm represents the aromatic protons. A peak appears at 4.4 ppm is due to methine proton. The signals at 3.4 and 2.9 ppm are assigned to methine and methylene protons respectively.

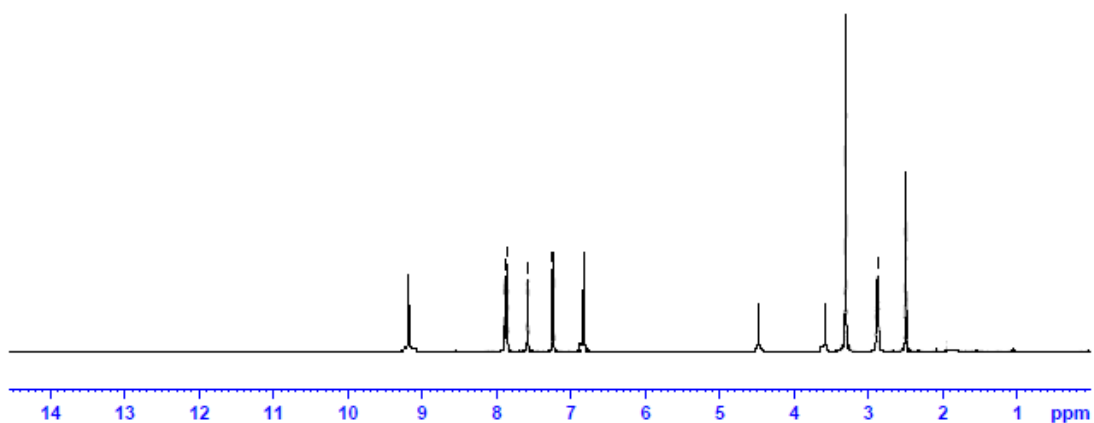


Fig.4.7. ^1H -NMR spectrum of 3-((4-aminophenyl)amino)-1-phenyl-3-(thiophen-2-yl)propan-1-one (MA12)

4.2.3. ^{13}C -NMR spectrum of 3-((4-aminophenyl)amino)-1-phenyl-3-(thiophen-2-yl)propan-1-one (MA12)

^{13}C -NMR spectrum of MA12 is shown in the Fig 4.8 has a peak at 199 ppm is due to carbonyl carbon. The signals from 135 to 127 ppm are attributed to the aromatic carbons. Methylene carbon exhibits a peak at 72 ppm. The presence of methine carbon is indicated by a peak at 58 ppm.

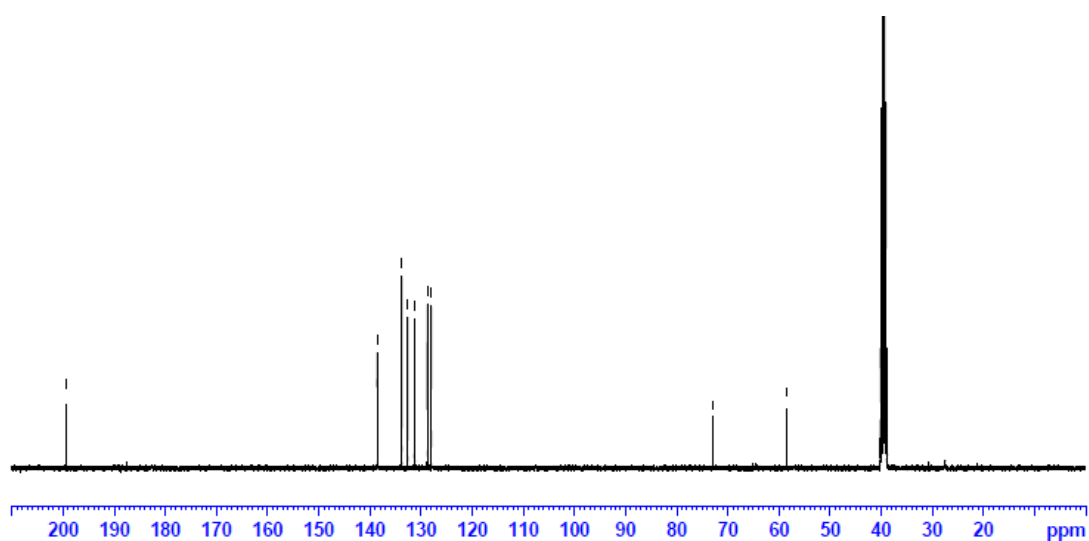


Fig.4.8. ^{13}C -NMR spectrum of 3-((4-aminophenyl)amino)-1-phenyl-3-(thiophen-2-yl)propan-1-one (MA12)

4.2.3. Mass spectrum of 3-((4-aminophenyl)amino)-1-phenyl-3-(thiophen-2-yl)propan-1-one (MA12)

Mass spectra of the compound MA12 is shown in the Fig. 4.9. The peak observed at m/z 321.97 indicates the molecular ion peak. The peak appearing at m/z 105.04 with high intensity is the base peak.

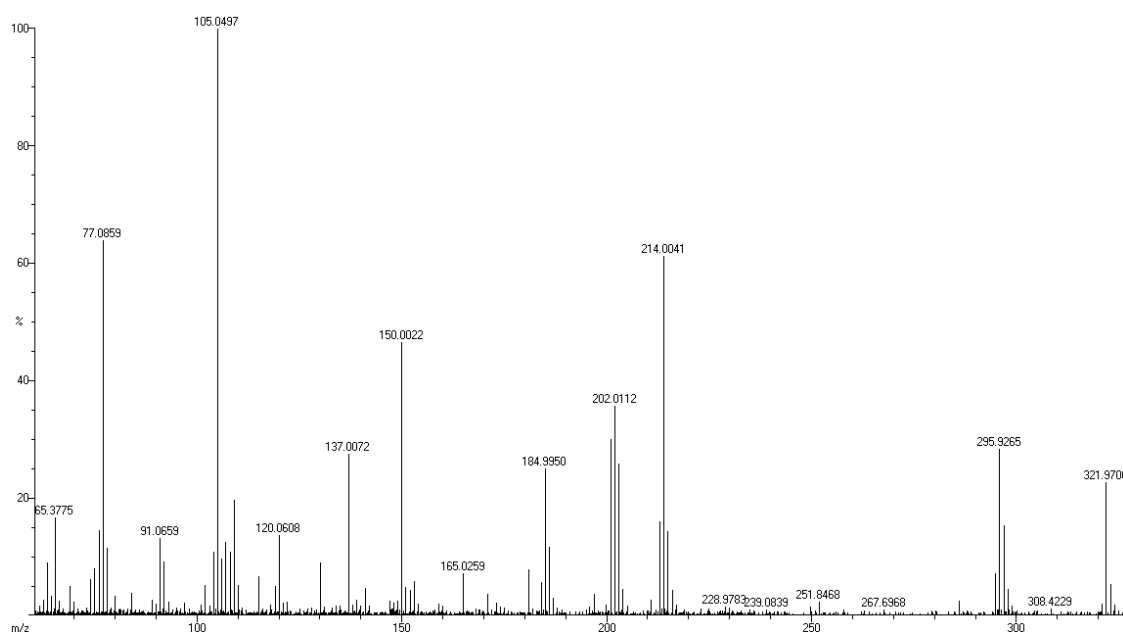


Fig.4.9. Mass spectrum of 3-((4-aminophenyl)amino)-1-phenyl-3-(thiophen-2-yl)propan-1-one (MA12)

4.2.5. Antimicrobial evaluation of MA12

The compound MA12 exhibits less activity against against *Moraxella*, *A.niger* and *trichophyton*. It has considerable activity against *B. subtilis* when compared to the positive standards. The compound is found to be more potent against fungi than the bacteria. Antifungal activity of the compound is found to be higher than the antibacterial activity. The results are shown in the Table 4.2 and Fig 4.10

S. No.	Pathogen	Zone of inhibition (mm/ μ L)				
		25 μ L	50 μ L	75 μ L	100 μ L	Control
1.	<i>B. subtilis</i>	10	12	15	18	32
2.	<i>Moraxella</i>	-	9	10	11	30
3.	<i>A. niger</i>	11	13	14	15	28
4.	<i>Trichophyton</i>	-	10	11	13	20

Table 4.2: Zone of of inhibition of MA12

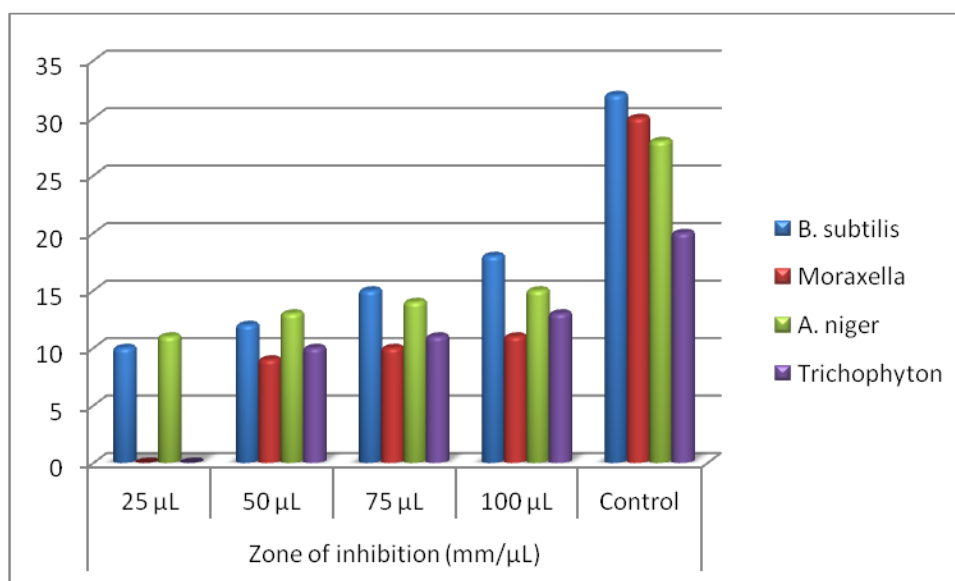
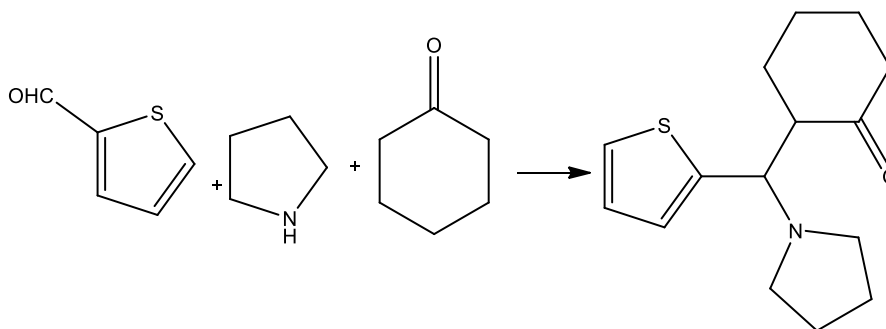


Fig.4.10.Zone of of inhibition of MA12

4.3. Synthesis of 2-(pyrrolidin-1-yl(thiophen-2-yl)methyl)cyclohexanone (MA13)

To the ethanolic solution of cyclohexanone, pyrrolidine (10.8 g, 0.1 M) was added followed by thiophene-2-carboxaldehyde (9.3 mL, 0.1 M). The reaction mixture was kept at ice cold condition over a magnetic stirrer and stirred for about 7 h. The solid separated out was washed filtered and dried over vacuum. (brown solid; M.P: 138 °C)



Scheme 4.3: Synthesis of 2-(pyrrolidin-1-yl(thiophen-2-yl)methyl)cyclohexanone (MA13)

4.3.1. IR spectrum of 2-(pyrrolidin-1-yl(thiophen-2-yl)methyl)cyclohexanone (MA13)

FT-IR spectrum of MA13 is shown in the Fig 4.11. NH stretching is noticed by a band at 3432 cm^{-1} . Aromatic CH frequency is exhibited by the band at 3072 cm^{-1} . A band at 2939 cm^{-1} indicates the C-H stretching of methine group. A sharp absorption band at 1646 cm^{-1} is due to the carbonyl stretching of cyclohexanone. The bands noticed at 1371 and 702 are attributed to C-N and C-S stretching respectively.

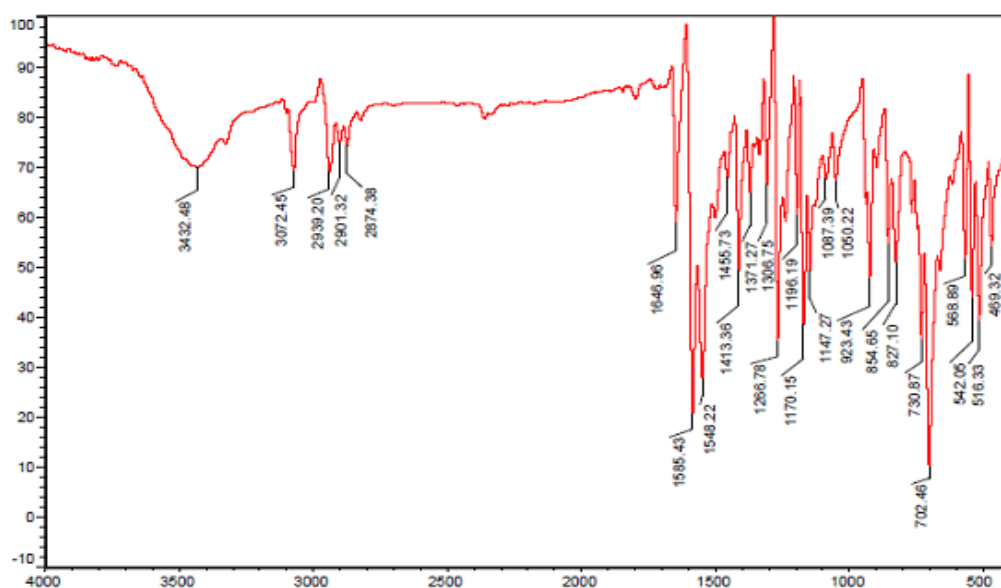


Fig.4.11. IR spectrum of 2-(pyrrolidin-1-yl(thiophen-2-yl)methyl)cyclohexanone (MA13)

4.3.2. $^1\text{H-NMR}$ spectrum of 2-(pyrrolidin-1-yl(thiophen-2-yl)methyl)cyclohexanone (MA13)

$^1\text{H-NMR}$ spectrum of MA13 is shown in the Fig 4.12. The signals exhibited from 7.9 to 6.9 ppm indicates the protons of indole ring. Methine proton shows a peak at 4.3 ppm. CH_2 protons of pyrrolidine and cyclohexanone are indicated by the signals appeared at 2.9 to 1.9 ppm.

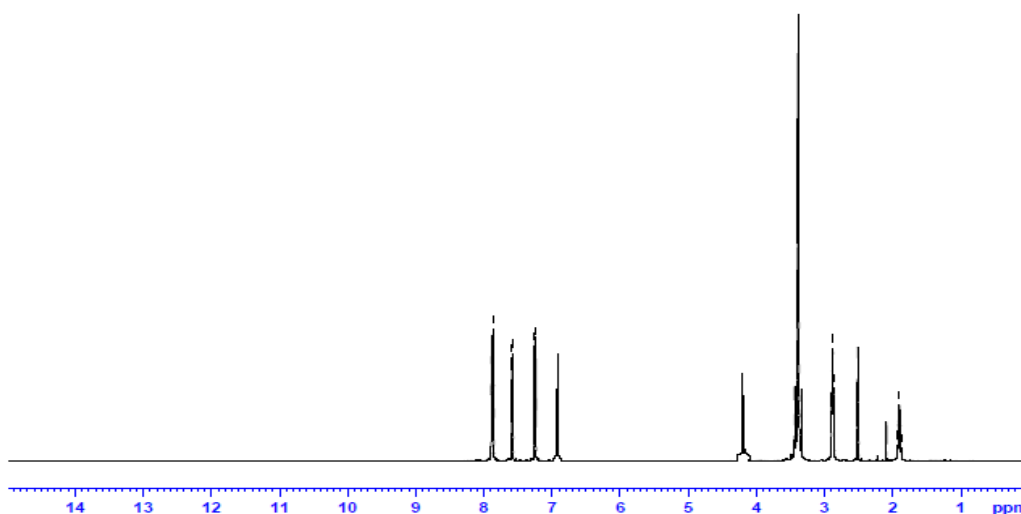


Fig. 4.12. $^1\text{H-NMR}$ spectrum of 2-(pyrrolidin-1-yl(thiophen-2-yl)methyl)cyclohexanone (MA13)

4.3.3. $^{13}\text{C-NMR}$ spectrum of 2-(pyrrolidin-1-yl(thiophen-2-yl)methyl)cyclohexanone (MA13)

$^{13}\text{C-NMR}$ spectrum of MA13 is shown in the Fig 4.13. A peak appears at 189 ppm is due to carbonyl carbon of cyclohexanone. The peaks noticed in the range of 135-122 ppm are indicating the thiophene carbons. The signals appeared in the range of 22 and 28 ppm are due to pyrrolidine and cyclohexanone carbons. The signal appeared at 64 ppm is indicating the methine carbon.

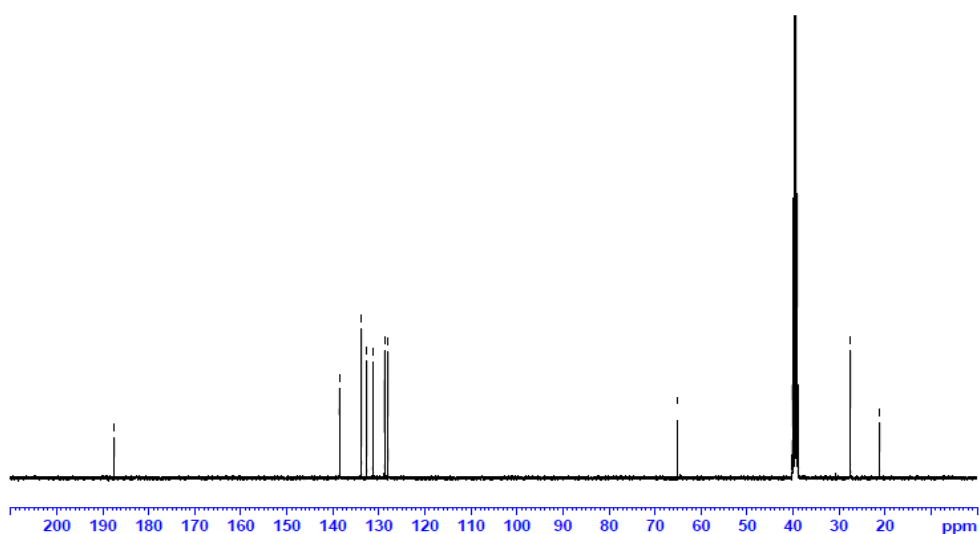


Fig.4.13. ^{13}C -NMR spectrum of 2-(pyrrolidin-1-yl(thiophen-2-yl)methyl)cyclohexanone (MA13)

4.3.4. Mass spectrum of 2-(pyrrolidin-1-yl(thiophen-2-yl)methyl)cyclohexanone (MA13)

Mass spectra of the compound MA13 has been given in the Fig. 4.14. The molecular ion peak appearing at m/z 263.13 well fit with the calculated molecular mass of the compound. Intensity of the peak shows that the molecular ion peak itself is the base peak.

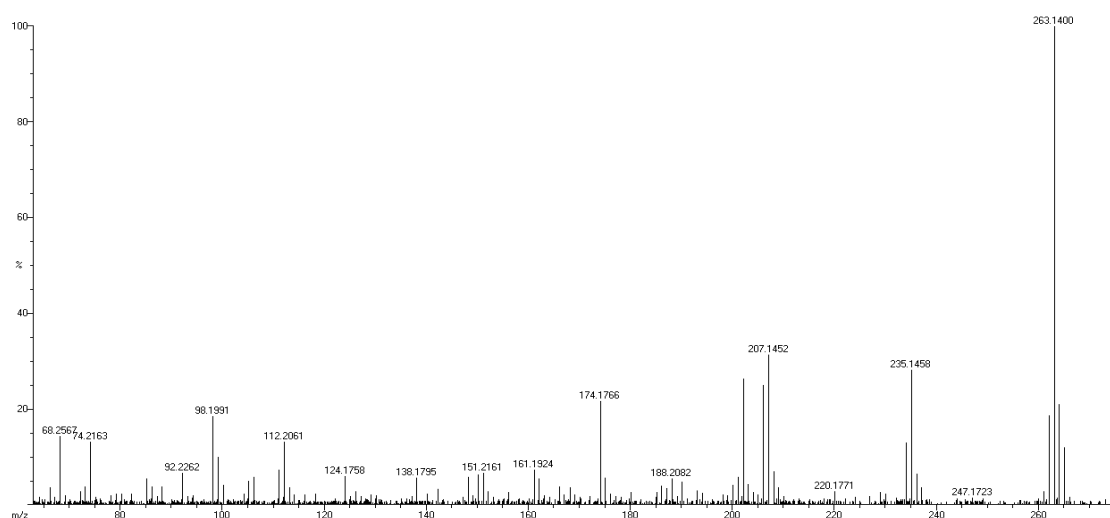


Fig.4.14. Mass spectrum of 2-(pyrrolidin-1-yl(thiophen-2-yl)methyl)cyclohexanone (MA13)

4.3.5. Antimicrobial evaluation of MA13

The compound MA13 possesses very less activity against *Moraxella*. It shows considerable activity against *B. subtilis*, *A.niger* and *Trichophyton*. Activity of the compound is higher in the case of gram positive bacteria than the gram negative bacteria. Potency of the compound against *A.niger* is found to be higher when compared to other strains. The results are shown in the Table 4.3 and Fig 4.15.

S. No.	Pathogen	Zone of inhibition (mm/ μ L)				
		25 μ L	50 μ L	75 μ L	100 μ L	Control
1.	<i>B. subtilis</i>	12	15	17	20	32
2.	<i>Moraxella</i>	-	-	7	9	30
3.	<i>A.niger</i>	13	15	18	20	28
4.	<i>Trichophyton</i>	9	10	11	12	20

Table 4.3: Zone of inhibition of MA13

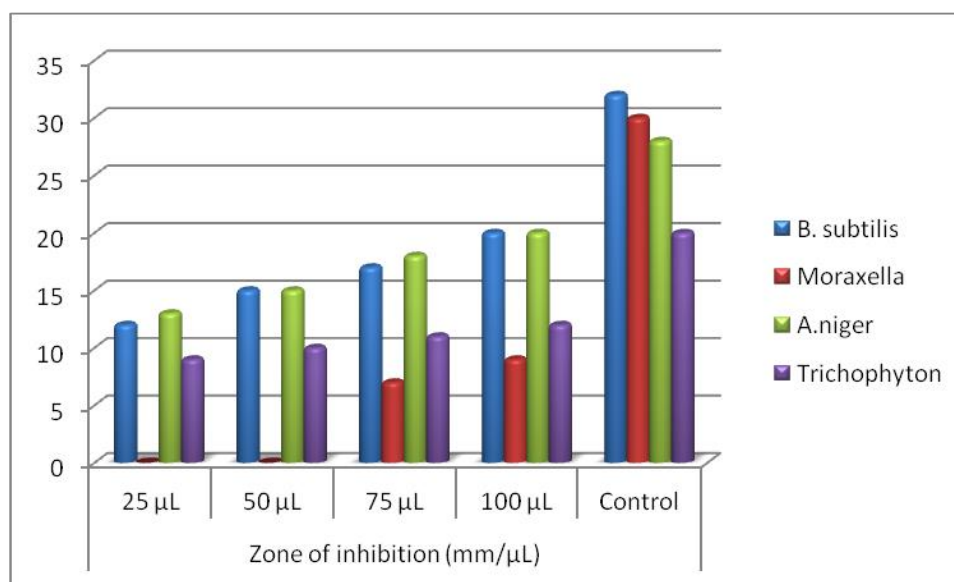
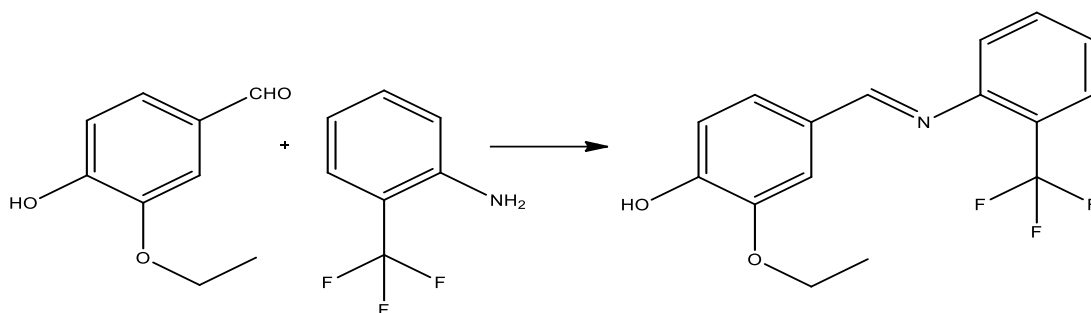


Fig.4.15.Zone of inhibition of MA13

Synthesis, characterization and DFT studies of MA14 & MA15

5.1. Synthesis of 2-ethoxy-4-(((2-(trifluoromethyl)phenyl)imino)methyl)phenol (MA14)

To the ethanolic solution of 3-ethoxy-4-hydroxy benzaldehyde (16.6 g, 0.1 M), 2-trifluoromethylaniline (9.9 g, 0.1 N) was added and refluxed for 6 h. The reaction mixture was cooled and poured in to a beaker containing crushed ice. The solid separated was washed, filtered and dried over vacuum and recrystallized using absolute ethanol.



Scheme 5.1: Synthesis of 2-ethoxy-4-(((2-(trifluoromethyl)phenyl)imino)methyl)phenol(MA14)

5.1.1. IR spectrum of 2-ethoxy-4-(((2-(trifluoromethyl)phenyl)imino)methyl)phenol (MA14)

The FT-IR spectrum of MA14 is presented in the Fig. 5.1. A broad band appeared at 3314 cm^{-1} shows OH stretching. Aromatic C-H stretching in phenyl ring exhibits a band at 3043 cm^{-1} . A sharp band

observed at 2926 cm^{-1} shows C-H stretching of methyl group. Strong absorption bands appeared at 2926 cm^{-1} and 2870 cm^{-1} are due to asymmetric and symmetric C-H stretching of methylene group. An absorption band at 1555 cm^{-1} indicates C=N stretching. A band appeared at 1025 cm^{-1} is due to C-F stretching.

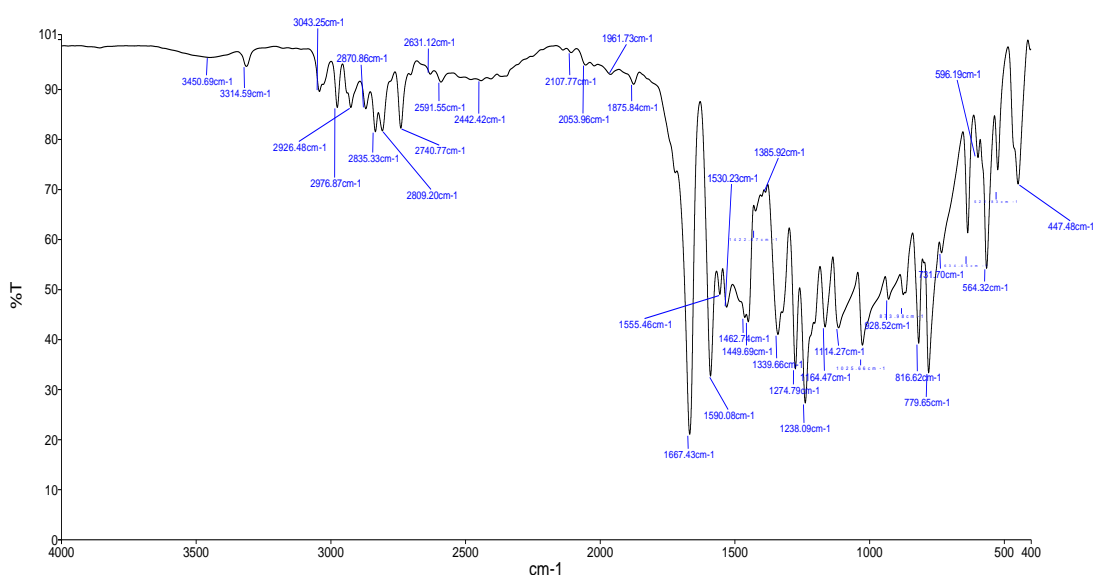


Fig.5.1. IR spectrum of 2-ethoxy-4-((2-(trifluoromethyl)phenyl)imino)methyl)phenol (MA14)

5.1.2. Mass spectrum of 2-ethoxy-4-((2-(trifluoromethyl)phenyl)imino)methyl)phenol (MA14)

Fig. 5.2 represents the mass spectra of the compound MA14. The molecular ion peak appearing at m/z 309.10 confirms the calculated molecular mass of the compound. The peak appearing with high intensity at m/z 293.10 is the base peak.

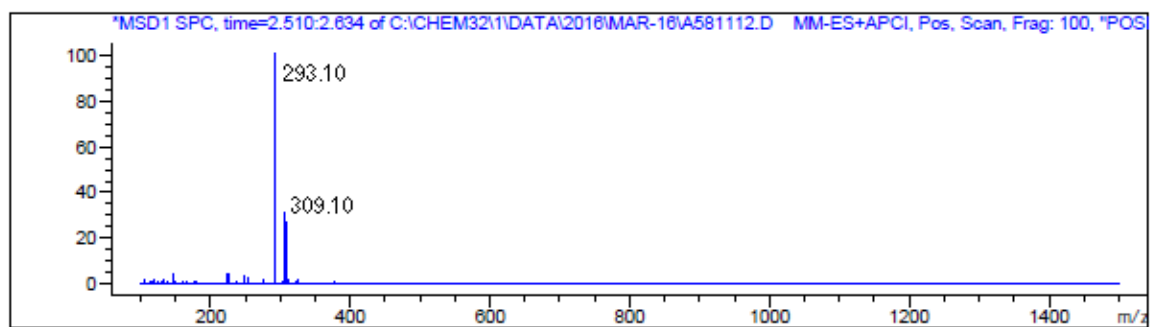


Fig.5.2. Mass spectrum of 2-ethoxy-4-(((2-(trifluoromethyl)phenyl)imino)methyl)phenol (MA14)

DFT Studies of 2-Ethoxy-4[(2-trifluoromethyl- phenylimino) methyl]phenol (MA14)

This study presents the molecular properties such as, vibrational spectra: FT-IR and FT-Raman, ^1H NMR and ^{13}C NMR chemical shifts, UV-Vis spectral parameters, HOMO, LUMO properties, atomic charges, NLO properties, NBO analysis, MEP surface and thermodynamic properties of 2-Ethoxy-4[(2-trifluoromethyl- phenylimino)methyl]phenol (**MA14**) molecule. Detailed analyses of structural, spectroscopic, magnetic, electronic, optical and thermodynamic properties of **MA14** molecule are not available in the literature. The quantum chemical investigations are performed by means of DFT/B3LYP method with 6-311++G(d,p) basis set, for the first time. The quantum chemical computation provides a powerful support for experimental studies.

All computational functions were carried out using Gaussian 03W program package running under Windows XP [91]. The geometrical optimization of **MA14** molecule was done using DFT method with Becke's three-parameter hybrid exchange correlation functional (B3LYP) [92–95]. The 6-311++G(d,p) basis set augmented

by d polarisation functions on heavy atoms and p polarisation functions on hydrogen atoms as well as diffuse functions for both hydrogen and heavy atoms was used [96,97]. The optimised molecular structure, harmonic vibrational frequencies, UV-Vis spectra, ^1H NMR and ^{13}C NMR spectra, the frontier molecular orbital (FMO), MEP, NLO properties, NBO analysis, Mulliken atomic charges and thermodynamic properties of title molecule were done using B3LYP/6-311++G(d,p) level.

The vibrational assignments were done with the help of Gauss View molecular visualisation program [98]. In addition, the calculated vibrational bands were justified by means of TED analysis and the assignments of the fundamental vibrational modes using VEDA 4 program [99]. The ^1H NMR and ^{13}C NMR chemical shifts were calculated within GIAO approach [100] applying the same method and the basis set as used for geometry optimization. The UV-Vis. calculations of the title molecule were performed by the time dependent-DFT (TD-DFT) method. The HOMO, LUMO energy values and their shapes were computed by the same level. On the basis of computed HOMO and LUMO energy values of the title molecule, the molecular properties such as, electron affinity (A), ionisation potential (I), chemical hardness (η), chemical softness (S), electronegativity (χ), chemical potential (μ), and electrophilicity index (ω) were computed. The NLO properties such as, dipole moment (μ), the mean polarisability (α_{total}), the first hyperpolarisability (β_0) were performed with the above mentioned computational level. The NBO analysis was done to know the interactions among the bonds and hyper

conjugative interactions in MA14 molecule. The MEP and its surfaces were simulated using the optimized molecular geometry of MA14 molecule.

Molecular geometry

The geometrical optimized molecular structure of MA14 molecule is shown in Figure 5.3. The computed geometrical parameters such as, bond lengths, bond angles and dihedral angles are summarised in Table 5.1. In the literature, experimental or calculated bond parameters for the molecule MA14 are not found; therefore the structure of MA14 molecule is compared with the available X-ray diffraction data of similar compound (*E*)- 2-ethoxy-6-[(phenylimino)methyl]phenol [101]. The calculated bond lengths at B3LYP method are slightly more than the experimental values; which is, due to the theoretical calculations that belong to the gaseous phase while the observed results are valid for solid phase of the molecule. The bond length of C13–C16 is 1.521 Å.

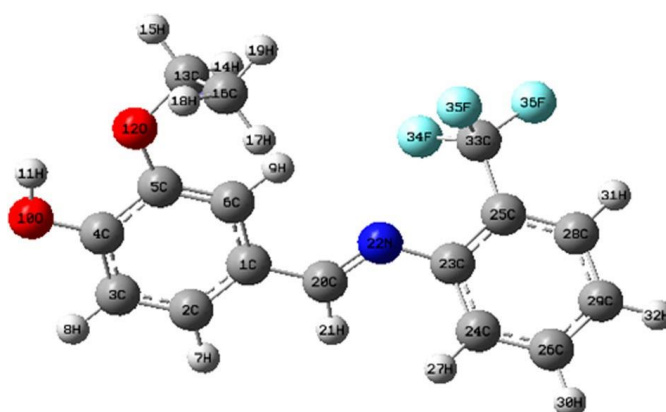


Figure.5.3. The optimised molecular structure of **MA14** .

Table 5.1. The optimised molecular geometric parameters of 2E42TP using B3LYP/6-311++G(d,p) basis set.

Bond parameters	B3LYP/6-311++G(d,p)	XRD^a
Bond lengths (Å)		
C1-C2	1.399	1.398
C1-C6	1.409	1.398
C1-C20	1.458	1.446
C2-C3	1.392	1.387
C4-C5	1.416	1.400
C4-O10	1.355	1.3514
C5-C6	1.381	1.382
C5-O12	1.370	1.365
C6-H9	1.081	
O10-H11	0.968	
O12-C13	1.440	1.432
C13-H14	1.094	
C13-H15	1.090	
C13-C16	1.521	1.502
C20-H21	1.099	
C20-N22	1.280	1.271
N22-C23	1.396	
C23-C24	1.404	1.377
C23-C25	1.413	
C24-C26	1.390	1.379
C24-H27	1.084	
C28-C29	1.393	
C33-F34	1.354	
C33-F35	1.354	
C33-F36	1.357	
Bond angles (°)		
C1-C2-C3	120.62	120.74
C1-C2-H7	119.73	
C3-C2-H7	119.64	
C3-C4-O10	120.13	

C5-C4-O10	119.74	118.22
C4-C5-C6	120.05	119.16
C4-C5-O12	113.16	
C6-C5-O12	126.78	125.81
C5-O12-C13	120.05	117.74
O12-C13-H14	109.33	
O12-C13-H15	104.07	
O12-C13-C16	112.54	
C1-C20-N22	122.90	122.94
H21-C20-N22	121.40	
C20-N22-C23	120.61	122.03
N22-C23-C24	122.15	124.16
N22-C23-C25	119.52	
C24-C23-C25	118.23	118.06
C23-C24-C26	121.03	121.12
C24-C26-C29	120.28	120.2
C25-C28-C29	120.70	120.8
C26-C29-C28	119.49	119.5
F34-C33-F35	106.85	
F34-C33-F36	106.25	
F35-C33-F36	106.13	
Dihedral angles (°)		
C6-C1-C2-C3	-0.32	-0.6
C6-C1-C20-N22	1.43	-1.6
C2-C3-C4-O10	179.68	179.26
O10-C4-C5-O12	-0.73	
O12-C5-C6-C1	-178.84	-178.76
C4-C5-O12-C13	-180.02	178.76
C6-C5-O12-C13	-0.84	-1.6
C25-C23-C24-C26	-1.30	-1.4
N22-C23-C25-C28	178.26	178.79
N22-C23-C25-C33	-2.16	
C24-C23-C25-C28	1.80	1.2

This elongation may be due to the repulsive nature between them which is, justified from Mulliken atomic charges as: C13 = -0.245 and C16 = -0.357 a.u. The calculated C5–O12 and C1–C20 bond lengths are 1.370 and 1.458 Å, respectively which are in agreement with XRD data [101]. The C20–N22, O10–H11, C5–O12 and C4–O10 bond lengths are 1.280, 0.968, 1.370 and 1.355 Å are agreeable with literature [101]. Similarly, the angles C1–C2–C3, C5–C4–O10 and C1–C20–N22 are 120.62°, 119.74° and 122.90° they are in agreement with literature [101]. The calculated dihedral angles N22–C23–C25–C33, O10–C4–C5–O12 and C6–C1–C20–N22 are -2.16°, -0.73° and 1.43° which show the planarity nature of the molecule. The angles C6–C5–O12: 126.78°/C4–C5–O12: 113.16° differ by 13.62° and this may be due to the intramolecular hydrogen bonding O10–H11 ... O12 with hyper conjugation interaction energy 8.24 kJ/mol.

Vibrational assignments

Vibrational spectral assignments are done at B3LYP/6-311++G(d,p) level for the present molecule which belongs to C1 point group. There are 36 atoms and have 102 vibrational modes which are active in both IR and Raman. The computed (unscaled and scaled) and observed vibrational frequencies, IR intensities, Raman intensities, vibrational assignments, force constant and reduced mass of vibrational assignments are summarised in Table 5.2. The calculated and observed FT-IR and FT-Raman spectra of MA14 molecule are given in Figure 5.4(a,b). The vibrational frequencies are justified on the basis of TED.

Table 5.2. The experimental and calculated frequencies of MA14 using B3LYP/6-311++G(d,p) level of basis set [Harmonic frequencies (cm⁻¹), FT- IR, FT- Raman (cm⁻¹)

S. No.	Observed frequencies			Vibrational assignments
	Scaled	FT-IR	FT-Raman	
1	3629.37	3450vw		vOH
2	3106.33			vCH
3	3104.39			vCH
4	3091.83			vCH
5	3086.03			vCH
6	3078.29		3076vw	vCH
7	3065.72			vCH
8	3062.82	3043w	3046vw	vCH
9	3017.38		3026vw	vCH
10	2999.01			vCH
11	2992.25	2976w	2978vw	vCH
12	2945.84			vCH
13	2936.17	2926w	2941vw	vCH
14	2908.13	2870w	2869vw	vCH
15	1627.12	1667vs	1661vs	vNC
16	1585.55	1590s	1586vs	vCC+vCC
17	1578.78			vCC+vCC+βCCC
18	1572.98			vCC+vCC
19	1556.55	1555vw	1554m	vCC+vCC+vCC
20	1486.94			βCCC+vOC+βHCC+βHCC
21	1468.57			βHCH+βHCH+ΓCHCH
22	1463.74			βHCC+βHCC
23	1450.2	1462vw	1462w	βHCH+βHCH
24	1438.6	1449vw		βHCC+βHCH

25	1430.86			$\beta\text{CCC}+\beta\text{HCC}+\beta\text{HCC}$
26	1422.16	1422vw		$\nu\text{CC}+\nu\text{CC}+\nu\text{CC}$
27	1387.36	1385vw	1387m	$\beta\text{HOC}+\beta\text{HCN}$
28	1369.96			$\Gamma\text{CHCH}+\Gamma\text{CHHH}$
29	1350.62	1339w		$\beta\text{HCN}+\Gamma\text{CHCH}+\Gamma\text{CHHH}$
30	1344.82		1316m	$\beta\text{HOC}+\beta\text{HCC}+\beta\text{HCN}$
31	1287.78	1274m	1273w	$\nu\text{CC}+\nu\text{CC}+\beta\text{HCO}$
32	1283.91			βHCO
33	1278.11			$\nu\text{CC}+\beta\text{HCC}$
34	1266.51	1238m	1239s	$\nu\text{CC}+\nu\text{CC}+\nu\text{OC}$
35	1253.94			$\beta\text{HCC}+\beta\text{HCN}$
36	1232.67			$\nu\text{CC}+\beta\text{HCC}$
37	1230.74			$\nu\text{OC}+\beta\text{HCC}$
38	1204.63			$\nu\text{CC}+\nu\text{NC}$
39	1173.7			$\nu\text{CC}+\beta\text{HOC}+\beta\text{HCC}$
40	1157.26	1164m		$\beta\text{HCC}+\Gamma\text{CHCO}$
41	1148.56			$\nu\text{CC}+\beta\text{HCC}+\beta\text{HCC}$
42	1132.12			$\nu\text{OC}+\beta\text{HCC}$
43	1112.79	1114w	1116vw	$\beta\text{CCC}+\nu\text{CC}+\nu\text{FC}$
44	1102.15			$\nu\text{CC}+\beta\text{HCC}+\beta\text{HCC}$
45	1076.05			$\nu\text{FC}+\nu\text{FC}+\Gamma\text{CCFF}$
46	1071.21			$\nu\text{FC}+\Gamma\text{CHCH}$
47	1069.28			$\nu\text{FC}+\nu\text{CC}+\Gamma\text{CHCH}$
48	1032.54	1025w		$\nu\text{FC}+\beta\text{HCC}+\beta\text{CCC}$
49	1016.11			$\nu\text{CC}+\nu\text{OC}$
50	1011.27			$\beta\text{CCC}+\nu\text{FC}$
51	969.7			τHCNC
52	962.93			$\Gamma\text{CCCH}+\Gamma\text{CCCH}$
53	958.1			$\nu\text{CC}+\nu\text{OC}+\nu\text{CC}$

54	934.9	928vw	939w	$\Gamma\text{CCCH}+\Gamma\text{CCCH}+\tau\text{HCCH}$
55	914.59			τHCCH
56	873.99			$\nu\text{CC}+\nu\text{OC}+\Gamma\text{CHCH}$
57	868.19			τHCCC
58	853.68			$\Gamma\text{CCCH}+\tau\text{HCCC}$
59	837.25	873vw	871vw	$\nu\text{NC}+\beta\text{CCC}$
60	801.48	816m	812vw	ΓCCCH
61	800.51			$\nu\text{OC}+\beta\text{HCC}+\beta\text{CCC}$
62	786.98	779s	784m	$\beta\text{HCC}+\Gamma\text{CHCO}$
63	758.94			$\Gamma\text{CCCH}+\tau\text{CCCC}+\Gamma\text{NCCC}$
64	743.47			$\Gamma\text{CCCH}+\tau\text{HCCC}+\tau\text{CCCC}$
65	735.73	731vw		νFC
66	716.4			βCCC
67	708.66			$\tau\text{CCCC}+\tau\text{CCCC}$
68	642.92			$\beta\text{CCC}+\beta\text{FCF}$
69	619.72	634m	639m	$\beta\text{CCC}+\beta\text{CCC}+\beta\text{CCC}$
70	604.25			τCCCC
71	579.11	596vw		$\nu\text{FC}+\tau\text{CCCC}+\Gamma\text{CCFF}$
72	572.35	564s	564w	$\beta\text{CCN}+\Gamma\text{CCFF}$
73	548.18			$\beta\text{CCO}+\beta\text{CCO}+\Gamma\text{FCFC}$
74	539.47			$\nu\text{OC}+\beta\text{CCC}$
75	525.94	522w	523vw	$\tau\text{CCCC}+\Gamma\text{NCCC}$
76	494.03			$\beta\text{CCC}+\beta\text{CCC}$
77	484.37			$\beta\text{CCN}+\beta\text{FCF}+\beta\text{FCF}$
78	477.6			τHOCC
79	462.13		467vw	$\beta\text{FCF}+\beta\text{FCF}$
80	446.66	447m		$\tau\text{CCCC}+\tau\text{CCCC}+\tau\text{CCCO}+\tau\text{CCCO}$
81	418.62			$\beta\text{CCO}+\beta\text{CCO}$

The absorption bands in the region of 3100–3700 cm^{-1} result the presence of O–H stretching mode for free hydroxyl group [102]. Intramolecular hydrogen bonding if present in benzene moiety would reduce νOH mode to 3200–3550 cm^{-1} [103]. Based on this conclusion, the observed FT-IR band at 3450 cm^{-1} and its corresponding harmonic value 3607 cm^{-1} is assigned to νOH (mode no: 1) with 100% contribution of TED. Generally, the O–H in-plane bending vibrations are observed in the region 1200–1350 cm^{-1} . The O–H in-plane bending vibration is assigned to 1379 cm^{-1} (mode no: 27) and observed values: 1385/1387 cm^{-1} FT-IR/FT-Raman and the O–H out-of plane bending vibration is assigned to 475 cm^{-1} (mode no: 78) with 88% TED contribution. These assignments find support from the literature [104].

The C–H stretching vibrations generally are found in the region 3000–3100 cm^{-1} in aromatic structure, which is, the characteristic region for the identification of νCH stretching vibrations [105]. In MA14, the νCH stretching modes are assigned to 3043/3046, 3076 cm^{-1} in FT- IR / FT-Raman and its corresponding harmonic values are 3044/3073 cm^{-1} (mode nos: 8, 4). The mode nos: 2, 3, 5, 6 and 7 also belong to νCH . The νCH stretching of aliphatic is assigned to 2870/2869 cm^{-1} in FT- IR/FT-Raman and its corresponding harmonic value is 2890 cm^{-1} (mode no: 14). These assignments are pure mode (> 92%) and they are also in line with the literature [105]. The C–H in-plane and out-of-plane bending vibrations are appeared in the regions: 1000–1600 cm^{-1} and 650–1000 cm^{-1} [102,106–108]. The mode nos: 22, 25, 36, 37, 41, 42, 44 and 52,

54, 58, 60, 64 are assigned to β CH and TCH modes, respectively and also find support from observed FT-IR/FT-Raman bands: 1449, 1422, and 928/939, 816/812 cm^{-1} . The in-plane and out-of-plane modes of $\text{C}_{20}\text{H}_{21}$ are attributed to mode nos: 30 and 51, respectively. These assignments have considerable TED value.

CH₂ vibrations

For the assignments of CH₂ group frequencies there are six fundamental vibrations associated with CH₂ group namely, $\nu_{\text{sym}}(\text{CH}_2)$ -symmetric stretch, $\nu_{\text{asy}}(\text{CH}_2)$ -asymmetric stretch, $\rho(\text{CH}_2)$ -rocking modes which belong to in-plane vibrations. In addition to that wagging and twisting modes of CH₂ group would be assigned as out-of-plane bending vibrations. The CH₂ ν_{asy} and CH₂ ν_{sym} vibrations would appear in the range 2700–3000 cm^{-1} [104]. The CH₂ ν_{asy} and ν_{sym} vibrations are assigned at 3026, 2941/2926 cm^{-1} in FT-Raman/FT-IR and its corresponding harmonic values are 2999, 2928 cm^{-1} (mode nos: 9, 12) with (>91%) contribution of TED. The other fundamental CH₂ group vibrations which are CH₂ scissoring, CH₂ rocking, CH₂ wagging and CH₂ twisting modes appear in the expected wave number region of 875-1475 cm^{-1} [109, 110]. According to TED (> 59%), the CH₂ scissoring mode is assigned to 1459 cm^{-1} (mode no: 21) with observed values 1462/1462 cm^{-1} in FT-IR/FT-Raman. Harmonic frequencies: 1342/1150 cm^{-1} (mode nos: 29, 40) with TED value (>33%) are assigned to $\omega\text{CH}_2/\text{TCH}_2$ modes, respectively. These assignments are in line with the literature [109, 110] and also find support from observed FT-IR bands: 1339 and 1164 cm^{-1} .

CH₃ vibrations

Methyl groups are referred as electron-donating substituents in the aromatic ring system. The CH₃ *ν*_{asy} vibrations are observed in the range 2925–3000 cm⁻¹ and CH₃ *ν*_{sym} vibrations in the range 2905–2940 cm⁻¹ [111, 112]. The CH₃ *ν*_{asy} and *ν*_{sym} vibrations are assigned at 2976/2978 cm⁻¹ FT-IR/FT-Raman, respectively and its corresponding harmonic values are: 2980, 2974 and 2918 cm⁻¹ (mode nos: 10, 11, 13). These assignments are within the expected region and also find support from TED value (> 79%). According to Socrates [113], the *β*_{asy} HCH and *β*_{sym} HCH modes of CH₃ group appear in the regions: 1440–1465 and 1370–1390 cm⁻¹, respectively. The weak FT-IR band around 1449 cm⁻¹ belongs to *β*_{asy} HCH mode it is in good agreement with harmonic value 1455 cm⁻¹ (mode no: 22). The *β*_{sym} HCH is assigned to harmonic frequencies 1441, 1430 cm⁻¹ (mode nos: 23, 24) with TED contribution (> 18%). The vibrational absorptions noticed in the region 900–1070 cm⁻¹ are due to *ρ*CH₃ mode [114]. The *ρ*CH₃ vibrations of CH₃ group appear as mixed vibrations. Based on this the calculated frequency 1065/869 cm⁻¹ (mode nos: 46/56) with considerable TED (> 33%) observed at 873/871 cm⁻¹ in FT-IR/FT-Raman are designated as in-plane and out-of- plane *ρ*CH₃ modes. The harmonic frequency 1361 cm⁻¹ (mode no: 28) having 66% TED value is attributed to wagging CH₃ which is justified with the help of Gauss View program.

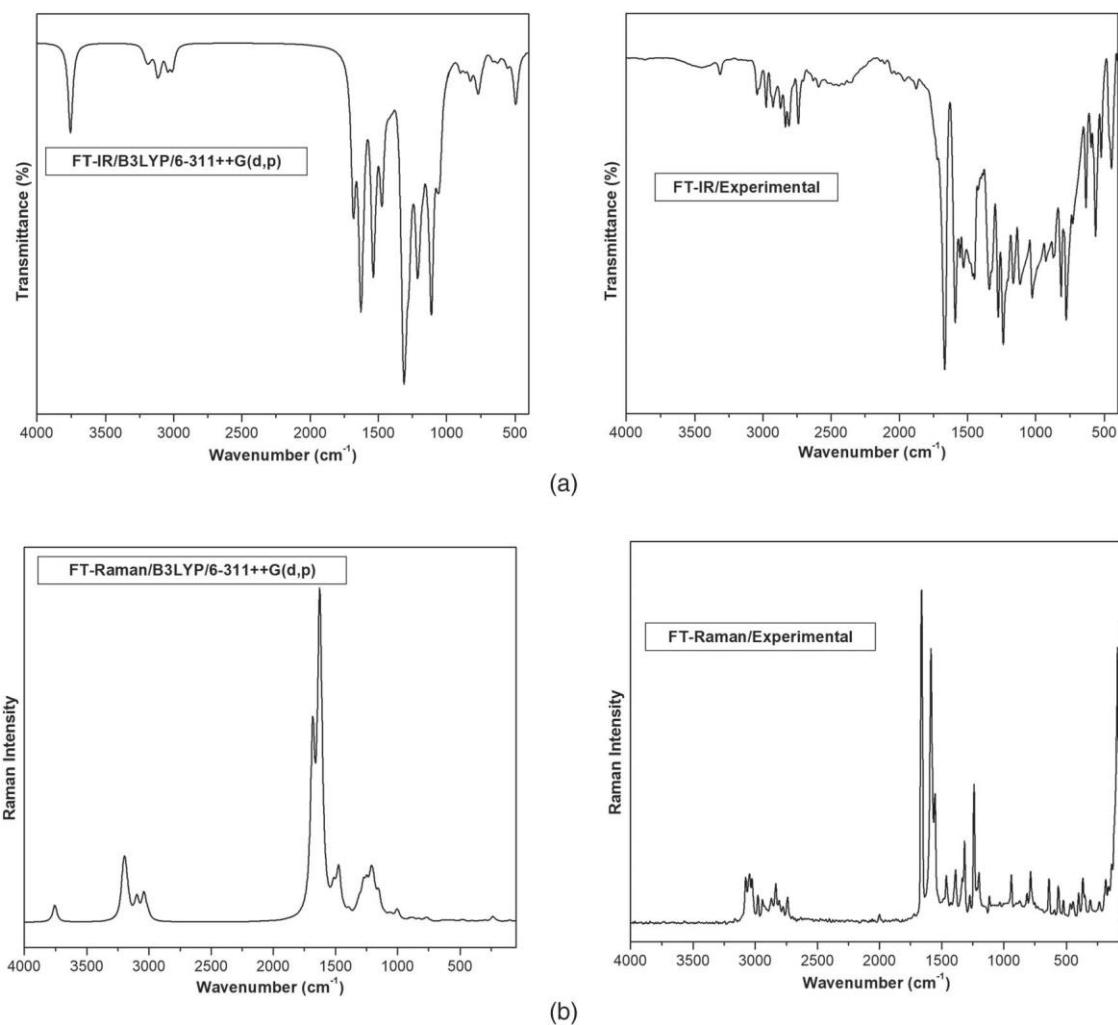


Fig.5.4. The combined theoretical and experimental FT-IR spectra and FT-Raman spectra of MA14 (a) & (b).

CN vibrations

The C=N stretching vibrations are assigned in the region 1500–1600 cm^{-1} by Silverstein [115] is close to the predicted region of 1600–1670 cm^{-1} [116]. In the present study, the CN stretching mode is assigned to very strong bands: 1667/1661 cm^{-1} in FT-IR/FT-Raman spectra and its corresponding harmonic value is 1617 cm^{-1} (mode no: 15). The mode no: 15 has moderate to strong intensity with TED value 64%. According to Silverstein [115] the $\nu_{\text{C-N}}$ vibrations are appeared in

the region: 1266–1382 cm^{-1} for aromatic amines. The $\nu\text{C-N}$ is assigned to 1197 cm^{-1} (mode no: 38) with no observed FT-IR/FT-Raman bands. The CN in-plane and out-of-plane bending vibrations are observed at 564/564 cm^{-1} and 522/523 cm^{-1} in FT-IR/FT-Raman spectra and its corresponding harmonic values are 569/523 cm^{-1} (mode nos: 72/75) with > 20% TED contribution.

C-C vibrations

The C–C ring stretching vibrations of aromatic group generally appear in the regions of 1280–1380; 1430–1465; 1470–1540; 1575–1590 and 1590–1625 cm^{-1} with variable intensity [117]. For the title molecule νCC vibrations are observed at 1590(s)/1586(vs) and 1555(vw)/1554(m) in FT-IR/FT-Raman spectra. These assignments find support from harmonic frequencies: 1576, 1569, 1563, 1547, 1413, 1280 and 1259 (mode nos: 16–19, 26, 31 and 34) in addition to their TED value (> 27%). The in- plane and out-of-plane bending modes of CCC are associated with smaller force constant than νCCC vibrations and hence they are assigned to lower frequencies. The harmonic in-plane CCC (1005, 832, 796, 712, 639 and 616 cm^{-1} /mode nos: 50, 59, 61, 66, 68 and 69) and out-of-plane CCC (704, 601, 576, 523, 444 and 342 cm^{-1} /mode nos: 67, 70, 71, 75, 80 and 84) bending modes have been found to be in line with the observed FT-IR bands: 634 and 596, 522, 447 cm^{-1} , respectively and their TED contributions are > 22%. The mode nos: 36 and 49 are attributed to νC25C33 and νC13C16 modes, respectively on the basis of TED value > 31%.

CO stretching

The C–O stretching vibrations are found in the range 1168–1310 cm^{-1} [118]. Bharanidharan [119], assigned the phenolic $\nu\text{C-O}$ mode at 1201 (m) cm^{-1} in FT-Raman spectrum. The $\nu\text{C4-O10}$ vibration is assigned to 1238 (m)/1239 (s) cm^{-1} in FT-IR/FT-Raman spectra and its corresponding harmonic value is 1259 cm^{-1} (mode no: 34). This assignment is further supported by TED value 50%. The mode no: 42 and 49 are attributed to $\nu\text{C5-O12}$ and $\nu\text{C13-O12}$ vibrations, respectively with considerable TED value (34 and 44%). The calculated wavenumbers: 545, 416 and 387, 186 cm^{-1} (mode nos: 73, 81 and 82, 92) are designated as $\beta\text{C4C5O12}$, $\beta\text{C3C4O10}$ and $\tau\text{C6C5C4O10}$, $\tau\text{H19C16C13O12}$ modes, respectively. Similarly $\beta\text{C5O12C13}/\tau\text{C5O12C13C16}$ modes are assigned to harmonic frequencies: 310/81 cm^{-1} (mode nos: 86/97), respectively. These assignments have considerable TED value (> 20%) and also find support from observed FT-Raman bands 183, 307, 72 cm^{-1} .

CF₃ vibrations

According to the work by Alpaslan [120], the harmonic wave number at 1113: FT-IR/1114 cm^{-1} is designated as $\nu\text{C-F}$ mode. Further, the $\nu\text{C-F}$ mode is assigned [121] at 1160 cm^{-1} /FT-IR in the case of 2,3-dichloro.5-trifluoromethyl pyridine. In this study, the bands 1114/1116, 731 cm^{-1} (FT-IR/FT-Raman) are assigned to νCF mode. These assignments are in line with calculated frequencies: 1106, 1069 and 731 cm^{-1} (mode nos: 43, 45 and 65) in addition to their TED value (> 13%). The CF deformation vibrations are expected to occur in the region 490–590 cm^{-1} [122]. The observed FT-Raman bands 467, 367 and

564, 234 cm^{-1} confirm the presence of in-plane and out-of-plane bending vibrations of CF_3 , respectively. The harmonic frequencies 481, 459, 375 and 569, 235 cm^{-1} (mode nos: 77, 79, 83 and 72, 89) are respectively in agreement with the experimental value. These assignments have TED value ($> 34\%$ and $> 19\%$), respectively.

NMR

The isotropic NMR chemical shift analysis is used to identify relative ionic species, to determine different number of protons and carbon atoms and functional groups in a molecular structure as well as to calculate reliable magnetic properties which provide an accurate prediction of molecular geometries [123–126]. The ^1H NMR and ^{13}C NMR chemical shift of MA14 molecule are calculated at B3LYP/6-311 G(d,p) level with TMS as an internal standard. The calculated ^1H NMR and ^{13}C NMR chemical shift values are given in Table-5.3.

Table 5.3- The theoretical (^1H and ^{13}C) chemical shifts (ppm) values of MA14.

Atoms	Theoretical	Atoms	Theoretical
H21	8.21	C23	158.92
H9	8.07	C4	157.65
H31	7.84	C5	150.47
H30	7.59	C26	137.32
H32	7.23	C1	134.56
H7	7.15	C33	134.52
H27	7.13	C28	132.26
H8	7.03	C2	132.10
H11	5.79	C25	130.54
H14	4.52	C29	127.90
H15	4.29	C24	121.79
H17	1.75	C3	117.37
H18	1.18	C6	111.74
H19	1.01	C13	66.33
C20	164.17	C16	13.99

The ^{13}C NMR chemical shift values are calculated in the range of 13.99–164.17 ppm, and ^1H NMR are calculated in the range of 1.01–8.21 ppm. The C_{20} , C_{23} , C_4 and C_5 atoms are connected with the electronegative atoms and their ^{13}C NMR chemical shift values are assigned at 164.17, 158.92, 157.65 and 150.47 ppm. These carbon atoms have more chemical shift values than other carbon atoms in MA14 molecule, and this is due to deshielding effect of electronegative N and O atoms. Carbon atoms of aromatic ring give resonance signals in the range of 100–150 ppm [123–126]. As the NMR chemical shift values for aromatic carbon atoms in MA14 molecule are calculated at the interval 111.74–158.92 ppm. Due to intra-molecular hydrogen bonding, the proton NMR chemical shift for H21 atom is found at 8.21 ppm. The aromatic rings produce large deshielding effects and their π -bonding electrons act as a conductor [123]. The chemical shift of proton numbered at H21 is highly deshielded when compare with other protons due to the influence of adjacent Nitrogen atom. The C_{13} and C_{16} atoms show least chemical shift 66.33 and 13.99 ppm which is due to their repulsive nature between them (-0.245 , -0.357 a.u) obtained from Mulliken atomic charges.

Natural bond orbital

The natural bond orbital (NBO) analysis is a calculated bonding orbital with maximum electron density (ED) which is used to determine intra-molecular and inter-molecular bonding interactions, bond structures, bond species and natural atomic charges in a molecular system. In addition, it is used to study inter-molecular charge transfers

(ICT) or hyperconjugation interactions and the stability between Lewis type filled orbitals and non-Lewis type vacancy orbitals. The hyperconjugation interaction energy (or the stabilisation energy, $E^{(2)}$) shows the interaction between donor and acceptor groups. The ED delocalisation between occupied bonded orbitals and unoccupied non-bonded orbitals corresponds to stabilise donor acceptor interaction [127]. The interactions result a loss of occupancy from the localised NBO of the idealised Lewis structure into an empty non-Lewis orbital. For each donor (i) and acceptor (j) orbital the stabilisation energy $E^{(2)}$ associated with the delocalisation $i \rightarrow j$ is estimated as

$$E^{(2)} = \Delta E_{ij} = q_i F(i, j)^2 / \epsilon_j - \epsilon_i$$

where q_i represents occupancy of donor orbital, ϵ_i and ϵ_j are the diagonal elements and $F(i, j)$ is the off diagonal NBO Fock matrix element [128,129].

Table 5.4: The second order perturbation theory analysis of Fock Matrix in NBO basis for MA14

Type	Donor NBO (i)	ED/e	Acceptor NBO (j)	ED/e	aE(2) kJ/mol	bE(j)-E(i) a.u.	cF(i,j) .u.
$\sigma-\sigma^*$	BD (1) C 1 - C 2	1.974	BD*(1) C 1 - C 6	0.02489	15.94	1.26	0.062
$\pi-\pi^*$	BD (2) C 1 - C 2	1.655	BD*(2) C 3 - C 4	0.36709	76.53	0.27	0.064
			BD*(2) C 5 - C 6	0.3416	80.58	0.28	0.065
			BD*(2) C 20 - N 22	0.16772	84.56	0.28	0.07
$\sigma-\sigma^*$	BD (1) C 1 - C 6	1.967	BD*(1) C 1 - C 2	0.02105	15.9	1.26	0.062
			BD*(1) C 5 - O 12	0.02968	22.47	1.03	0.067
$\sigma-\sigma^*$	BD (1) C 2 - H 7	1.979	BD*(1) C 1 - C 6	0.02489	20.13	1.08	0.065
			BD*(1) C 3 - C 4	0.02137	13.31	1.09	0.052
$\pi-\pi^*$	BD (2) C 3 - C 4	1.654	BD*(2) C 1 - C 2	0.39924	91.13	0.29	0.072
			BD*(2) C 5 - C 6	0.3416	73.05	0.29	0.063
$\sigma-\sigma^*$	BD (1) C 3 - H 8	1.978	BD*(1) C 1 - C 2	0.02105	14.31	1.09	0.055
			BD*(1) C 4 - C 5	0.03795	17.32	1.04	0.059
$\pi-\pi^*$	BD (2) C 5 - C 6	1.712	BD*(2) C 1 - C 2	0.39924	71.59	0.3	0.066
			BD*(2) C 3 - C 4	0.36709	78.78	0.29	0.068
$\sigma-\sigma^*$	BD (1) C 6 - H 9	1.974	BD*(1) C 1 - C 2	0.02105	18.74	1.1	0.063
$\sigma-\sigma^*$	BD (1) O 10 - H 11	1.986	BD*(1) C 3 - C 4	0.02137	20.29	1.31	0.071
$\sigma-\sigma^*$	BD (1) C 16 - H 18	1.988	BD*(1) C 13 - H 14	0.02227	10.75	0.89	0.043
$\sigma-\sigma^*$	BD (1) C 16 - H 19	1.980	BD*(1) O 12 - C 13	0.02841	19.92	0.77	0.054
$\sigma-\sigma^*$	BD (1) C 20 - H 21	1.985	BD*(1) C 1 - C 6	0.02489	18.37	1.1	0.062
$\pi-\pi^*$	BD (2) C 20 - N 22	1.911	BD*(2) C 1 - C 2	0.39924	32.05	0.36	0.051
$\sigma-\sigma^*$	BD (1) N 22 - C 23	1.980	BD*(1) C 1 - C 20	0.03152	13.26	1.27	0.057
$\pi-\pi^*$	BD (2) C 23 - C 24	1.625	BD*(2) C 20 - N 22	0.16772	30.5	0.29	0.043
			BD*(2) C 25 - C 28	0.35769	75.1	0.28	0.064
			BD*(2) C 26 - C 29	0.33407	94.14	0.28	0.072
$\sigma-\sigma^*$	BD (1) C 24 - C 26	1.978	BD*(1) N 22 - C 23	0.02452	16.23	1.16	0.06
$\sigma-\sigma^*$	BD (1) C 24 - H 27	1.978	BD*(1) C 23 - C 25	0.03226	17.99	1.07	0.061
$\pi-\pi^*$	BD (2) C 25 - C 28	1.692	BD*(2) C 23 - C 24	0.36845	88.37	0.29	0.071
			BD*(2) C 26 - C 29	0.33407	70.67	0.29	0.063
$\pi-\pi^*$	BD (2) C 26 - C 29	1.655	BD*(2) C 23 - C 24	0.36845	77.86	0.28	0.065
			BD*(2) C 25 - C 28	0.35769	97.11	0.28	0.072
			BD*(2) C 23 - C 25	0.03226	19.58	1.07	0.063
$\sigma-\sigma^*$	BD (1) C 28 - H 31	1.978	BD*(1) C 24 - C 26	0.01482	15.56	1.1	0.057
$\sigma-\sigma^*$	BD (1) C 29 - H 32	1.980	BD*(1) C 4 - C 5	0.03795	23.64	1.13	0.072
$n-\sigma^*$	LP (1) O 10	1.978	BD*(1) C 3 - C 4	0.36709	124.22	0.35	0.096
$n-\pi^*$	LP (2) O 10	1.855	BD*(1) C 5 - C 6	0.02413	28.53	1.14	0.079
$n-\sigma^*$	LP (1) O 12	1.958	BD*(1) O 10 - H 11	0.01385	8.24	0.97	0.039
			BD*(1) C 5 - C 6	0.3416	112.63	0.35	0.092
$n-\pi^*$	LP (2) O 12	1.860	BD*(2) C 5 - C 6	0.3416	112.63	0.35	0.092
			BD*(1) C 13 - C 16	0.01431	22.72	0.7	0.057
$n-\sigma^*$	LP (1) N 22	1.868	BD*(1) C 1 - C 20	0.03152	12.18	0.83	0.045
			BD*(1) C 20 - H 21	0.04227	53.14	0.73	0.088
			BD*(1) C 23 - C 24	0.03025	23.43	0.9	0.065
			BD*(2) C 23 - C 24	0.36845	32.05	0.36	0.05
$n-\sigma^*$	LP (2) F 34	1.954	BD*(1) C 25 - C 33	0.05387	23.56	0.79	0.059
$n-\sigma^*$	LP (3) F 34	1.937	BD*(1) C 33 - F 35	0.09886	39.83	0.65	0.071
			BD*(1) C 33 - F 36	0.08849	44.31	0.64	0.074
$n-\sigma^*$	LP (3) F 35	1.938	BD*(1) C 33 - F 34	0.09801	39.83	0.65	0.071
$n-\sigma^*$	LP (2) F 36	1.956	BD*(1) C 25 - C 33	0.05387	23.35	0.79	0.059
$n-\sigma^*$	LP (3) F 36	1.943	BD*(1) C 33 - F 34	0.09801	42.05	0.65	0.073

The NBO data computed for the molecule MA14 at B3LYP/6-311++G(d,p) is given in Table 5.4. The larger $E^{(2)}$ value the more intensive is the interaction between electron donors and acceptors i.e., the more donation tendency from electron donors to electron acceptors and greater the extent of conjugation of the whole system. The strong hyperconjugation interactions are computed between π & σ bonding electrons of the CC, CH, CO, OH, CN single and double bonds, π^* and σ^* antibonding ones of CC, CH, CO, OH, and CF single and CN double bonds. In addition, other strong hyperconjugation interactions are also found between the lone pair n electrons of O, N, F atoms and σ^* and π^* antibonding ones of C–C, O–H, C–H and C–F bonds. The π bond electrons are weaker than σ bond electrons. Therefore, π bonded groups have less ED than σ bonded ones. For the MA14 molecule, the EDs of the π bonds in the donor (i) groups are calculated at the interval of 1.625e–1.911e, whereas the EDs of the σ bonds in the donor (i) groups are found between 1.967e–1.988e. The EDs of lone pair n electrons of O, N, and F atoms in donor (i) groups are found between 1.855e–1.978e. The strongest hyperconjugation interactions occur from lone pair n electrons of O10 and O12 atoms to an antibonding π^* electrons of C3–C4 and C5–C6, with interaction energy $E^{(2)} = 124.22$ and 112.63 kJ/mol. It is evident from Table 5.4 the hydrogen (H11) is towards the oxygen (O12) and hence, the intra- molecular interaction takes place between the C5–O12 and O10–H11 group (O–H ... C–O). Due to this reason the LP O12 transfer energy (8.24 kJ/mol) to acceptor antibonding orbital σ^* O10–H11. The stabilisation energy values for π (C1–C2) \rightarrow π^* (C20–N22), π (C3–C4) \rightarrow π

* $(C1-C2)$, $\pi(C23-C24) \rightarrow \pi^*(C26-C29)$, $\pi(C25-C28) \rightarrow \pi^*(C23-C24)$ and $\pi(C26-C29) \rightarrow \pi^*(C25-C28)$ are computed as 84.56, 91.13, 94.14, 88.37 and 97.11 kJ/mol. Likewise, the $\sigma(C1-C6) \rightarrow \sigma^*(C5-O12)$, $\sigma(O10-H11) \rightarrow \sigma^*(C3-C4)$, $\sigma(C2-H7) \rightarrow \sigma^*(C1-C6)$, $\sigma(C16-H19) \rightarrow \sigma^*(O12-C13)$, $\sigma(C28-H31) \rightarrow \sigma^*(C23-C25)$ hyper conjugation interactions are obtained as 22.47, 20.29, 20.13, 19.92 and 19.58 kJ/mol.

UV-Visible

The UV-Vis electronic absorption spectrum of the MA14 molecule is recorded experimentally in the region 200–800 nm using DMSO solvent. The calculated and recorded UV-Vis spectroscopic parameters and its corresponding electronic transitions are given in Table 5.5.

Table 5.5: The electronic transition of MA14

Calculated at B3LYP/6-311++G(d,p)	Oscillator strength and gap (eV/nm)	Calculated band gap (nm)	Experimental band gap (eV/nm)	Type
Excited State-1	Singlet-A ($f = 0.5694$)	3.7180 eV/333.47 nm	362.90 nm	$\pi-\pi^*$
78 \rightarrow 81	0.17474			
79 \rightarrow 81	-0.21206			
80 \rightarrow 81	0.58917			
Excited State-2	Singlet-A ($f = 0.0348$)	4.0189 eV/308.50 nm	308.35 nm	$\pi-\pi^*$
76 \rightarrow 81	-0.1417			
79 \rightarrow 81	0.59947			
80 \rightarrow 81	0.23103			
Excited State-3	Singlet-A ($f = 0.1254$)	4.3369 eV/285.88 nm	267.50 nm	$\pi-\pi^*$
78 \rightarrow 81	0.58777			
79 \rightarrow 81	0.13888			
80 \rightarrow 81	-0.11967			
80 \rightarrow 82	0.18743			
80 \rightarrow 83	-0.2103			

In addition, the simulated and recorded UV-Vis. Spectra are also given in Figure 5.5. The absorptions observed at 362.90 and 308.35 nm in the experimental UV-Vis spectrum using DMSO solvent can be assigned to $\pi \rightarrow \pi$ electronic transition in the MA14 molecule. According to Frank-Condon principle the maximum absorption peak (λ_{\max}) in a UV-Vis spectrum corresponds to vertical excitation. The calculated UV-Vis spectrum shows an intense peak at 333.47 nm with an oscillator strength $f = 0.5694$ which is in line with the experimental $\lambda_{\max} = 362.90$ nm. This electronic absorption corresponds to the transition from the ground state to the first excited state and is described as one electron excitation from the HOMO to the LUMO. Similarly, an electronic transition at 308.50 nm with an oscillator strength $f = 0.0348$ is in line with the observed data 308.35 nm. The absorption wavelength (λ), oscillator strength (f) and excitation energies are calculated at TD-DFT/B3LYP/6-311++G(d,p) level, for MA14 molecule. The band gap energy between HOMO and LUMO indicates the electrical transport properties of molecules [130].

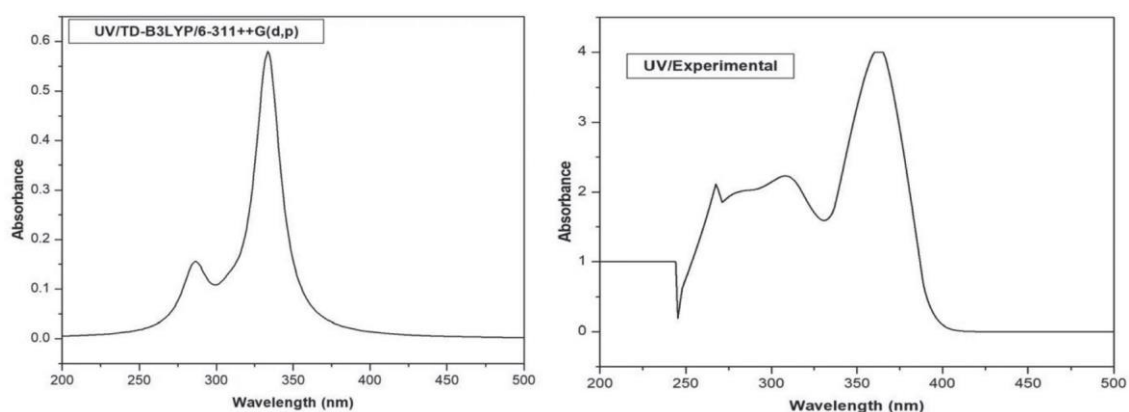


Fig.5.5. Theoretical and experimental UV-Vis spectrum of **MA14**.

The MEP is associated with the ED and is generally an important descriptor to identify the sites for electrophilic and nucleophilic reactions as well as hydrogen bonding interactions [131, 132]. MEP has vital role to explain the hydrogen bonding, chemical reactivity, presence of intra-molecular and inter-molecular interactions, electronegativity and structure activity of molecule [133]. The MEP surface denotes the distance from a molecule at which a positive (test) charge experiences a certain amount of repulsion or attraction. The negative electrostatic potential indicates a possibility of an attraction of proton by the concentrated ED in the molecules, while positive electrostatic potential indicates repulsion of the proton by the atomic nuclei where the nuclear charge is incompletely shielded due to the existence of low electron density. Therefore, the regions with red coloured parts represents negative electrostatic potential while blue ones represent the regions of positive electrostatic potential. Additionally, green coloured parts represent the regions of zero potential. The MEP surface of MA14 molecule is calculated using the optimized molecular structure at B3LYP with 6-311++G(d,p) level and its 3D plot is shown in Figure 5.6. The negative regions of MEP map are mainly localized on O10, N22, F34, F35 and F36 atoms indicating the possible sites for electrophilic reactivity due to the electronegative property of these mentioned atoms. The positive region of MEP map localised on hydrogen atoms indicates the possible sites for nucleophilic attack.

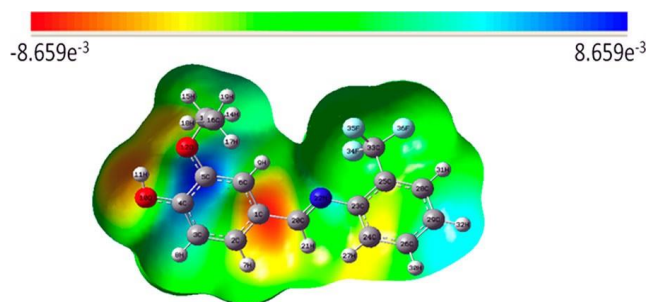


Fig.5.6. MEP Plot of MA14

HOMO–LUMO

The highest occupied molecular orbital (HOMO) and the lowest unoccupied molecular orbital (LUMO) play an essential role in quantum chemistry. These orbitals play a vital role in terms of electric properties as well as they determine the way the molecule interacts with other species [134–136]. Both orbitals take part in chemical reaction. The energy of the HOMO relates to the ionisation potential, whereas LUMO energy corresponds to the electron affinity. These orbitals are also called as frontier molecular orbitals (FMOs) which may be used to predict the absorption centres of the inhibitor molecule for corrosion of metal surfaces [137]. In order to provide a prudent qualitative indication of the excitation energies, HOMO and LUMO energies and HOMO–LUMO gap energy are done at B3LYP method with 6-311++G(d,p) level. The calculated values of HOMO and LUMO energies and HOMO–LUMO band gap energy of MA14 molecule are listed in Table 5.6.

Table 5.6. The Physico-chemical properties of MA14.

Parameters	Values
HOMO	-6.095 eV
LUMO	-1.986 eV
Energy gap	4.109 eV
Ionisation potential [$I = -E_{\text{HOMO}}$]	6.095 eV
Electron affinity [$A = -E_{\text{LUMO}}$]	1.986 eV
Electronegativity [$\chi = (I + A)/2$]	4.041 eV
Chemical potential [$\mu = -\chi$]	-4.041 eV
Chemical hardness [$\eta = (I - A)/2$]	2.055 eV
Chemical softness [$S = 1/2\eta$]	0.487 eV
Electrophilicity index [$\omega = \mu / 2\eta$]	3.982 eV

The HOMO and LUMO plot for MA14 molecule is given in Figure 5.7. The molecules which have more HOMO–LUMO energy band gap are called as ‘hard molecules’, whereas the molecules with a small HOMO–LUMO energy band gap are called as ‘soft molecules’. Therefore, the molecules with the least HOMO–LUMO gap become more reactive. The computed HOMO and LUMO energy values for the MA14 molecule are found as –6.095 and –1.986 eV. The energy band gap between the HOMO and LUMO is obtained as 4.109 eV. The HOMO is localised on the whole molecule except ethyl group, CF₃ and hydrogen atoms whereas; LUMO is localised over the whole molecule except ethoxy group bonded with C₅ atom and CF₃ group. Normally larger the aromatic system, smaller is the HOMO–LUMO gap, which is due to the presence of mobile pi electrons in the aromatic ring. So, F₃ negative is not involved in HOMO–LUMO part which is due to the presence of high electronegative fluorine group

attached with the aromatic ring. The calculated energy band gap between the HOMO and LUMO directly reveals that the charge transfer occurs within the molecule.

Density of state spectrum (DOS) is used to find out the contribution of groups with the molecular orbitals (HOMO–LUMO). DOS plot indicates the density of electrons per orbital and demonstrates an easy view of character of molecular orbitals in a certain energy range. The DOS spectrum is shown in Figure 5.8. The energy range from –20 eV to –5 eV is called as filled orbitals and from –5 eV to 0 eV are called as virtual orbitals. The virtual orbitals are empty and also called as acceptor orbitals, whereas filled orbitals are called as donor orbitals. The green and red lines in the DOS spectrum show the HOMO and LUMO levels, respectively. A high intensity DOS at a particular energy level means that there are many states available for occupation. A zero intensity DOS reveals that there are no states which can be occupied by the system. The frontier molecular orbital (FMO) analysis is done in order to get the molecular orbital information with Gaussian curves of unit height and full width at half maximum (FWHM) of 0.3 eV using the Gausssum 2.2 program [138, 139]. The variations found on the peaks are due to movement of electrons between the C = C and C–C in the rings of the molecule. The obtained FMO energies are given in Table 5.7.

Table 5.7. The frontier molecular orbitals of MA14

Occupancy	Orbital Energies (a.u)	Orbital Energies (eV)	Kinetic Energy (a.u)
O76	-0.295	-8.027	1.599
O77	-0.278	-7.564	1.221
O78	-0.260	-7.075	1.460
O79	-0.248	-6.748	1.537
O80	-0.224	-6.095	1.645
V81	-0.074	-2.014	1.534
V82	-0.038	-1.034	1.424
V83	-0.022	-0.599	1.267
V84	-0.012	-0.326	0.672
V85	-0.012	-0.326	0.949

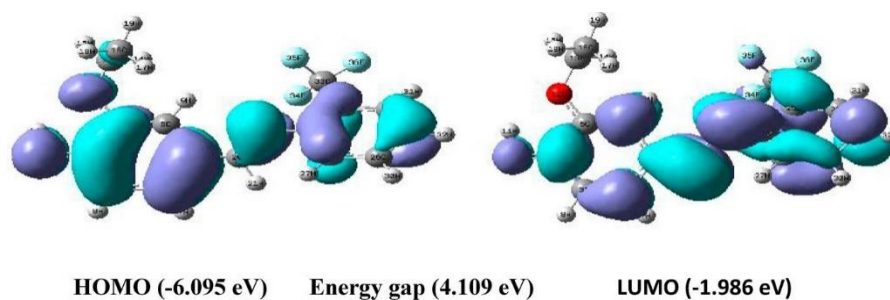


Fig.5.7. HOMO LUMO plots of MA14

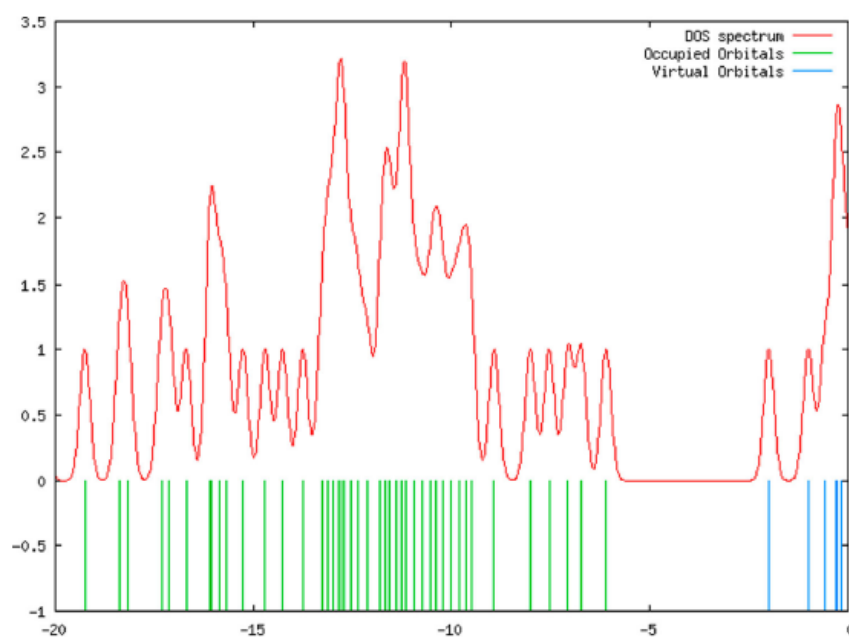


Fig.5.8. Density of state spectrum of MA14

Mulliken atomic charges

Mulliken analysis is one of the simplest and most common method used to determine the electronic partial distribution of molecular atomic charges in a molecular system. It arises from Mulliken population analysis [140]. The calculation of effective charges plays a vital role in the field of quantum chemistry computation. This calculation describes the charge of every atom as positive or negative in a molecular system which plays an important role to increase or decrease the bond length between the atoms. The review of literature depicts that the effective atomic charge distribution plays an essential role in the field of chemical calculation to the molecular system, as the atomic charges effect dipole moment, polarisability, acidity–basicity behaviour, electronic structure and other properties of the molecular system [141]. It is also used to determine the electrostatic potential surfaces [142–144]. The Mulliken atomic charges of MA14 molecule are calculated using B3LYP/6-311++G(d,p) level and are given in Table 5.8. The Mulliken charge plot is shown in Figure 5.9. From the Table 5.8 it is noticed that all hydrogen atoms have positive charges. It is clear that H₁₁ and H₈ atoms have more positive charge compare to other hydrogen atoms and this is due to the electro negative property of O₁₀ atom. The computed Mulliken atomic charges of H₁₁ and H₈ are 0.305 and 0.196 a.u. The atomic charges of carbon atoms are found either positive or negative at the interval –1.131 to +1.050 a.u. The most positive/negative Mulliken atomic charge of carbon atoms are at C₁/C₂₃ as +1.050/–1.131 which is due to the C₂₀ = N₂₂ linkage in between two benzene rings.

Table 5.8. The Mulliken atomic charges of MA14

Atoms	Charges (a.u.)	Atoms	Charges (a.u.)
C1	1.050	H19	0.137
C2	-0.727	C20	-0.032
C3	-0.288	H21	0.103
C4	-0.703	N22	0.302
C5	0.016	C23	-1.131
C6	-0.169	C24	-0.293
H7	0.159	C25	0.964
H8	0.196	C26	-0.037
H9	0.134	H27	0.167
O10	-0.240	C28	0.168
H11	0.305	C29	-0.548
O12	-0.208	H30	0.178
C13	-0.245	H31	0.184
H14	0.165	H32	0.160
H15	0.190	C33	0.386
C16	-0.357	F34	-0.067
H17	0.149	F35	-0.068
H18	0.15	F36	-0.156

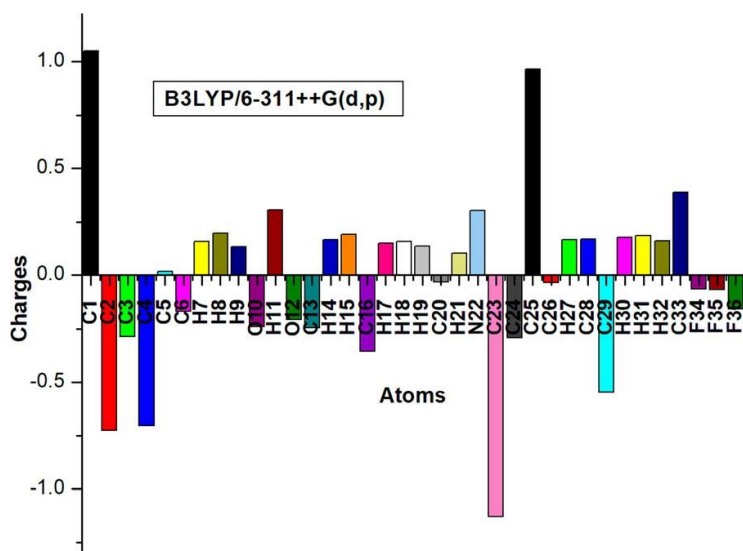


Figure 5.9. The Mulliken atomic charges of MA14.

PES SCAN

The aim of the conformational analysis of MA14 molecule is to provide a model for the molecular structure. Potential energy scan (PES) is a relationship between the energy of the molecule and its geometry. PES is important to visualise and understand the relationship between potential energy and molecular geometry and also help to understand how to compute chemistry programs, locate and characterise structures of interest [145]. Figure 5.10 shows the performance of PES scan for dihedral angle C5–O12–C13–C16 using B3LYP 6- 311++G(d,p) method for the title molecule.

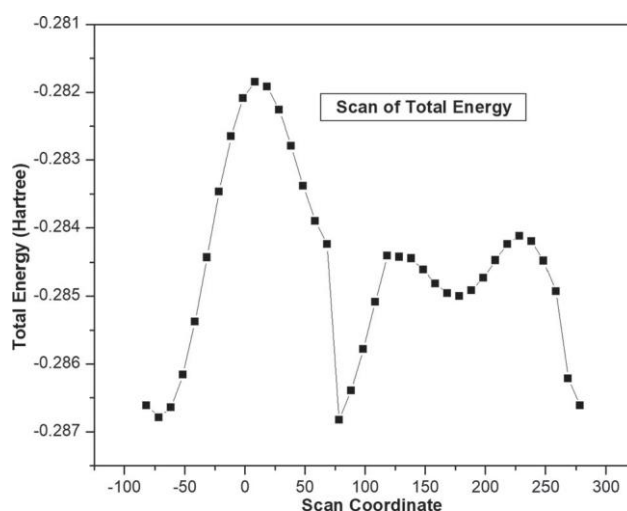


Figure 5.10. The potential energy surface around C5-O12-C13-C16 dihedral angle of MA14 molecule

The PES scan is carried out at the torsion angle C5–O12–C13–C16 using a 10° step size and considering the full 360° range for 2E42TP. The conformational energy profile shows three maxima with an energy values

-0.281846, -0.284118 and -0.284411 (hartree) and four minima with energy -0.286826, -0.286785, -0.286612 and -0.284996 (hartree). The energy values obtained from the scan output reveal that the structure has the dihedral angle C5-O12-C13-C16 at scan coordinate 78.4487 and possess minimum energy.

Thermodynamic properties

The standard thermodynamic functions as heat capacity ($C_{p,m}^0$), entropy (S_m^0) and enthalpy (H_m^0) rotational constants, temperature and zero-point vibrational energy (ZPVE) for MA14 are computed using B3LYP/6-311++G(d,p) basis set at room temperature of 298.15 K, under 1 atm pressure in vacuum and the results are shown in Table 5.9. The partition function plays an important role for both thermodynamic equilibrium and thermodynamic parameters. It has four species which are translational, electronic, vibrational and rotational one. It is used to find thermo- dynamic variables (heat capacity, entropy, equilibrium constants, total energy, pressure, thermal energy and rate constants, etc.) of a system. It is well known that total energy of any molecular system is the sum of electronic, vibrational, rotational and translational energies ($E = E_e + E_v + E_r + E_t$). The computed minimum total energy (-1123.178 a.u), ZPVE (170.428 kcal/mol) and total thermal energy (182.756 kcal/mol) are calculated. The major contribution to thermal energy comes from vibrational energy with 180.979 cal/mol \times K value, whereas minor values belong to electronic energy with 0.000 cal/mol \times K, translational and rotational energies with 0.889 cal/mol \times K one.

Likewise, the calculated heat capacity (C_v) and entropy (S) values are calculated as 74.956 and 149.514 cal/mol \times K, respectively. The contributions of electronic, translational, rotational and vibrational energy to heat capacity and entropy are found as 0.000, 2.981, 2.981 and 68.995 cal/mol \times K and 0.000, 43.082, 34.909 and 71.524 cal/mol \times K, respectively. The computed rotational constants (GHz) for MA14 are found as 0.481, 0.142 and 0.122 GHz, respectively.

Table 5.9. Thermodynamic properties of MA14 molecule.

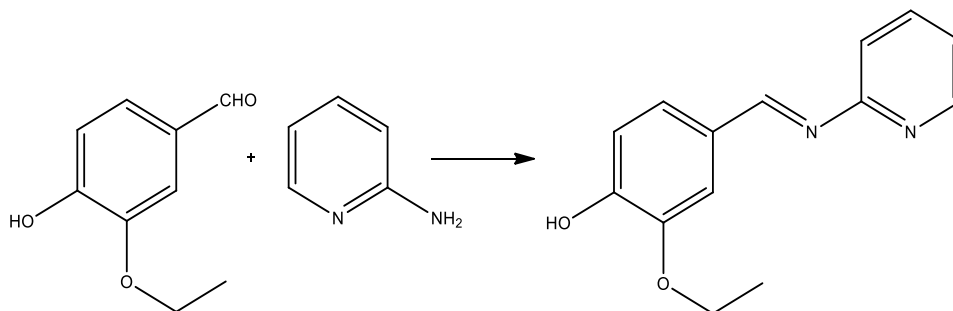
Zero-point vibrational energy 170.428 (kcal/mol) Rotational constants (GHz) A(0.481), B(0.142), C(0.122) E(RB+HF-LYP) = -1123.178 a.u			
	<i>E</i> (Thermal) kcal/mol	<i>C_v</i> (Specific heat)cal/mol \times K	<i>S</i> (Entropy) cal/mol \times K
Total energy	182.756	74.956	149.514
Electronic	0.000	0.000	0.000
Translational	0.889	2.981	43.082
Rotational	0.889	2.981	34.909
Vibrational	180.979	68.995	71.524

For the first time a complete vibrational analysis was performed for MA14 molecule. The detailed interpretations of the vibrational spectra were carried out. The vibrational assignments were justified with the help of TED. The optimised geometrical parameters were calculated and compared with the reported XRD values. The calculated dihedral angles N22-C23-C25-C33, O10-C4-C5-O12 and C6-C1-C20-N22 are -2.16, -0.73 and 1.43° which showed the planarity nature of the molecule. The first order hyperpolarisability (β_0) value was seventy times more than that of urea and hence the present molecule possessed good NLO

property. The $\nu_{\text{O10-H11}}$ mode was observed at higher frequency due to high energy transfer from LPO10 to π^* C3–C4 (124.22 kJ) anti-bonding orbital. The experimental band at 363 nm was attributed mainly due to a HOMO \rightarrow LUMO transition which was predicted as $\pi \rightarrow \pi^*$ transition. The physico-chemical properties, Mulliken atomic charges, MEP and thermodynamic properties were also calculated. The H₁₁ atom had more positive charge compared to other hydrogen atoms which was due to the electronegative property of O10 atom. The most positive/negative Mulliken atomic charge of carbon atoms were at C1/C23 as +1.050/–1.131 which was due to the C20 = N22 linkage in between two benzene rings. The potential energy surface was obtained depending on the C5–O12–C13–C16 torsional angle.

5.2. Synthesis of 2-Ethoxy-4-(pyridin-2-yliminomethyl)-phenol (MA15)

To the ethanolic solution of 3-ethoxy-4-hydroxy benzaldehyde (16.6 g, 0.1 M), 2-aminopyridine (9.4 g, 0.1 M) was added and refluxed for 6 h. The reaction mixture was cooled and poured in to a beaker containing crushed ice. The solid separated was washed, filtered and dried over vacuum and recrystallized using absolute ethanol.



Scheme 5.2: Synthesis of 2-Ethoxy-4-(pyridin-2-yliminomethyl)-phenol (MA15)

5.2.1. IR spectrum of 2-Ethoxy-4-(pyridin-2-yliminomethyl)-phenol (MA15)

The FT-IR spectrum of MA15 is depicted in the Fig. 5.11. A broad intense band appeared at 3263 cm^{-1} indicates OH stretching. Aromatic C-H stretching shows a band at 3061 cm^{-1} . A sharp band appeared at 2949 cm^{-1} shows C-H stretching of methyl group. Strong absorption bands appeared at 2829 cm^{-1} and 2749 cm^{-1} are due to asymmetric and symmetric C-H stretching of methylene group. An absorption band at 1544 cm^{-1} indicates C=N stretching. A band appeared at 1150 cm^{-1} is due to C-O-C stretching.

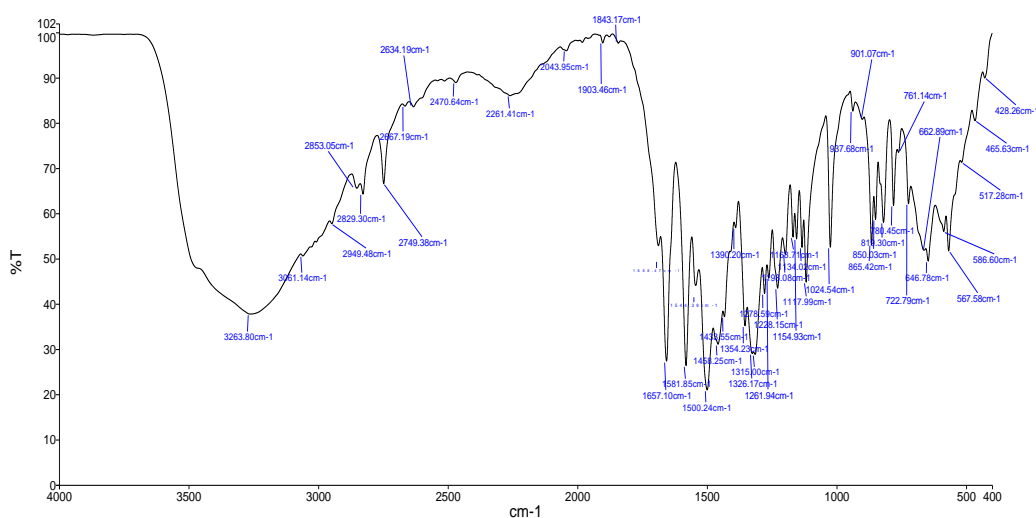


Fig.5.11. IR spectrum of 2-Ethoxy-4-(pyridin-2-yliminomethyl)-phenol (MA15)

5.2.2. Mass spectrum of 2-Ethoxy-4-(pyridin-2-yliminomethyl)-phenol (MA15)

Mass spectra of the compound MA15 has been depicted in the Fig. 5.12. The peak appearing at m/z 242.11 is the molecular ion peak ($M+1$). The intense peak noticed at m/z 226.11 is assigned as base peak.

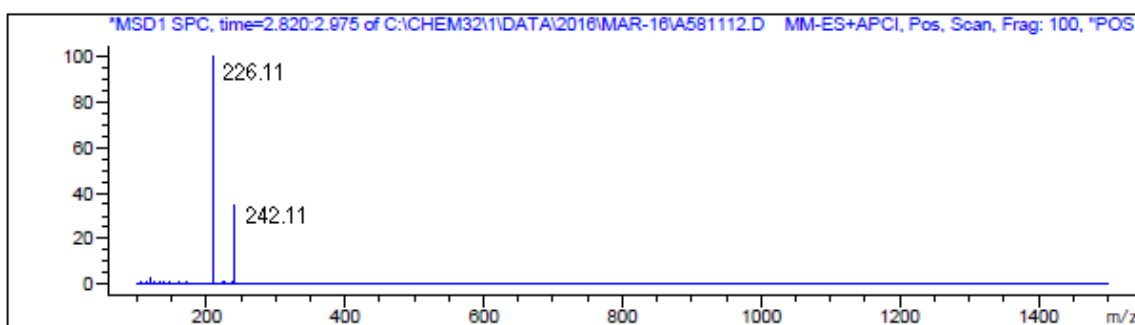


Fig.5.12. Mass spectrum of 2-Ethoxy-4-(pyridin-2-yliminomethyl)-phenol (MA15)

The experimental FT-IR and FT-Raman spectra of the title compound are compared with the theoretical spectra in Fig. 5.13 & 5.14 respectively. The scaled calculated harmonic vibrational frequencies at B3LYP/6-311++G(d,p) level, observed vibrational frequencies are tabulated in Table 5.10. Harmonic frequencies are calculated for gas phase of an isolated compound while the experimental ones are obtained for its solid phase. Hence, there is disagreement between the observed and the calculated frequencies in some modes. In order to improve the agreement between the calculated and the experimentally observed values, the calculated harmonic frequencies have been scaled down by 0.9668.

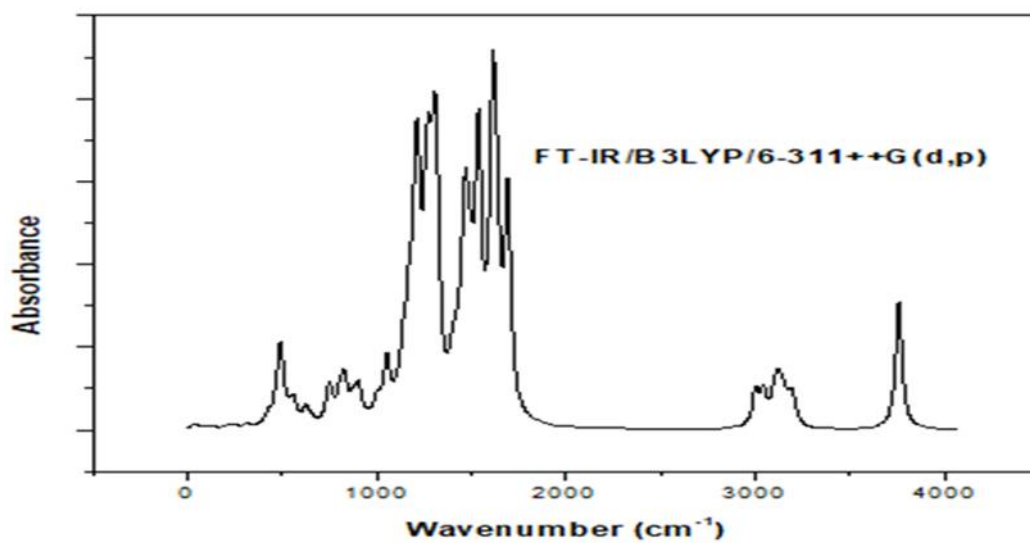


Fig.5.13.IR spectrum of MA15

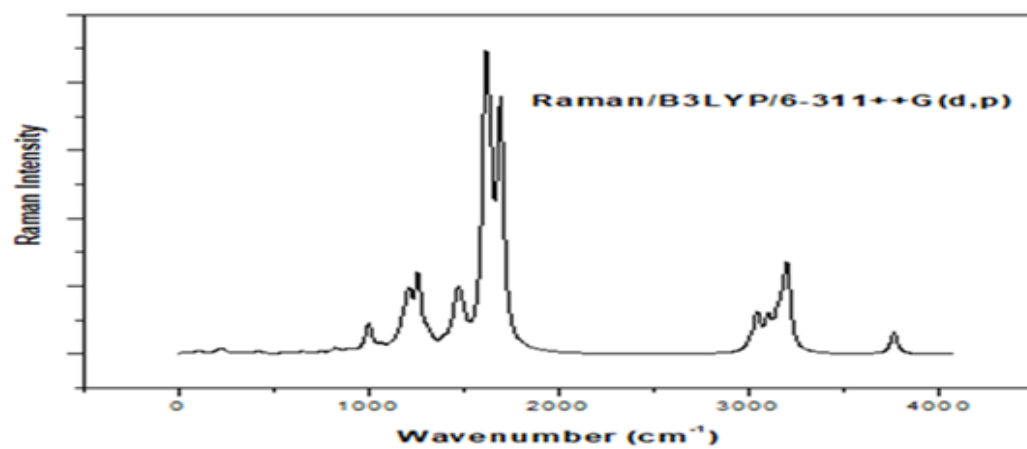


Fig.5.14.Raman spectrum of MA15

The frequencies obtained by theoretical method are in accordance with the observed FT-IR and FT-Raman spectra. The present molecule belongs to C_1 point group. The OH stretching are extremely sensitive to the formation of hydrogen bonding. The absorption bands in the region 3700-3100 cm^{-1} result the presence of O-H stretching mode. In the present work, the OH stretching vibration is assigned at 3263 cm^{-1} and its harmonic value is calculated at 3633 cm^{-1} . This decrease in ν_{OH} is due to intra-molecular hydrogen bonding. If it is present in a six membered ring moiety, the ν_{OH} mode would be reduced to 3200-3500 cm^{-1} . The CH stretching vibrations are normally observed in the region 3100-3000 cm^{-1} for the benzene ring and less than 3000 cm^{-1} for non-aromatic compounds. In the present work, the CH stretching vibrations are assigned at 3025, 2980 and 2947 cm^{-1} in FT-Raman spectrum and its calculated values are: 3016, 2991 and 2944 cm^{-1} . The CH bending vibrations are assigned at 1023, 1067 cm^{-1} . It is difficult to assign ν_{CN} vibrations, since there is mixing of several vibrations are possible. Silverstein et al assigned CN stretching absorption in the region 1500-1600 cm^{-1} . In the present work, the band observed at 1657 cm^{-1} has been assigned to CN stretching vibration and its corresponding calculated frequency is 1634 cm^{-1} . The CN in-plane bending vibration is observed at 1354 cm^{-1} in FT-IR and 1353 cm^{-1} in FT-Raman. The ring stretching vibrations are very important in the spectrum of benzene and their derivatives are highly characteristic of the aromatic ring itself. The bands between 1400 and 1650 cm^{-1} in benzene derivatives are usually assigned to C=C stretching modes. For the title molecule, the CC stretching

vibrations are undoubtedly assigned to 1438 cm^{-1} in FT-IR and 1430 cm^{-1} in FT-Raman. These assignments are within the characteristic region and also find support from harmonic value 1436 cm^{-1} . The CC in-plane bending vibration is assigned at 959 cm^{-1} and its corresponding harmonic value is 967.8 cm^{-1} . The carbonyl stretching vibrations has been most extensively studied by IR spectroscopy. This multiply bonded group is highly polar and therefore gives rise to an intense IR absorption band $1168\text{-}1310\text{ cm}^{-1}$. Based on the above conclusion, the observed bands 1117 cm^{-1} : FT-IR/ 1113 cm^{-1} : FT-Raman however with weak intensity and its corresponding harmonic value 1130 cm^{-1} is designated as νCO mode is observed in the present investigation. The in-plane and out-of-plane vibrations are listed in Table.

Table 5.10. The experimental and calculated frequencies of MA15 using B3LYP/6-311++G(d,p) level of basis set [Harmonic frequencies (cm⁻¹), FT- IR, FT- Raman (cm⁻¹)

S. No.	Observed frequencies			Vibrational Assignments
	Scaled	FTIR	FTIRaman	
1	3633	3263.8(m)		vOH
2	3104			vCH
3	3091			vCH
4	3089			vCH
5	3082			vCH
6	3065			vCH
7	3063	3061.14(vw)	3052.94(m)	vCH
8	3040			vCH
9	3016		3025.61(m)	vCH
10	2997			vCH
11	2991		2980.16(vw)	vCH
12	2944	2949.48(vw)	2947.04(m)	vCH
13	2936			vCH
14	2901	2853.05(v)	2848.62(m)	vCH
15	1635	1657.1(vs)	1646.1(vs)	vNC)
16	1583	1581.85(vs)		vCC+vCC
17	1580		1577.27(vs)	vCC+vCC+vCC
18	1561			vNC+vCC+vCC
19	1547	1544.39(vw)	1544.88(s)	vNC+vCC+vCC+βCCC
20	1486			vCC+vCC+vCC+vOC
21	1469	1458.25(vw)	1456.83(m)	βHCH+βHCH
22	1451			βHCH+βHCH
23	1446			vNC+βHCC+βHCN
24	1437	1438.55(w)	1430.07(vw)	βHCH
25	1422			vCC+vCC+vCC+βHCC
26	1406		1407.01(vw)	vNC+βHCC+βHCC
27	1386	1390.2(vw)	1388.83(vw)	vCC+βHOC+βHCN+ΓCHCH

28	1368			$\Gamma\text{CHCH}+\Gamma\text{CHHH}$
29	1353	1354.23(w)	1353.69(vw)	$\beta\text{HCN}+\Gamma\text{CHCH}+\Gamma\text{CHHH}$
30	1344	1326.17(vw)	1317.95(m)	$\beta\text{HOC}+\beta\text{HCN}+\Gamma\text{CHCH}$
31	1284			βHCO
32	1278	1278.59(m)		$\nu\text{NC}+\beta\text{HCC}+\beta\text{HCN}$
33	1266	1261.94(w)	1262.92(vw)	$\nu\text{CC}+\nu\text{CC}+\nu\text{CC}+\nu\text{OC}$
34	1256			βHCC
35	1240			$\nu\text{NC}+\nu\text{CC}$
36	1232	1228.15(m)	1224.62(m)	νOC
37	1215			νNC
38	1174	1168.71(w)	1198.56(vw)	$\nu\text{CC}+\beta\text{HOC}+\beta\text{HCC}$
39	1157	1154.93(vw)		$\Gamma\text{CHCO}+\Gamma\text{CHCH}$
40	1133	1134.02(m)		$\nu\text{CC}+\nu\text{CC}+\beta\text{HCC}+\beta\text{HCC}+\beta\text{HCC}$
41	1130			$\nu\text{OC}+\nu\text{CC}+\beta\text{HCC}+\beta\text{HCC}$
42	1102		1113.08(w)	$\nu\text{CC}+\beta\text{HCC}+\beta\text{HCC}$
43	1080			$\nu\text{CC}+\nu\text{CC}+\beta\text{HCC}+\beta\text{HCC}$
44	1067		1067.46(w)	$\nu\text{CC}+\beta\text{HCC}+\beta\text{CCO}$
45	1032	1024.54(vs)	1023.91(w)	$\nu\text{CC}+\nu\text{CC}+\beta\text{HCC}$
46	1016			$\nu\text{CC}+\nu\text{OC}$
47	973			$\tau\text{HCCH}+\tau\text{HCCH}+\Gamma\text{CCNH}$
48	971.6			$\beta\text{CCN}+\beta\text{CCC}+\Gamma\text{CCNH}$
49	967.8			$\beta\text{CCC}+\tau\text{HCCH}+\tau\text{HCCH}+\Gamma\text{CCNH}$
50	957.1		959.56(vw)	$\nu\text{CC}+\nu\text{CC}$
51	947.5	937.68(vw)	938.03(vw)	τHCCH
52	914.6	901.07(vw)		$\Gamma\text{CCCH}+\tau\text{HCCC}$
53	875			$\nu\text{CC}+\nu\text{OC}+\beta\text{HCC}$
54	868.2	865(s)		τHCCO
55	859.5			$\tau\text{HCCH}+\tau\text{HCCH}$
56	843	850.03(m)		$\nu\text{NC}+\beta\text{CCC}+\tau\text{HCCH}$
57	803.4	819.3(m)	824.33(w)	$\Gamma\text{CCCH}+\tau\text{HCCC}$
58	798.6			$\nu\text{OC}+\Gamma\text{CCCH}$
59	788.9			$\Gamma\text{CHCO}+\Gamma\text{CHCH}$

60	774.4	780.45(s)	780.08(w)	Γ CHCO+ τ CNCC+ Γ CNCNC
61	727			τ HCCN+ τ CNCC+ τ CCCN
62	721.2	722.79(w)	722.32(vw)	ν OC+ β CCC
63	709.6			τ CCCC5+ τ CCCC
64	637.1	646.78(w)	639.1(m)	β CCN+ β CCN
65	614.9			β CCN+ β CCC+ β NCN
66	603.3			τ CCCC
67	559.8	567.58(m)	566.97(vw)	β CCO
68	539.5			ν OC+ β CCC+ β CCO
69	525	517.28(vw)	514.12(vw)	τ CCCC+ τ CCCN+ Γ CNCNC
70	492			β CCC
71	476.6			β NCN+ τ HOCC
72	470.8	465.63(vw)		τ HOCC
73	446.7			τ CCCC+ τ CCCC+ τ CCCO+ τ CCCO
74	412.8	428.26(vw)	426.59(w)	β CCO+ β CCO
75	407			τ CNCC+ τ CCCC+ τ CCCN
v: Stretching, β :in-plane-bending, Γ :out-of-plane bending, τ :Torsion, vw: very weak, w:weak,				
m:medium, s:strong, scaling factor:0.9668(Radom et al.,)				

Summary and Conclusion

The research work deals with the synthesis and characterisation of some azomethines and β -amino carbonyl compounds using Schiff condensation pathway and Mannich reaction respectively. Fifteen new compounds have been synthesized using simple synthetic procedure based on the recent literatures.

Twelve compounds listed below have been synthesized via Schiff Condensation

- (2, 3-Dichloro-benzylidene)-(1-phenyl-ethyl)-amine **(MA1)**
(4-Isopropyl-benzylidene)-(3-trifluoromethyl phenyl)-amine **(MA2)**
N-(4-isopropylbenzylidene)-4-nitro-2-(trifluoromethyl)aniline **(MA3)**
3-(trifluoromethyl)-N-(3,4,5-trimethoxybenzylidene)aniline **(MA4)**
3-methyl-2-((3,4,5-trimethoxybenzylidene)amino)butanoic acid **(MA5)**
(E,E)-1,1'-(pentane-2,4-diylidene)bis(3-phenylurea) **(MA6)**
4-(((5-bromopyridin-2-yl)imino)methyl)phenol **(MA7)**
1-phenyl-3-(thiophen-2-ylmethylene)urea **(MA8)**
5-bromo-N-(2,3-dichlorobenzylidene)pyridin-2-amine **(MA9)**
5-bromo-N-(thiophen-2-ylmethylene)pyridin-2-amine **(MA10)**
2-ethoxy-4-(((2-(trifluoromethyl)phenyl)imino) methyl)phenol **(MA14)**
2-Ethoxy-4-(pyridin-2-yliminomethyl)-phenol **(MA15)**

Three compounds mentioned below have been synthesized via Mannich reaction.

- 3-morpholino-1-(3-nitrophenyl)-3-(thiophen-2-yl)propan-1-one **(MA11)**
3-((4-aminophenyl)amino)-1-phenyl-3-(thiophen-2-yl)propan-1-one **(MA12)**
2-(pyrrolidin-1-yl(thiophen-2-yl)methyl)cyclohexanone **(MA13)**

All the compounds have been characterized using FTIR, ¹H & ¹³C-NMR and mass spectral studies. The results of the spectral investigation are found to be in amicable agreement with the proposed structures of the synthesized compounds.

Antimicrobial screening has been carried out at various concentrations for thirteen compounds MA1-MA13. Four bacterial pathogens viz., *Staphylococcus aureus*, *Escherichia coli*, *Bacillus subtilis*, *Moraxella* and three fungi strains viz., *Candida albicans*, *Aspergillus niger*, *Trichophyton* have been selected at random for the investigation. Hilton Agar dilution method employed for antimicrobial screening and Ofloxacin, Amphotericin B and Gentamicin were used as positive standards. Compound, MA10 possessed excellent antimicrobial activity against the tested bacteria and fungi pathogens. Zone of inhibition of MA10 is higher than the positive standard. Presence of thiophene ring and bromo substituted pyridine ring present in the compound may be the reason for its potency. Compounds MA7, MA9 and MA11 are exhibited equal antimicrobial activity compared to the standard drug. Compound MA6 exhibited moderate antimicrobial activity compared to the standard drugs. Considerable activity has been found in the compounds MA1, MA3, MA8 against bacteria stain and moderate activity noticed against fungi pathogens. Zone of inhibition of the compounds MA4 and MA5 are moderate against bacteria strains. Compounds MA12 and MA13 possessed very less activity against all the tested microbial strains.

Density functional theory (DFT) studies have been carried out for the compounds MA13 and MA14. Characteristic absorption frequencies have been well established by FTIR spectral characterization and it is correlated with FT-Raman spectral studies.

References

1. I. Iovel, L. Golomba, J. Popelis, A. Gaukhman and E. Lukevics, *Chemistry of Heterocyclic compounds* 36 **(2000)** 264
2. Adnan dib, *International Journal of ChemTech Research* 5 **(2013)** 204
3. Veera Raghavulu Nagavolu, Shankarananth Velusamy, Sridhar Chechugari, Prasanna Raju Yalavarthi and Manasa Karani, *Indian Journal of Pharmaceutical Education and Research* 51 **(2017)**
4. Sunita Bhagat, Nutan Sharma and Tejpal Singh Chundawat, *Hindawi Journal of Chemistry*, Article ID 909217 **(2013)**
5. Jumbad H. Tomma, Mustafa S. Khazaal and Ammar H. Al-Dujaili, *Arabian Journal of Chemistry* 7 **(2014)** 157
6. Emad Yousif, Ahmed Majeed, Khulood Al-Sammarrae, Nadia Salih, Jumat Salimon and Bashar Abdullah, *Arabian Journal of Chemistry* 10 **(2017)** 1639
7. Rishikesh V. Antre, A. Cendilkumar, Divakar Goli, Ganesh S. Andhale, and Rajesh J. Oswal, *Saudi Pharmaceutical Journal* 19 **(2011)** 233
8. Hina Zafar, Abdul Kareem, Asif Sherwani, Owais Mohammad, Mohammad Azam Ansari, Haris M.Khan and Tahir AliKhan, *Journal of Photochemistry and Photobiology B: Biology* 142 **(2015)** 8
9. Yixiao Dong, Waqar U.Hassan, Robert Kennedy, Udo Greiser, Abhay Pandit, Yolanda Garcia and Wenxin Wang, *Acta Biomaterialia* 10 **(2014)** 2076
10. Eliene Leandrode Araújo, Hellen Franciane, Gonçalves Barbosa, Edward Ralph Dockal and Éder Tadeu Gomes Cavaleiro, *International Journal of Biological Macromolecules* 95 **(2017)** 168

11. B.Kavitha, M.Sravanthi and P.Saritha Reddy, Journal of Molecular Structure 1185 **(2019)** 153
12. A. M. Iglesias, V. Miranda-soto, D. A. Pompa-Monroy , J. G. Martínez-Ortiz, G. K. Díaz-Trujillo and L. J. Villarreal-Gómez, Indian Journal of Pharmaceutical Sciences 81 **(2019)** 333
13. Bhushan Nazirkar, Mustapha Mandewale and Ramesh Yamgar, Journal of Taibah University for Science 13 **(2019)** 440
14. Ikram Saadaoui, Fatma Krichen, Bochra Ben Salah, Riadh Ben Mansour, Nabil Miled, Ali Bougatef and Mohamed Kossentini, Journal of Molecular Structure 1180 **(2019)** 344
15. Shahzad Murtaza, Muhammad Shoaib Akhtar, Farina Kanwal, Aadil Abbas, Shoaib Ashiq and Saima Shamim, Journal of Saudi Chemical Society 21 **(2017)** 329
16. Mokhles M.Abd-Elzaher, Ammar A.Labib, Hanan A.Mousa, Samia A.Moustafa, Mamdouh M.Ali and Ahmed A.El-Rashedy, Beni-Suef University Journal of Basic and Applied Sciences 5 **(2016)** 85
17. Salam A.H.Al-AmeriMahmoud N.A.Al-JibouriTaghreed M.D.Musa, Journal of Saudi Chemical Socceity 18 2014 802
18. Asha B.Thomas, Rabindra K.Nanda, Lata P.Kothapalli and Sunil C.Hamane, Arabian Journal of Chemistry 9 (2016) S79
19. P.MangaveniG.DurgaP.BhushanavathiP.Sarada, Materials Today Proceedings 5 2018 25862
20. Azza A.Abou-Hussein and Wolf gang Linert Spectrochimica Acta Part A: Molecular and Biomolecuar Spectroscopy 117 2014 763
21. Hanan F.Abd El-halim, M.M.Omar and Gehad G.Mohamed, Spectrochimica Acta Part A: Molecular and Biomolecular Spectroscopy 78 **(2011)** 36

22. Gehad G.MohamedM.M.Omar and Ahmed M.M.Hindy, *Spectrochimica Acta Part A: Molecular and Biomolecular Spectroscopy* 62 **(2005)** 1140
23. Divyaraj Puthran Boja Poojary Nikil Purushotham Nandam Harikrishna Soukhyarani GopalNayak Vinuta Kamat, *Heliyon* 5 **(2019)** e02233
24. Y.Harinath, D.Harikishore Kumar Reddy, B.Naresh Kumar, Ch.Apparao and K.Seshaiah, *Spectrochimica Acta Part A: Molecular and Biomolecular Spectroscopy* 101 **(2013)** 264
25. Piotr Przybylski, Adam Huczynski, Krystian Pyta, Bogumil Brzezinski, Franz Bartl, *Current Organic Chemistry* 13 **(2009)** 124
26. Zhanyong Guo, Rong Xing, Song Liu, Zhimei Zhong, Xia Ji, Lin Wang and Pengcheng Li, *Carbohydrate Research* 342 **(2007)** 1329
27. Shū Kobayashi, Naohiro Aoyama and Kei Manabe, *Wiley Online Library* 2 (2003) 124
28. Shū Kobayashi, Masaharu Ueno, Susumu Saito, Yumiko Mizuki, Haruro Ishitani, and Yasuhiro Yamashita, *Proceedings of the National Academy of Sciences of the United states of America* 15 **(2004)** 5476
29. Nanyan Fu and Thomas T.Tidwell, *Tetrahedron* 64 **(2008)** 10465
30. P Rathelot, P Vanelle, M Gasquet, F Delmas, MP Crozet, P Timon-David and J Maldonado, *European Journal of Medicinal Chemistry* 30 **(1995)** 503
31. Misbah ur Rehman, Muhammad Imran and Muhammad Arif, *American Journal of Applied Chemistry* 4 **(2013)** 59
32. Dueke-Eze, C. U, Fasina, T. M and Idika. N, *African Journal of Pure and Applied Chemistry* 5 **(2011)** 13
33. Francis K. Ngounoue, Evans N. Mainsah, Aseng M. Conde , Awawou G. Paboudam, Sally-Judith E. Ntum, Walter K.

- Ndamukong, Choumkeu Mbakop Vanessa and Peter T Ndifon, *Der Pharma Chemica* 7 **(2015)** 101
34. A. V. G. S. Prasad, K Trinagaraju, Boyina Gopala Rao, Y. Usha, P. Sudha Reddy, P. Venkateswara Rao, *International journal of innovative research and development* 2 **(2013)** 39
35. R Nirmal, Cr Prakash, K Meenakshi and P Shanmuga pandiyan, *Journal of Young Pharmacists* 2 **(2010)** 162
36. Mohammad Sayed Alam, Dong-Ung Lee and Md. Latiful Bari, *Journal of the Korean Socceity for Applied Biological Chemistry* 57 **(2014)** 613
37. Shahzad Murtaza, Muhammad Shoaib Akhtar, Farina Kanwal, Aadil Abbas, Shoaib Ashiq and Saima Shamim, *Journal of Saudi Chemical Socceity* 21 **(2017)** S359
38. Dharmarajan Sriram, Perumal Yogeewari, Naga Sirisha Myneedu and Vivek Saraswat, *Bioorganic and Medicinal Chemistry Letters* 16 **(2006)** 2127
39. Krishnan Suresh Kumar, Swastika Ganguly and Erik De Clercq, *European Journal of Medicinal Chemistry* 45 **(2010)** 5474
40. Fatiha Benachenhou, Abderrezzak Mesli and Roger Guilard, *Arabian Journal Chemistry* 6 **(2013)** 313
41. Mounira Mesbah, Tahar Douadi, Farida Sahli, Saifi Issaadi, Soraya Boukazoula, Salah Chafaa, *Journal of molecular structure*, 1151 **(2018)** 41
42. Angamaly Antony Shanty, Jessica Elizabeth Philip, Eeettinil kunnathil JoseSneha, Maliyeckal R, Prathapachandra Kurup, Sreedharan nair, Balachandran and Puzhavorparambil Velayudhan Mohanan, *Bioorganic Chemistry*, 70 **(2017)** 67
43. Hossein Naeimi, Hashem Sharghi, Fariba Salimi and Khadijeh Rabiei, *Heteroatom Chemistry* 19 **(2008)** 1

44. Dong-Mei Ye, Hou-Li Zhang, Li Wang, Qi-Ying Yao, Yuan Lin and Kun Li, Asian Journal of chemistry 25 **(2013)** 4629
45. Vladimir P. Petrovic, Dusica Simijonovic, Zorica D. Petrovic and Svetlana Markovic, Chemical Papers 69 **(2015)** 1244
46. Subrahmanian Supriya, Aravamudhan Raghavan, V.R. Vijayaraghavan, Kandasamy Chinnakali, Hoong-Kun Fun and J. Subramanian, Polyhedron 26 **(2007)** 3217.
47. Po-Jung J. Huang, D. Youssef, T. Stanley Cameron and Amitabh Jhaa, Platinum Open Access Journal for Organic Chemistry 16 **(2008)** 165.
48. Chew Hee Ng, Yih Tong Lim, Norhayati Moris and Siang Guan Teoh, Polyhedron 22 **(2003)** 521.
49. Scott K. Bur and Stephen. F. Martin, Tetrahedron 57 **(2001)** 3221.
50. Dhananjay V. Bondar, Research Journey 165 **(2019)** 270
51. Afshin Fassihi, Daryoush Abedi, Lotfollah Saghaie, Razieh Sabet, Hossein Fazeli, Ghasem Bostaki, Omid Deilami and Hekmatollah Sadinpour, European Journal of Medicinal Chemistry 44 **(2009)** 2145
52. K. Shanmuga Bharathi, A. Kalilur Rahiman, K. Rajesh, S. Sreedaran, P.G. Aravindan, D. Velmurugan and V. Narayanan, Polyhedron. 25 **(2006)** 2859.
53. Zhi-Liang Yuan, Jia-Jun Jiang and Min Shi, Tetrahedron. 65 **(2009)** 6001
54. Arun M. Isloor, Balakrishna Kalluraya and Prashanth Shetty, European Journal of Medicinal Chemistry 44 **(2009)** 3784
55. Kakul Husain, Mohammad Abid and Amir Azam, European Journal of Medicinal Chemistry 43 **(2008)** 393

56. Chalugaraju K C and Ishwar Bhat K, International Journal of ChemTech Research 2 **(2010)** 1368
57. U. Sankappa Rai, Arun M. Isloor, Prakash Shetty, Nishitha Isloor, Shridhar Malladi and Hoong-Kun Fun, European Journal of Medicinal Chemistry 45 **(2010)** 6090
58. M. Lakshmi Kantam, Koosam Mahendar, Bojja Sreedhar, Boyapati. M. Choudary, Suresh K. Bhargava and Steven H. Priver, Tetrahedron 66 **(2010)** 5042.
59. Trupti S. Chitre, Santosh Panda, Shital M. Patil, Aparna S. Chothe, G. Vignesh, Amol B. Salake and Muthu K. Kathiravan, Advances in Biological Chemistry 1 **(2011)** 7
60. Ahlam J. Abdulghani and Nada M. Abbas, Bioinorg Chemistry and Applications 706262 **(2011)** 1
61. Ebru Mete, Halise Inci Gul, Sinan Bilginer, Oztekin Algul, Mehmet Emin Topaloglu, Medine Gulluce and Cavit Kazaz, Molecules 16 **(2011)** 4660
62. Arthur Y. Shaw, Chun-Yi Chang, Mei-Yuan Hsu, Pei-Jung Lu, Chia-Ning Yang, Hui-Ling Chen, Cheng-Wei Lo, Chung-Wai Shiau and Ming-Kai Chern, European Journal of Medicinal Chemistry 45 **(2010)** 2860
63. Amanda P. Neves, Kelly C.B. Maia, Maria D. Vargas, Lorenzo C. Visentin, Annelise Casellato, Miguel A. Novak and Antônio S. Mangrich, Polyhedron 29 **(2010)** 2884
64. Elizabeth Malamidou-Xenikaki, Christina Vlachou and Xenophon N. Stampelos, Tetrahedron. 62 **(2006)** 9931
65. Elena Maria Mosoarca, Ingo Pantenburg, Ramona Tudose, Gerd Meyer, Nicolae Calin Popa, Adelina Han, Radostina Alexandrova, Reni Kalfin, Wolfgang Linert and Otilia Costisor, Inorganica Chimica Acta 370 **(2011)** 460.

66. Bikash Karmakar and Julie Banerji, Tetrahedron Letters 52 **(2011)** 4957
67. Arpit D. Shah, Devanshi J. Raval, Viraj P. Jatakiya, Dr. Dhrubo Jyoti Sen and R. Badmanaban, International Journal of Drug Development & Research. 4 **(2012)** 205
68. Sachin A. Pishawikar and Harinath N. More, Arabian Journal of Chemistry 10 **(2017)** S2714
69. S. Sheik Mansoor, K. Aswin, K. Logaiya and S.P.N. Sudhan, Journal of Saudi Chemical Society 19 **(2015)** 379.
70. Pandeya S N and Neha Rajput, Indo Global Journal of Pharmaceutical Sciences 2 **(2012)** 76.
71. Surendra N. Pandeya and Neha Rajput, International Journal of Medicinal Chemistry 237965 **(2012)** 1
72. Sindhu T. J, Meena Chandran, K Krishnakumar and A R Bhat, Journal of Pharmacy Research 1 **(2013)** 992.
73. G. Vishnuvardhanaraj, D. Tamilvendan and M. Amaladasan, International Journal of Pharmacy and Pharmaceutical Sciences 5 **(2013)** 821
74. Rimpay Gupta, Haq N. Sheikh, Bansil Kalsotra and Vishal Singh, Journal of Saudi Chemical Society 20 **(2016)** 291
75. Wafaa S. Hamama, Mohamed A. Ismail, Hanaa A. Al-Saman and Hanafi H. Zoorob, Journal of Advanced Research 4 **(2013)** 115
76. Rathi Paresh P, More Vishal S, Deshmukh V.K and Chaudhari S. R, International Journal of Pharmaceutical Research 10 **(2013)** 30
77. Rita Bamnola and S P Shrivatava, Indian Journal of Chemistry 53B **(2014)** 1128
78. Baldwin Mathew V, Meena Chandran, K Krishnakumar and A.R Bhat, Journal of Pharmacy Research 1 **(2013)** 970

79. Jiangke Qin, Wenli Lan, Zhong Liu, Jun Huang, Huang Tang and Hengshan Wang, *Chemistry Central Journal* 7 **(2013)** 1
80. Veerababurao Kavala, Chunchi Lin, Chun-Wei Kuo, Hulin Fang and Ching-Fa Yao, *Tetrahedron* 68 **(2012)** 1321
81. Someshwar D. Dindulkar, Vedavati G. Puranik and Yeon Tae Jeong, *Tetrahedron Letters* 53 **(2012)** 4376
82. Onkara.P, A.Sunil Kumar, S.Kanakaraju, B.Prasanna, Y.Pydisetty and G.V.P.Chandramoul, *International Journal of Pharma and Bio Sciences* 4 **(2013)** 263.
83. Suman Bala, Neha Sharma, Anu Kajal, Sunil Kamboj, and Vipin Saini, *International Journal of Medicinal Chemistry* 191072 **(2014)** 1
84. M. Sivakami, B. Natarajan, M.Vijayachandrasekar, S. Ram Kumar Pandian and Krishnan Sundar, *International Journal of Pharmacy and Pharmaceutical Sciences* 6 **(2014)** 59
85. K.Chakkaravarthi, K.Gokulakrishnan, T.Suman and D.Tamilvendan, *International Journal of Pharma and Bio Sciences* 5 **(2014)** 580
86. Beena Thomas, Anju LS and Jyoti Harindran, *International Journal of Research in Pharmacy and Chemistry* 4 **(2014)** 351
87. Sayan Dutta Gupta, Manish Kumar Bommaka, Gisela I. Mazaira, Mario D. Galigniana, Chavali Venkata Satya Subrahmanyam, Naryanasamy Lachmana Gowrishankar and Nulgumnalli Manjunathaiah Raghavendra, *International Journal of Biological Macromolecules* 80 **(2015)** 253
88. Hitendra M. Patel, *Green and Sustainable Chemistry* 5 **(2015)** 137
89. Sheela Joshi, Purni Bilgaiyan and Anju Pathak, *Arabian Journal of Chemistry* 10 **(2013)** S1180

90. Gheorghe Roman, *Mini-Reviews in Organic Chemistry* 10 **(2013)** 27
91. M.J. Frisch, G.W. Trucks, H.B. Schlegel, G.E. Scuse-
ria, M.A. Robb, J.R. Cheeseman, J.A. Montgomery, T.J. Vreven, K.N. Kudin,
J.C. Burant, J.M. Millam, S.S. Iyengar, J., Tomasi, V. Barone, B.
Mennucci, M. Cossi, G. Scal-
mani, N. Rega, G.A. Petersson, H.
Nakatsuji, M. Hada, M. Ehara, K. Toyota, R. Fukuda, J. Hasegawa,
M. Ishida, T., Nakajima, Y. Honda, O. Kitao, H. Nakai, M. Klene,
X. Li, J.E. Knox, H.P. Hratchian, J.B. Cross, C. Adamo, J.
Jaramillo, R. Gomperts, R.E. Stratmann, O. Yazyev, A.J., Austin,
R. Cammi, C. Pomelli, J.W. Ochterski, P.Y. Ayala, K. Morokuma,
G.A., Voth, P. Salvador, J.J. Dannenberg, V.G. Zakrzewski, S.
Dapprich, A.D. Daniels, M.C. Strain, O. Farkas, D.K. Malick, A.D.
Rabuck, K. Raghavachari, J.B. Foresman, J.V. Ortiz, Q. Cui, A.G.
Baboul, S. Clif-
ford, J. Cioslowski, B.B. Stefanov, G. Liu, A.,
Liashenko, P. Piskorz, I. Komaromi, R.L. Martin, D.J. Fox, T. Keith,
M.A. Al-Laham, C.Y. Peng, A. Nanayakkara, M. Challacombe,
P.M.W. Gill, B. Johnson, W., Chen, M.W. Wong, C. Gonza-
lez, J.A. Pople, Gaussian 03, Revision E.01, Gaussian, Inc., Pittsburgh, PA,
2003.
92. C.T. Lee, W.T. Yang and R.G. Parr, *Physical Review B* 37 **(1988)**
785
93. R.G. Parr and W. Yang, *Density Functional Theory of Atoms and
Molecules* (Oxford University Press, New York, **1989**).
94. A.D. Becke, *Journal of Chemical Physics* 98 **(1993)** 5648.
95. P.J. Stephens, F.J. Devlin, C.F. Chabalowski and M.J. Frisch,
Journal of Physical Chemistry 98 **(1994)** 11623.
96. G.A. Petersson and M.A. Allaham, *Journal of Chemical Physics* 94
(1991) 6081
97. G.A. Petersson, A. Bennett, T.G. Tensfeldt, M.A. Allaham, W.A.
Shirley and J.J. Mantzaris, *Journal of Chemical Physics* 89 **(1988)**
2193

98. A. Frisch, R. D. Dennington II, T. A. Keith, J. Milliam, A.B. Nielsen, A.J. Holder, J. Hiscocks, GaussView Reference, Version 4.0. Gaussian Inc., Pittsburgh, **2007**.
99. M.H. Jamroz, *Vibrational Energy Distribution Analysis VEDA 4*, Warsaw, **2004**.
100. R. Ditchfield, *Journal of Chemical Physics* 56 (**1972**) 5688.
101. C. Albayrak, B. Kosar, S. Demir, M. Odabasoglu and O. Büyükgüng, *Journal of Molecular Structure* 963 (**2010**) 211.
102. N.B. Colthup, L.H. Daly and E. Wiberley, *Introduction to Infrared and Raman Spectroscopy* (Academic Press, New York, **1964**).
103. D. Michalska, D.C. Bienko, A.J. Abkowicz-Bienko and Z. Latajka, *Journal of Physical Chemistry* 100 (**1996**) 17786
104. G. Litvinov, *Proceedings of the XIII International Conference on Raman Spectroscopy*, Wurzburg, Germany, **1992**.
105. N. Özbek, G. Kavak, Y. Özcan, S. İde and N. Karacan, *Journal of Molecular Structure* 919 (**2009**) 154
106. L.J. Bellamy, *The Infrared Spectra of Complex Molecules* (Wiley, New York, **1975**).
107. R.M. Silverstein and F.X. Webster, *Spectroscopic Identification of Organic Compounds* (Wiley, New York, **1998**).
108. B.H. Stuart, *Infrared Spectroscopy: Fundamentals and Applications* (Wiley, England, **2004**).
109. H. Alyar, A. Ünal, N. Özbek, S. Alyar and N. Karacan, *Spectrochimica Acta Part A: Molecular and Biomolecular Spectroscopy* 91 (**2012**) 39
110. S.P.V. Chamundeeswari, E.R.J.J. Samuel and N. Sundaraganesan, *European Journal of Chemistry* 2 (**2011**) 136

111. D. Lin-Vien, N.B. Colthup, W.G. Fateley, and J.A. Grasselli, *The Handbook of Infrared and Raman Characteristic Frequencies of Organic Molecules*, Academic Press, Boston, MA, **1991**.
112. N. Roeges, *A Guide to the Complete Interpretation of Infrared Spectra of Organic Structures* (Wiley, New York, **1994**).
113. G. Socrates, *Infrared Characteristic Group Frequencies* (Wiley, New York, **1980**).
114. F.R. Dolish, W.G. Fateley and F.F. Bentely, *Characteristic Raman Frequencies of Organic Compounds* (Wiley, New York, **1997**).
115. R.M. Silverstein and F.X. Webster, *Spectroscopic Identification of Organic Compounds*, 6th ed. (Wiley, New York, **2003**).
116. S. Subashchandrabose, C. Meganathan, Y. Erdogdu, H. Saleem, C. Jajkumar and P. Latha, *Journal of Molecular Structure* 1042 (**2013**) 37
117. G. Varsanyi, *Assignments for Vibrational Spectra of 700 Benzene Derivatives* (Wiley, New York, **1974**).
118. A.R. Berenji, S.F. Tayyari, M. Rahimizadeh, H. Eshghi, M. Vakili and A. Shiri, *Spectrochimica Acta Part A: Molecular and Biomolecular Spectroscopy* 102 (**2013**) 350
119. S. Bharanidharan, H. Saleem, A. Nathiya, A. Arokiasamy and V. Thanikachalam, *International Letters of Chemistry* 60 (**2015**) 168
120. Y.B. Alpaslan, H. Gokce, G. Alpaslan and M. Macit, *Journal of Molecular Structure* 1097 (**2015**) 171.
121. R. Sangeetha, S. Seshadri and M.P. Rasheed, *International Journal of Academic Research and Development* 2 (**2017**) 653
122. G. Socrates, *Infrared and Raman Characteristic Group Frequencies* (Wiley, New York, **2001**).

123. L.G. Wade Jr, *Organic Chemistry* (Pearson Prentice Hall, New Jersey, **2006**).
124. R.J. Anderson, D.J. Bendell and P.W. Groundwater, *Organic Spectroscopic Analysis* (The Royal Society of Chemistry, Sanderland, UK, **2004**).
125. H.O. Kalinowski, S. Berger and S. Braun, *Carbon-13 NMR Spectroscopy* (Wiley, Chichester, **1988**).
126. K. Pihlaja and E. Kleinpeter, editors, *Carbon-13 Chemical Shifts in Structural and Stereochemical Analysis* (VCH Publishers, Deerfield Beach, **1994**).
127. F. Wienhold and C.R. Landis, *Valency and Bonding-A Natural Bond Orbital Donor-Acceptor Perspective* (Cambridge University Press, New York, **2005**).
128. J. Liu, Z. Chen and S.F. Yuan, *Journal of Zhejiang University Science B* **6** (**2005**) 584
129. S. Gunasekaran, R.A. Balaji, S. Kumaresan, G. Anand and S. Srinivasan, *Canadian Journal of Analytical Science and Spectroscopy* **53** (**2008**) 149
130. K. Fukui, *Science* **218** (**1982**) 747
131. E. Scrocco and J. Tomasi, *Advances in Quantum Chemistry* **11** (**1978**) 115
132. F.J. Luque, J.M. Lopez and M. Orozco, *Theoretical Chemistry Accounts* **03** (**2000**) 343
133. J.S. Murray and K. Sen, *Molecular Electrostatic Potentials: Concepts and Applications* (Elsevier Science B.V, Amsterdam, The Netherlands, **1996**).
134. M. Govindarajan, S. Periandy and K. Carthigayen, *Spectrochimica Acta Part A: Molecular and Biomolecular Spectroscopy* **97** (**2012**) 411

135. M. Govindarajan and M. Karabacak, *Spectrochimca Acta Part A: Molecular and Biomolecular Spectroscopy* 96 **(2012)** 421
136. C. Ravikumar, I.H. Joe and V.S. Jayakumar, *Chemical Physics Letters* 460 **(2008)** 552
137. R.M. Issa, M.K. Awad and F.M. Atlam, *Materials and Corrosion* 61 **(2010)** 709
138. N. M. O'Boyle, A. L. Tenderholt and K. M. Langner, *Journal of Computational Chemistry* 29 **(2008)** 839
139. R. Hoffmann, *Solids and Surfaces: A Chemist's View of Bonding in Extended Structures* (VCH Publishers, New York, **1988**).
140. R.S. Mulliken, *Journal of Chemical Physics* 23 **(1955)** 1833
141. I. Sidir, Y.G. Sidir, M. Kumalar and E. Tasal, *Journal of Molecular Structure* 964 **(2010)** 134
142. V. Balachandran and K. Parimala, *Spectrochimca Acta Part A: Molecular and Biomolecular Spectroscopy* 96 **(2012)** 340
143. A. Lakshmi and V. Balachandran, *Journal of Molecular Structure* 1033 **(2013)** 40
144. S. Ramalingama, M. Karabacak, S. Periandy, N. Puviarasan and D. Tanuja, *Spectrochimca Acta Part A: Molecular and Biomolecular Spectroscopy* 96 **(2012)** 212.
145. E.G. Lewars, *Computational Chemistry: Introduction to the theory and Applications of Molecular and Quantum Mechanics*, 2nd ed. (Springer, New York, **2011**).

Publication(s)

1. **K.K. Mohammed Ameen**, M. Syed Ali Padusha, Ajitha Devi and F.M. Mashood Ahamed, Synthesis, Characterization and Antimicrobial Studies of Some Azomethine Compounds Derived Via Schiff Base Condensation Chemistry, Journal of Natural Remedies 21 **(2020)** 84.
2. **K.K. Mohammed Ameen**, M. Syed Ali Padusha, Ajitha Devi and F.M. Mashood Ahamed, Synthesis, Characterization, DFT and Microbial Studies of Some Azomethine and β -amino derivatives, High Technology Letters 26 **(2020)** 870.

Source details

Feedback > Compare sources >

Vietnam Journal of Chemistry

Scopus coverage years: from 2020 to Present

Publisher: Wiley-Blackwell

E-ISSN: 2572-8288

Subject area: [Chemistry: General Chemistry](#)

Source type: Journal

[View all documents >](#)

[Set document alert](#)

[Save to source list](#) [Source Homepage](#)

SJR

SNIP

CiteScore

Improved CiteScore methodology

CiteScore value counts the citations received in the last 4 years to articles, reviews, conference papers, book chapters and data papers published in the last 4 years, and divides this by the number of publications published in the last 4 years.

Current source has not enough data to display citescore value. [Learn more >](#)

CiteScoreTracker 2021

$$0.4 = \frac{106 \text{ Citations to date}}{237 \text{ Documents to date}}$$

Last updated on 06 March, 2022 • Updated monthly

[View CiteScore methodology >](#) [CiteScore FAQ >](#)

Spectroscopic analysis, DFT studies and molecular docking of 2,3-dichloro-benzylidene-(2-trifluoromethyl-phenol)-amine

Mohammed Ameen K. K.¹, Towseef Ahmad Hajam², Syed Ali Padusha M.^{1*},
Saleem H.², D. Partha Sarathi¹

¹PG and Research Department of Chemistry, Jamal Mohamed College, Affiliation with Bharathidasan University, Trichy 620 020, India

²Department of Physics, Annamalai University, Annamalainagar 608 002, India

Submitted July 6, 2021; Revised September 21, 2021; Accepted December 28, 2021

Abstract

2,3-dichloro-benzylidene-(2-trifluoromethyl-phenol)-amine (2DBTP) has been synthesized and characterized by various spectroscopic techniques including FT-IR, FT-Raman, UV-Vis and ¹H, ¹³C NMR spectroscopy. The equilibrium geometry and harmonic vibrational frequencies were investigated by density functional theory (DFT) at B3LYP/6-311++G(d,p) basis set. The vibrational wavenumber assignments were made on the basis of total energy distribution (TED) calculations using Veda 4 program. The harmonic wavenumbers calculated at DFT were in line with the experimental values. The non-linear optical properties (NLO) were calculated. Stability of the molecule arises from hyperconjugative interactions and charge delocalization was analyzed by natural bond orbital (NBO) analysis. Molecular electrostatic potential (MEP), Mulliken atomic charges were also calculated. The energy gap of the molecule was found by HOMO and LUMO calculation. TD-DFT calculations have been carried out on the optimized geometry to further understand the electronic transitions in the UV-Vis spectrum of the compound. In addition, the ¹H and ¹³C NMR chemical shift values of 2DBTP in the ground state were also calculated using Gauge invariant atomic orbital (GIAO) method. The molecular docking solved the binding mode of 2XCT complex with the ligand. The investigated molecule revealed the inhibition activity of the ligand against anti-bacterial protein topoisomerase DNA gyrase enzyme (PDB ID: 2XCT).

Keywords. FT-IR, FT-RAMAN, NLO, NBO, NMR, docking studies.

1. INTRODUCTION

The Schiff base compounds or dynamic imine compounds are the condensed products of primary amines with carbonyl compounds were firstly reported by Hugo Schiff.^[1,2] These compounds have numerous applications in various fields such as biological, analytical and inorganic chemistry. They also play a great role as an intermediate in catalysts, dyes, organic synthesis, corrosion inhibitors, polymer stabilizers and pigments.^[3] Schiff bases have achieved great importance in medicinal and pharmaceutical fields due to broad spectrum of biological activities like anti-bacterial,^[4] anti-inflammatory,^[5] anti-fungal, anti-cancer and herbicidal^[6,7] activities. The electron conjugated system in compounds with donor-acceptor benzene derivatives display extremely large second-order optical nonlinearities. The conformation of molecules of aromatic compounds that are substituted with π -electron donors and acceptors

which exhibit intra-molecular charge transfer. In addition, the Schiff base is of special interest in literature which shows thermochromic and photochromic properties.^[8,9] Xuan and Zhai^[10] have recorded and analyzed the FT-IR and FT-Raman spectra of the methyl 2,5-dichlorobenzoate molecule in the solid phase. The bond parameters were calculated using DFT with 6-311G(d,p) and 6-311++G(d,p) basis sets and compared with the experimental data. Arjunan and Mohan^[11] reported the vibrational spectra of 2-chloro-4-methylaniline and 2-chloro-6-methylaniline. Utilizing the observed FT-IR and FT-Raman data, a complete vibrational assignment and analysis of the fundamental modes of the compounds were carried out. The manifestations of NH- π interactions and the influence of bulky chlorine and methyl group on the vibrational modes of the amino group were investigated.

In the present study, the vibrational and structural properties of Schiff base derivative:

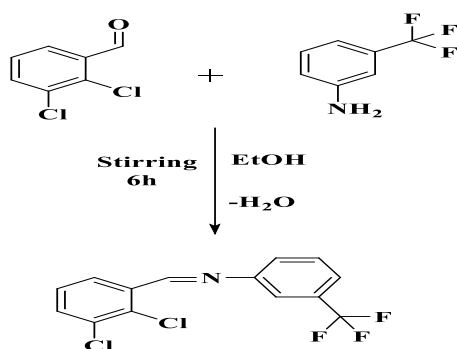
2DBTP have been studied by Gaussian 03 W software with basis set 6-311++G(d,p). The detailed interpretation of the vibrational spectra of the title molecule was justified on the basis of TED. NBO analysis was used to quantify the redistribution of electron density (ED) at various bonding and antibonding and $E^{(2)}$ energies, providing unambiguous evidence of stabilization arising from hyper conjugation of various intra-molecular interactions. The non-linear optical (NLO) behavior, molecular electrostatic potential (MEP) and thermodynamic properties of the title molecule were also calculated. The electronic transition was studied using TD-DFT method. UV spectroscopic studies, as well as HOMO and LUMO analyses have been utilized to explain charge transport information within the molecule.

2. MATERIALS AND METHODS

2.1. Synthesis procedure

Synthesis method of the compound is depicted schematically in scheme 1.

0.01 M (1.72 g) 2,3-dichloro benzaldehyde and 0.01 M (1.63 g) 2-amino benzotrifluoride were dissolved in 40 ml ethanol and the solution was taken in 100 ml round-bottom flask. The reaction mixture was stirred for 3 h at room temperature in the presence of 10 drops of glacial acetic acid. The completion of the reaction was ensured by TLC. After completion the mixture was poured into crushed ice, crude solid developed was filtered, washed with water, dried in air and recrystallized using ethanol.



Scheme 1: Synthesis of 2,3-dichloro-benzylidene-(2-trifluoromethyl-phenol)-amine

2.2. Instrumentation

KBr pellet with FT-IR Shimadzu spectrometer was used to record FT-IR spectrum in the spectral range

of 4000-400 cm^{-1} . The spectrum was recorded with a scanning speed of 10 cm^{-1} per minute at room temperature with the spectral resolution of 2.0 cm^{-1} . The FT-Raman spectrum was recorded in the region 4000-50 cm^{-1} using 1064 nm line of Nd: YAG laser as excitation wavelength on Bruker IFS 66v spectrophotometer equipped with a FRA 106 FT-Raman module with spectral resolution of 4 cm^{-1} . ^1H NMR spectrum was recorded on Bruker 400 MHz spectrometer and ^{13}C NMR spectrum was recorded on Bruker 100 MHz spectrometer. The UV-Vis absorption spectrum was recorded in the range of 200-800 nm using Shimadzu-2600 spectrometer.

2.3. Computational procedure

The optimization of structure and vibrational assignments were performed by Gaussian 03 W software package^[12] at DFT/B3LYP/6-311++G(d,p) level of theory. Density functional theory (DFT) method is more beneficial for its low computational cost with high accuracy. These important properties make DFT more practical and feasible for computations of different molecules. The geometry of 2DBTP was optimized using DFT/B3LYP method.^[13,14] At the optimized geometry for the title molecule no imaginary frequency was obtained, therefore a true minimum on the potential energy surface was found. The vibrational assignments were performed using GaussView 5.0 program package.^[15,16] The wavenumber values computed at DFT level contains known systematic errors due to the negligence of electron correlation. In order to improve the calculated values in agreement with the experimental values, a spectral uniform scaling factor was used to offset the systematic errors due to the anharmonicity of vibrational bands. Hence, the vibrational frequencies calculated at DFT level were scaled down by proper scaling factor.^[17, 18] The assignments of the calculated normal modes were made on the basis of TED analysis. The TEDs were computed from quantum chemically calculated vibrational frequencies using VEDA 4 program.^[19] The electronic absorption spectrum for optimized molecule was calculated with time dependent density functional theory (TD-DFT) at B3LYP/6-311++G(d,p) level. In order to investigate the nucleophilic and electrophilic attacks of the title compound the molecular electrostatic potential surface was evaluated. The ^1H and ^{13}C NMR chemical shifts were calculated with GIAO approach.^[20] NBO analysis, Mulliken atomic charges and thermodynamic properties of title molecule were computed at same level. Further, to show NLO activity of 2DBTP molecule, the dipole moment,

linear polarizability and first order hyperpolarizability were obtained from molecular polarizabilities based on theoretical calculations.

3. RESULTS AND DISCUSSION

3.1. Molecular geometry

The optimized structural parameters of 2DBTP molecule are calculated by DFT/B3LYP/6-311++G(d,p) basis set are listed in table 1. The optimized molecular structure with atomic numbering is shown in figure 1. The calculated geometric parameters can be used as foundation to calculate other parameters for 2DBTP. The conformational analysis is carried out by means of the potential energy surface scan with DFT/B3LYP method at 6-311++G(d,p) basis set. During the scan, all the geometrical parameters were simultaneously relaxed; while the dihedral angle $C_{18}-C_{16}-C_{25}-F_{28}$ was allowed to vary in the steps of 10° , ranging from 0° to 360° in a total of 36 steps. For this rotation minimum energy of -0.166252 Hartrees for $C_{18}-C_{16}-C_{25}-F_{28}$ which is shown in figure 2. In the present work, we have focused on the most stable form of 2DBTP molecule to clarify molecular structure assignments of vibrational spectra. The carbon and hydrogen atoms are bonded with σ -bonds in the benzene ring and the substitution of chlorine atoms for hydrogen reduces the electron

density (ED) at the ring carbon atom. In 2DBTP, the C–Cl bond length varies from 1.735 to 1.748 Å which is due to the steric effect produced by the C=N linkage, respectively. The substitution at carbon atoms in a benzene ring exerts large attraction on the valence electron cloud of hydrogen atoms, which causes increase in C–H force constants that results the decrease in corresponding bond length. The actual change in the C–H bond length would be influenced by the combined effects of the inductive-mesomeric interaction and the electric dipole field of the polar substituent. The calculated bond lengths of C_4-C_5 , C_5-C_6 and C_1-C_6 are 1.387, 1.389 and 1.393 Å, whereas C_1-C_2 , C_2-C_3 and C_3-C_4 are 1.402, 1.414 and 1.404 Å this variation is due to the attachment of electron withdrawing group (Cl and C=N linkage). Similarly, the bond lengths of $C_{18}-C_{21}$, $C_{17}-C_{19}$, $C_{15}-C_{17}$ and $C_{15}-C_{16}$ are 1.394, 1.391, 1.403 and 1.412 Å, respectively which are in a good agreement with the literature,^[21] whereas the C–H bond lengths of benzene rings in 2DBTP varies from 1.082 to 1.084 Å. The benzene ring appears to be little distorted because of the C=N group linkage as seen from the bond angle $C_2-C_3-C_4$ is calculated as 118.41° which is smaller than typical hexagonal angle of 120° . The dihedral angles $C_3-C_{12}-N_{13}-C_{15}$, $C_{25}-C_{16}-C_{15}-N_{13}$ and $C_2-C_3-C_{12}-N_{13}$ are 177.153° , -2.764° and -9.963° , which show the non-planar nature of the compound.

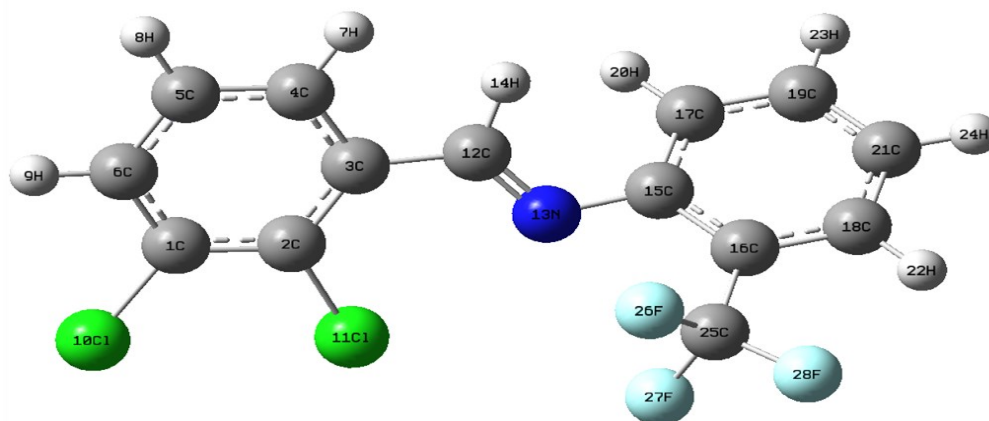


Figure 1: The optimized molecular structure of 2DBTP

3.2. Vibrational Assignments

The 2DBTP molecule has 28 atoms and belongs to C_1 point group symmetry; hence 78 fundamental vibrations are possible which are active in both IR and Raman spectra. For visual comparison, the observed and calculated FT-IR and FT-Raman spectra of 2DBTP at DFT/B3LYP level using 6-311++G(d,p) basis set are shown in figures 3(a,b),

respectively. The detailed vibrational assignments of fundamental modes of 2DBTP along with the calculated FT-IR and FT-Raman frequencies, IR and Raman intensities, force constant, reduced mass and normal mode descriptions (characterized by TED) are summarized in table 2. The vibrational assignments obtained at DFT/B3LYP/6-311++G(d,p) force field are generally greater than the experimental values due to neglect of

anharmonicity in the real system. These discrepancies can be corrected explicitly either by computing anharmonic corrections or by introducing the scaled field or directly scaling the calculated wavenumbers with proper scaling factor.^[17,18]

Table 1: The optimized molecular geometric parameters of 2DBTP using B3LYP/6-311++G(d,p) basis set

Parameters	B3LYP/6-311++G(d,p)	Lit*
Bond lengths (Å)		
C1-C2	1.402	
C1-C6	1.393	
C1-C110	1.748	
C2-C3	1.414	
C2-C111	1.735	
C3-C4	1.404	
C3-C12	1.472	
C4-C5	1.387	
C4-H7	1.084	
C5-C6	1.389	
C5-H8	1.083	
C6-H9	1.082	
C12-N13	1.273	1.280
C12-H14	1.099	1.099
N13-C15	1.399	1.396
C15-C16	1.412	1.413
C15-C17	1.403	1.404
C16-C18	1.393	
C16-C25	1.509	
C17-C19	1.391	
C17-H20	1.084	

C18-C21	1.394	1.393
C25-F26	1.355	
C25-F27	1.350	
C25-F28	1.356	
Angles (°)		
C2-C1-C110	121.18	
C6-C1-C110	117.66	
C1-C2-C111	119.09	
C3-C2-C111	121.75	
C2-C3-C4	118.41	
N13-C12-H14	120.66	
N13-C15-C16	119.84	
N13-C15-C17	121.49	
C16-C25-F27	112.56	
F26-C25-F27	107.08	106.85
F26-C25-F28	106.31	106.25
F27-C25-F28	106.45	106.13
Dihedral (°)		
C6-C1-C2-C111	-179.004	
C110-C1-C2-C111	0.778	
C1-C2-C3-C4	-0.748	
C1-C2-C3-C12	179.181	
C111-C2-C3-C4	178.383	
C111-C2-C3-C12	-1.688	
C2-C3-C12-N13	-9.963	
C2-C3-C12-H14	172.058	
C3-C12-N13-C15	177.153	
N13-C15-C16-C25	-2.764	
N13-C15-C17-C19	-177.180	

*Taken from Ref. [21].

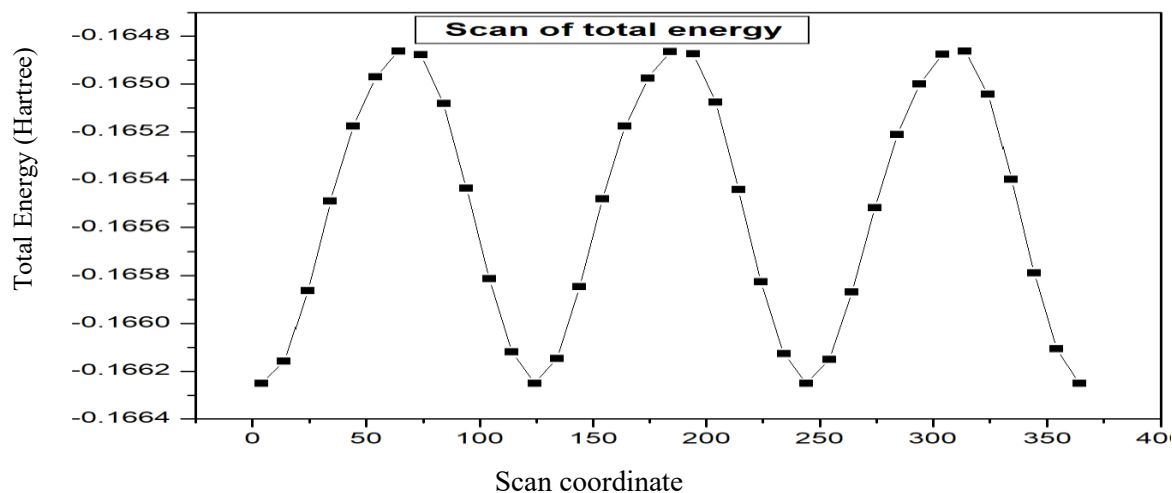


Figure 2: The potential energy surface around C18-C16-C25-F28 dihedral angle of 2DBTP

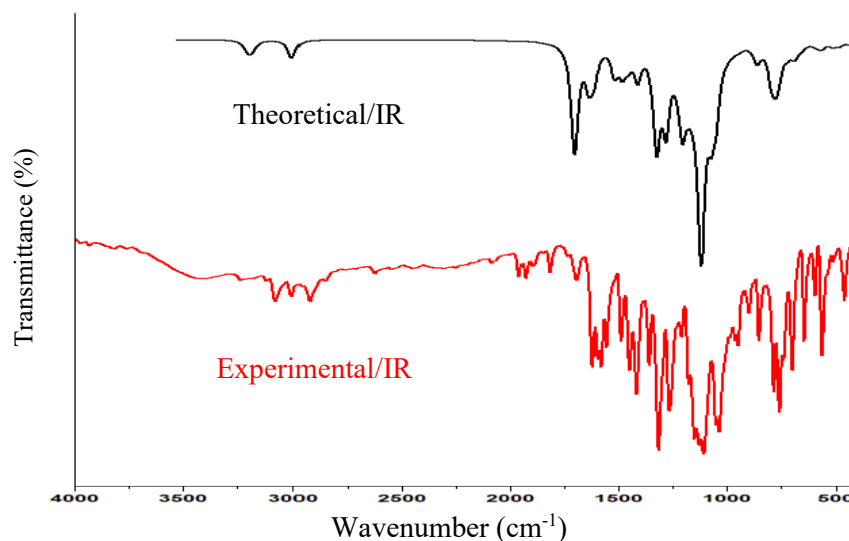


Figure 3a: The combined theoretical and experimental FT-IR spectra of 2DBTP

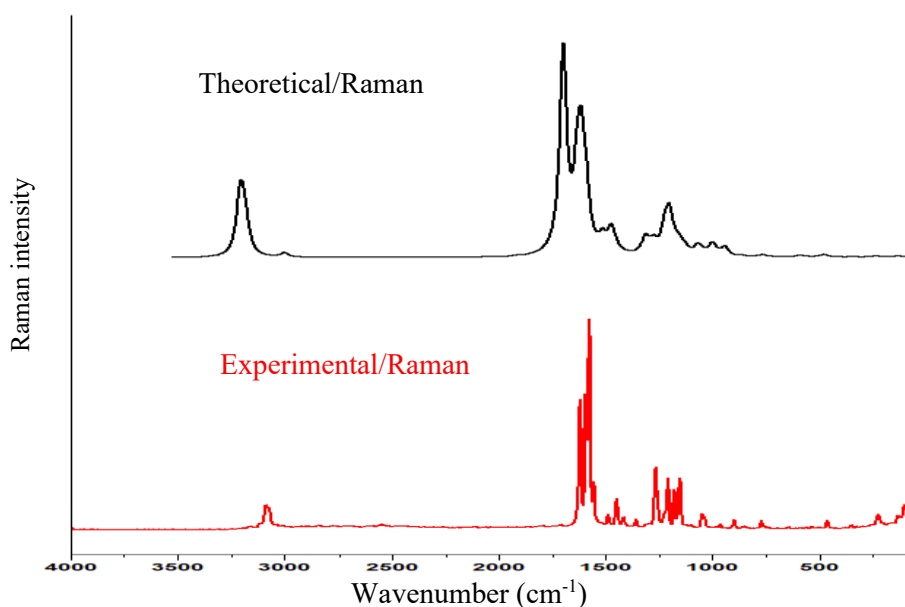


Figure 3b: The combined theoretical and experimental FT-Raman spectra of 2DBTP

3.2.1. CH Vibrations

In aromatic compounds, the C–H stretching vibrations usually fall in the range of 3044–3087 cm^{-1} .^[21] These vibrations are not being affected due to the nature and position of the substituent. In 2DBTP, the $\nu_{\text{C-H}}$ vibrations are found at 3117, 3077/3085, 3002 cm^{-1} in FT-IR/FT-Raman and their corresponding harmonic values are 3085, 3081 and 3046 cm^{-1} (mode nos: 1, 2 and 7) are pure modes with > 96 % TED values. The mode nos: 3–6 are also pure modes with > 98 % TED values are designated as $\nu_{\text{C-H}}$ modes. The $\nu_{\text{C-H}}$ of aliphatic group is observed at 2851 cm^{-1} in FT-IR and its corresponding harmonic value is 2880 cm^{-1} (mode no: 8). The C–H in-plane bending vibrations were appeared in the range 1000–1300 cm^{-1} in the

substituted benzenes and the out-of-plane bending vibrations in the range 750–1000 cm^{-1} .^[22] The mode nos: 14–16, 22, 24–26, and 37, 38, 40, 41, 43, 45 are assigned to β_{CH} and Γ_{CH} modes, respectively and also find support from observed FT-IR/FT-Raman bands: 1449, 1417, 1178, 1150, 1128/1449, 1417, 1180, 1153 cm^{-1} . The in-plane and out-of-plane bending modes of $\text{C}_{12}\text{-H}_{14}$ are assigned at 1355 and 964 cm^{-1} (mode nos: 18 and 35), respectively which are in good agreement with the observed FT-IR/FT-Raman bands: 1358/1358 cm^{-1} and 963/963 cm^{-1} , these assignments are having > 64 % contribution of TED.

3.2.2. CN Vibrations

According to Socrates^[23] the $\nu_{\text{C=N}}$ stretching

vibrations appear around 1600-1670 cm^{-1} and Babu *et al.*,^[24] assigned $\nu_{\text{C=N}}$ vibration at 1611/1627 cm^{-1} in FT-IR/FT-Raman spectra. Which is further supported by earlier studies^[21,25] $\nu_{\text{C=N}}$ stretching bands: 1667/1661 and 1657/1646 cm^{-1} in FT-IR/FT-Raman spectra. Based on the above literatures, the scaled harmonic wavenumber 1633 cm^{-1} (mode no: 9) is assigned to $\nu_{\text{C}_{12}=\text{N}_{13}}$ (76 % TED value) in which the calculated value is in good agreement with the experimental values: 1621/1620 cm^{-1} in FT-IR/FT-Raman spectra. The $\nu_{\text{C=N}}$ stretching modes are expected in the region 1100-1300 cm^{-1} ^[26] and in the present study, $\nu_{\text{C}_{15}=\text{N}_{13}}$ mode is observed at 1210/1209 cm^{-1} in FT-IR/FT-Raman bands and its corresponding calculated value is 1215 cm^{-1} (mode no: 23) with considerable TED value. The mode nos: 49, 59 and 67, 74 are assigned to $\beta_{\text{C}_3-\text{C}_{12}=\text{N}_{13}}$, $\beta_{\text{C}_{17}-\text{C}_{15}-\text{N}_{13}}$ and $\tau_{\text{C}_2-\text{C}_3-\text{C}_{12}=\text{N}_{13}}$, $\tau_{\text{C}_{12}=\text{N}_{13}-\text{C}_{15}-\text{C}_{17}}$ modes, respectively.

3.2.3. CC Vibrations

The $\nu_{\text{C-C}}$ ring vibrations are expected to fall in the regions: 1280-1380; 1430-1465; 1470-1540; 1575-1590 and 1590-1625 cm^{-1} with variable intensity.^[27] In the present study, $\nu_{\text{C-C}}$ vibrations are observed at 1580(m)/1578(vs), 1556(m)/1557(m), 1315(s), 1266(m)/1266(m) cm^{-1} in FT-IR/FT-Raman spectra. These assignments find support from harmonic frequencies: 1571, 1553, 1548, 1529, 1280 and 1262 cm^{-1} (mode nos: 10-13, 19, 21). The harmonic in-plane and out-of-plane deformations of CCC are 1030, 1006, 825, 731, 723, 629, 556 cm^{-1} (mode nos: 32, 34, 42, 46, 47, 50, 53) and 740, 690, 576, 502, 350, 288, 228 cm^{-1} (mode nos: 45, 48, 51, 56, 62, 65, 67) are in line with the observed FT-IR values: 1037, 986, 563 and 740, 700, 595, 511, 350 cm^{-1} , respectively. These assignments are further justified by the TED values. The $\nu_{\text{C}_3-\text{C}_{12}}$ and $\nu_{\text{C}_{16}-\text{C}_{25}}$ modes are assigned to harmonic frequencies: 1156 and 1270 cm^{-1} (modes nos: 25 and 20), respectively. The mode nos: 71/70 and 66/73 respectively belongs to $\beta_{\text{C}_2\text{C}_3\text{C}_{12}/\beta_{\text{C}_{18}\text{C}_{16}\text{C}_{25}}}$ and $\tau_{\text{C}_1\text{C}_2\text{C}_3\text{C}_{12}/\tau_{\text{C}_{21}\text{C}_{18}\text{C}_{16}\text{C}_{25}}}$ modes. These modes also have considerable TED values.

3.2.4. CF₃ Vibrations

Lipp and Seliskar^[28] have studied the infrared spectra of a number of mono- and di-substituted fluorine derivatives and those of tri- and tetra-fluoro benzene by Rastogi *et al.*^[29] They have assigned the frequency 1250 cm^{-1} to C–F stretching mode of vibration. In the vibrational spectra of related

compounds, the band due to the C–F stretching vibration^[23,30] may be found over a wide frequency range 1000-1360 cm^{-1} , since the vibration is easily affected by adjacent atoms or groups. In the present investigation, the C–F stretching vibrations are calculated at 1110, 1076, 1067 cm^{-1} (mode nos: 28, 30, 31) find support from the observed values 1108, 1051/1049 cm^{-1} in FT-IR/FT-Raman are in line with the reported values 1114/1116 cm^{-1} in FT-IR/FT-Raman spectra.^[21] The C–F deformation vibrations generally appear in the region 490-590 cm^{-1} .^[23] The harmonic frequencies 490, 463, 453 and 576, 573 cm^{-1} (mode nos: 57-59 and 51, 52) are attributed to β_{CF} and Γ_{CF} modes, respectively. These assignments are further supported by their TED value (> 17 %).

3.2.5. CCl Vibrations

The vibrations that belong to the bond formed between the ring and the halogen atoms are worth to discuss here, since mixing of vibrations are possible due to lower molecular symmetry and the presence of heavy atoms on the periphery of molecule.^[31] Generally, the $\nu_{\text{C-Cl}}$ absorption is obtained in the broad region between 550 and 850 cm^{-1} .^[32] Therefore, the bands found at 459/462 cm^{-1} in FT-IR/FT-Raman are being designated to $\nu_{\text{C-Cl}}$ stretching mode of vibration and the corresponding force constant contribute nearly 40 % to the TED, are in line with the corresponding harmonic value 463 cm^{-1} (mode no: 58). The calculated harmonic value at 723 cm^{-1} (mode no: 47) is also attributed to $\nu_{\text{C-Cl}}$ mode. The calculated harmonic frequencies 418, 215 and 228, 220 cm^{-1} (mode nos: 60, 69 and 67, 68) having considerable TED values are assigned to β_{CCCl} and Γ_{CCCl} modes, respectively.

3.3. NMR Analysis

The NMR isotropic chemical shifts are continuously being used as an aid to identify the reactive organic as well as ionic species.^[33] The Gauge invariant atomic orbital (GIAO) ¹H and ¹³C chemical shift calculations of the present molecule has been made on the optimized geometry at B3LYP/6-311++G(d,p) method and experimental values are listed in table 3. The ¹H NMR is interesting since the hydrogen atom is the smallest of all atoms and its chemical shift will be more susceptible to intermolecular interactions. The typical range of ¹³C NMR chemical shift in organic molecules is greater than 100 ppm.^[33,34] The singlet observed at 8.86 ppm is attributed to =C–H proton. The protons of aromatic rings give the multiplets in the region 7.37-

7.88 ppm. Aromatic proton adjacent to fluorine atoms appear at 7.88 ppm and aromatic proton adjacent to chlorine atoms appear at 7.71 ppm, respectively. Similarly, the multiplets appear in the region 122.6-149.65 ppm are attributed to aromatic carbon atoms. A singlet appear at 158.69 ppm is assigned to azomethine carbon. Whereas the signals appeared at 149.65 and 127.78 ppm are due to C-Cl and C-F₃ respectively. The ¹H and ¹³C NMR spectra of 2DBTP are shown in figures 4(a,b).

3.4. NBO Analysis

The NBO analysis results of the prominent charge-transfer interactions in the isolated gas-phase molecule of 2DBTP. It is an essential tool to study inter- and intra-molecular bonding interactions and also a convenient basis to investigate charge transfer or hyperconjugative interactions in the molecular system. Some orbitals are electron donors and some are electron acceptors, the energy difference between the bonding and anti-bonding orbitals makes the molecule susceptible for interactions.^[35,36] The large energy difference $E^{(2)}$ value means the strong interaction that implies the more donating and accepting tendency of electrons from one orbital to other. Delocalization of ED between occupied Lewis type (bond or lone pair) NBO orbitals and formally unoccupied (anti-bond or Rydberg) non-Lewis NBO orbital corresponds to a stabilizing donor-acceptor interaction. NBO analysis have been performed on 2DBTP at DFT/B3LYP/6-311++G(d,p) level in order to elucidate the intra-molecular rehybridization and delocalization of ED within the molecule. The strong hyperconjugative interactions are computed between π and σ bonding electrons of CC, CCl, CH, CN, CF and π^* and σ^* anti-bonding ones of CC, CCl, CH, CN, CF. The π bond electrons are weaker than σ bond electrons. Therefore, π bonded groups have less ED than C bonded groups. In the present study, the electron densities (EDs) of π bonds in the donor (i) groups are calculated at the interval of 1.632e to 1.915e, whereas the EDs of the σ bonds in the donor (i) groups are calculated between 1.966e to 1.995e. Similarly, the EDs of lone pair n electrons of Cl, N, and F atoms in donor (i) groups are found between 1.861e to 1.993e. The $E^{(2)}$ energy values and types of transitions are listed in table 4. The strongest hyperconjugation interactions occur from lone pair n electrons of F₂₇, N₁₃ and Cl₁₀, Cl₁₁ to an anti-bonding

σ^* and π^* electrons of C₂₅-F₂₈, C₁₂-H₁₄ and C₁-C₂ with interaction energies $E^{(2)} = 44.73, 54.18$ and $59.87, 67.36$ kJ/mol. Lone pairs Cl₁₁ \rightarrow π^* C₁-C₂ and Cl₁₀ \rightarrow π^* C₁-C₂ transfer hyperconjugation energies 67.36 and 59.87 kJ/mol, respectively. It is evident from the table 9 that the Cl₁₁/C₂ and Cl₁₀/C₁ atoms possess Mulliken atomic charge: 0.675/-0.750 and 0.465/0.682 a.u. respectively, which cause greater inter-atomic force in between Cl₁₁-C₂ on comparing with Cl₁₀-C₁, hence more energy transfer to the anti-bonding orbital (C₁-C₂). The stabilization energy values for π (C₃-C₄) \rightarrow π^* (C₁-C₂), π (C₅-C₆) \rightarrow π^* (C₃-C₄), π (C₁₅-C₁₇) \rightarrow π^* (C₁₉-C₂₁) and π (C₁₉-C₂₁) \rightarrow π^* (C₁₆-C₁₈) are computed as 89.91, 92.01, 91.76 and 96.36 kJ/mol. Similarly, the σ (C₃-C₄) \rightarrow σ^* (C₂-Cl₁₁), σ (C₅-C₆) \rightarrow σ^* (C₁-Cl₁₀), σ (C₁₆-C₁₈) \rightarrow σ^* (C₁₅-C₁₆) and σ (C₁₈-H₂₂) \rightarrow σ^* (C₁₅-C₁₆) hyperconjugation interactions are obtained as 19.92, 19.08, 19.41 and 19.62 kJ/mol.

Table 3: Theoretical and experimental (¹H & ¹³C) NMR isotropic chemical shifts (ppm) of 2DBTP

Atoms	Calculated (B3LYP/6-311++G(d,p))	Exp. δ (ppm)
H14	8.39	8.86
H22	7.85	7.88
H9	7.61	7.71
H23	7.59	7.58
H7	7.41	7.46
H8	7.27	7.43
H24	7.26	7.40
H20	6.97	7.37
C12	163.52	158.69
C15	157.96	149.65
C1	150.69	135.08
C2	148.29	134.43
C3	140.51	134.0
C4	139.97	133.58
C19	137.46	133.10
C6	137.42	129.16
C25	133.73	127.78
C18	132.02	126.69
C16	130.18	126.62
C5	129.45	126.55
C21	129.01	126.22
C17	121.54	122.6

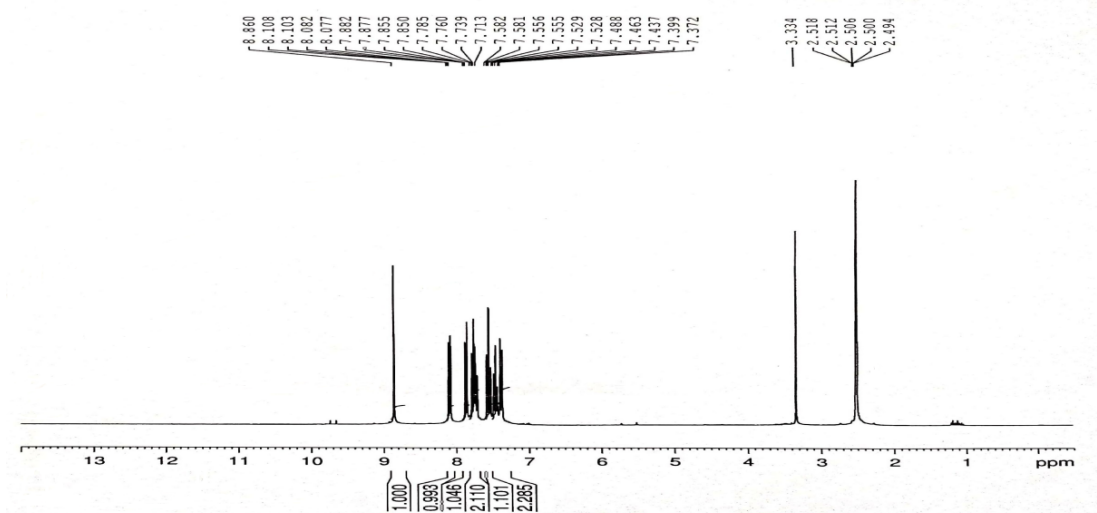
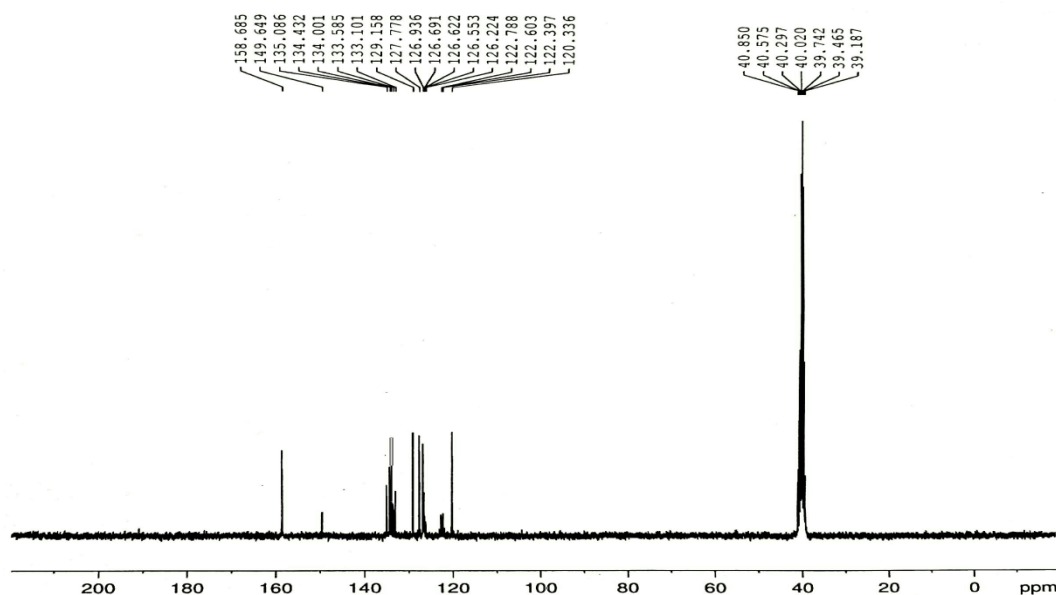
Figure 4a: ^1H NMR spectrum of 2DBTPFigure 4b: ^{13}C NMR spectrum of 2DBTP

Table 4: The second order perturbation theory analysis of Fock Matrix in NBO basis for 2DBTP

Type	Donor NBO (i)	ED/e	Acceptor NBO (j)	ED/e	$^a\text{E}^{(2)}$ KJ/mol	$^b\text{E}(j)-\text{E}(i)$ a.u.	$^c\text{F}(I,j)$ a.u.
$\pi-\pi^*$	BD (2) C1 – C2	1.68605	BD*(2) C3 – C4	0.3772	69.33	0.31	0.065
			BD*(2) C5 – C6	0.32425	78.37	0.31	0.068
$\sigma-\sigma^*$	BD (1) C1 – C6	1.97509	BD*(1) C1 – C2	0.0415	17.99	1.27	0.066
$\sigma-\sigma^*$	BD (1) C1 – C110	1.98764	BD*(1) C2 – C3	0.03758	10.71	1.25	0.051
$\sigma-\sigma^*$	BD (1) C2 – C3	1.96857	BD*(1) C1 – C2	0.0415	16.82	1.25	0.064
			BD*(1) C1 – C110	0.02847	18.83	0.87	0.056
$\sigma-\sigma^*$	BD (1) C2 – C111	1.98744	BD*(1) C1 – C6	0.02707	11.38	1.27	0.053
$\sigma-\sigma^*$	BD (1) C3 – C4	1.9671	BD*(1) C2 – C3	0.03758	17.24	1.23	0.064
			BD*(1) C2 – C111	0.02697	19.92	0.86	0.057
			BD*(1) C4 – C5	0.0144	11.46	1.28	0.053
$\pi-\pi^*$	BD (2) C3 – C4	1.63316	BD*(2) C1 – C2	0.43342	89.91	0.25	0.067

			BD*(2) C5 – C6	0.32425	79.79	0.28	0.066
			BD*(2) C12 – N13	0.13707	76.15	0.29	0.069
σ - σ^*	BD (1) C3 – C12	1.9727	BD*(1) C1 – C2	0.0415	8.28	1.2	0.044
			BD*(1) N13 – C15	0.02607	17.66	1.12	0.061
σ - σ^*	BD (1) C4 – C5	1.97877	BD*(1) C3 – C4	0.02027	12.55	1.26	0.055
σ - σ^*	BD (1) C4 – H7	1.97817	BD*(1) C2 – C3	0.03758	17.95	1.06	0.06
			BD*(1) C5 – C6	0.01714	15.06	1.1	0.056
σ - σ^*	BD (1) C5 – C6	1.972	BD*(1) C1 – C6	0.02707	14.02	1.26	0.058
			BD*(1) C1 – Cl10	0.02847	19.08	0.86	0.056
π - π^*	BD (2) C5 – C6	1.64914	BD*(2) C1 – C2	0.43342	89.75	0.25	0.067
			BD*(2) C3 – C4	0.3772	92.01	0.28	0.071
			BD*(1) C3 – C4	0.02027	15.94	1.07	0.057
σ - σ^*	BD (1) C6 – H9	1.97773	BD*(1) C1 – C2	0.0415	18.07	1.06	0.061
π - π^*	BD (2) C12 – N13	1.91454	BD*(2) C3 – C4	0.3772	31.59	0.36	0.05
σ - σ^*	BD (1) C12 – H14	1.98523	BD*(1) C2 – C3	0.03758	17.53	1.07	0.06
σ - σ^*	BD (1) N13 – C15	1.97855	BD*(1) C3 – C12	0.03353	15.86	1.23	0.061
σ - σ^*	BD (1) C15 – C16	1.96558	BD*(1) C12 – N13	0.01136	9.79	1.32	0.05
			BD*(1) C16 – C18	0.0193	18.03	1.27	0.066
σ - π^*	BD (1) C15 – C17	1.97161	BD*(2) C12 – N13	0.13707	4.23	0.73	0.025
			BD*(1) C15 – C16	0.03214	17.28	1.25	0.064
			BD*(1) C17 – C19	0.01482	12.43	1.28	0.055
π - π^*	BD (2) C15 – C17	1.63163	BD*(2) C12 – N13	0.13707	29.5	0.29	0.043
			BD*(2) C16 – C18	0.35207	74.98	0.28	0.064
			BD*(2) C19 – C21	0.32768	91.76	0.29	0.072
σ - σ^*	BD (1) C16 – C18	1.9724	BD*(1) N13 – C15	0.02607	14.77	1.15	0.057
			BD*(1) C15 – C16	0.03214	19.41	1.26	0.068
			BD*(1) C21 – H24	0.01324	8.83	1.16	0.044
π - π^*	BD (2) C16 – C18	1.69042	BD*(2) C15 – C17	0.3682	89.04	0.29	0.071
			BD*(2) C19 – C21	0.32768	71.42	0.29	0.063
σ - σ^*	BD (1) C17 – C19	1.97737	BD*(1) N13 – C15	0.02607	16.32	1.15	0.06
σ - σ^*	BD (1) C17 – H ₂ O	1.97815	BD*(1) C15 – C16	0.03214	18.03	1.07	0.061
			BD*(1) C19 – C21	0.01612	14.98	1.1	0.056
σ - σ^*	BD (1) C18 – C21	1.97834	BD*(1) C16 – C18	0.0193	13.35	1.27	0.057
σ - σ^*	BD (1) C18 – H22	1.9775	BD*(1) C15 – C16	0.03214	19.62	1.07	0.063
			BD*(1) C19 – C21	0.01612	15.02	1.1	0.056
σ - σ^*	BD (1) C19 – C21	1.97958	BD*(1) C17 – C19	0.01482	11.42	1.28	0.053
π - π^*	BD (2) C19 – C21	1.65546	BD*(2) C15 – C17	0.3682	78.99	0.28	0.065
			BD*(2) C16 – C18	0.35207	96.36	0.28	0.072
σ - σ^*	BD (1) C19 – H23	1.97978	BD*(1) C15 – C17	0.02938	16.15	1.08	0.058
			BD*(1) C18 – C21	0.0153	15.31	1.1	0.057
σ - σ^*	BD (1) C21 – H24	1.97996	BD*(1) C16 – C18	0.0193	15.65	1.09	0.057
			BD*(1) C17 – C19	0.01482	15.65	1.1	0.057
n - σ^*	LP (1) Cl10	1.99255	BD*(1) C1 – C2	0.0415	5.19	1.46	0.038
n - σ^*	LP (2) Cl10	1.96866	BD*(1) C1 – C2	0.0415	20.33	0.85	0.057
			BD*(1) C1 – C6	0.02707	15.73	0.87	0.051
n - π^*	LP (3) Cl10	1.91997	BD*(2) C1 – C2	0.43342	59.87	0.3	0.065

n- σ^*	LP (1) C111	1.99276	BD*(1) C1 – C2	0.0415	4.98	1.45	0.037
			BD*(1) C2 – C3	0.03758	6.65	1.45	0.043
n- σ^*	LP (2) C111	1.96217	BD*(1) C1 – C2	0.0415	18.74	0.84	0.055
			BD*(1) C2 – C3	0.03758	21.25	0.83	0.058
n- π^*	LP (3) C111	1.89675	BD*(2) C1 – C2	0.43342	67.36	0.3	0.067
n- σ^*	LP (1) N13	1.8613	BD*(1) C3 – C12	0.03353	12.76	0.79	0.045
			BD*(1) C12 – H14	0.0436	54.18	0.72	0.089
			BD*(1) C15 – C17	0.02938	20.29	0.9	0.061
			BD*(2) C15 – C17	0.3682	37.7	0.37	0.055
n- σ^*	LP (2) F26	1.9544	BD*(1) C16 – C25	0.05459	23.39	0.78	0.059
			BD*(1) C25 – F27	0.09654	20.13	0.66	0.051
			BD*(1) C25 – F28	0.089	16.53	0.64	0.046
n- σ^*	LP (3) F26	1.93768	BD*(1) C25 – F27	0.09654	39.33	0.65	0.071
			BD*(1) C25 – F28	0.089	44.6	0.64	0.074
n- σ^*	LP (2) F27	1.95171	BD*(1) C16 – C25	0.05459	24.35	0.78	0.06
			BD*(1) C25 – F26	0.09876	20.04	0.65	0.05
			BD*(1) C25 – F28	0.089	17.91	0.64	0.047
n- σ^*	LP (3) F27	1.93583	BD*(1) C25 – F26	0.09876	41.76	0.64	0.072
			BD*(1) C25 – F28	0.089	44.73	0.64	0.074
n- σ^*	LP (2) F28	1.95565	BD*(1) C16 – C25	0.05459	23.6	0.79	0.06
			BD*(1) C25 – F26	0.09876	15.86	0.65	0.045
			BD*(1) C25 – F27	0.09654	20.29	0.66	0.051
n- σ^*	LP (3) F28	1.94245	BD*(1) C25 – F26	0.09876	43.68	0.65	0.074
			BD*(1) C25 – F27	0.09654	38.41	0.66	0.07

^aE⁽²⁾ means energy of hyper conjugative interaction (stabilization energy).

^bEnergy difference between donor (i) and acceptor (j) nbo orbitals.

^cF(I, j) is the Fock matrix element between I and j nbo orbitals.

3.5. UV-Vis spectral analysis

The lowest singlet to singlet spin-allowed excited states are taken into account for the TD-DFT calculation to investigate the electronic properties of the molecular system. The experimental λ_{\max} values are obtained from the UV-Vis spectrum recorded in DMSO. The calculation was also performed in gas phase and DMSO, ethanol solvents. The calculated and the experimental absorption wavelengths (λ_{\max}) are given in table 5. The observed and the calculated UV-Vis spectra of 2DBTP are shown in figure 5. The energy gap between HOMO and LUMO is an

important tool to determine the molecular electrical transport properties.^[37] In the electronic absorption spectra, the calculated λ_{\max} values are obtained at 278.74, 278.23 and 277.37 nm in DMSO, ethanol and gas phase with higher oscillator strengths $f = 0.4609, 0.4252$ and 0.2540 is attributed to the most prominent $\pi \rightarrow \pi^*$ transition which are in good line with the experimental $\lambda_{\max} = 267.50$ nm. As can be seen in figure 5 across the solvents against the gas phase there is red shift i.e., bathochromic shift the absorption of radiation is shifted towards longer wavelength with decrease in energy gap.

Table 5: The experimental and computed UV-Vis parameters of 2DBTP

Solvent	TD-DFT/B3LYP/6-311++G(d,p)				
	Oscillator strength (f)	λ_{\max} (nm)	Band gap (eV)	Experimental λ_{\max} (nm)	Type
DMSO	0.4609	278.74	4.4481	267.50	$\pi - \pi^*$
Ethanol	0.4252	278.23	4.4563	-	$\pi - \pi^*$
Gas	0.2540	277.37	4.4701	-	$\pi - \pi^*$

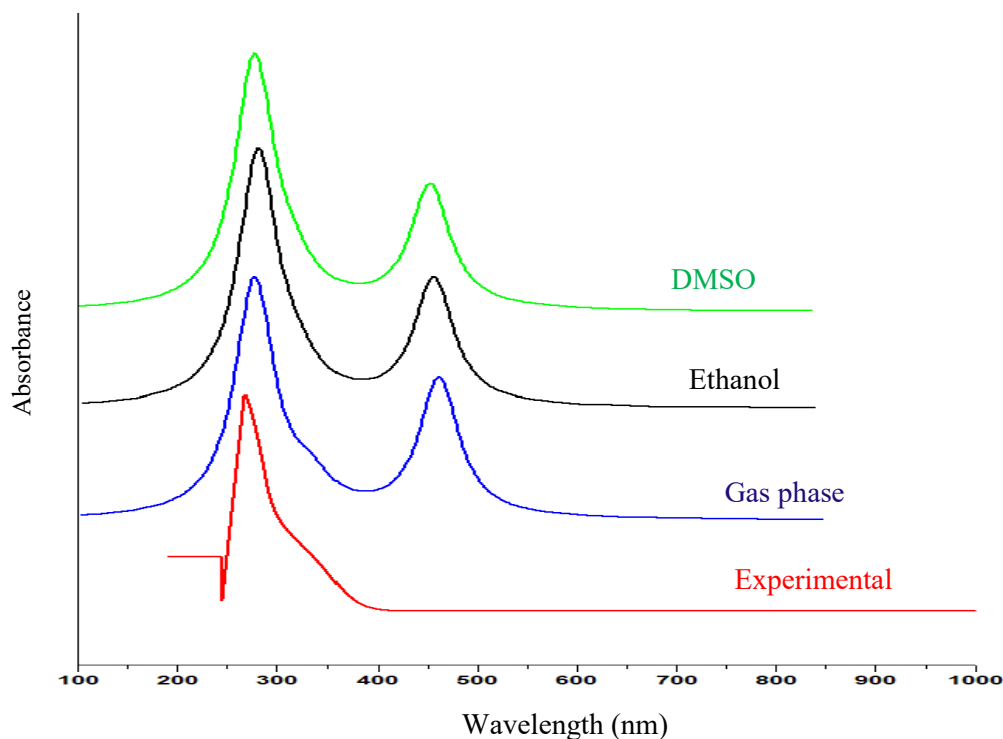


Figure 5: Theoretical and experimental UV-Vis spectra of 2DBTP

3.6. Molecular electrostatic potential

The reactivity of a chemical compound is determined by molecular electrostatic potential map (MEP) which differentiates the electrophilic and nucleophilic sites in a molecule.^[38] For this purpose the MEP has been calculated for 2DBTP compound at B3LYP/6-311++G(d,p) level. From MEP plot as shown in figure 6 the negative regions represented

by red color, are preferable sites for electrophilic attack and the positive regions represented by blue color are favored nucleophilic attack. It is obvious from figure 6 that the regions around CF_3 , CCl and $\text{C}=\text{N}$ represents the negative potential regions. These negative and positive sites help to predict the regions in a compound responsible for non-covalent interactions.^[39]

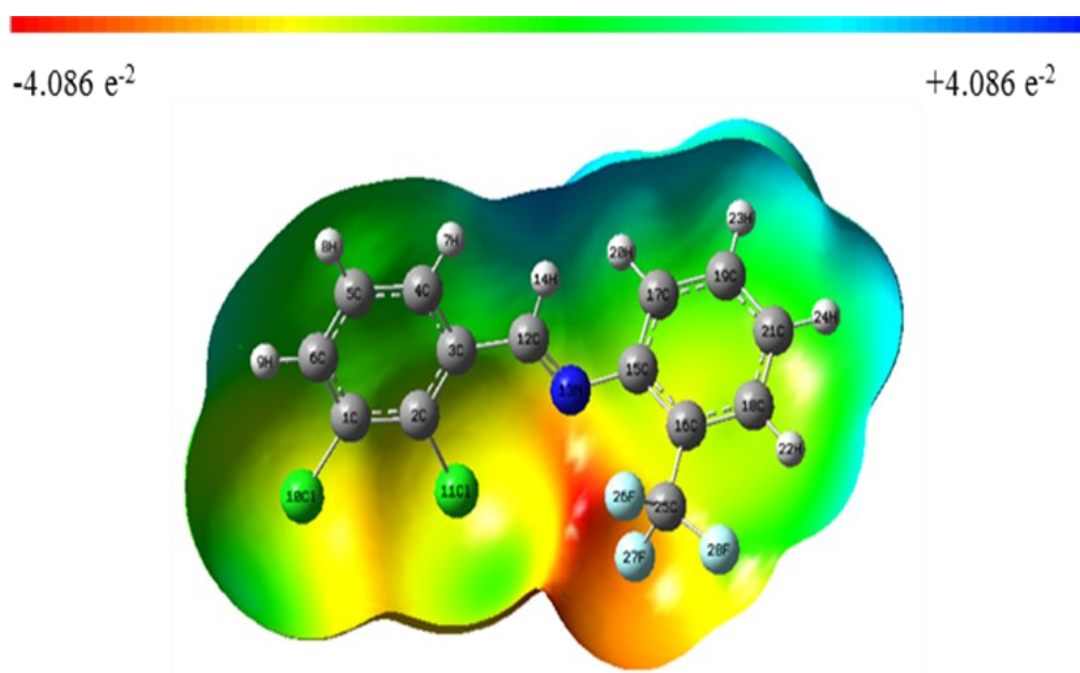


Figure 6: MEP Plot of 2,3-dichloro-benzylidene-(2-trifluoromethyl-phenol)-amine

3.7. HOMO-LUMO analysis

The HOMO energy characterizes the ability of electron donating orbitals, whereas LUMO energy characterizes the ability of electron accepting^[40] and the energy gap between HOMO and LUMO characterizes the stability of a molecule. It is also an important tool to determine the molecular electrical transport properties because it is a measure of electron conductivity.^[37] The electronic absorption corresponds that is mainly described by one electron excitation from HOMO to LUMO, an increase in values a molecule becomes more stable and decreases the intermolecular charge transfer which makes a compound to be NLO active.^[41] We have obtained a plot of the frontier molecular orbital of the first and the last five orbitals of a molecule of each group (HOMO and LUMO) to analyze the

main atomic contributions for these orbitals. The importance of observing these plots were to determine the chemical reactivity of 2DBTP. The HOMO (-6.748 eV), LUMO (-2.476 eV) and the energy gap values are 4.272 eV obtained using B3LYP/6-311++G(d,p) basis set. The HOMO-LUMO pictures are shown in figure 7. DOS spectrum is used to calculate the contribution of groups to the molecular orbitals. The DOS plot shows population analysis for each orbital and demonstrates a simple view character of the Mos in a certain range. DOS spectrum is shown in figure 8, in which the lines start from -20 eV to -5 eV, are called filled orbitals and the lines start from -5 eV to 0 eV, are called virtual orbitals. The physico-chemical properties and frontier molecular energies for 2DBTP are given in tables 6 and 7, respectively.

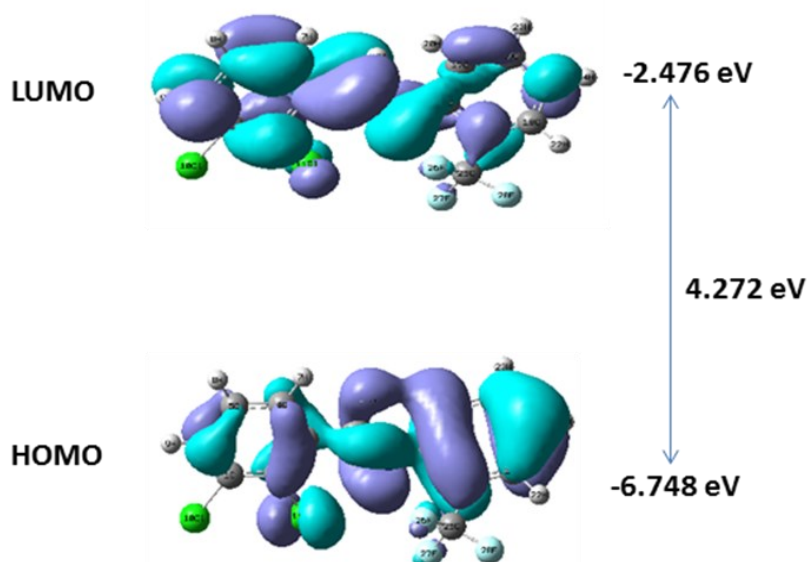


Figure 7: HOMO, LUMO Plots and energy band gap of 2DBTP

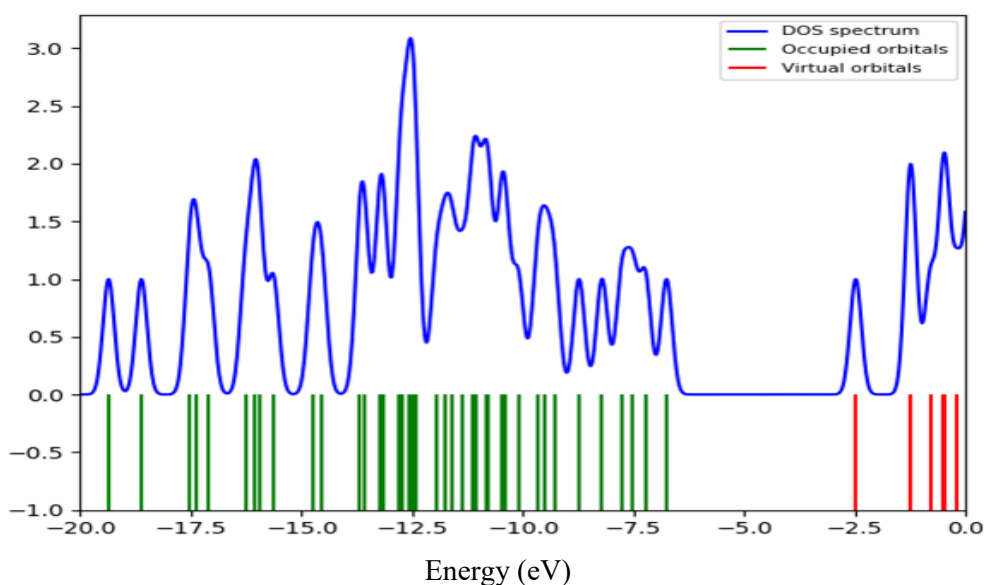


Figure 8: Density of State Spectrum of 2DBTP

Table 6: The Physico-chemical properties of 2DBTP

Parameters	Values
HOMO (eV)	-6.748
LUMO (eV)	-2.476
Energy gap (eV)	4.272
Ionization potential [I = -E _{HOMO}] (eV)	6.748
Electron affinity [A = -E _{LUMO}] (eV)	2.476
Electronegativity [$\chi = (I+A)/2$]	4.612
Chemical Potential [$\mu = -\chi$]	-4.612
Chemical Hardness [$\eta = (I-A)/2$]	2.136
Chemical Softness [S = I/2 η]	2.970
Electrophilicity Index [$\omega = \mu^2/2\eta$]	4.980

Table 7: The frontier molecular orbitals of 2DBTP

Occupancy	Orbital energies (a.u)	Orbital energies (eV)	Kinetic energy (a.u)
O76	-0.3006	-8.183	1.826
O77	-0.2841	-7.730	1.227
O78	-0.2764	-7.521	1.665
O79	-0.2655	-7.225	1.738
O80	-0.2474	-6.732	1.560
V81	-0.0912	-2.482	1.516
V82	-0.0462	-1.257	1.452
V83	-0.0442	-1.203	1.442
V84	-0.0283	-0.770	1.379
V85	-0.0197	-0.536	0.947

3.8. Nonlinear optical properties

A good NLO material has been frequently used in communication technology, signal processing, optical memory devices and optical switches. The NLO property originates with delocalized π electrons of an organic compound and increase with increasing conjugation in a compound. The presence of electron donor group and an electron acceptor group also increase the NLO properties. The static dipole moment (μ), the linear polarizability (α_0) and the first order hyperpolarizability (β_0) using the x, y, z components are calculated using the following equations.^[42]

$$\mu = \sqrt{\mu_x^2 + \mu_y^2 + \mu_z^2}$$

$$\beta_0 = \sqrt{\beta_x^2 + \beta_y^2 + \beta_z^2}$$

$$\alpha_0 = \frac{1}{3} (\alpha_{xx} + \alpha_{yy} + \alpha_{zz})$$

$$\beta_0 = \left[(\beta_{xxx} + \beta_{xyy} + \beta_{xzz})^2 + (\beta_{yyy} + \beta_{yzz} + \beta_{yxx})^2 + (\beta_{zzz} + \beta_{zxx} + \beta_{zyy})^2 \right]^{2/3}$$

Larger the dipole moment, stronger will be the intermolecular interactions.^[43] The dipole moment (μ), the linear polarizability (α_0) and the first order hyperpolarizability (β_0) are calculated at B3LYP/6-311++G(d,p) level and are summarized in table 8.

The dipole moment (μ) value for 2DBTP compound is 2.1750 D. The calculated linear polarizability (α_0) and first hyperpolarizability (β_0) for 2DBTP compound are 0.431×10^{-30} and 6.065×10^{-30} esu, respectively. Urea is one of the prototype materials which is used as a reference

material and frequently used for comparative purpose in the study of the NLO properties. The calculated values of μ and β_0 for 2DBTP compound are greater than those of urea (μ and β_0 of urea are 1.3732 D and 0.3728×10^{-30} esu).^[44] Theoretically, the first-order hyperpolarizability (β_0) of the title compound is 16.26 times higher than urea, which indicates that the 2DBTP compound possess good NLO property.

3.9. Mulliken atomic charges

Mulliken atomic charge calculation^[45] has an important role in the application of quantum chemical calculation to molecular system. Because of atomic charges affect dipole moment, polarizability, electronic structure and more properties of molecular system. The total atomic charges of 2DBTP molecule obtained by Mulliken population analysis at B3LYP/6-311++G(d,p) basis set is listed in table 9 and plotted in figure 9. From the results, it is clear that the substitution of Cl_2 and CF_3 groups in the aromatic rings leads to the redistribution of ED. The C_1 (0.682 a.u) carbon is linked with C_6 -H₉ and C_2 (-0.750 a.u) carbon atom with C_3 - C_{12} has different atomic charges which may be due to their adjacent proton and carbon atoms. Highest positive atomic charge is at C_{16} (1.228 a.u) which is due to the inductive effect of CF_3 group and least charge at C_{15} (-1.793 a.u) which is due to attachment of electronegative nitrogen (N_{11}) atom.

Table 8: The calculated dipole moment (μ), polarizability (α_0) and first-order hyperpolarizability (β_0) values of 2DBTP

Parameters	B3LYP/6-311++G(d,p) Debye
Dipole moment μ	
μ_x	1.9162
μ_y	-1.0272
μ_z	-0.0581
μ	2.1750 Debye
Polarizability (α_0) $\times 10^{-30}$ esu	
α_{xx}	187.250
α_{xy}	-19.235
α_{yy}	138.051
α_{xz}	9.217
α_{yz}	5.085
α_{zz}	317.997
α_0	0.431×10^{-30} esu
Hyperpolarizability (β_0) $\times 10^{-30}$ esu	
β_{xxx}	403.098
β_{xxy}	-30.771
β_{xyy}	42.161
β_{yyy}	-93.904
β_{xxz}	85.733
β_{xyz}	14.029
β_{yyz}	5.594
β_{xzz}	239.027
β_{yzz}	-20.389
β_{zzz}	-31.223
β_0	6.065×10^{-30} esu

Standard value for urea ($\mu = 1.3732$ Debye, $\beta_0 = 0.3728 \times 10^{-30}$ esu); esu-electrostatic unit.

Table 9: The Mulliken atomic charges of 2DBTP

Atoms	Charges (a.u.)	Atoms	Charges (a.u.)
C1	0.682	C15	-1.793
C2	-0.750	C16	1.228
C3	0.238	C17	-0.230
C4	-0.343	C18	0.279
C5	-0.664	C19	-0.171
C6	-0.234	H20	0.174
H7	0.169	C21	-0.376
H8	0.177	H22	0.186
H9	0.202	H23	0.176
C110	0.465	H24	0.165
C111	0.675	C25	0.515
C12	-0.969	F26	-0.073
N13	0.476	F27	-0.056
H14	0.082	F28	-0.158

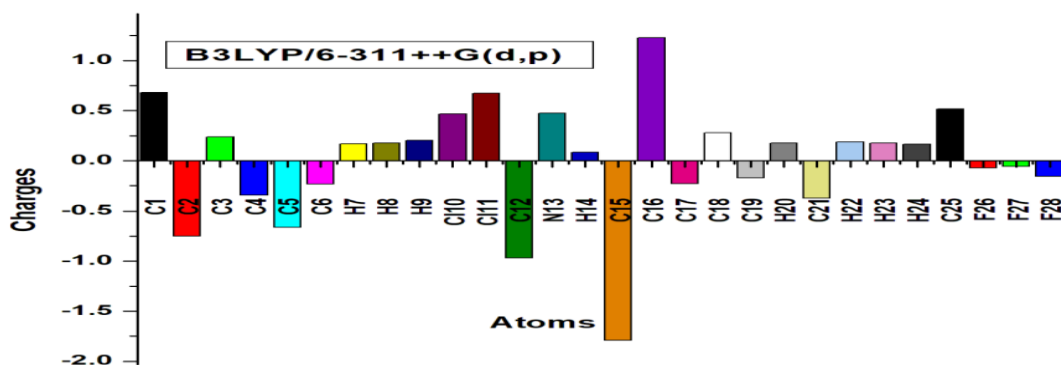


Figure 9: The Mulliken atomic charges of 2DBTP

3.10. Thermodynamic properties

The thermodynamic quantities such as the enthalpy (H), heat capacity at constant volume (C_v) due to vibrational motion and entropy (S) for 2DBTP molecule were calculated at B3LYP/6-311++G(d,p) basis set at the temperature of 298.15K, and at the pressure of 1 atmosphere. The structure dependent thermodynamic properties of the molecule are given in table 10. The thermal energy (E_{therm}) was calculated as the sum of the thermal energy corrections for molecular translation (E_{trans}), rotation (E_{rot}) and vibration (E_{vib}) at 298.15 K. The total

electronic energy gives the total energy of the molecular system relative to separate nuclei and electrons. The zero-point vibrational energy (ZPVE) is attributed from the vibrational motion of the molecular systems at 0K and is the sum of the contributions from all the vibrational modes of the molecular system. The computed minimum total energy -1813.2694 a.u, zero point vibrational energy 117.39168 kcal/mol and total thermal energy 128.111 kcal/mol are calculated. The calculated vibrational energies contribute 126.333 kcal/mol to thermal energy, 58.118 cal/mol \times K to specific heat and 61.378 cal/mol \times K to entropy.

Table 10: Thermodynamic properties of 2DBTP

Zero-Point Vibrational Energy 117.39168 (kcal/mol)			
Rotational Constants (GHz) A(0.54822), B(0.15006), C(0.13320)			
E(RB+HF-LYP) = -1813.2694 a.u			
Molecular mass = 316.998 amu			
	E (Thermal) kcal/mol	C_v (Specific heat) cal/mol \times K	S (Entropy) cal/mol \times K
Total Energy	128.111	64.079	139.182
Translational	0.889	2.981	43.157
Rotational	0.889	2.981	34.638
Vibrational	126.333	58.118	61.387

3.11. Molecular docking

The docking studies reported in the present study are performed using Glide program^[46,47] version 6.3, Schrodinger software. Molecular docking study is performed on topoisomerase DNA enzymes to find the binding and interaction properties of synthesized compound. The 3D crystallographic structure of topoisomerase was downloaded from Protein Data Bank (PDB ID: 2XCT). The protein complex was

prepared by Protein Preparation Wizard in Maestro of Schrodinger software. The synthesized compound exhibits Glide score, Glide energy and Emodel value as -2.713, -31.467 and -43.422 kcal/mol are in line with the Glide score, Glide energy and Emodel value for the standard drug Norfloxacin as -7.29, -54.230 and -83.073 kcal/mol. This shows that the present compound possesses anti-bacterial activity. The protein ligand interactions are shown in figure 10.

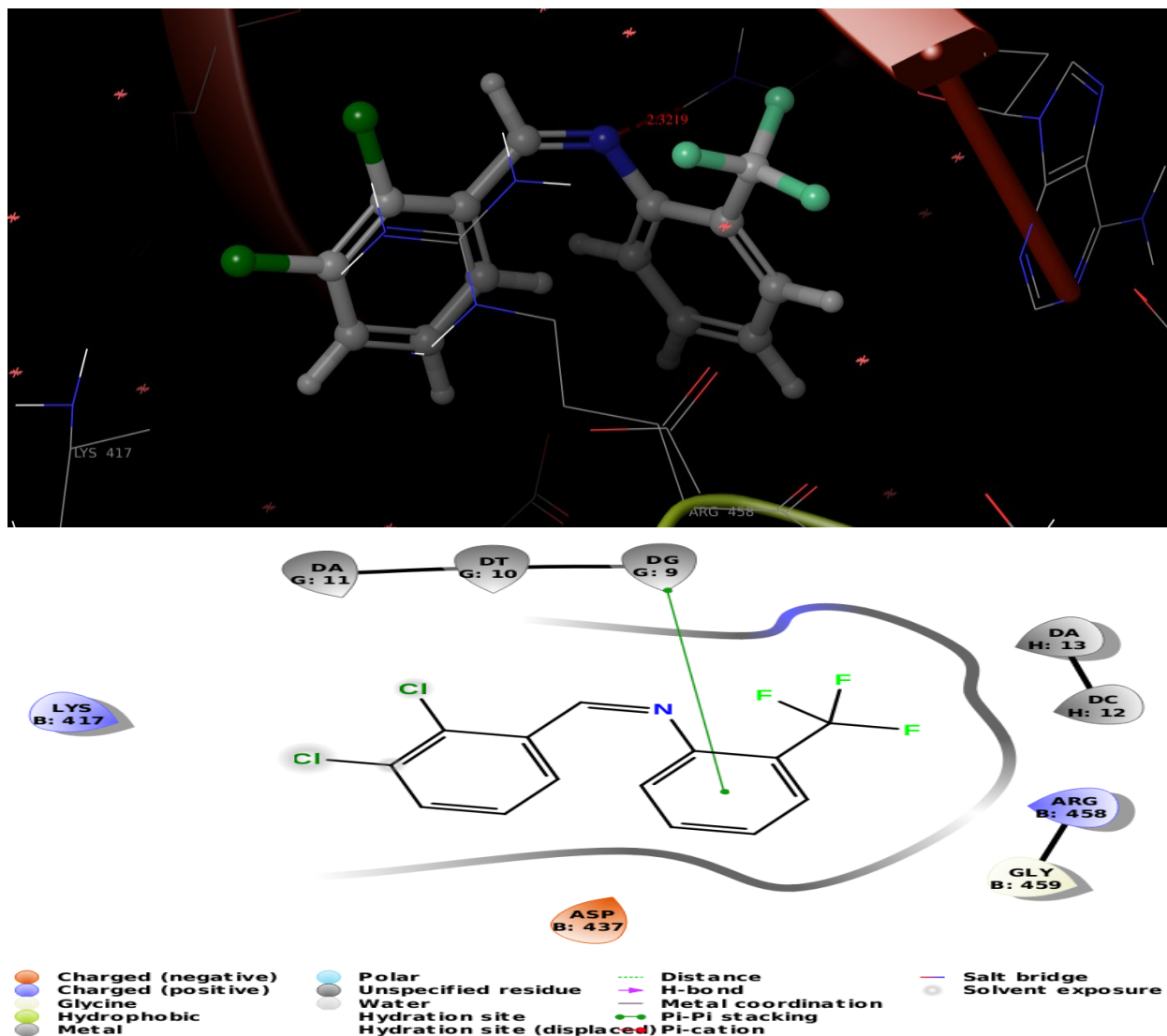


Figure 10: 2D and 3D interactions of 2DBTP

4. CONCLUSION

The title molecule was synthesized and characterized by spectral analysis such as FT-IR, FT-Raman NMR and UV-Vis. A complete vibrational analysis was carried out for the first time on 2DBTP molecule. The bond parameters were calculated. The Cl_{11} - C_2 was shortened due to the steric effect. The NBO results reflect the charge transfer occurred within the molecule and the maximum energy transfer took place from $n\text{-}\pi^*$ bonding orbital of chlorine atom to anti-bonding orbital of C_1 - C_2 . Lone pair Cl_{11} transferred more energy 67.36 kJ/mol to C_1 - C_2 anti-bonding orbitals compared with Cl_{10} : 59.87 kJ/mol was due to the effect of inter-atomic force between Cl_{11} - C_2 . The β_0 value of 2DBTP is 16.26 times larger than urea, hence the molecule had good NLO property. The recorded UV-Vis spectral value agreed well with calculated value in DMSO solvent. The λ_{max} 267.5

nm was assigned to $\pi\text{-}\pi^*$ type. MEP gives the visual representation of the chemically active sites and comparative reactivity of atoms. The region around C_{15} atom possessed the most negative potential. Mulliken population analysis revealed that the most positive and most negative mulliken atomic charges at C_{16} (1.228 a.u)/ C_{15} (-1.793 a.u) were due to the inductive effect of CF_3 group and electronegative N_{11} atom. The synthesized 2DBTP ligand exhibited excellent ligand-protein interactions with the amino acids. The obtained docking results revealed that the titled compound possessed anti-bacterial activity.

Acknowledgements. Authors gratefully thank Sophisticated Analytical Instrument Facility (SAIF), IIT Madras and Department of Chemistry, Jamal Mohamed College, Tiruchirappalli, Affiliation to Bharathidasan University, Tamilnadu for spectral studies.

REFERENCES

- Z. Cimerman, S. Miljanic, N. Galic. Schiff bases derived from aminopyridines as spectrofluorimetric analytical reagents, *Croat. Chem. Acta*, **2000**, 73(1), 81-95.
- H. Schiff. Mittheilungen aus dem Universitätslaboratorium in Pisa: Eine neue Reihe organischer Basen, *Justus Liebigs Ann. Chem.*, **1864**, 131(1), 118-119.
- C. M. Da Silva, D. L. da Silva, L. V. Modolo, R. B. Alves, M. A. de Resende, C. V. B. Martins, A. de Fatima. Schiff bases: A short review of their antimicrobial activities, *J. Adv. Res.*, **2011**, 2(1), 1-8.
- K. Cheng, Q. Z. Zheng, Y. Qian, L. Shi, J. Zhao, H. L. Zhu. Synthesis, antibacterial activities and molecular docking studies of peptide and Schiff bases as targeted antibiotics, *Bioorg. Med. Chem.*, **2009**, 17, 7861-7871.
- M. T. Cocco, C. Congiu, V. Lilliu, V. Onnis. Synthesis and in vitro antitumoral activity of new hydrazinopyrimidine-5-carbonitrile derivatives, *Bioorg. Med. Chem.*, **2006**, 14(2), 366-372.
- B. S. Creaven, B. Duff, D. A. Egan, K. Kavanagh, G. Rosair, V. R. Thangella, M. Walsh. Anticancer and antifungal activity of copper (II) complexes of quinolin-2(1H)-one-derived Schiff bases, *Inorg. Chim. Acta.*, **2010**, 363(14), 4048-4058.
- K. Singh, M. S. Barwa, P. Tyagi. Synthesis, characterization and biological studies of Co(II), Ni(II), Cu(II) and Zn(II) complexes with bidentate Schiff bases derived by heterocyclic ketone, *Eur. J. Med. Chem.*, **2006**, 41(1), 147-153.
- A. Koll. Specific features of intramolecular proton transfer reaction in Schiff bases, *Int. J. Mol. Sci.*, **2003**, 4(7), 434-444.
- S. Manivannan, S. Dhanuskodi. Synthesis, crystal growth, structural and optical properties of an organic NLO material, *J. Crys. Growth.*, **2004**, 262(1-4), 473-478.
- X. Xuan, C. Zhai. Quantum chemical studies of FT-IR and Raman spectra of methyl 2,5-dichlorobenzoate, *Spectrochim. Acta Part A.*, **2011**, 79(5), 1663-1668.
- V. Arjunan, S. Mohan. Fourier transform infrared and FT-Raman spectra, assignment, ab initio, DFT and normal co-ordinate analysis of 2-chloro-4-methylaniline and 2-chloro-6-methylaniline, *Spectrochim. Acta Part A.*, **2009**, 72(2), 436-444.
- M. J. Frisch, G. W. Trucks, H. B. Schlegel, G. E. Scuseria, M. A. Robb, J. R. Cheeseman, J. A. Montgomery, T. J. Vreven, K. N. Kudin, J. C. Burant, J. M. Millam, S. S. Iyengar, J. Tomasi, V. Barone, B. Mennucci, M. Cossi, G. Scalmani, N. Rega, G. A. Petersson, H. Nakatsuji, M. Hada, M. Ehara, K. Toyota, R. Fukuda, J. Hasegawa, M. Ishida, T. Nakajima, Y. Honda, O. Kitao, H. Nakai, M. Klene, X. Li, J. E. Knox, H. P. Hratchian, J. B. Cross, C. Adamo, J. Jaramillo, R. Gomperts, R. E. Stratmann, O. Yazyev, A. J. Austin, R. Cammi, C. Pomelli, J. W. Ochterski, P. Y. Ayala, K. Morokuma, G. A. Voth, P. Salvador, J. J. Dannenberg, V. G. Zakrzewski, S. Dapprich, A. D. Daniels, M. C. Strain, O. Farkas, D. K. Malick, A. D. Rabuck, K. Raghavachari, J. B. Foresman, J. V. Ortiz, Q. Cui, A. G. Baboul, S. Clifford, J. Cioslowski, B. B. Stefanov, G. Liu, A. Liashenko, P. Piskorz, I. Komaromi, R. L. Martin, D. J. Fox, T. Keith, M. A. Al-Laham, C. Y. Peng, A. Nanayakkara, M. Challacombe, P.M.W. Gill, B. Johnson, W. Chen, M. W. Wong, C. Gonzalez, J. A. Pople, Gaussian 03, Revision E.01, Gaussian, Inc., Pittsburgh, PA, **2003**.
- A. D. Becke. Density-functional thermochemistry. I. The effect of the exchange-only gradient correction, *J. Chem. Phys.*, **1993**, 98(492), 5648-5652.
- C. T. Lee, W.T. Yang, R. G. Parr. Development of the Colle-Salvetti correlation-energy formula into a functional of the electron density, *Phys. Rev. B.*, **1988**, 37(2), 785-789.
- M. J. Frisch, G. W. Trucks, H. B. Schlegel, G. E. Scuseria, M. A. Robb, J. R. Cheeseman, G. Scalmani et al. Gaussian 09, Revision d. 01, Gaussian Inc, Wallingford CT 201, **2009**.
- A. Frisch, H. P. Hratchian, R. D. Dennington, II, T. A. Keith, John Millam, B. Nielsen, A. J. Holder, J. Hiscocks, GaussView Version 5.0.8, Gaussian Inc, Wallingford, CT, USA, **2009**.
- L. Radom, J. A. Pople. Molecular orbital theory of the electronic structure of organic compounds. IV. Internal rotation in hydrocarbons using a minimal Slater-type basis, *J. American. Chem. Soc.*, **1970**, 92(16), 4786-4795.
- J. A. Pople, A. P. Scott, M. W. Wong, L. Radom. Scaling factors for obtaining fundamental vibrational frequencies and zero-point energies from HF/6-31G* and MP2/6-31G* harmonic frequencies, *Israel J. Chem.*, **1993**, 33(3), 345-350.
- M. H. Jamroz. Vibrational Energy Distribution Analysis, VEDA 4, Warsaw, **2004**.
- K. Wolinski, J. F. Hilton, P. Pulay. Efficient Implementation of the Gauge-Independent Atomic Orbital Method for NMR Chemical Shift Calculations, *J. Am. Chem. Soc.*, **1990**, 112(23), 8251-8826.
- T. A. Hajam, H. Saleem, M. S. A. Padhusa, K. K. Mohammed Ameen. Synthesis, quantum chemical calculations and molecular docking studies of 2-ethoxy-4[(2-trifluoromethyl-phenylimino) methyl] phenol, *Mol. Phys.*, **2020**, 118(24), 1-19.
- V. Krishnakumar, N. Prabavathi. Analysis of vibrational spectra of 1-chloro-2,4-dinitrobenzene based on density functional theory calculations, *Spectrochim. Acta Part A.*, **2009**, 72A, 738-742.
- G. Socrates. Infrared and Raman Characteristic group frequencies, 3rd ed., John Wiley, Chicester, **2001**.
- N. R. Babu, S. Subashchandrabose, M.S.A. Padusha, H. Saleem, Y. Erdogdu. Synthesis and spectral characterization of hydrazone derivative of furfural using experimental and DFT method, *Spectrochim. Acta A.*, **2014**, 120, 314-322.

25. T. A. Hajam, H. Saleem, M. S. A. Padusha, K. K. Mohammed Ameen. Quantum Mechanical Study, Spectroscopic (FT-IR, FT-Raman and UV-Vis) Study, NBO, NLO Analysis and Molecular Docking Studies of 2-Ethoxy-4-(Pyridine-2yliminomethyl)-Phenol, *Polycycl. Aromat. Compd.*, Taylor and Francis, **2021**, 1-24.
26. R. M. Silverstein, G. C. Bassler, T. C. Morrill. Spectrometric Identification of Organic Compounds, Fifth ed., John Wiley and Sons Inc., Singapore, **1991**.
27. G. Varsanyi. Assignments for vibrational spectra of 700 benzene derivatives, Wiley, New York, **1974**.
28. E. D. Lipp, C. J. Seliskar. The vibrational spectrum of fluorobenzene, *J. Mol. Spectrosc.*, **1978**, 73(2), 290-304.
29. V. K. Rastogi, M. A. Palafox, R. P. Tanwar, L. Mittal. 3,5-Difluorobenzonitrile: ab initio calculations, FTIR and Raman spectra, *Spectrochim. Acta Part A*, **2002**, 58(9), 1987-2004.
30. C. J. Pouchert. Aldrich Library of Infrared Spectra, Wisconsin, USA, **1975**.
31. R. K. Yadav, N. P. Sing, R. A. Yadav. Vibrational studies of trifluoromethyl benzene derivatives: II 5-amino-2-fluoro and 5-amino-2-chloro benzotrifluorides, *Indian J. Phys.*, **2003**, 77, 421-427.
32. V. Arjunan, S. Mohan. Fourier transform infrared and FT-Raman spectral analysis and ab initio calculations for 4-chloro-2-methylaniline and 4-chloro-3-methylaniline, *J. Mol. Struct.*, **2008**, 892(1-3), 289-299.
33. H. O. Kalinowski, S. Berger, S. Brawn. Carbon 13 NMR spectroscopy, John Wiley and Sons, Chichester, **1988**.
34. D. A. Kleinman. Nonlinear dielectric polarization in optical media, *Phys. Rev.*, **1962**, 126(6), 1977.
35. J. Liu, Z. Chen, & S. Yuan. Study on the prediction of visible absorption maxima of azobenzene compounds. *J. Zhejiang Univ. Sci.*, **2005**, 6B(6), 584-589.
36. C. James, A. A. Raj, R. Reghunathan, V. S. Jayakumar, I. H. Joe. Structural conformation and vibrational spectroscopic studies of 2,6-bis(p-N,N-dimethyl benzylidene)cyclohexanone using density functional theory, *J. Raman Spectrosc.*, **2006**, 37(12), 1381-1392.
37. K. Fukui. Role of frontier orbitals in chemical reactions, *Science*, **1982**, 218(4574), 747-754.
38. M. Yavuz, H. Tanak. Density functional modelling studies on N-2-Methoxyphenyl-2-oxo-5-nitro-1-benzylidenemethylamine, *J. Mol. Struct. Theochem.*, **2010**, 961(1-3), 9-16.
39. S. Y. Ebrahimipour, M. Abaszadeh, J. Castro, M. Seifi. Synthesis, X-ray crystal structure, DFT calculation and catalytic activity of two new oxido-vanadium (V) complexes containing ONO tridentate Schiff bases, *Polyhedron.*, **2014**, 79, 138-150.
40. G. Gece. The use of quantum chemical methods in corrosion inhibitor studies, *Corros. Sci.*, **2008**, 50(11), 2981-2992.
41. S. Muthu, A. Prabhakaran. Vibrational spectroscopic study and NBO analysis on tranexamic acid using DFT method, *Spectrochim Acta Part A.*, **2014**, 129, 184-192.
42. C. Albayrak, M. Odabasoglu, A. Ozek, O. Buyukgungor. Synthesis, spectroscopic characterizations and quantum chemical computational studies of (Z)-4-[(E)-(4-fluorophenyl) diazenyl]-6-[(3-hydroxypropylamino) methylene]-2-methoxycyclohexa-2,4-dienone, *Spectrochim. Acta Part A.*, **2012**, 85(1), 85-91.
43. S. Sakthivel, T. Alagesan, S. Muthu, Christina Susan Abraham, E. Geetha. Quantum mechanical, spectroscopic study (FT-IR and FT-Raman), NBO analysis, HOMO-LUMO, first order hyperpolarizability and docking studies of a non-steroidal anti-inflammatory compound, *J. Mol. Struct.*, **2017**, 1156, 645-656.
44. Y. B. Alpaslan, G. Alpaslan, A. A. Agar, N. O. Iskeleli, E. Oztekin. Experimental and density functional theory studies on (E)-2-[(2-(hydroxymethyl) phenylimino) methyl] benzene-1, 4-diol, *J. Mol. Struct.*, **2011**, 995(1-3), 58-65.
45. V. K. Rastogi, M. A. Palafox, L. Mittal, N. Peica, W. Kiefer, K. Lang, P. Ohja. FTIR and FT-Raman spectra and density functional computations of the vibrational spectra, molecular geometry and atomic charges of the biomolecule: 5-bromouracil, *J. Raman Spectrosc.*, **2007**, 38(10), 1227-1241.
46. Prime. Version 3.6, Schrodinger, LLC, New York, NY, USA, **2014**.
47. R. A. Friesner, R. B. Murphy, M. P. Repasky, L. L. Frye, J. R. Greenwood, T. A. Halgren, P. C. Sanschagrin, D. T. Mainz. Extra precision glide: Docking and scoring incorporating a model of hydrophobic enclosure for protein-ligand complexes, *J. Med. Chem.*, **2006**, 49(21), 6177-6196.

Corresponding author: Syed Ali Padusha M.

PG and Research Department of Chemistry

Jamal Mohamed College

Affiliation with Bharathidasan University, Trichy 620 020, India

E-mail: Syedalipadusha26@gmail.com/syedlipadusha@gmail.com.

Table 2: The experimental and calculated frequencies of 2DBTP using DFT/6-311++G(d,p) level of basis set [harmonic frequencies (cm^{-1}), IR, Raman intensities (Km/mol)], reduced masses (amu) and force constants ($\text{mdyn}\text{\AA}^{-1}$)

Mode No	Calculated Frequencies (cm^{-1})		Observed Frequencies (cm^{-1})		IR Intensity ^b	Raman Intensity ^c	Reduced Mass	Force Constant	Vibrational Assignments $\geq 10\%$ (TED) ^d
	Un scaled	Scaled ^a	FT-IR	FT Raman					
1	3211	3085	3117(vw)		4.24	99.67	1.09	6.64	$\nu\text{C}_{18}\text{H}_{22}$ (96)
2	3207	3081	3077(vw)	3085(w)	2.29	107.47	1.10	6.64	$\nu\text{C}_5\text{H}_8$ (99)
3	3193	3068			9.19	85.04	1.10	6.58	$\nu\text{C}_{21}\text{H}_{24}$ (99)
4	3192	3067			6.01	52.31	1.09	6.55	$\nu\text{C}_6\text{H}_9$ (99)
5	3185	3060			5.49	34.50	1.09	6.52	$\nu\text{C}_{17}\text{H}_{20}$ (99)
6	3173	3049			2.84	19.00	1.09	6.45	$\nu\text{C}_4\text{H}_7$ (98)
7	3170	3046	3002(vw)		4.15	29.13	1.09	6.44	$\nu\text{C}_{19}\text{H}_{23}$ (96)
8	2998	2880	2851(vw)		33.07	23.67	1.09	5.75	$\nu\text{C}_{12}\text{H}_{14}$ (100)
9	1700	1633	1621(m)	1620(s)	198.08	3886.1	8.60	14.63	$\nu\text{N}_{13}\text{C}_{12}$ (76)
10	1635	1571	1580(m)	1578(vs)	58.43	1274.9	5.83	9.19	$\nu\text{C}_{17}\text{C}_{19}$ (30) + $\nu\text{C}_{18}\text{C}_{21}$ (50)
11	1616	1553	1556(w)	1557(w)	10.91	1214.7	5.80	8.93	$\nu\text{C}_1\text{C}_2$ (46) + $\nu\text{C}_3\text{C}_4$ (30)
12	1611	1548			40.09	793.29	6.10	9.33	$\nu\text{C}_{18}\text{C}_{21}$ (15) + $\nu\text{C}_{15}\text{C}_{16}$ (19)
13	1591	1529			6.63	824.97	5.82	8.67	$\nu\text{C}_5\text{C}_6$ (45) + $\nu\text{C}_3\text{C}_4$ (21)
14	1516	1457	1449(m)	1449(w)	48.27	332.07	2.64	3.57	$\beta\text{H}_{20}\text{C}_{17}\text{C}_{15}$ (24) + $\beta\text{H}_{22}\text{C}_{18}\text{C}_{21}$ (23)
15	1480	1422			39.59	25.63	2.37	3.06	$\beta\text{C}_{15}\text{C}_{16}\text{C}_{18}$ (11) + $\beta\text{H}_{23}\text{C}_{19}\text{C}_{21}$ (27) + $\beta\text{H}_{24}\text{C}_{21}\text{C}_{19}$ (21)
16	1475	1417	1417(s)	1417(vw)	2.81	557.97	2.21	2.83	$\beta\text{H}_7\text{C}_4\text{C}_3$ (21) + $\beta\text{H}_8\text{C}_5\text{C}_6$ (23)
17	1453	1396			24.64	112.58	1.94	2.41	$\beta\text{H}_9\text{C}_6\text{C}_5$ (22) + $\beta\text{H}_{14}\text{C}_{12}\text{N}_{13}$ (30)
18	1410	1355	1358(m)	1358(vw)	55.48	15.19	1.86	2.18	$\beta\text{H}_{14}\text{C}_{12}\text{N}_{13}$ (75)
19	1332	1280	1315(vs)		1.72	60.80	4.51	4.72	$\nu\text{C}_{19}\text{C}_{21}$ (30) + $\nu\text{C}_{15}\text{C}_{16}$ (36)
20	1322	1270			160.54	19.09	2.62	2.70	$\beta\text{C}_{15}\text{C}_{16}\text{C}_{18}$ (12) + $\nu\text{C}_{16}\text{C}_{25}$ (24) + $\beta\text{H}_{22}\text{C}_{18}\text{C}_{21}$ (24)
21	1313	1262	1266(m)	1266(m)	16.33	454.31	6.90	7.01	$\nu\text{C}_4\text{C}_5$ (32) + $\nu\text{C}_1\text{C}_2$ (31)
22	1278	1228			127.66	343.15	2.74	2.64	$\nu\text{C}_{16}\text{C}_{25}$ (17) + $\beta\text{H}_{20}\text{C}_{17}\text{C}_{15}$ (39)
23	1265	1215	1210(w)	1209(w)	5.43	32.51	2.69	2.54	$\nu\text{N}_{13}\text{C}_{15}$ (44)
24	1226	1178	1178(vw)	1180(w)	20.26	734.73	1.73	1.53	$\nu\text{N}_{13}\text{C}_{15}$ (14) + $\beta\text{H}_7\text{C}_4\text{C}_3$ (27) + $\beta\text{H}_9\text{C}_6\text{C}_5$ (16)
25	1203	1156	1150(vw)	1153(w)	118.37	1322.1	2.09	1.78	$\nu\text{C}_3\text{C}_{12}$ (26) + $\beta\text{H}_9\text{C}_6\text{C}_5$ (62)
26	1188	1141			7.92	74.01	1.12	0.93	$\nu\text{C}_{19}\text{C}_{21}$ (11) + $\beta\text{H}_{20}\text{C}_{17}\text{C}_{15}$ (10) + $\beta\text{H}_{23}\text{C}_{19}\text{C}_{21}$ (29) +


27	1175	1129	1128(vw)		37.46	191.54	1.68	1.37	$\beta\text{H}_{24}\text{C}_{21}\text{C}_{19}(31)$
28	1155	1110	1108(w)		38.21	351.77	2.15	1.69	$\beta\text{H}_8\text{C}_5\text{C}_6(38) + \beta\text{C}_2\text{C}_1\text{C}_6(15)$
29	1129	1085			10.29	205.59	2.34	1.76	$\nu\text{C}_{18}\text{C}_{21}(16) + \nu\text{F}_{28}\text{C}_{25}(17) + \beta\text{H}_{23}\text{C}_{19}\text{C}_{21}(11)$
30	1120	1076			224.03	5.50	8.25	6.10	$\nu\text{C}_5\text{C}_6(17) + \beta\text{H}_7\text{C}_4\text{C}_3(11) + \beta\text{H}_9\text{C}_6\text{C}_5(14)$
31	1111	1067	1051(w)	1049(vw)	151.74	11.71	4.15	3.01	$\nu\text{F}_{27}\text{C}_{25}(53) + \nu\text{F}_{26}\text{C}_{25}(14)$
32	1072	1030	1037(m)		48.11	175.07	5.94	4.03	$\nu\text{F}_{26}\text{C}_{25}(41) + \nu\text{F}_{28}\text{C}_{25}(25)$
33	1069	1027			57.01	215.40	2.57	1.73	$\nu\text{C}_4\text{C}_5(20) + \beta\text{C}_1\text{C}_2\text{C}_3(13) + \nu\text{Cl}_{11}\text{C}_2(12) + \beta\text{C}_2\text{C}_1\text{C}_6(10)$
34	1047	1006	986(vw)		88.99	122.16	7.29	4.71	$\nu\text{C}_{19}\text{C}_{21}(19) + \nu\text{F}_{28}\text{C}_{25}(14) + \beta\text{H}_{22}\text{C}_{18}\text{C}_{21}(10)$
35	1003	964	963(vw)	963(vvw)	7.43	410.45	1.55	0.92	$\nu\text{C}_{19}\text{C}_{21}(14) + \beta\text{C}_{17}\text{C}_{19}\text{C}_{21}(25) + \beta\text{C}_{18}\text{C}_{21}\text{C}_{19}(20)$
36	998	959			1.77	124.29	1.35	0.79	$\Gamma\text{C}_{12}\text{C}_3\text{N}_{13}\text{H}_{14}(64)$
37	986	947	949(vw)		0.39	65.37	1.34	0.77	$\tau\text{H}_{20}\text{C}_{17}\text{C}_{19}\text{H}_{23}(17) + \tau\text{H}_{23}\text{C}_{19}\text{C}_{21}\text{H}_{24}(44)$
38	970	932			4.34	22.58	1.39	0.77	$\Gamma\text{C}_4\text{C}_3\text{C}_5\text{H}_7(11) + \tau\text{H}_8\text{C}_5\text{C}_6\text{H}_9(75)$
39	943	906			5.43	462.03	5.19	2.72	$\tau\text{H}_{20}\text{C}_{17}\text{C}_{19}\text{H}_{23}(36) + \Gamma\text{C}_{18}\text{C}_{16}\text{C}_{21}\text{H}_{22}(45)$
40	920	884	899(w)	898(vw)	0.38	7.17	1.37	0.68	$\nu\text{C}_3\text{C}_{12}(15) + \nu\text{Cl}_{10}\text{C}_1(12) + \beta\text{C}_3\text{C}_{12}\text{N}_{13}(21) + \beta\text{C}_2\text{C}_1\text{C}_6(19)$
41	883	848	853(m)		0.43	20.94	1.53	0.70	$\Gamma\text{C}_4\text{C}_3\text{C}_5\text{H}_7(52) + \tau\text{H}_9\text{C}_6\text{C}_1\text{C}_2(33)$
42	859	825			30.98	54.99	6.22	2.71	$\tau\text{H}_{20}\text{C}_{17}\text{C}_{19}\text{H}_{23}(31) + \Gamma\text{C}_{18}\text{C}_{16}\text{C}_{21}\text{H}_{22}(22) + \tau\text{H}_{23}\text{C}_{19}\text{C}_{21}\text{H}_{24}(25)$
43	795	764		771(vw)	40.69	1.80	1.60	0.59	$\nu\text{N}_{13}\text{C}_{15}(14) + \beta\text{C}_{17}\text{C}_{19}\text{C}_{21}(14) + \beta\text{C}_{18}\text{C}_{21}\text{C}_{19}(30) + \beta\text{C}_{16}\text{C}_{18}\text{C}_{21}(10)$
44	783	752	759(m)		23.42	25.02	2.58	0.93	$\Gamma\text{C}_4\text{C}_3\text{C}_5\text{H}_7(18) + \tau\text{H}_9\text{C}_6\text{C}_1\text{C}_2(29) + \tau\text{C}_1\text{C}_6\text{C}_2\text{C}_3(19)$
45	770	740	740(m)		49.91	73.11	1.57	0.55	$\tau\text{C}_{15}\text{C}_{17}\text{C}_{21}\text{C}_{19}(10) + \Gamma\text{N}_{13}\text{C}_{15}\text{C}_{17}\text{C}_{16}(16)$
46	761	731			6.34	70.11	6.21	2.12	$\Gamma\text{C}_{19}\text{C}_{17}\text{C}_{21}\text{H}_{23}(56) + \tau\text{C}_{17}\text{C}_{19}\text{C}_{18}\text{C}_{21}(10) + \tau\text{C}_{18}\text{C}_{16}\text{C}_{21}\text{C}_{19}(12)$
47	753	723			17.79	24.46	7.54	2.52	$\nu\text{F}_{27}\text{C}_{25}(14) + \beta\text{C}_{17}\text{C}_{19}\text{C}_{21}(35)$
48	718	690	700(s)		13.76	16.33	3.35	1.02	$\nu\text{Cl}_{11}\text{C}_2(14) + \nu\text{Cl}_{10}\text{C}_1(13) + \beta\text{C}_4\text{C}_5\text{C}_6(49)$
49	686	659	645(m)		22.58	29.28	6.69	1.85	$\tau\text{H}_9\text{C}_6\text{C}_1\text{C}_2(16) + \tau\text{C}_1\text{C}_6\text{C}_4\text{C}_5(11) + \tau\text{C}_3\text{C}_2\text{C}_4\text{C}_5(37) + \Gamma\text{Cl}_{11}\text{C}_1\text{C}_3\text{C}_2(17)$
50	655	629			8.01	33.36	7.24	1.83	$\beta\text{C}_1\text{C}_6\text{C}_5(10) + \beta\text{C}_3\text{C}_{12}\text{N}_{13}(41)$
51	600	576	595(w)		1.66	95.35	5.34	1.13	$\beta\text{C}_{16}\text{C}_{18}\text{C}_{21}(32)$
52	596	573			0.93	34.89	7.04	1.48	$\nu\text{F}_{27}\text{C}_{25}(10) + \tau\text{C}_{15}\text{C}_{17}\text{C}_{21}\text{C}_{19}(21) + \Gamma\text{C}_{25}\text{C}_{16}\text{F}_{27}\text{F}_{28}(17) + \tau\text{C}_{21}\text{C}_{18}\text{C}_{16}\text{C}_{25}(11)$
53	579	556	562(s)		4.77	55.87	5.73	1.13	$\beta\text{C}_{15}\text{C}_{17}\text{C}_{19}(14) + \Gamma\text{C}_{25}\text{C}_{16}\text{F}_{27}\text{F}_{28}(28)$
54	563	541			8.94	25.88	5.98	1.12	$\beta\text{C}_{15}\text{C}_{17}\text{C}_{19}(34)$
55	554	532			1.48	31.19	6.66	1.21	$\beta\text{C}_{15}\text{C}_{17}\text{C}_{19}(14)$
								1.21	$\Gamma\text{F}_{27}\text{C}_{16}\text{F}_{26}\text{C}_{25}(37)$

56	523	502	511(vw)		0.33	3.02	4.08	0.66	$\tau C_1C_6C_4C_5(35) + \tau C_3C_2C_4C_5(14) + \Gamma Cl_{10}C_2C_6C_1(13) + \Gamma Cl_{11}C_1C_3C_2(28)$
57	510	490			7.97	62.05	6.31	0.97	$\beta F_{27}C_{25}F_{28}(39)$
58	482	463	459(m)	462(vw)	6.85	218.16	8.02	1.10	$\nu Cl_{11}C_2(40) + \beta F_{27}C_{25}F_{28}(39)$
59	472	453			0.28	126.69	6.12	0.80	$\beta C_{17}C_{15}N_{13}(22) + \beta F_{26}C_{25}F_{28}(41)$
60	435	418			5.08	41.31	5.80	0.65	$\beta C_1C_2Cl_{11}(18) + \beta C_2C_1Cl_{10}(23)$
61	412	396			0.54	59.13	10.63	1.06	$\nu Cl_{10}C_1(27) + \beta C_2C_1C_6(13) + \beta F_{26}C_{25}F_{27}(10)$
62	364	350		350(vvw)	0.56	39.97	6.56	0.51	$\beta F_{26}C_{25}F_{27}(16) + \tau C_{15}C_{17}C_{21}C_{19}(12)$
63	347	333			0.45	54.35	7.20	0.51	$\beta F_{26}C_{25}F_{27}(10) + \beta F_{26}C_{25}F_{28}(11) + \Gamma F_{27}C_{16}F_{26}C_{25}(32)$
64	330	317			3.17	82.61	9.94	0.64	$\beta C_{15}C_{16}C_{18}(13) + \nu C_{16}C_{25}(27) + \beta F_{27}C_{25}F_{28}(10)$
65	300	288			1.99	19.24	6.32	0.33	$\tau C_{17}C_{19}C_{18}C_{21}(52)$
66	269	258			6.09	121.36	5.68	0.24	$\beta C_{17}C_{15}N_{13}(10) + \Gamma F_{27}C_{16}F_{26}C_{25}(11) + \Gamma Cl_{11}C_1C_3C_2(13) + \tau C_1C_2C_3C_{12}(15)$
67	237	228			2.19	214.21	4.55	0.15	$\tau C_2C_3C_{12}N_{13}(11) + \tau C_1C_6C_4C_5(14) + \tau C_3C_2C_4C_5(14) + \Gamma Cl_{10}C_2C_6C_1(21)$
68	229	220		224(vw)	1.04	162.18	7.45	0.23	$\tau C_{17}C_{19}C_{18}C_{21}(13) + \Gamma Cl_{10}C_2C_6C_1(16) + \Gamma Cl_{11}C_1C_3C_2(10)$
69	224	215			0.06	80.79	27.49	0.82	$\beta C_1C_2Cl_{11}(43) + \beta C_2C_1Cl_{10}(44)$
70	185	178			1.63	89.19	7.05	0.14	$\beta C_{12}N_{13}C_{15}(10) + \beta C_{18}C_{16}C_{25}(39)$
71	149	143			0.24	54.67	7.93	0.10	$\beta C_2C_3C_{12}(14) + \tau C_{21}C_{18}C_{16}C_{25}(35)$
72	133	128			1.16	725.13	4.72	0.05	$\tau C_1C_6C_2C_3(35) + \tau C_{12}N_{13}C_{15}C_{17}(18)$
73	113	109		100(vw)	0.31	219.92	5.18	0.04	$\tau C_{17}C_{19}C_{18}C_{21}(15) + \tau C_{21}C_{18}C_{16}C_{25}(44)$
74	68	65		66(w)	1.26	741.22	9.22	0.03	$\tau C_1C_6C_2C_3(12) + \tau C_{12}N_{13}C_{15}C_{17}(28)$
75	55	53			0.20	298.10	9.81	0.02	$\beta C_3C_{12}N_{13}(13) + \beta C_{12}N_{13}C_{15}(17) + \tau C_{18}C_{16}C_{25}F_{26}(28)$
76	40	38			0.22	185.26	15.26	0.01	$\beta C_{12}N_{13}C_{15}(12) + \tau C_{18}C_{16}C_{25}F_{26}(52)$
77	32	31			0.32	289.12	11.83	0.01	$\tau C_3C_{12}N_{13}C_{15}(37) + \tau C_1C_2C_3C_{12}(34)$
78	13	12			0.19	3430.3	9.61	0.00	$\tau C_2C_3C_{12}N_{13}(65) + \tau C_{12}N_{13}C_{15}C_{17}(22)$

v: Stretching, β : in-plane-bending, Γ : out-of-plane bending, τ : Torsion, vw: very weak, vvw: very very weak, w: weak, s: strong, vs: very strong,

^aScaling factor: 0.9608 (Random et al., 1970 and Pople *et al.*, 1993).^[17,18] ^bIR absorption intensities. ^cRaman intensities. ^dTotal energy distribution calculated

at B3LYP/6-311++G(d,p) level. ^dTotal energy distribution calculated at DFT/B3LYP/6-311++G(d,p)level

 The power of the Web of Science™ on your mobile device, wherever inspiration strikes. [Dismiss](#) [Learn More](#)

General Information

Web of Science Coverage

[Return to Search Results](#)

BULLETIN OF ENVIRONMENT PHARMACOLOGY AND LIFE SCIENCES

[Share This Journal](#)

ISSN / eISSN **2277-1808**

Publisher **ACAD ENVIRONMENT & LIFE SCIENCES, C/O DR MANISH KUMAR 27, B N PURAM, NEAR BANSHI VIHAR COLONY, PASCHIM PURI RD, SIKANDRA-BODLA, UTTAR, INDIA, AGRA, 28200**

General Information

Journal Website

[Visit Site](#)

Publisher Website

[Visit Site](#)

Frequency

Monthly

Issues Per Year

12

Country / Region

INDIA

Web of Science Coverage

Feedback





Synthesis, Characterization, DFT and antimicrobial studies of some azomethine and β -amino derivatives

Mohammed Ameen K.K.¹, M. Syed Ali Padusha^{2*}, Ajitha Devi³ and F.M. Mashood Ahamed⁴

^{1,2,4}PG& Research Department of Chemistry, Jamal Mohamed College (Affiliated to Bharathidasan University), Tiruchirappalli, Tamilnadu

³Department of Chemistry, Government Victoria College, Palakkad, Kerala

*Author for correspondence: [syedalipadusha@gmail.com](mailto:syedali-padusha@gmail.com)

ABSTRACT

In the present work, three phenol derivatives Schiff and Mannich Bases were prepared and characterized using analytical and spectral methods such as FT-IR, ¹H-NMR, ¹³C-NMR and Mass Spectral Studies. The molecular structure, vibrational frequencies and intensity vibrational bands were analyzed for Schiff base derived by treating 2-ethoxy-4-(((2-(trifluoromethyl)phenyl)imino)methyl)phenol and interpreted with the help of Density Functional Theory (DFT) method with basis set 6-311++G(d,p). Further all the compounds are screened for Anti-microbial activity by disc diffusion method. Synthesized compounds such as (1-phenyl-ethyl)-amine(MA1), (3-trifluoromethyl phenyl)-amine (MA2) and 4-nitro-2-(trifluoromethyl) aniline(MA3) compounds found to have antibacterial and antifungal activity

Key words: Mannich Bases- Imines-azomethine compounds-DFT

Received 04.12.2020

Revised 03.01.2021

Accepted 19.01.2021

INTRODUCTION

A reaction in which two molecules combine to form a single molecule is called condensation reaction. Usually a small molecule water is removed in this reaction [1]. Formation of peptide bond during the combination amino acid is because of condensation reaction, a covalent bond forms between the amine nitrogen of one amino acid and the carboxyl carbon of the second amino acid. Condensation reaction proceeds in a step-wise fashion to produce the addition product. It is a versatile class of reactions that can occur in acidic or basic conditions or in the presence of a catalyst. There are several type of condensation reactions exist, viz., aldol condensation, Claisen condensation, Knoevenagel condensation, Dieckman condensation (intramolecular Claisen condensation), Schiff Condensation and Mannich Condensation [2]. Of these several condensation reaction studied, the products of Schiff and Mannich reactions gained much attention among the researchers in the fields like Organic, Organometallic and Pharmaceutical chemistry due to their wide biological applications. The present research work focused on synthesis of organic compounds via Schiff and Mannich reactions. Hence, it is essential to highlight the importance of Schiff and Mannich Bases. German chemist, Hugo Schiff in 1864 produced Schiff bases by reacting primary amines and carbonyl compounds [3-5]. Schiff base is also known as imine or azomethine group. Schiff bases are active against a wide range of organisms since they play an important role in living organisms, such as decarboxylation, transamination and C-C bond cleavage. Biological Properties Azomethine group of these compounds has a great attention as precursor in huge organic synthesis due to their biological applications such as, anticancer, CNS depressant, antibacterial, anti-inflammatory [6-8], anticonvulsant, anti-tumor, analgesic [9-11], anti- hypertensive activity, anti HIV activity, antimicrobial activity [12,13], anticovelcent [14], anti-tubercular [15], anti-cancer [16], anti-oxidant [17], plant growth inhibitors, and insecticidal properties. Schiff base ligands are essential in the field of coordination chemistry, especially in the development of complexes of Schiff bases because these compounds are potentially capable of forming stable complexes with metal ions. Metal-imine complexes have been widely investigated due to antitumor and herbicidal use. They can work as models for biologically important species. Ligands and complexes that include sulfur and nitrogen have wide applications for the synthesis of drugs. Drug resistances properties of Schiff base against antibacterial agents may be enhanced by the preparation of metal complexes, using a process of chelation with the coordination of transition metal ions. Schiff bases

have N atoms as their basic elements. Schiff base derivatives containing donor atom can act as good chelating agents for the transition of metal ions [18].

Photo- and thermochromic properties of Schiff bases find used in the following modern technologies: optical computers, to measure and control the intensity of the radiation, in imaging systems, in the molecular memory storage, as organic materials in reversible optical memories and photodetectors in biological systems [19, 20]. Photochromic properties of Schiff compounds make them as photo stabilizers, dyes for solar collectors, solar filters. They are also exerted in optical sound recording technology [19]. Among others, worthy of interest in the properties associated with Schiff rules include: properties of liquid crystal [20], chelating ability [21], thermal stability [22], optical nonlinearity [23] and the ability to create the structure of a new type of molecular conductors using electrical properties to proton transfer [24]. Because of its thermal stability Schiff bases can be used as stationery phase in gas chromatography. The optical nonlinearity of these compounds allows us to use them as electronic materials, opto-electronic (in optical switches) and photonic components [25]. Imine derivatives can be exerted to obtain conductive polymers. Schiff bases as an electrical conductor possess a variety range of uses: as catalysts in photo electrochemical processes, electrode materials and micro-electronic equipment, organic batteries or electrochromic display device (graphical output devices). Due to the presence of the imine group, the electron cloud of the aromatic ring and electronegative nitrogen, oxygen and sulfur atoms in the Schiff bases molecules [26], these compounds effectively prevent corrosion of mild steel, copper, aluminium and zinc in acidic medium. Carl Mannich developed a product by reacting formaldehyde and a primary or secondary amine or ammonia and a compound containing acidic proton, the final product formed is a β -amino-carbonyl compound also known as a Mannich base [27, 28]. The Mannich reaction is an example of nucleophilic addition of an amine to a carbonyl group followed by dehydration to the Schiff base. The Mannich-Reaction is employed in the organic synthesis of natural compounds such as peptides, nucleotides, antibiotics, and alkaloids (e.g. tropinone). Mannich compounds are used to possess potent activity like anti-inflammatory, anticancer, antibacterial, antifungal and antimicrobial activities [29].

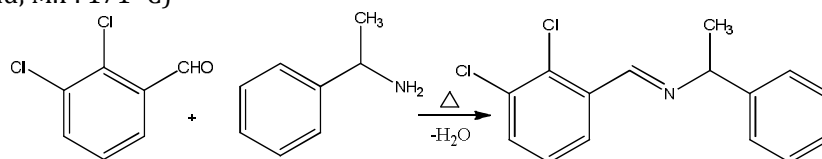
MATERIAL AND METHODS

Synthesis of azomethine compounds via Schiff reaction (MA1-MA3)

Melting points were measured in an open capillary on Mel-Temp apparatus and are uncorrected. IR spectra were recorded on Perkin Elmer spectrometer using KBr pellets. ^1H and ^{13}C NMR spectra were recorded on a Bruker AM-400 spectrometer for solution in DMSO- d_6 with tetramethylsilane (TMS) as an internal standard. All the chemical shifts values were recorded as δ ppm. Mass spectra were recorded by EI method and HRMS was measured on a JEOL GC mate II mass spectrometer. Commercially obtained reagents were used without further purification. All reactions were monitored by TLC with silica gel-G coated plates.

Synthesis of (2, 3-Dichloro-benzylidene)-(1-phenyl-ethyl)-amine (MA1)

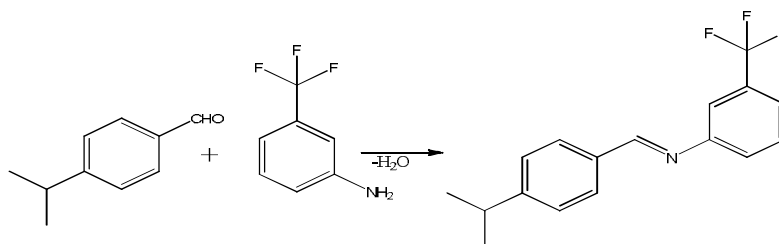
To the ethanolic solution of 1-phenylethanamine (12.8 mL, 0.1 M), 2,3-dichlorobenzaldehyde (17.5 g, 0.1 M) was added and refluxed for 6 h. The mixture was poured into a beaker contain crushed ice. The solid separated out was washed, filtered and dried over vacuum and recrystallized using ethanol. (Colour: Deep Brown solid; M.P: 171 $^{\circ}\text{C}$)



Scheme:1 - Synthesis of (2, 3-Dichloro-benzylidene)-(1-phenyl-ethyl)-amine (MA1)

Synthesis of (4-Isopropyl-benzylidene)-(3-trifluoromethyl phenyl)-amine (MA2)

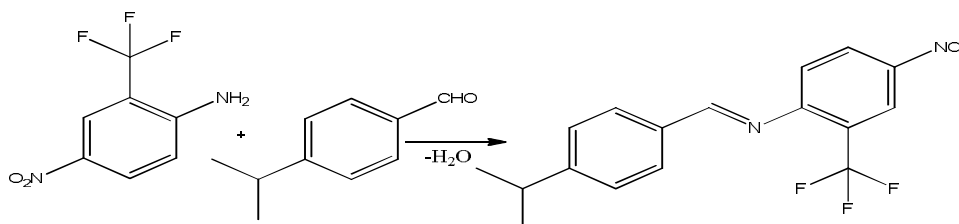
To the ethanolic solution of 4-isopropyl benzaldehyde (14.8 mL, 0.1 M), 3-amino benzotrifluoride. (16.0 mL, 0.1 M) was added. The reaction mixture was taken in a RB flask and kept over a magnetic stirrer and stirred for 6 h. The solid separated out was washed, filtered, and dried over vacuum and recrystallized using absolute ethanol. (Colour: Colourless solid; M.P: 180 $^{\circ}\text{C}$)



Scheme: 2- Synthesis of (4-Isopropyl-benzylidene)-(3-trifluoromethyl phenyl)-amine (MA2)

Synthesis of N-(4-isopropylbenzylidene)-4-nitro-2-(trifluoromethyl) aniline (MA3)

To the ethanolic solution of 2-amino-5-nitrobenzenetrifluoride (20.4 g, 0.1 M), 4-isopropylbenzaldehyde (15.0 mL, 0.1M) was added. The reaction mixture was taken in a RB flask and kept over a magnetic stirrer and stirred for 6 h. The solid separated out was washed, filtered, and dried over vacuum and recrystallized using absolute ethanol. (Colour: Brown solid; M.P: 106 °C)



Scheme: 3- Synthesis of N-(4-isopropylbenzylidene)-4-nitro-2-(trifluoromethyl) aniline (MA3)

Antimicrobial study

Antibacterial activity evaluated against *E.coli* and *S.aureus* and antifungal activity performed against *Aspergillusniger* by disc diffusion method. Known concentration of compound at 100µg/disc were preloaded and placed over the agar surface seeded with test pathogen. Zone of inhibition for bacteria recorded after 24 h and antifungal activity confirmed after 5 days. ofloxacin and cyclohexamide used as positive control DMSO used as negative control. Relative inhibitory zone was calculated as follows

$$\text{RIZD} = \frac{\text{Zone of Test} - \text{Zone of negative control}}{\text{zone of PC} \times 100}$$

RESULT AND DISCUSSION**Spectral and Antimicrobial studies of (MA1)**

The FT-IR spectrum of MA1 is presented in the **Fig. 1**. Aromatic C-H stretching in phenyl ring exhibits a band at 3068 cm^{-1} . A strong absorption band appeared at 2964 cm^{-1} is due to C-H stretching. An absorption band at 1562 cm^{-1} indicates C=N stretching. A band appeared at 719 is due to C-Cl stretching. ^1H - NMR spectrum of MA1 in the **Fig 2**. The peaks ranges from 7.2-7.5 are due to aromatic protons. Presence of azomethine and methine protons revealed from the peaks exhibited at 6.9 ppm and 5.9 ppm respectively. Methyl protons exhibited peak at 1.5 ppm. **Fig. 3** represents the ^{13}C -NMR spectrum of MA1. Azomethine carbon exhibits a peak at 162 ppm. Aromatic carbons show signals from 120 to 128 ppm. A peak appeared at 72 ppm shows the presence of methine carbon. A peak obtained at 22 ppm is due to methyl carbon. Mass spectrum of (2, 3-Dichloro-benzylidene)-(1-phenyl-ethyl)-amine (MA1) is shown in the **Fig 4**. Exact mass of MA1 has been confirmed by its m/z appeared at 277.04.

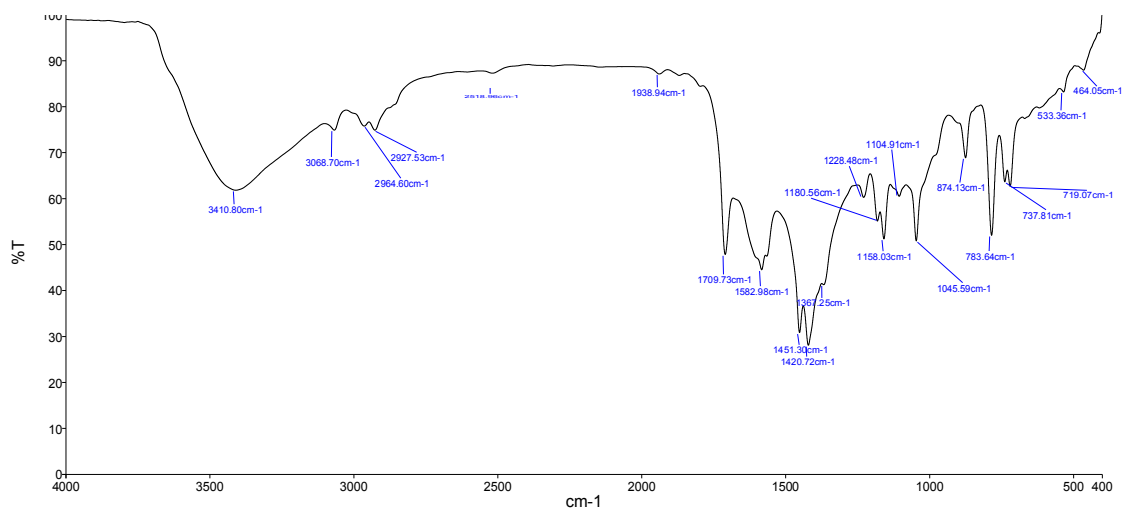


Fig. 1. FTIR spectrum of (2, 3-Dichloro-benzylidene)-(1-phenyl-ethyl)-amine (MA1)

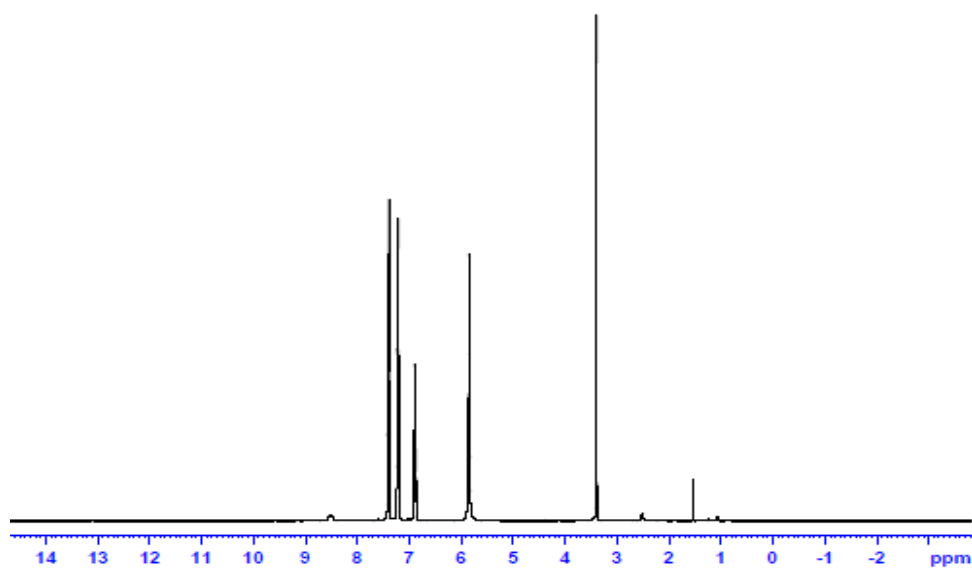


Fig. 2. ¹H-NMR spectrum of (2, 3-Dichloro-benzylidene)-(1-phenyl-ethyl)-amine (MA1)

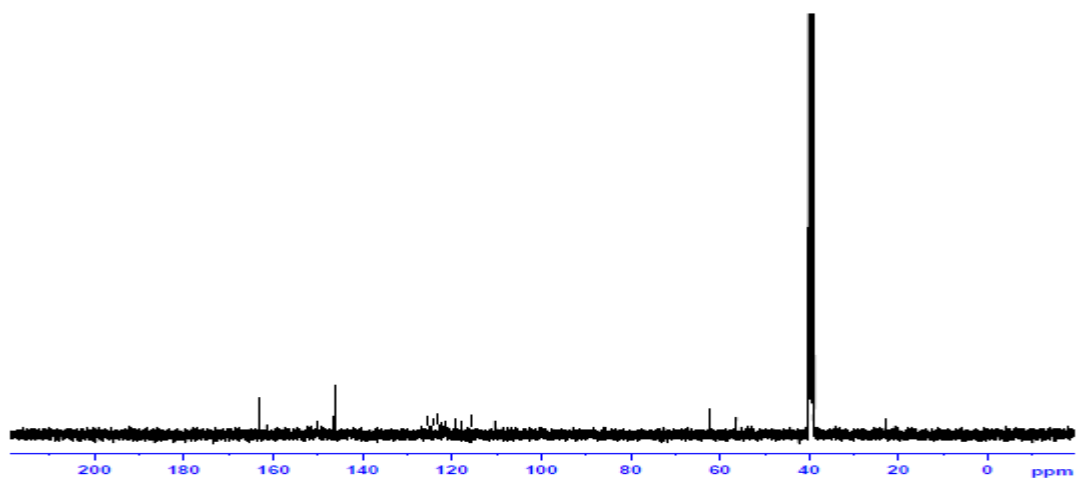


Fig. 3. ¹³C-NMR spectrum of (2, 3-Dichloro-benzylidene)-(1-phenyl-ethyl)-amine (MA1)

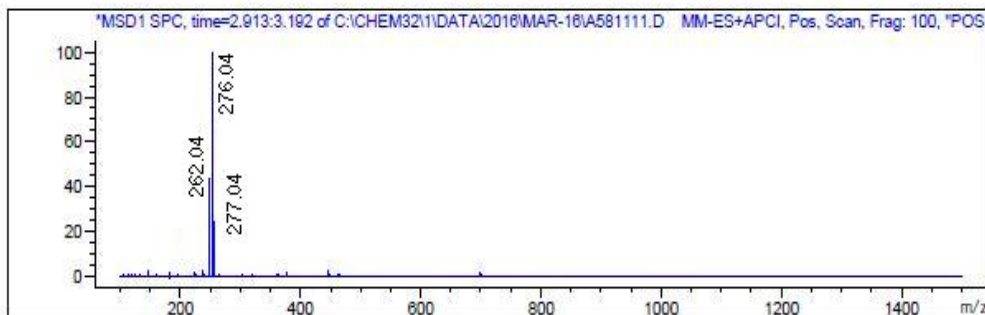


Fig. 4. Mass spectrum of (2, 3-Dichloro-benzylidene)-(1-phenyl-ethyl)-amine (MA1)

Spectral and Antimicrobial studies of (MA2)

The FT-IR spectrum of MA2 is presented in the **Fig. 5**. Aromatic C-H stretching in phenyl ring exhibits a band at 2965 cm^{-1} . A strong absorption band appeared at 2876 cm^{-1} is due to C-H stretching. An absorption band at 1631 cm^{-1} indicates C=N stretching. A band appeared at 660 is due to C-F stretching. $^1\text{H-NMR}$ spectrum of MA2 has been given in the **Fig. 6**. A peak at 8.5 ppm indicates the azomethine proton. The signals ranges from 6.9 to 7.5 ppm are assigned to aromatic protons. A peak observed at 2.5 ppm indicates methine protons. Methyl protons are assigned by the signal obtained at 1.1 ppm . $^{13}\text{C-NMR}$ of the compound MA2 has been presented in the **Fig. 7**. Azomethine carbon shows a peak at 161 ppm . The peaks ranging from 124 - 138 indicate the aromatic carbons. CF_3 carbon is indicated by a peak at 122 ppm . Mass Spectrum of (4-Isopropyl-benzylidene)-(3-trifluoromethyl phenyl)-amine. (MA2) given in **Fig. 8** represents the mass spectrum of the compound MA2. The peak appearing at $m/z\ 291.12$ confirms the calculated molecular mass of the compound. The intense peak at $m/z\ 248.12$ is the base peak.

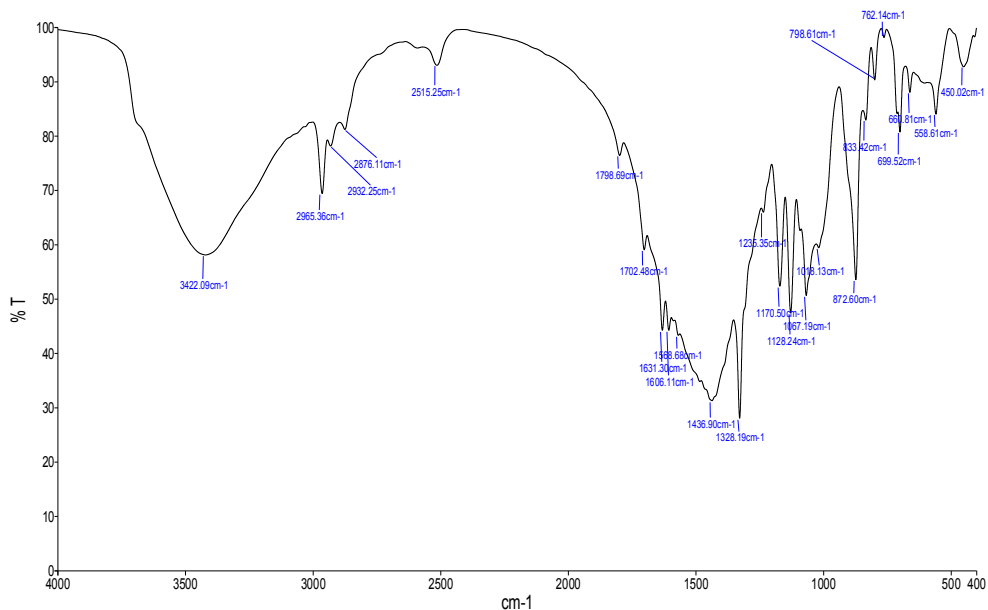


Fig. 5. IR Spectrum of (4-Isopropyl-benzylidene)-(3-trifluoromethyl phenyl)-amine (MA2)

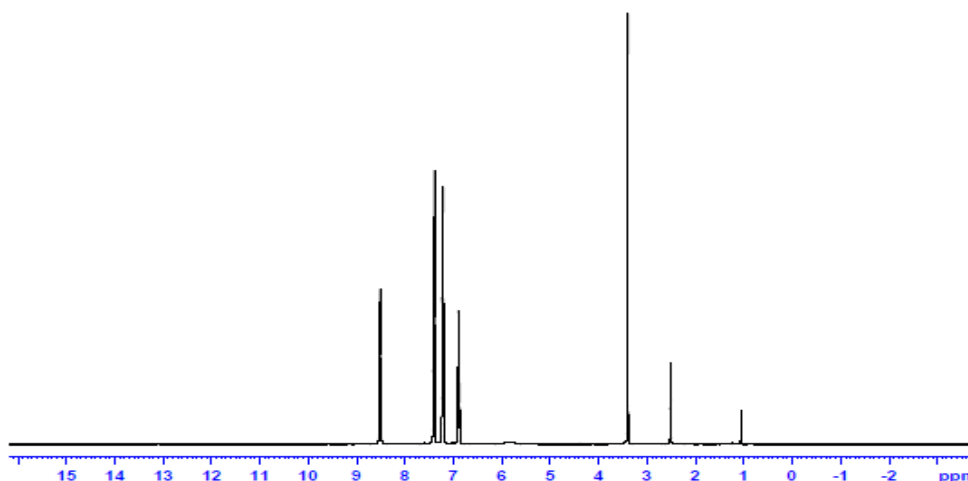


Fig. 6¹H-NMR Spectrum of (4-Isopropyl-benzylidene)-(3-trifluoromethylphenyl)amine (MA2)

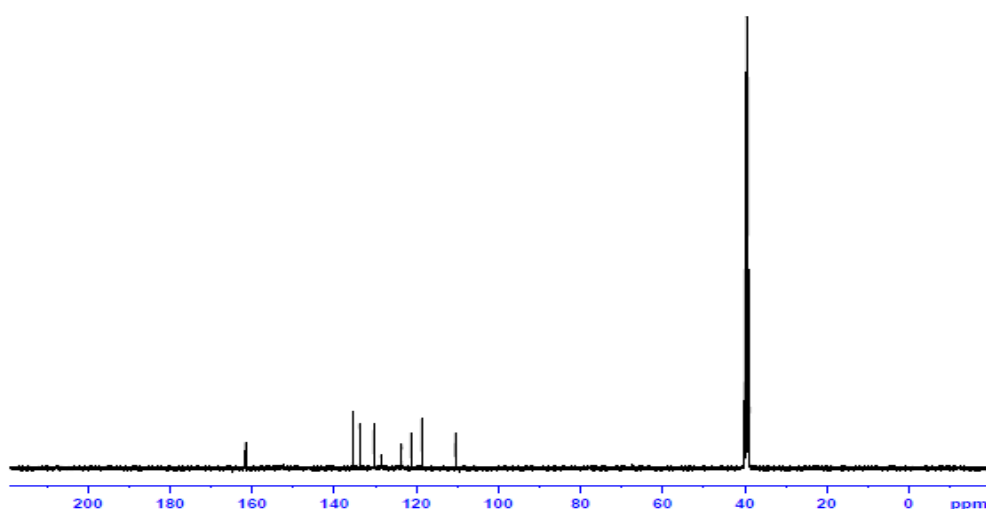


Fig. 7.¹³C-NMR Spectrum of (4-Isopropyl-benzylidene)-(3-trifluoromethyl phenyl)-amine. (MA2)

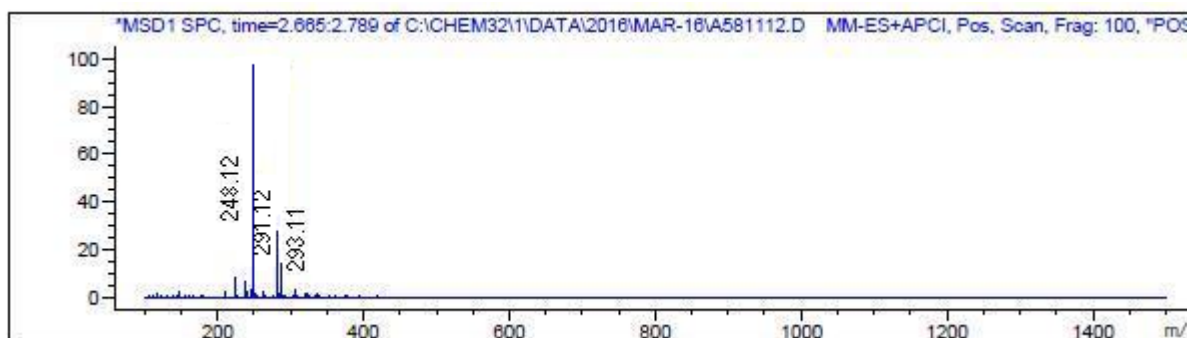


Fig. 8 Mass Spectrum of (4-Isopropyl-benzylidene)-(3-trifluoromethyl phenyl)-amine. (MA2)

Spectral and Antimicrobial studies of (MA3)

FT-IR spectrum of MA3 is shown in the **Fig. 9**. The band appears at 3314 cm^{-1} is due to NH stretching. Aromatic C-H and C=C stretching frequencies are indicated by the bands at 2988 and 1492 cm^{-1} respectively. Carbonyl stretching frequency of ester is noticed by a band at 1697 cm^{-1} . ¹H-NMR spectrum of N-(4-isopropylbenzylidene)-4-nitro-2-(trifluoromethyl)aniline (MA3) given in the **Fig. 10**. A peak at 8.5 ppm indicates the azomethine proton. The signals ranges from 6.9 to 7.5 ppm are assigned to aromatic protons. A peak observed at 2.5 ppm indicates methine protons. Methyl protons are assigned by the signal obtained at 1.2 ppm. ¹³C-NMR of the compound MA3 is presented in the **Fig. 11**. Azomethine carbon

shows a peak at 162 ppm. The signal appeared at 146 ppm is due to nitro group carbon bonded in aromatic ring. The peaks ranging from 122-135 indicate the aromatic carbons. CF₃ carbon is indicated by a peak at 121 ppm. **Fig. 12** represents the mass spectrum of the compound MA3. The molecular ion peak appearing at m/z 336.31 confirms the calculated molecular mass of the compound. The peak appearing with high intensity at m/z 293.11 is the base peak.

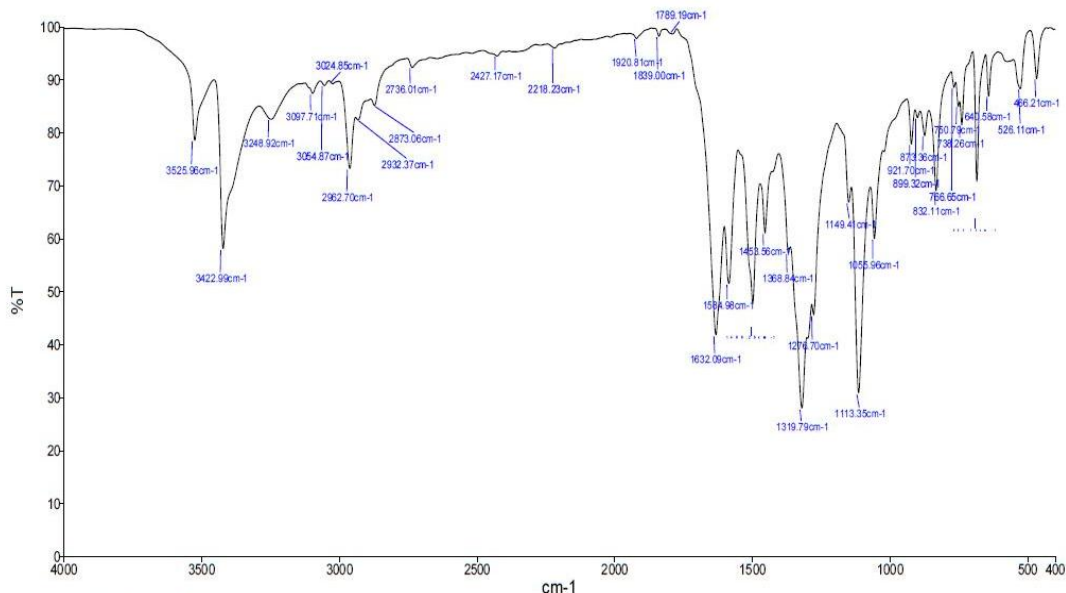


Fig. 9. IR spectrum of N-(4-isopropylbenzylidene)-4-nitro-2-(trifluoromethyl)aniline (MA3)

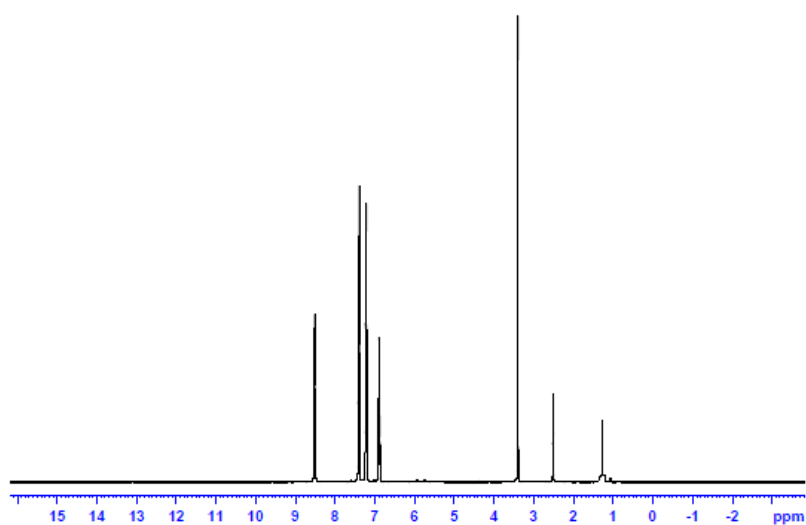


Fig. 10. ¹H-NMR spectrum of N-(4-isopropylbenzylidene)-4-nitro-2-(trifluoromethyl)aniline (MA3)

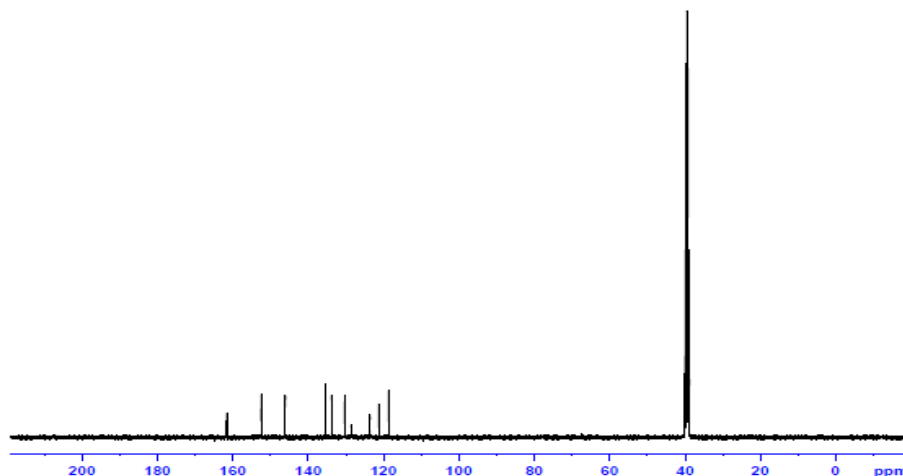


Fig. 11. ^{13}C -spectrum of N-(4-isopropylbenzylidene)-4-nitro-2-(trifluoromethyl)aniline (MA3)

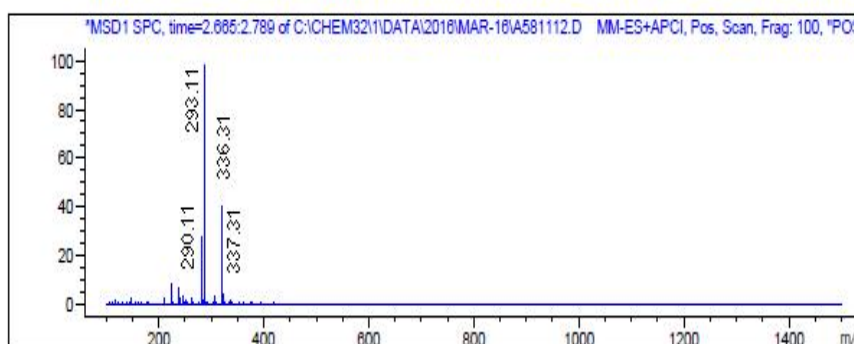


Fig. 12. Mass spectrum of N-(4-isopropylbenzylidene)-4-nitro-2-(trifluoromethyl)aniline

Antibacterial effect

Zone of inhibition of the compound MA1 –MA3 is given in the Table 1 reveals that the compound exhibits very less activity against *E.coli*. It shows moderate activity against *A. niger*. Potency of the compound is found to be high against *S. aureus*. All the three compound is found to be potent against gram positive bacteria and less active against gram negative bacteria and moderate against fungi strain when compared to the standard drug employed. All the test pathogens were highly sensitive to MA3 than MA1 and MA2. The compound MA2 possesses very high activity against *S. aureus*, less activity against *E.coli* and considerable activity against the fungi strain, *A. niger* when compared to the positive standard. In general the compound exhibit moderate activity against fungi pathogen and potent against gram positive bacteria. **Fig. 13** represent the results of the antimicrobial evaluation of the compound MA1 to MA3 Compared with standard. MA1 found 76% RIZD against fungi but moderate against bacterial pathogen. Similarly MA2 found better against Staphylococcus and It shows 50 % RIZD against *E.coli* and *A.niger*. the another derivative MA3 is found to posses greater activity than standard against *S. aureus* and *E. coli*but moderate activity against *A. niger*. The compound is more active against bacterial stain than the fungi when compared to the positive standard. Many investigators have observed the importance of azomethines for their antibacterial and antifungal [30]

Table 1. Zone of inhibition mm in diameter

TEST PATHOGEN	MA1	MA2	MA3	STANDARD	NC
<i>S. aureus</i>	20	19	30	20	2
<i>E. coli</i>	18	16	30	24	3
<i>A. niger</i>	25	18	20	30	3

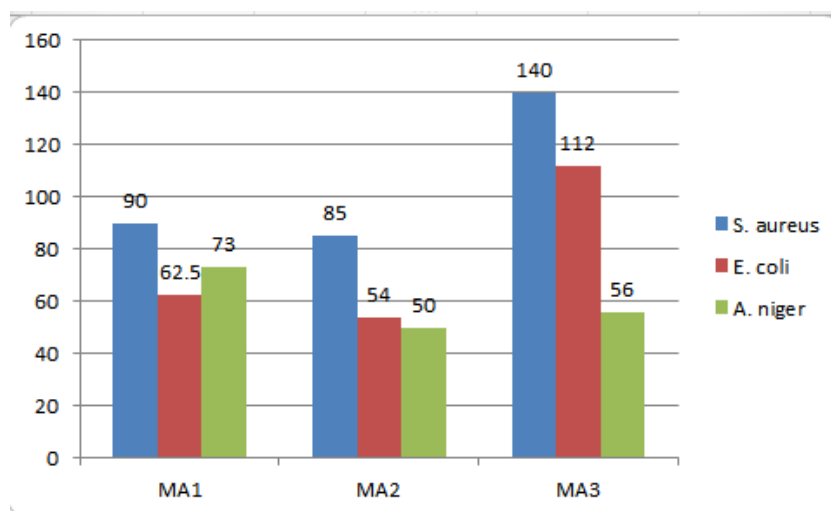


Figure . Relative inhibitory zone of diameter

CONCLUSION

Biologically potent compounds having more Nitrogen in their structure were effected through condensation Schiff and Mannich base reactions. FT-IR, ¹H-NMR, ¹³C-NMR and Mass Spectral data of all the compounds corroborated with the structure proposed in the scheme concerned. The results of the antimicrobial studies reveal that, the compounds have found to possess highest activity at 100 µg for all the selected microorganism.

REFERENCES

- Fakirov S (2019). Condensation Polymers: Their Chemical Peculiarities Offer Great Opportunities. Progress in Polymer Science; 89: 1-18.
- Bruckner, Reinhard (2002). Advanced Organic Chemistry (First Ed.). San Diego, Harcourt Academic Press; 414-427.
- Cimerman, Miljanić S, and Galić N (2000). Schiff bases derived from aminopyridines as spectrofluorimetric analytical reagents. CroaticaChemicaActa; 73(1): 81-95.
- Schiff (1864). Communications from the University Laboratory in Pisa: a new series of organic bases. Justus Liebigs Annalen der Chemie; 131(1): 118-119.
- Dhar D. N and Taploo C. L (1982). Schiff bases and their applications. Journal of Scientific and Industrial Research; 41(8): 501-506.
- Sathe B. S, Jaychandran .E, Jagtap V. A, and Sreenivasa G. M (2011). Synthesis characterization and anti-inflammatory evaluation of new fluorobenzothiazole schiff's bases. International Journal of Pharmaceutical Research and Development; 3 (3): 164-169.
- Sondhi S. M, Singh N, Kumar A, Lozach O, and Meijer L (2006). Synthesis, anti- inflammatory, analgesic and kinase (CDK-1, CDK-5 and GSK-3) inhibition activity evaluation of benzimidazole/benzoxazole derivatives and some Schiff's bases. Bioorganic and Medicinal Chemistry; 14(11): 3758-3765.
- Pandey A, Dewangan D, Verma S, Mishra A, and Dubey R. D (2011). Synthesis of schiff bases of 2-amino-5-aryl-1, 3, 4-thiadiazole and its analgesic, anti-inflammatory, anti-bacterial and anti-tubercular activity. International Journal of ChemTech Research; 3(1): 178-184.
- Chandramouli C, Shivanand M. R, Nayanbhai T. B, Bheemachari B, and Udupi R. H (2012). Synthesis and biological screening of certain new triazoleschiff bases and their derivatives bearing substituted benzothiazole moiety. Journal of Chemical and Pharmaceutical Research; 4(2): 1151-1159.
- Chinnasamy R. P, Sundararajan R, and Govindaraj S (2010). Synthesis, characterization, and analgesic activity of novel schiff base of isatin derivatives. Journal of Advanced Pharmaceutical Technology and Research; 1(3): 201342- 347.
- Mounika K, Anupama B, Pragathi J, and Gyanakumari C (2010). Synthesis, characterization and biological activity of a Schiff base derived from 3-ethoxy salicylaldehyde and 2-amino benzoic acid and its transition metal complexes. Journal of Scientific Research; 2(3): 513-524.
- Venkatesh P (2011). Synthesis, characterization and antimicrobial activity of various schiff bases complexes of Zn (II) and Cu(II) ions. Asian Journal of Pharmaceutical and Health Sciences; 1(1): 8-11.
- Chaube A. K. and Pandeya S. N (2012). Synthesis & anticonvulsant activity (Chemo Shock) of Schiff and Mannich bases of Isatin derivatives with 2-Amino pyridine (mechanism of action). International Journal of PharmTech Research; 4(4):590-598.
- Aboul-Fadl T, Mohammed F. A, and Hassan E. A (2003). Synthesis, antitubercular activity and pharmacokinetic studies of some Schiff bases derived from 1- alkylisatin and isonicotinic acid hydrazide (INH). Archives of Pharmacol Research; 26(10):778-784.

15. Miri R, Razzaghi-asl N, and Mohammadi M. K (2013). QM study and conformational analysis of an isatin Schiff base as a potential cytotoxic agent, *Journal of Molecular Modeling*; 19(2):727-735.
16. Ali SM, Azad MA, Jesmin M, Ahsan S, Rahman MM, Khanam JA, Islam MN, Shahriar SM (2012). In vivo anticancer activity of Vanillin semicarbazone, *Asian Pacific Journal of Tropical Biomedicine*; 2(6):438-442.
17. Wei D, Li N, Lu G, and Yao K (2006). Synthesis, catalytic and biological activity of novel dinuclear copper complex with Schiff base. *Science in China B*; 49(3): 225-229.
18. Chohan Z. H, Praveen M, and Ghaffar A (1997). Structural and biological behaviour of Co(II), Cu(II) and Ni(II) metal complexes of some amino acid derived Schiff- bases, *Metal-Based Drugs*; 4(5): 267-272.
19. Tanaka K, Shimoura R., Caira M. R (2010). Synthesis, crystal structures and photochromic properties of novel chiral Schiff base macrocycles. *Tetrahedron Lett*; 51(2):449-452.
20. Pistolis G, Gegiou D, Hadjoudis E (1996). Effect of cyclodextrin complexation on thermochromic Schiff bases. *J. Photochem. Photobiol. A: Chem*; 93(2-3): 179-184.
21. Mocanu A. S, Ilis M, Dumitrascu F, Ilie M, Circu V (2010). Synthesis, mesomorphism and luminescence properties of palladium(II) and platinum(II) complexes with dimeric Schiff base liquid crystals. *Inorg.Chim.Acta*; 363(4):729-736.
22. Issa Y. M, Sherif O. E, Abbas S. M (1998). Chelation behaviour of Ce(III), Th(IV), and UO₂ (VI) with 5,7-Dihydroxy-6-formyl-2-methylbenzopyran-4-one Schiff bases. *Monatshefte fur Chemie*; 129: 985-998.
23. Atta A. M., Shaker N. O., Maysour N. E (2006). Influence of the molecular structure on the chemical resistivity and thermal stability of cured Schiff base epoxy resins. *Prog. Org. Coat*; 56:100-110.
24. Jia J. H, Tao X. M, Li Y. J, Sheng W. J (2011). Synthesis and third-order optical nonlinearities of ferrocenyl Schiff base. *Chem. Phys. Lett*; 514(1-3):114-118.
25. Amany M. A (1992). Ibrahim Electrical and thermal behaviour of some Schiff bases and their charge transfer complexes with acidic acceptors. *Thermochim.Acta*; 197(1): 211-217.
26. Emregül K. C, Düzgün E, Atakol O (2006). The application of some polydentate Schiff base compounds containing aminic nitrogens as corrosion inhibitors for mild steel in acidic media. *Corr. Sci*; 48: 3243-3260.
27. Carl Mannich, Krösche, W (1912). "About a condensation product from formaldehyde, ammonia and antipyrine ", *Archiv der Pharmazie*; 250(1): 647-667.
28. Blicke, F. F (2011). The Mannich Reaction, *Organic Reactions*; 1(10): 303-341.
29. Bala S, Sharma N, Kajal A, Kamboj S and Saini V (2014). Mannich Bases: An Important Pharmacophore in Present Scenario. *International Journal of Medicinal Chemistry*; 2014: 191072.
30. Neelakantan M, Esakkiammal M, Mariappan S, Dharmaraja J, Jeyakumar T. Synthesis, Characterization and Biocidal Activities of Some Schiff Base Metal Complexes. *Indian J Pharm Sci* 2010; 72: 216-222.

CITATION OF THIS ARTICLE

Mohammed Ameen K.K, M. Syed Ali Padusha, Ajitha Devi and F.M. Mashood Ahamed- Synthesis, Characterization, DFT and antimicrobial studies of some azomethine and β -amino derivatives . *Bull. Env. Pharmacol. Life Sci.*, Vol 10[2] January 2021 : 105-114.